VOLUME 39 JUNE 1961 NUMBER 6

Canadian Journal of Physics

Published by THE NATIONAL RESEARCH COUNCIL

OTTAWA CANADA

CANADIAN JOURNAL OF PHYSICS

Under the authority of the Chairman of the Committee of the Privy Council on Scientific and Industrial Research, the National Research Council issues THE CANADIAN JOURNAL OF PHYSICS and five other journals devoted to the publication, in English or French, of the results of original scientific research. Matters of general policy concerning these journals are the responsibility of a joint Editorial Board consisting of: members representing the National Research Council of Canada; the Editors of the Journals; and members representing the Royal Society of Canada and four other scientific societies.

Manuscripts for publication should be submitted to Dr. H. E. Duckworth, Editor, Canadian Journal of Physics, Hamilton College, McMaster University, Hamilton, Ontario.
For instructions on preparation of copy, see **NOTES TO CONTRIBUTORS** (back cover).

Proof, correspondence concerning proof, and orders for reprints should be sent to the Manager, Editorial Office (Research Journals), Division of Administration and Awards, National Research Council, Ottawa 2, Canada.

Subscriptions, renewals, requests for single or back numbers, and all remittances should be sent to Division of Administration and Awards, National Research Council, Ottawa 2, Canada. Remittances should be made payable to the Receiver General of Canada, credit National Research Council.

The journals published, frequency of publication, and subscription prices are:

Canadian Journal of Biochemistry and Physiology	Monthly	$9.00 a year
Canadian Journal of Botany	Bimonthly	$6.00 a year
Canadian Journal of Chemistry	Monthly	$12.00 a year
Canadian Journal of Microbiology	Bimonthly	$6.00 a year
Canadian Journal of Physics	Monthly	$9.00 a year
Canadian Journal of Zoology	Bimonthly	$5.00 a year

The price of regular single numbers of all journals is $2.00.

Canadian Journal of Physics

Issued by THE NATIONAL RESEARCH COUNCIL OF CANADA

VOLUME 39 JUNE 1961 NUMBER 6

ON THE RELATION BETWEEN THE OLD AND THE NEW DEFINITION OF THE INTERNATIONAL METRE[1]

K. H. HART AND K. M. BAIRD

ABSTRACT

In October, 1960, the Eleventh General Conference of Weights and Measures adopted as the new definition of the International Metre, 1,650,763.73 wavelengths in vacuum of the unperturbed .606 μ line of Kr86. The present paper reports measurements, in terms of the new definition, on four copies of the metre which were well known in terms of the former International Metre prototype. They indicate no significant discontinuity in the metre, as a result of the transition to the new definition, and they demonstrate the accuracy to which the metre based on the old definition was realized in practice.

INTRODUCTION

Between 1889 and October, 1960, the International Metre was defined by the distance between two lines engraved on a platinum iridium bar which was kept at Sèvres, near Paris, at the International Bureau of Weights and Measures. Its relation to spectroscopic wavelength standards was known through several careful comparisons with the red line of cadmium, which were made at several laboratories since 1892. By making use of this known relationship, the metre has now been redefined as being equal to 1,650,763.73 wavelengths in vacuum of the unperturbed .606 μ line of Kr86 (Eleventh General Conference of Weights and Measures, Paris, France, October, 1960). An idea of the accuracy with which one would expect that the International Metre based on the new definition reproduces the old standard, can be given by a brief account of the steps leading to the new definition.

Referring to Table I, the last column gives what the present authors consider as "best values" for the relation between the vacuum wavelength of the red line of Cd and the former International Metre, derived from the various classical experiments; these values can be taken to indicate the degree of scatter in the comparisons as well as any possible drift in the length of the metre shown up by the experiments.

In the table, an asterisk indicates the value for the relation as originally published; a value is also given for the wavelength in standard air, which

[1]Manuscript received February 8, 1961.
Contribution from the Division of Applied Physics, National Research Council, Ottawa, Canada.
Issued as N.R.C. No. 6303.

TABLE I

Determinations of the relation between the Cd red line and the International Metre

Observations	Wavelength in air as originally given	Wavelength in standard air	Wavelength in vacuum
Michelson and Benoît (1895)	6438.4722*	6438.4691	6440.2486
Benoît, Fabry, and Pérot (1913)	.4696*	.4703	.2498
Watanabe and Imaizumi (1928)	.4685*	.4682	.2477
Sears and Barrell (1934)		.4718	.2513*
Kösters and Lampe (1934)		.4684	.2479*
Kösters (1938)	.4700*	.4692	.2487
Romanova *et al.* (1942)		.4693	.2488*
Average		.4695	.2490
N.R.C.		.4684	.2479

*Value reported in original papers.

has been deduced from the original value by making use of present knowledge; these values are useful in tracing the historical development of the new definition of the metre. The relation between the values of the last two columns is according to the Edlèn formula for the refractive index of standard air (1953).

It was not a straightforward matter to arrive at suitable values for Table I because, since the various measurements were made, new factors affecting the results have been disclosed from time to time by other experimenters as well as by those involved in the original measurements. For this reason, the values 4 to 7 inclusive differ from those of similar tables which have been published (see, for example, Barrell 1948).

The value originally reported by Michelson was corrected to standard air by making allowance for an assumed value for the relative humidity involved in his measurement, and for a revised value for the coefficient of thermal dilatation of the metre bar; the value of Benoît *et al.* was corrected for the same revised value of the coefficient; the value of Watanabe and Imaizumi was corrected for .03% CO_2 which is contained in standard air but which was not included in their original measurement. These three corrections follow Sears and Barrell (1934) and are generally accepted.

The original values of Sears and Barrell (1934) and of Kösters and Lampe (1934) have been taken from a joint report of Sears and Kösters (1935) containing an exhaustive analysis of their experiments; this report stated that the *vacuum* values quoted in Table I above were to be considered definitive values, although values for standard air (derived by different formulae in the two cases) were then given as having more interest at that time.

The original published value of Kösters (1938) is known to be in error because the Cd lamp which he used had a large content of argon with consequent pressure shift (Engelhard 1959). However, in Köster's determination, the metre bar was compared directly with the .565 μ line of natural Kr and the latter was then compared with the Cd red line. From Köster's paper the value found by him for the relation of the .565 μ line to the metre could be inferred, and by making use of the known relation of this line with the Cd red line, the corrected values in the table were obtained.

The value of Romanova *et al.* (1942) is their published "best value" for the vacuum wavelength.

For convenience, the corresponding relation derived from the measurement described in the present paper is also given in Table I.

Shortly after the measurement of Benoît *et al.* in 1905, the angstrom unit was defined by making use of the relation reported by them for the wavelength of the Cd line in standard air, viz., $\lambda = 6438.4696 \times 10^{-10}$ metre; the definition was made such that if this ratio were correct, 1 angstrom would equal 10^{-10} metre. The same ratio was provisionally sanctioned by the Seventh General Conference of Weights and Measures in 1927 and, after several years of uncertainties and ambiguities in the specified conditions for the excitation of the Cd line, a standard Cd lamp was specified by the International Committee of Weights and Measures in 1935 and the International Astronomical Union in 1937.

When the International Advisory Committee for the Definition of the Metre considered the matter in 1953, the mean of all the corrected known values for the ratio of the Cd red line to the metre was not significantly different from the 1905 value by which the angstrom unit was defined, even though in the meantime it was found that that 1905 value ought to have been corrected (as given in Table I). On the basis of this evidence, the recommendation was made that, in the redefinition of the metre, the ratio sanctioned in 1927 for the relation between the Cd red line and the metre be accepted, assuming that any error in this ratio was not significant insofar as the metre was concerned, and thereby making the angstrom unit by definition exactly equal to 10^{-10} metre. This relation was to be converted to vacuum by means of the Edlèn formula for the refractive index of air, which had been officially adopted in 1952 by the Joint Commission for Spectroscopy, and it was to be used to establish a new definition of the metre by direct comparison of the vacuum wavelength of the Cd red line with the wavelength of whichever spectral line was decided on as being the most suitable for the new standard.

This procedure was followed, and in 1960, the Eleventh General Conference of Weights and Measures ratified a new definition of the metre based on the .606 μ line of Kr86; this line had in the meantime been found to be the most suitable and its relation with the Cd red line had been checked by five different laboratories within a spread of three parts in 10^8, or .03 μ in the metre (C.I.P.M. 1958).

With the adoption of the new definition of the metre, it became necessary for national laboratories to equip themselves to measure, in terms of the wavelength standard, length scales like the old standard metre bars; these will continue to have great importance in scientific and legal measurement. A comparator for this purpose was built at N.R.C. (Baird 1961).

Although it had been decided in 1953 that the relation between the old metre and the Kr wavelengths was known with sufficient accuracy through the Cd line as intermediary, it was nevertheless of considerable interest to verify that measurements by new techniques, using the new definition for the metre, did not result in a serious discontinuity in scientific and legal length measurement. It is clear, from the last column of Table I above, that

a discontinuity of the order of $.002 \times 10^{-10}$ metre in the wavelength, or 0.3 μ in a metre, might well have been expected. This impression is only strengthened by a detailed study of the measurements on which the relation was based and the difficulties and uncertainties involved. As the comparator at N.R.C. was the only one at the time in a position for making such a verification, it was used for the measurement of four 1-metre bars, which were already well known in relation to the international prototype, and the results were communicated to the Eleventh General Conference. These measurements are described next.

MEASUREMENT PROCEDURE

The bars which were measured were the following:

(1) A platinum iridium bar, M-16, which was kindly loaned by the National Physical Laboratory of Great Britain; this bar is one of the original set from which the prototype metre was chosen and is very stable; it was re-engraved and calibrated in 1956 so that the lines are very good and the defining direction is straight, but there are some longitudinal scratches. New lines were engraved at 0, 50 cm, and at 100 cm for both 0° C and 20° C.

(2) A platinum iridium bar, M-4, kindly loaned by the United States Bureau of Standards; this bar is also from the original set but has very old lines (likely more than 40 years) engraved at every millimeter. It had a very high density of longitudinal scratches and was not straight, so that the position of the bar had to be readjusted in the comparator between measurements on the 0–50-cm and 50–100-cm intervals. However, the calibrations of all the intervals were extremely well known over a long period of time.

(3) A nickel bar, M-306, the former Canadian legal copy of the metre. Its lines were also old.

(4) An invar bar, M-169, repolished and engraved in 1952, with very good lines and relatively free from scratches. It has a fairly high rate of growth (0.081 μ per year) but its equation is well known through intercomparison at B.I.P.M. and with other bars at N.R.C.

By means of the N.R.C. interference comparator, the length of an interval up to 50 cm could be determined in terms of wavelengths in about half an hour with a standard deviation in the single determination of 0.12 μ. This deviation was mostly due to the pointing on the lines of the metre bar by the visual microscope with which the instrument is at present equipped. All known sources of systematic error in the interferometric observations were reduced or corrected for to the extent that they would not together contribute an error of more than a few hundredths of a micron in a metre to the final result (Baird 1961). The source of the Kr86 standard wavelengths conformed in all respects to the recommendation adopted by the C.I.P.M. in 1960 and therefore contributed negligible error.

The bars were measured in two steps, viz., the intervals 0 to 50 cm and 50 to 100 cm. In order to test for any possible effect due to bad collimation or uneven illumination, some measurements were made with the microscope in two orientations having the relation given by a rotation of π radians about

its axis, and for each position, the bars were measured in the normal and in the end-for-end reversed positions; no significant effect was observed due to these changes.

The temperatures of the bars were measured with respect to a platinum resistance thermometer by means of thermocouples. In addition to the individual calibration of the thermocouple bridge and the platinum thermometer, the whole setup was checked by occasional simultaneous independent measurements of the temperature of the bar made in co-operation with the group responsible for temperature standards at N.R.C. As a result of these checks and tests of the variation of the temperature along the bar ($<.006°$ C from end to end) it was found that the average temperature of the bar was known with certainty to $\pm 0.002°$ C. The measurements were all made within 0.3° of 20.0° C and the coefficients of thermal dilatation were well known; hence the uncertainty in the length measurement due to the effect of temperature was less than .02 μ in the metre.

The bars were mounted free from strain at their normal Airy points with a slight modification to take into account the interferometer mirror attached to one end. The latter with its mounting was equivalent in weight to about one centimeter of length of the bar. The length error due to this modification is less than .01 μ (Rolt 1929). With the exception of M-4, the bars were measured by displacement along a straight line joining the mid-points of the lines defining the metre interval.

Observations were taken by three observers of this laboratory, and in addition, Mr. B. Page of the National Bureau of Standards made observations in the case of M-4. The latter observations were particularly significant because Mr. Page has made pointings on this particular bar for a good many years and the length, according to his pointings, is known to a few hundredths of a micron in their relation to the former International Metre. No significant difference was found between observations by Mr. Page and those of the N.R.C. observers.

The only other source of uncertainty is that due to the statistical fluctuation, which is indicated in Table II and referred to later.

RESULTS

The results of the measurements are given in Table II. The column M/λ_{vac} gives the number of vacuum wavelengths found for the former International

TABLE II

Comparison of four 1-metre bars with Kr86 standard

Standard	Equation (at 20° C)	M/λ_{vac}	$\Delta L = M^1 - M$	No. of obs.	σ
M-16	1 m − 0.54 μ	1,650,764.16 m^{-1}	−0.26 μ	30	0.22 μ
M-4	1 m+167.37	3.92	−0.11	10	.11
M-169	1 m+ 1.15	4.09	−0.22	14	.19
M-306	1 m+269.91	4.13	−0.24	25	.20
Average		1,650,764.08	−0.21		
Relation according to new definition of metre		M^1/λ_{vac} = 1,650,763.73			

Metre, M, by the use of the bar listed in the first column as intermediary, taking into account the known calibration of these bars in terms of M, given in the second column. The fourth column gives the corresponding differences, expressed in microns, between the new and the old metre. The numbers of determinations and the standard deviations, σ, for single determinations are given in the last two columns.

The two bars M-16 and M-169 were also intercompared directly on a transverse comparator. Their difference was found to be only 0.07 μ different from the result given by the comparisons with the Kr86 wavelengths.

From Table II, it is seen that the measurements on these four bars indicate a difference between the old and the new metre of from $-0.11\ \mu$ to $-0.26\ \mu$ with an average of $-0.20\ \mu \pm 0.044\ \mu$ (95% confidence). This value was used to infer the vacuum wavelength of the Cd line which is given at the bottom of Table I.

CONCLUSIONS

Having regard to the upper limits, which can be attributed to the various sources of systematic error and to the statistical confidence limits, it is reasonable to assume that the value found for the average relation of the four bars to the newly defined metre is accurate to $\pm 0.1\ \mu$. The relation of the average length of the four bars to the old metre prototype, M, can also be assumed to be known to $\pm 0.1\ \mu$ as shown by past experience (Leclerc 1958) and as confirmed by the scatter found amongst the four bars. Therefore, the measurements indicate that the metre, according to the new definition, is shorter than the metre as formerly defined by $0.2\ \mu$ to within $\pm 0.2\ \mu$ with a considerable degree of certainty. The amount of this discontinuity is barely significant in relation to past calibrations of individual bars in terms of the old metre, and certainly is not important as regards any scientific or industrial measurements done in the past.

On the other hand, the results also confirm that, on the old basis, the International Metre has been constant and has been realized in practice to an accuracy of better than $\pm 0.2\ \mu$. A substantial part of the scatter in the values presented in Table I is undoubtedly due to the techniques used for comparison with wavelengths and to uncertainties in the reproduction of the Cd red line.

ACKNOWLEDGMENTS

The authors wish to acknowledge the assistance of Mrs. B. Potvin in making the measurements described in this paper, and of Dr. L. G. Turnbull for the intercomparison of M-16 and M-169.

REFERENCES

BAIRD, K. M. 1961. Rev. Sci. Instr. **32**. May issue.
BARRELL, H. 1948. Research, **1**, 533.
BENOÎT, J. R., FABRY, C., and PÉROT, A. 1913. Trav. Bur. Int. Poids Mesures, **15**, 3.
C.I.P.M. 1958. Procès-verbaux C.I.P.M. **26B**, M-15.
EDLÈN, B. 1953. J. Opt. Soc. Am. **43**, 339.
ENGELHARD, E. 1959. National Physical Laboratory 11th Symposium on Interferometry.

KÖSTERS, W. 1938. Physik. Z. **39**, 245.
KÖSTERS, W. and LAMPE, P. 1934. Physik. Z. **15**, 224.
LECLERC, G. 1958. Procès-verbaux C.I.P.M. **26B**, M-41.
MICHELSON, A. A. and BENOÎT, J. R. 1895. Trav. Bur. Int. Poids Mesures, **11**, 3.
ROLT, F. H. 1929. Gauges and fine measurement, Vol. 1 (Macmillan and Co., London).
ROMANOVA, M. F., WAHRLICH, G. V., KARTASHEV, A. I., and BATARCHUKOVA, N. R. 1942. Compt. rend. acad. sci. U.R.S.S. **37**, 46.
SEARS, J. E. and BARRELL, H. 1934. Phil. Trans. A, **233**, 143.
SEARS, J. E. and KÖSTERS, W. 1935. Procès-verbaux C.I.P.M. **17**, 113.
WATANABE, N. and IMAIZUMI, M. 1928. Proc. Imp. Acad. (Tokyo), **4**, 350.

GAMMA-RAY ANGULAR CORRELATIONS FROM ALIGNED NUCLEI PRODUCED BY NUCLEAR REACTIONS[1]

A. E. Litherland and A. J. Ferguson

ABSTRACT

Two general procedures for the measurement and analysis of angular correlations of gamma radiations from nuclear reactions are described which have wide applications in nuclear spectroscopy for the determination of spins and gamma-ray multipolarities. Cases can be studied by these methods when the reaction proceeds through a compound state too complex to allow the usual analysis to be made, for example where several levels overlap or where direct interaction is dominant. The basis of these procedures is to exploit the simplifications brought about by making the reacting system axially symmetric. A sharp gamma-ray-emitting state formed in such a system can be regarded as aligned and described in terms of a relatively small number of population parameters for the magnetic substates. In the first procedure, a state Y^* is prepared by a nuclear reaction $X(h_1h_2)Y^*$ in which h_2 is unobserved. The state Y^* has axial symmetry about the beam axis. From coincidence angular correlation measurements of two cascade gamma rays from Y^*, the unknown population parameters for Y^* together with the nuclear spins and gamma-ray multipolarities can be determined. In the second procedure, h_2 is measured in a small counter at 0° or 180° relative to the incident beam. It is then shown that the quantum numbers of the magnetic substates of Y^* which can be populated do not exceed the sum of the spins of X, h_1, and h_2. In cases where the sum of the spins does not exceed $\frac{1}{2}$, the angular correlation of the gamma rays from the aligned state depends only upon the properties of the states in the residual nucleus. Theoretical expressions for angular correlations from aligned states are given, together with a method whereby existing extensive tables of coefficients can be used to calculate them. The results of two recent experiments are discussed as examples.

I. INTRODUCTION

The determination of the spins and parities of nuclear states as well as of a number of associated nuclear parameters has rested very largely on angular distribution measurements of nuclear reactions. This is a consequence of the intimate connection which the concepts of spin and parity have with the rotation and reflection of co-ordinate systems. The general theory of such processes exploits the invariance properties of the system through the use of the statistical tensors of Fano and Racah (1959), as has been described in a number of well-known papers. The formalism and, to a large degree, the notation of the survey of Devons and Goldfarb (1957) will be used in the present paper.

The interpretation of the simplest angular distribution, namely the angular distribution of an outgoing gamma radiation with respect to a bombarding beam and without observation of its polarization, is usually attended by ambiguity. The reason for this is that such a simple experiment does not provide very much information. More specifically, the results of a typical experiment can be represented by the formula

$$W(\theta) = a_0P_0(\cos\theta)+a_2P_2(\cos\theta)+a_4P_4(\cos\theta) \tag{1}$$

[1]Manuscript received February 23, 1961.
Contribution from the Physics Division, Atomic Energy of Canada Limited, Chalk River, Ontario.
Issued as A.E.C.L. No. 1231.

where $W(\theta)$ is the intensity of the reaction observed at the angle θ relative to the incident beam and the a_k are the coefficients of the corresponding Legendre polynomials, $P_k(\cos\theta)$. It frequently happens that the angular distribution coefficients are a function of several unquantized parameters, for example, channel spin mixtures and orbital mixtures for the incoming particles and a multipole mixture for the outgoing gamma ray. Thus, it may be possible to adjust the parameters to fit the measured a_2/a_0 and a_4/a_0 for several choices of the spin of the state. In such a case, the spin could not be determined from the measurements.

It has been pointed out by Ferguson and Rutledge (1957) and by Biedenharn (1960) that substantially more information can be obtained from a triple correlation such as the reaction $(p\gamma\gamma)$. Assuming the axis of quantization to be defined by the incoming particle beam, the intensity of the two gamma rays in coincidence will be a function of the polar angles θ_1 and θ_2 for each radiation and the relative azimuthal angle ϕ between them. In this case, the intensity is given by the series

$$W(\theta_1, \theta_2, \phi) = \sum_{k_1 k_2 \kappa} a^{\kappa}_{k_1 k_2} X^{\kappa}_{k_1 k_2}(\theta_1, \theta_2, \phi) \tag{2}$$

where the $X^{\kappa}_{k_1 k_2}(\theta_1, \theta_2, \phi)$ are functions whose angular dependence has the form $P^{\kappa}_{k_1}(\cos\theta_1) P^{\kappa}_{k_2}(\cos\theta_2)\cos\kappa\phi$. k_1 and k_2 are limited by the multipolarities of the two gamma rays and are even if the nuclear states have sharp spin and parity. κ is positive or zero, may be even or odd, and does not exceed the smaller of k_1 and k_2. With the latter restricted to 4, corresponding to quadrupole radiation, the series (2) has 19 terms (Ferguson and Rutledge (1957) hereinafter designed FR). Provided the compound state has sharp spin and parity, then usually no more than five unquantized parameters comprising channel spin and orbital and multipole mixing will occur. Over a sufficiently varied set of points, the angle functions of series (2) are linearly independent, so that the coefficients $a^{\kappa}_{k_1 k_2}$ can all be determined, and it may be seen that the amount of available information, i.e. the number of measurable parameters, generously exceeds the number of unknowns. No experimental use has yet been made of this general approach. A number of investigators, Hoogenboom (1958), Litherland *et al.* (1959), and Broude *et al.* (1959) for example, have extracted a limited amount of information by the use of geometrical configurations, or "geometries", with one detector fixed and the other moving in a horizontal plane.

These considerations are predicated on the assumption that all of the states concerned have definite spins and parities. While this will be generally true for the lower states of the cascade, it will be obtained for the state into which an incident particle is captured only if this is a sharp, well-isolated resonance. The lighter nuclei under neutron, proton, or alpha-particle bombardment provide abundant instances where this requirement is satisfied. However, for deuteron bombardment and in the middle-weight and heavier nuclei, such isolated resonant structure is rare, the reaction ordinarily being dominated by stripping or direct interaction type of behavior for which the compound

state has no definite spin. Here the description in terms of statistical tensors contains so many arbitrary parameters that, despite the large amount of information available, the analysis of the system must be regarded as impractical at present. It is the object of the present paper to describe some types of experiment wherein the representation of the system is greatly simplified so as to permit the results to be interpreted. The essence of the idea is to consider a state of sharp spin and parity, which is one of the later stages of a transmutation process, prepared in a way such that there are certain strong limitations on the populations of the magnetic substates. The subsequent decay of this state can then be treated as if it were aligned. The cases we will be concerned with are those in which the angular distribution of a gamma ray emitted by the state is measured and those in which the correlation of two gamma rays in cascade from the state is measured. In the latter, the amount of information that can be extracted from the correlation is the same as for the $(p\gamma\gamma)$ triple correlation discussed above and will usually be well in excess of the number of arbitrary parameters describing the system. This method has been used by Warburton and Rose (1958) to establish the spin of the 6.89-Mev state of C^{14}. It is conjectured by these workers that the contrast between results for different spin choices will generally be much less marked than it was in the C^{14} study and they conclude that the method is probably of limited use. This is a question which has not been studied and does not appear to be amenable to a theoretical scrutiny. However, in the use made of triple angular correlations to date, clear-cut results have generally been found. We are proposing here that the method has indeed wide applicability and is one of the most powerful methods available for the determination of spins and multipole mixtures.

The ideas involved here can be grouped into two parts which we will call, for convenience, method I and method II. Method I is that in which a state of definite spin and parity is formed by a transmutation process involving incident and outgoing particles and proceeding through a compound state which may not have sharp spin and parity. The incident beam defines the axis of quantization and the outgoing particles are not observed. It can then be shown that the magnetic substates of the system are uncorrelated with each other and that they are symmetrically populated. The angular correlations of the radiations from this state will then be governed by a or $a-\frac{1}{2}$ polarization parameters according to whether the spin a is integral or half-integral. The measurement of the correlations of two cascade gamma rays following this will thus normally provide sufficient information to determine these parameters as well as multipole mixtures of the two radiations.

The theoretical expressions for such correlations are given in Section II of this paper together with the modifications necessary to allow for the finite size of the gamma-ray detectors. In Sections II and III a procedure is given for obtaining the theoretical correlation coefficients from the table of coefficients prepared by FR. In Section IV an experiment is discussed which provides a good illustration of method I. This is the experiment on the angular distributions and correlations of the gamma rays from the 4.24-Mev state in Mg^{24} discussed recently by Batchelor *et al.* (1960).

Method II consists of forming a state in a way similar to that of method I, but with the difference that the outgoing particle is detected in a counter located at either 0° or (near) 180° relative to the incident beam. Then, since the orbital magnetic quantum numbers for the incoming and outgoing particles are zero, the populations of the magnetic substates of the state under consideration will be limited by the spins of the target nucleus and of the incident and emergent particles.

In Section V theoretical expressions are given for the angular distribution of the gamma rays with respect to the axis defined by the incident and emergent particles. These expressions include the first order corrections for the finite size of the counter detecting the emergent particle. In Section VI the experimental results from the reaction $Mg^{26}(\alpha,n\gamma)Si^{29}$ are discussed. In this example the observation of the neutrons at 0° selects the magnetic substates $\pm\frac{1}{2}$ of the gamma-emitting state. Consequently there is no arbitrary parameter associated with the populations and the angular distribution coefficients depend only upon the properties of the residual nucleus Si^{29}. Theoretical expressions for such angular correlations are given and a method described whereby existing extensive tables of coefficients can be used to calculate them.

II. METHOD I

A state which is formed as the final one in a nuclear reaction involving the capture of an unpolarized particle incident along the z-axis followed by the emission of one or more unobserved radiations in cascade is clearly symmetric about the z-axis. The state is then aligned, this alignment being indistinguishable from the alignment achieved by methods other than nuclear reactions as summarized, for example, by Blin-Stoyle and Grace (1957). For an axially symmetric state with angular momenta a and a' only the tensor parameters $\rho_{k0}(aa')$ are different from zero as is readily seen from the requirement of invariance under rotation through an arbitrary angle about the z-axis. This treatment of correlations resulting from nuclear reactions is specifically considered by Biedenharn (1960). If, further, the state considered has definite parity, and if no polarization is present in the incident particles and target, then only the tensor parameters having even k will be non-zero. This again follows readily by considering reflection of the system in the origin, equivalent, in this case, to a proper rotation through 180° about the y-axis. We will henceforth make the assumption that the state has both spin and parity definite.

Using the standard relation connecting a statistical tensor and density matrix:

$$\langle a\alpha|\rho|a\alpha'\rangle = \sum_{k_a\kappa_a} (-)^{a-\alpha'}(a\alpha,a-\alpha'|k_a\kappa_a)\rho_{k_a\kappa_a}(aa), \tag{3}$$

we find that the restriction $\kappa = 0$ implies that $\alpha' = \alpha$. The notation of Devons and Goldfarb is used here where α designates a magnetic quantum number of the state a; in general Greek letters designate the magnetic substates of states for which the corresponding Latin letter designates the spin magnitude.

$\langle a\alpha|\rho|a\alpha'\rangle$ is an element of the density matrix and $(a\alpha,a-\alpha'|k_a\kappa_a)$ is a Clebsch–Gordan vector addition coefficient. It is readily found that evenness of k_a implies symmetry between the population of the positive and negative magnetic substates, that is

$$\langle a-\alpha|\rho|a-\alpha\rangle = \langle a\alpha|\rho|a\alpha\rangle.$$

For convenience we will abbreviate the notation for these elements and introduce $P(\alpha) = \langle a\alpha|\rho|a\alpha\rangle$ to indicate the population of the substate α. Due to the symmetry between positive and negative values only the positive values and zero need be considered, but care must be taken not to ignore the contributions arising from negative values which normally occur in the summations.

The number of independent parameters required to describe the state a with the present limitations is $a+1$ or $a+\frac{1}{2}$ depending on whether a is integral or half-integral. The angular correlations are homogeneous in these parameters so that one parameter can be identified as a normalization factor which need not be measured. The essential number of parameters is consequently a or $a-\frac{1}{2}$. If the state decays with the emission of two gamma rays in cascade then two more unquantized parameters comprising the multipole mixing of the transitions must be expected. As a specific example, the correlation between two cascade gamma rays from a state of spin 5 will entail seven parameters. As we have seen, the measurement of such a correlation can yield 18 parameters so that ample information for the determination of the unknowns is generally available. We term the procedure based on these considerations method I. It consists of a bombardment experiment in which the incident beam direction is identified with the z-axis, the disintegration particles from the compound state are not observed, and the coincident correlations are measured relative to the z-axis of two cascade radiations, generally gamma rays, from a state below the compound state. The process is illustrated in Fig. 1. x and y are the spins of the target nucleus and compound nucleus

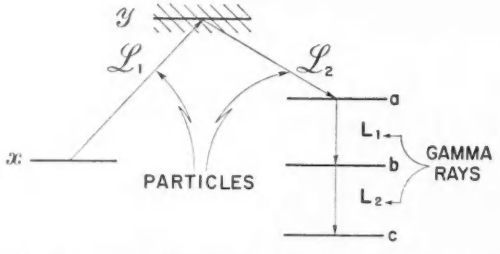

FIG. 1. Schematic energy level diagram to illustrate the quantum numbers used. The analysis of the paper is concerned with the gamma-ray cascade $aL_1\,b\,L_2c$. The quantum numbers $x\,y\,\mathscr{L}_1\mathscr{L}_2$ belong to the details of the formation of the state 'a' and are not involved directly in the analysis. x is the spin of the target nucleus, y is the spin of the compound state formed by capture of the particle with total angular momentum $\mathscr{L}_1$. $\mathscr{L}_2$ is the total angular momentum of the outgoing particle which in method I is not observed and in method II is observed in a counter located on the beam axis. The cross hatching on the state y indicates that it need not have sharp spin and parity. All of the details of the formation of the state 'a' are contained in the populations of its magnetic substates, $P(\alpha)$, which are treated as unknowns to be found from the angular correlations of the gamma rays.

and $\mathscr{L}_1$ and $\mathscr{L}_2$ the total angular momenta of incoming and outgoing particles respectively. a, b, and c are the spins of the subsequent states between which the radiations with multipolarities, L_1 and L_2, are observed. x, y, $\mathscr{L}_1$, and $\mathscr{L}_2$ and any interfering mixtures contained in them are immaterial to the analysis, which proceeds entirely from parameters describing the state a.

The expression for the correlation can be obtained immediately from one given by Devons and Goldfarb (1957) for two cascade radiations from an unpolarized state of spin a. We will assume as they do that the cascade proceeds through the states b and c with the emission of radiation of multipolarity 2^{L_1} and 2^{L_2}. The required expression is obtained from equation (11.33) of Devons and Goldfarb (1957) by removing the assumption that the initial state is unpolarized. It is

$$(4)\qquad W \sim \sum \rho_{k0}(aa)\,\langle c||L_2||b\rangle\,\langle c||L_2'||b\rangle^*\,\langle b||L_1||a\rangle\,\langle b||L_1'||a\rangle^*$$

$$\times \epsilon^*_{k_1\kappa_1}(L_1L_1')\,\epsilon^*_{k_2\kappa_2}(L_2L_2')\,\hat{a}^2\hat{k}_1\hat{k}_2 \begin{Bmatrix} b & L_1 & a \\ b & L_1' & a \\ k_2 & k_1 & k \end{Bmatrix} \hat{b}^2\hat{k}_2 \begin{Bmatrix} c & L_2 & b \\ c & L_2' & b \\ 0 & k_2 & k_2 \end{Bmatrix}$$

$$\times (k_2\kappa_2,\, k_1\kappa_1|k0)\;(00\;k_20|k_20)\cdot\hat{c}.$$

The summation in equation (4) is over $k\,k_1k_2\kappa_1\kappa_2L_1L_1'L_2L_2'$. The basic change required to remove the condition of a unpolarized is to replace the factor $\delta_{k_a0}/\hat{a}$ of the original equation by $\rho_{k0}(aa)$, in which k is assumed even as discussed above. The other δ-functions have been removed, putting in the explicit parameters demanded by them. From the Clebsch–Gordan coefficient $(k_2\kappa_2,k_1\kappa_1|k0)$ we must have $\kappa_1 = -\kappa_2 = \kappa$. The coefficient $(00k_20|k_20) = 1$. The circumflex over any index or quantum number, e.g. a, indicates the function

$$\hat{a} = (2a+1)^{1/2}.$$

The angular dependence of the correlation is contained specifically in the factors $\epsilon_{k_1\kappa_1}(L_1L_1')$ and $\epsilon_{k_2\kappa_2}(L_2L_2')$. These can both be written as

$$(5)\qquad \epsilon_{k\kappa}(L\,L') = c_{k0}(L\,L')\,D^k_{\kappa0}(\mathscr{R})$$

$$= \frac{\hat{L}\,\hat{L}'(-)^{L'-1}}{\sqrt{2\pi}\,\hat{k}}\,(L1,\,L'-1|k0)\;.\;Y^{\kappa*}_k\,(\theta,\phi)$$

where $c_{k0}(L\,L')$ is a radiation parameter for gamma rays as described by Devons and Goldfarb, $D^k_{\kappa0}(\mathscr{R})$ is an element of the rotation matrix for the rotation $\mathscr{R} = (\phi,\theta,0)$ which brings the z-axis into the direction of the counter. The second line of equation (5) is obtained by substituting explicit expressions for these quantities. $Y^\kappa_k(\theta,\phi)$ is the spherical harmonic of the polar angles θ and ϕ.

The reduced matrix elements, $\langle b||L_1||a\rangle$, etc. are real. The usual multipole amplitude ratios are defined by*

*We write the reduced matrix elements in the normal order. The consistent use of this convention will avoid the confusion of sign (Ofer 1959) which arises from the convention of Biedenharn and Rose (1953). The penalty for using the normal order is the appearance of factors of the type $(-)^{L-L'}$ in the formulae. We feel, however, that this is a smaller difficulty from the experimentalists' viewpoint than the one of having the sign of a mixing ratio depend on whether the transition involved is the first or last one in the correlation.

$$\delta_1 = \frac{\langle b||L_1+1||a\rangle}{\langle b||L_1||a\rangle}, \tag{6a}$$

$$\delta_2 = \frac{\langle c||L_2+1||b\rangle}{\langle c||L_2||b\rangle}. \tag{6b}$$

Finally the second $9-j$ symbol of the formula can be reduced to a Racah coefficient through

$$\begin{Bmatrix} c\ L_2\ b \\ c\ L_2'\ b \\ 0\ k_2\ k_2 \end{Bmatrix} = \frac{(-)^{c+k_2-L_2-b}}{\hat{c}\,\hat{k}_2} W(bL_2bL_2', ck_2).$$

Dropping constant factors which affect only the normalization of the expression we have

$$W \sim \sum \rho_{k0}(aa)\ \delta_1^{p_1}\ \delta_2^{p_2}(-)^{f_1}\ \hat{L}_1\hat{L}_1'\hat{L}_2\hat{L}_2' \tag{7}$$

$$\times(L_1 1, L_1'-1|k_1 0)\ (L_2 1, L_2'-1|k_2 0)\ (k_1-\kappa, k_2\kappa|k0)$$

$$\times \begin{Bmatrix} b\ L_1 a \\ b\ L_1' a \\ k_2\ k_1\ k \end{Bmatrix} W(bL_2bL_2', ck_2)\ Y_{k_1}^{\kappa}(\theta_1\phi_1)\ Y_{k_2}^{-\kappa}(\theta_2\phi_2).$$

The summation is over $k\ k_1 k_2 \kappa L_1 L_1' L_2 L_2'$. $f_1 = c-b+L_1'-L_2+L_2'+k_2$. k_1 and k_2 are even as a consequence of the states b and c having definite parity. We thus have

$$(k_1-\kappa, k_2\kappa|k0) = (k_1\kappa, k_2-\kappa|k0).$$

The summation over κ extends over positive and negative values which can be grouped in pairs

$$\begin{aligned}(k_1-\kappa, k_2\kappa|k0)\ Y_{k_1}^{\kappa}\ Y_{k_2}^{-\kappa} &+ (k_1\kappa, k_2-\kappa|k0)\ Y_{k_1}^{-\kappa}\ Y_{k_2}^{\kappa} \\ &= (k_1-\kappa, k_2\kappa|k0)\ [Y_{k_1}^{\kappa}\ Y_{k_2}^{-\kappa} + Y_{k_1}^{\kappa *}\ Y_{k_2}^{-\kappa *}] \\ &= (k_1-\kappa, k_2\kappa|k0)\ 2\ \mathrm{Re}\ [Y_{k_1}^{\kappa}(\theta_1,\phi_1)\ Y_{k_2}^{-\kappa}(\theta_2,\phi_2)]\end{aligned}$$

revealing that W is real, which is known, of course, as a general result. For explicit evaluation we write the spherical harmonics in terms of the associated Legendre polynomials (Condon and Shortley 1951)

$$Y_k^{\kappa}(\theta,\phi) = (-)^{(\kappa+|\kappa|)/2}\frac{\hat{k}}{\sqrt{4\pi}}\left[\frac{(k-|\kappa|)!}{(k+|\kappa|)!}\right]^{1/2} P_k^{|\kappa|}(\cos\theta)e^{i\kappa\phi}$$

and

$$\mathrm{Re}\ [Y_{k_1}^{\kappa}(\theta_1,\phi_1)\ Y_{k_2}^{-\kappa}(\theta_2,\phi_2)] \tag{8}$$

$$= \frac{(-)^{|\kappa|}}{4\pi} 2^{1-\delta_{\kappa 0}}\hat{k}_1\hat{k}_2\left[\frac{(k_1-|\kappa|)!\ (k_2-|\kappa|)!}{(k_1+|\kappa|)!\ (k_2+|\kappa|)!}\right]^{1/2} P_{k_1}^{|\kappa|}(\cos\theta_1)\ P_{k_2}^{|\kappa|}(\cos\theta_2)\cos\kappa\ \phi.$$

$$= \frac{(-)^{|\kappa|}}{4\pi} 2^{1-\delta_{\kappa 0}} X_{k_1k_2}^{\kappa}(\theta_1,\theta_2,\phi).$$

The terms representing interfering multipoles are duplicated in the summation of equation (7). It is consequently convenient to contract this formula and write

$$(9)\quad W \sim \sum{}' 2^n \rho_{k0}(aa)\, \delta_1^{p_1}\, \delta_2^{p_2} (-)^{f_2}\, \hat{L}_1 \hat{L}_1' \hat{L}_2 \hat{L}_2' \times (L_1 1, L_1' -1 | k_1 0)(L_2 1, L_2' -1 | k_2 0)\ (k_1 -\kappa, k_2 \kappa | k 0) \times \begin{Bmatrix} b & L_1 & a \\ b & L_1' & a \\ k_2 & k_1 & k \end{Bmatrix} W\,(bL_2\, bL_2',\, ck_2)\, X^{\kappa}_{k_1 k_2}\,(\theta_1, \theta_2, \phi).$$

The summation here is over $k\ k_1 k_2 \kappa L_1 L_1' L_2 L_2'$. The prime on the $\sum$ indicates the restriction $L_1 \leqslant L_1'$, $L_2 \leqslant L_2'$, and $\kappa \geqslant 0$. The duplication is accounted for by the factor 2^n. n is equal to the number of pairs $(L_1 L_1')$ and $(L_2 L_2')$ in which the interfering multipoles are different, plus zero for $\kappa = 0$ and plus one for $\kappa > 0$. $f_2 = c - b + L_1' - L_2 + L_2' + k_2 + |\kappa|$.

Equation (9) has the form of equation (2) so that the explicit expression for the coefficients $a^{\kappa}_{k_1 k_2}$ can be written down. The indices $k_1 k_2$, which characterize the angle functions $X^{\kappa}_{k_1 k_2}(\theta_1, \theta_2, \phi)$, are even and κ is integral and not greater than the smaller of k_1 and k_2. If $L_1, L_1', L_2, L_2' \leqslant 2$, then $(k_1 k_2 \kappa)$ may in general have the values (000), (020), (040), (200), (220), (221), (222), (240), (241), (242), (400), (420), (421), (422), (440), (441), (442), (443), (444). These 19 sets of indices define 19 corresponding angle functions which are mutually orthogonal in the intervals $0 \leqslant \theta_1 \leqslant \pi$, $0 \leqslant \theta_2 \leqslant \pi$, $0 \leqslant \phi \leqslant 2\pi$ and are thus linearly independent.

Extensive tabulations of the coefficients occurring in equation (9) have been made for which a convenient bibliography is given by Gibbs and Way (1958, 1959). The more extensive tabulations are by Simon *et al.* (1954) and Smith and Stevenson (1957). Composite coefficients in which several of the factors are combined and which facilitate numerical work considerably have been tabulated by Sharp *et al.* (1953), Ferentz and Rosenzweig (1955), Rose (1958), and Wapstra *et al.* (1959). The tabulation of FR is calculated specifically for $(p\gamma\gamma)$ reactions, but can be conveniently used in the present application with some limitations. Its use will be discussed in detail.

The variables in equation (9) that are generally to be found from experiment are the various $\rho_{k0}(aa)$, δ_1, and δ_2. The population parameters, $P(\alpha)$, constitute an alternate set of variables to the $\rho_{k0}(aa)$ and are related linearly to them. The choice between these two is largely a matter of convenience and is discussed further in Section IV. In some instances there may be knowledge of the details of the formation of the state of spin a which imposes a limit on k. In such cases it is convenient to use the $\rho_{k0}(aa)$ variables so that the restriction can be explicitly imposed. The $P(\alpha)$ have the important restriction that they must be positive. The formulation in terms of these parameters allows this restriction to be easily imposed.

The functions defined by Biedenharn (1960) and given by

$$P_{kk_1k_2}\,(\Omega_0 \Omega_1 \Omega_2) = (4\pi)^{3/2} \frac{i^{\,k+k_1-k_2}}{\hat{k}\,\hat{k}_1\,\hat{k}_2^2} \sum_{\kappa,\kappa_1,\kappa_2} (k\kappa, k_1\kappa_1 | k_2 \kappa_2)(-)^{\kappa} Y^{\kappa}_k\,(\Omega_0)\ Y^{\kappa_1}_{k_1}\,(\Omega_1)\ Y^{-\kappa_2}_{k_1}(\Omega_2),$$

where $\Omega_i = (\theta_i,\phi_i)$ represent the polar angles of the initial, first, and second radiations, play a role in triple correlation theory analogous to that of the Legendre polynomials in double correlation theory. Specializing these functions for $\theta_0 = \phi_0 = 0$, and introducing the population parameters $P(\alpha)$, the correlation function becomes

$$(10)\quad W \sim \sum P(\alpha)\,\delta_1^{p_1}\delta_2^{p_2}(-)^{f_3}\hat{k}\,\hat{k}_1\hat{k}_2\,(a\alpha,a-\alpha|k0) \times G_{k\,k_1k_2}(L_1L_1'\,b\,a)\,F_{k_2}(L_2L_2'\,b\,c)\,P_{k\,k_1k_2}(\theta_1,\theta_2,\phi).$$

The summation is over $\alpha k\,k_1k_2L_1L_1'L_2L_2'$. $f_3 = a-L_2+L_2'+(k-k_1-k_2)/2-\alpha$. $G_{k\,k_1k_2}(L_1L_1'\,b\,a)$ is the coefficient defined and tabulated by Rose (1958) and $F_{k_2}(L_2L_2'\,b\,c)$ is that tabulated by Ferentz and Rosenzweig (1955). The coefficients $Z_1(L_2bL_2'b;k_2c)$ defined and tabulated by Sharp *et al.* (1953) are related to the $F_{k_2}(L_2L_2'bc)$ coefficients by

$$Z_1(Lb\,L'b;ck) = \hat{b}\,(-)^{L+L'+b-c}\,\mathrm{Re}\,i^{\,(L'-\pi'-L+\pi+3k)}\,F_k(L\,L'b\,c)$$

where π and π' are 0 for electric and 1 for magnetic radiations.

The formulae developed so far have assumed ideal counters of negligible size. The modifications required for counters of finite size have been considered by Rose (1958) and Ferguson (1961). For counters with axial symmetry about a line through the target the correlation function from equation (9) is

$$(11)\quad W \sim \sum 2^n\,\rho_{k0}(aa)\,\delta_1^{p_1}\,\delta_2^{p_2}(-)^{f_2}\,\hat{L}_1\hat{L}_1'\hat{L}_2\hat{L}_2' \times(L_11,L_1'-1|k_10)\,(L_21,L_2'-1|k_20)\,(k_1-\kappa,k_2\kappa|k0) \times\begin{Bmatrix} b & L_1 & a \\ b & L_1' & a \\ k_2 & k_1 & k \end{Bmatrix} W(bL_2\,bL_2',ck_2)\,Q_{k_1}\,Q_{k_2}\,X^{\kappa}_{k_1k_2}\,(\theta_1,\theta_2,\phi)$$

where Q_{k_1} and Q_{k_2} are attenuation factors for the counters that detect the gamma rays 1 and 2 and are defined by

$$Q_k = \frac{J_k}{J_0},$$

$$J_k = \int_0^{\pi} \epsilon(\xi)\,P_k(\cos\xi)\,\sin\xi\,d\xi,$$

where $\epsilon(\xi)$ is the efficiency of the counter for a gamma ray propagating at an angle ξ to the axis of the counter. Tabulations of Q_k are given by Gove and Rutledge (1958), Rutledge (1959), and Rose (1953). In equation (11) the polar angles θ_1, θ_2, and ϕ define the position of the axes of the counters. The summation in equation (11) is over $k\,k_1k_2\kappa L_1L_1'L_2L_2'$ with $L_1 \leqslant L_1'$, $L_2 \leqslant L_2'$, and $\kappa \geqslant 0$.

The angular resolution corrections are applied to equation (10) in exactly the same way, that is, by the introduction of the two factors Q_{k_1} and Q_{k_2}. It may be of interest that the corrections required for counters not having axial symmetry can be applied in principle. They involve, however, substantially more complication, which can normally be avoided through the use of cylindrical counters.

The table of FR has been found to facilitate considerably the calculation of theoretical results. These have been prepared specifically for $(p\gamma\gamma)$ reactions, where p signifies here a particle of arbitrary spin, using the channel spin formalism and assuming that the compound state as well as the succeeding ones have sharp spin and parity. It is readily shown that the capture of a particle from a channel spin state, s, through orbital momentum l into a state of spin a gives rise to populations

$$P(\alpha) \propto (s\alpha, l0|a\alpha)^2.$$

Different channel spins combine incoherently, so that a mixture of channel spins having intensities $T(s)$ gives rise to populations

$$P(\alpha) \propto \sum_s T(s)(s\alpha, l0|a\alpha)^2.$$

By choosing $l = a$ for even–even nuclei or $l = a \pm \frac{1}{2}$ for even–odd nuclei, then any distribution of the populations, $P(\alpha)$, can be represented by an equivalent set of $T(s)$. Thus the tables of FR can be used by substituting for $P(\alpha)$ the variable $T(s)$. It should be stressed that this variable is completely fictitious and bears no relation to the actual formation of the state a as envisaged in the present application. The tabulation is limited to $l \leqslant 3$, which limits its use to $\alpha \leqslant 3$. While it appears to be true that cases for $a > 3$ could be accommodated if knowledge of the formation provided assurance that substates $\alpha > 3$ were not populated, the loss of generality makes this approach unattractive.

The triple correlation function obtained from the tables can be written

$$(12)\quad W = \sum{}'(-)^{f_4} D^{\kappa}_{k_1k_2}\,(sabcll'L_1L_1'L_2L_2')\;T(s)\;\delta_1^{p_1}\delta_2^{p_2}Q_{k_1}Q_{k_2}X^{\kappa}_{k_1k_2}(\theta_1,\theta_2,\phi)$$

the summation being over $k_1k_2\kappa sL_1L_1'L_2L_2'$. $f_4 = L_2+L_2'+k_1$. $D^{\kappa}_{k_1k_2}$ $(sabcll'L_1L_1'$ $L_2L_2')$ is the coefficient tabulated by FR. Introducing the definition of $D^{\kappa}_{k_1k_2}$ $(sabcll'L_1L_1'L_2L_2')$, equation (12) can be written

$$(13)\quad W = \hat{b}^2\sum{}'\,2^n(-)^{f_5}\,Z(lal'a, sk)\,\hat{L}_1\hat{L}_1'\hat{L}_2\hat{L}_2'\,(k_1-\kappa,k_2\kappa|k0)$$
$$\times(L_11,L_1'-1|k_10)\;(L_21,L_2'-1|k_20)\begin{Bmatrix} b & L_1 & a \\ b & L_1' & a \\ k_2 & k_1 & k \end{Bmatrix} W(bL_2\,bL_2',ck_2)$$
$$\times T(s)\;\delta_1^{p_1}\delta_2^{p_2}\,Q_{k_1}Q_{k_2}\,X^{\kappa}_{k_1k_2}(\theta_1,\theta_2,\phi).$$

The summation is over $k\;k_1k_2\kappa sL_1L_1'L_2L_2'$.

$$f_5 = s+a+b+c+L_1'+L_2+L_2'+k_2+\kappa+(l-l'-k)/2$$

$Z(lal'a, sk)$ is the coefficient defined by Blatt and Biedenharn (1952). Comparing equation (13) with equation (11), it is evident that they are identical if

$$\rho_{k0}(aa) = \frac{1}{\hat{a}^2}\sum_s\;(-)^{f_5-f_2}\,Z(lal'a, sk)\;T(s).$$

Only one value of l is required. Recognizing also that k, k_1, and k_2 are even, we obtain

$$\rho_{k0}(aa) = \frac{1}{\hat{a}^2} \sum_s (-)^{s+a-k/2} Z(lala, sk)\, T(s). \tag{14}$$

By substituting this expression for $\rho_{k0}(aa)$ in equation (3) we obtain for $P(\alpha)$

$$P(\alpha) = \sum_s (s\alpha, a-\alpha|l0)^2\, T(s). \tag{15}$$

Further discussion of the use of these results is given in Section III.

III. APPLICATIONS OF METHOD I

We will discuss in this section practical aspects of the application of the ideas of Section II. Section IV describes as a specific example, the reaction $Mg^{24}(pp'\gamma\gamma)Mg^{24}$ (Batchelor *et al.* 1960) and also some possible future applications.

The compound state formed by the capture of a particle with an energy of several million electron volts or more must be expected to have mixed spins and parities. The state formed after the emission of a particle is very likely to be a bound state and to have sharp spin and parity, thus satisfying the requirements for the application of method I. Reactions of the type $(pp'\gamma\gamma)$, $(\alpha p\gamma\gamma)$, $(dp\gamma\gamma)$, $(dn\gamma\gamma)$, $(d\alpha\gamma\gamma)$, $(He^3\, p\gamma\gamma)$, etc. generally have these characteristics. Details of the formation of the first gamma-emitting state are immaterial to the analysis, so that the reaction may proceed via direct interaction, a compound nucleus, or any combination of these without affecting the results. The processes $(pp'\gamma\gamma)$ and $(\alpha\alpha'\gamma\gamma)$ involve compound state excitations of lower energy than generally obtained for processes induced by deuterons, He^3, and particles of high internal energy. Few competing reactions will be present, resulting in simple gamma spectra, so that these inelastic scattering processes offer a particularly suitable field for the application of the method. Cases can be found where the radiation from the state a of Fig. 1 is a particle instead of a gamma ray, and the particle–gamma correlation can be treated by this approach provided the state a has the necessary sharp spin and parity. Gamma-ray transitions are the only possible ones among the bound states, and since interest is usually focussed on the lower states, gamma-ray studies will play the principal role in applications.

The correlation function of method I is described by equation (2) in which the coefficients $a^{\kappa}_{k_1k_2}$ are functions of the population parameters, $P(\alpha)$, and the multipole amplitude ratios δ_1 and δ_2. It is, in principle, possible to fit a set of experimental points using equation (2) and then from the coefficients, $a^{\kappa}_{k_1k_2}$, so determined, find the population parameters and multipole mixtures consistent with them. If some spins are unknown then a number of sets of possible spin assignments must be examined and it can be expected that generally, for one set only, parameters can be found that are consistent with all of the coefficients. Such a procedure is analogous to the use normally made of equation (1) in analyzing angular distributions. However, a practical difficulty in this procedure is that it is necessary to make measurements sufficient in number and in the ranges of the angles to determine all of the coefficients. Under fairly general conditions there are 19 coefficients, and since

it is usually desirable to measure a number of points rather greater than the number of parameters, a considerable number of measurements is evidently needed.

Since the information content of equation (2) is great, it is sufficient in most cases to obtain by experiment only a part of it. This can be done by fixing two of the angles (θ_1,θ_2,ϕ) at either 0°, 90°, or 180° and varying the third one. This choice of angles causes the functions $X^{\kappa}_{k_1k_2}(\theta_1,\theta_2,\phi)$ to vanish for κ odd. The correlation as a function of the variable angle will then have the form of equation (1) and will provide information in the form of the ratios a_2/a_0 and a_4/a_0. It can be written

$$W^i(\theta) = \sum_k a_k^i\,(abc)\,P_k(\cos\theta)$$

where $a_k^i\,(abc)$ is the coefficient of the Legendre polynomial of order k for the spin sequence $a \to b \to c$. The superscript i distinguishes between a number of possible arrangements obtained by fixing different pairs of angles at certain of the three indicated positions. Seven such arrangements are shown in Fig. 2.

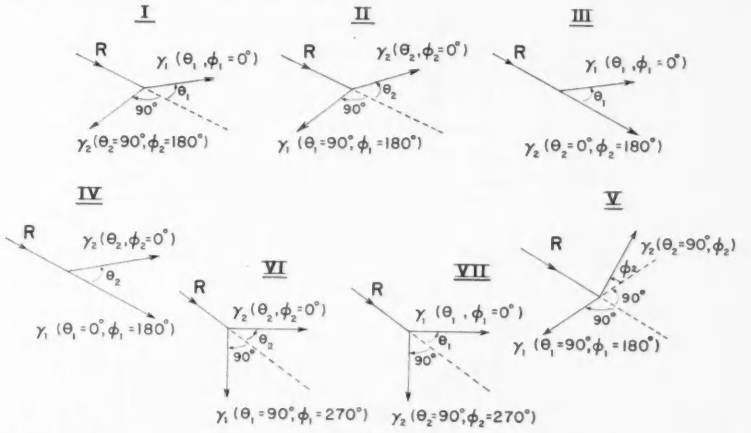

FIG. 2. Diagrams showing the locations and motions of the two counters for various special cases. The diagrams are stereographic projections of the counter directions in three dimensions. The incident beam R and one counter always lie in the horizontal plane. In cases I to IV the directions R, γ_1, and γ_2 are coplanar. In cases VI and VII one counter lies on the perpendicular to the horizontal plane and below it. In case V one counter, γ_2, moves in azimuth about the beam direction.

Here independent azimuthal angles have been assigned to each ray which are related to ϕ by $\phi_1-\phi_2=\phi$. The values of the three fixed angles are given for each case and the remaining unspecified one is variable. For cases I to IV the incident beam and the two gamma-ray directions are coplanar. For cases VI and VII the fixed counter is in a plane perpendicular to that containing the beam and the moving gamma-ray counter. For case V both the moving ray and the fixed one lie in a plane whose perpendicular is the beam direction. In this case it is clearly immaterial which gamma-ray counter is moved.

The series (2), with the restrictions described in Section II and with κ even, has 14 terms rather than the 19 terms obtained when the odd κ are present. Thus more than 14 independent quantities cannot be obtained from measurements made in these "geometries". Although the information obtained from the different cases is not always independent of the others, a sufficient number of these is available to establish the unknown parameters. It is advantageous to know the normalization of the cases relative to each other. Thus if a_k^i is a Legendre polynomial coefficient for a case, i, the a_0^i/a_0^0, a_2^i/a_0^0, and a_4^i/a_0^0, where a_0^0 is a particular coefficient, will be significant quantities rather than only a_2^i/a_0^i and a_4^i/a_0^i when the relative normalizations are unknown.

The direct angular distributions of the two individual gamma rays are also described in terms of the parameters used for the coincidence correlations and provide additional information. Indeed, these may be regarded as further geometries which supplement the others. Formulae for these distributions are easily obtained from equation (7) by integrating over all directions of the unobserved radiation. The only surviving terms will have $k_i = \kappa = 0$ where i is 1 or 2 depending on whether the first or second transition is unobserved.

Formulae for the coefficients for each case are readily obtained by specializing the angles as indicated. The associated Legendre polynomials $P_{k_1}^{\kappa}(\theta_1)$ and $P_{k_2}^{\kappa}(\theta_2)$, where κ is even, can each be expressed as a sum of the ordinary Legendre polynomials $P_k(\theta_1)$ and $P_k(\theta_2)$. In terms of the tabulation of Ferguson and Rutledge the reduction can be written

$$(16) \qquad u_k^i(abcsL_1L_1'L_2L_2') = \sum_{k_1k_2\kappa} Q_{k_1}\, Q_{k_2}\, \alpha_k^{i\ \kappa}{}_{k_1k_2}\, D_{k_1k_2}^{\kappa}\, (sabcll'L_1L_1'L_2L_2').$$

The complete Legendre polynomial coefficients are obtained from

$$(17) \qquad a_k^i(abc) = \sum{}' u_k^i(abcsL_1L_1'L_2L_2')\, T(s)\, \delta_1^{p_1}\, \delta_2^{p_2}.$$

The summation is over $sll'L_1L_1'L_2L_2'$ with $l \leqslant l'$, $L_1 \leqslant L_1'$, $L_2 \leqslant L_2'$. The factor 2^n required in the contracted sum (as in, for example, equation (9)) has been included in the tabulated coefficients.

Case V of Fig. 2 is slightly different. A Fourier cosine series arises naturally from the specialization of θ_1 and θ_2 made in this case. Thus the expansion used here in place of equation (1) is

$$W(\phi) = \sum_k a_k \cos k\ \phi.$$

The coefficients $\alpha_k^{i\ \kappa}{}_{k_1k_2}$ are tabulated by FR.* It is important to note the occurrence of the attenuation factors Q_{k_1} and Q_{k_2} in equation (16). This shows that the effect of finite counter solid angle is not to attenuate each term of the expansion by a simple factor Q_k. The attenuation factors of all orders

*Earlier copies covered only cases I to IV and contained some errors. In subsequent copies the values were extended to include all the cases of Fig. 2 and the errors were corrected.

A group of errors has been recently found in the main table of $D_{k_1k_2}^{\kappa}$ $(sabcll'L_{12}L_{12}'L_2L_2')$ arising from an incorrect Clebsch–Gordan coefficient, $(k\kappa,k_2\kappa_2|k_1\kappa_1) = (40,43|43)$, used as input. This has caused the coefficients having $k_1k_2\kappa = 443$, $a \geqslant 2$, $ll' = 22$, 13, and 33 to be incorrect. This will not affect the cases discussed here since for them κ is even.

of k_1 and k_2 occur in each coefficient and the effects are complicated and unpredictable. This point was first noticed and discussed by Hoogenboom (1958).

The evaluation of equation (16) with the aid of a desk calculator is not difficult, so that, within the limitations of FR, the necessary theoretical coefficients are readily obtained. They can also be obtained with greater range, but less convenience, from the tables of Rose (1958) and of Ferentz and Rosenzweig (1955).

In Tables I to IV are given the coefficients of the Legendre polynomial

TABLE I

Legendre polynomial coefficients, $u_k^i(abc\alpha L_1 L_1' L_2 L_2')$, of equation (18), for various cases and the spin sequence $abc = 0 \to 2 \to 0$, $\alpha = 0$, $L_2 = L_2' = 2$ for all entries. Cases VI, VII, γ_1, and γ_2 are isotropic due to $a = 0$

	k		
Case	0	2	4
I	1.2908	−.8583	.6641
II	1.2908	−.8583	.6641
III	1.0000	.3049	.6641
IV	1.0000	.3049	.6641
V*	1.1620	.4362	.3632

*In this case the expansion $W(\phi) = \Sigma_k a_k \cos k\phi$ is assumed.

coefficients for the spin sequence $a \to 2 \to 0$, where a takes the values 0, 1, 2, and 3. All of the cases of Fig. 2 are included as well as the angular distribution of the first gamma ray with the second unobserved and of the second gamma ray with the first unobserved, which are readily obtained by a similar calculation. The latter are designated respectively as cases γ_1 and γ_2. The transformation of equation (15), from the channel spin, s, to the magnetic quantum number, α, has been included. These coefficients can be designated by $u_k^i(abc\alpha L_1 L_1' L_2 L_2')$. The Legendre polynomial coefficients for any case, i, excepting case V, will be written as

$$a_k^i(abc) = \sum{}' u_k^i(abc\alpha L_1 L_1' L_2 L_2')\, P(\alpha)\, \delta_1{}^{p_1}\, \delta_2{}^{p_2} \tag{18}$$

with the summation over $\alpha L_1 L_1' L_2 L_2'$ and with $L_1 \leqslant L_1'$, $L_2 \leqslant L_2'$. Case V as before assumes a Fourier cosine series and the coefficients belong to $\cos k\phi$ rather than $P_k(\cos\theta)$. The attenuation coefficients $Q_2 = .9239$ and $Q_4 = .7623$ have been used in computing the tables. These are appropriate to 5-in. diameter by 6-in. long NaI(Tl) scintillators situated with their front faces 6.2 inches from the target and for gamma rays of minimum absorption coefficient, i.e. having energies of about 5 Mev. For crystals of other sizes and for other gamma-ray energies, these attenuation factors can be approximated by suitably adjusting the distance between the counter and the target. In this way the tabulation is applicable to a fairly wide range of experimental conditions.

An interesting feature of the coefficients is that for pure quadrupole radiation ($L_1 L_1' = 22$); there are three pairs of cases, I–II, III–IV, and VI–VII in which

TABLE II

Legendre polynomial coefficients, $u_k^i(abc\alpha L_1L_1'L_2L_2')$, of equation (18), for various cases and the spin sequence $abc = 120$. $L_2 = L_2' = 2$ for all entries

		L_1L_1'								
		11			12			22		
		k								
Case	α	0	2	4	0	2	4	0	2	4
I	0	0.4809	0.5436	0.0000	0.5249	0.9151	0.0000	0.8052	0.1906	−0.3622
	1	2.1990	0.0966	0.0000	0.9067	−3.7782	0.0000	2.1468	0.4590	−0.9660
II	0	0.9694	0.9772	−0.7244	0.2201	−0.5044	−1.0799	0.8052	0.1906	−0.3622
	1	1.7105	−0.3370	0.7244	1.2115	−2.3587	1.0799	2.1468	0.4590	−0.9660
III	0	1.4619	0.4796	0.0000	0.0000	2.7285	0.0000	0.5381	0.0807	0.3622
	1	1.5381	−1.1198	0.0000	0.0000	0.1346	0.0000	2.4619	0.3766	−1.6904
IV	0	0.9076	0.3095	0.7244	1.2395	0.4090	1.0799	0.5381	0.0807	0.3622
	1	2.0924	−0.9497	−0.7244	−1.2395	2.4540	−1.0799	2.4619	0.3766	−1.6904
VI	0	1.1230	0.0991	0.0000	−1.4596	0.0954	0.0000	0.8820	−0.2485	0.0000
	1	2.1971	−0.0991	0.0000	0.0281	−0.0954	0.0000	1.3913	0.2485	0.0000
VII	0	1.0571	−0.0326	0.0000	−0.5249	1.9649	0.0000	0.8820	−0.2485	0.0000
	1	2.2630	0.0326	0.0000	−0.9067	−1.9649	0.0000	1.3913	0.2485	0.0000
V*	0	0.6451	−0.4322	0.0000	−0.7302	0.7873	0.0000	1.5072	−0.2161	−0.7264
	1	2.2109	−0.0480	0.0000	1.3744	1.3600	0.0000	1.4089	0.1440	0.0000
γ_1	0	1.0000	−0.0924	0.0000	0.0000	1.2395	0.0000	1.0000	−0.4619	0.0000
	1	2.0000	0.0924	0.0000	0.0000	−1.2395	0.0000	2.0000	0.4619	0.0000
γ_2	0	1.0000	0.4619	0.0000	0.0000	0.0000	0.0000	1.0000	−0.4619	0.0000
	1	2.0000	−0.4619	0.0000	0.0000	0.0000	0.0000	2.0000	0.4619	0.0000

*In this case the expansion $W(\phi) = \Sigma_k a_k \cos k\phi$ is assumed.

TABLE III

Legendre polynomial coefficients, $u_k^i(abc\alpha L_1 L_1' L_2 L_2')$, of equation (18), for various cases and the spin sequence $abc = 220$. $L_2 = L_2' = 2$ for all entries

		L_1L_1'								
		11			12			22		
		k								
Case	α	0	2	4	0	2	4	0	2	4
I	0	1.6419	0.0565	0.0000	0.4686	−2.0398	0.0000	1.2059	−0.9483	0.2131
	1	1.4527	0.0565	0.0000	0.9892	−4.1223	0.0000	1.9876	−0.2613	0.8658
	2	2.4389	−1.1799	0.0000	0.1041	3.0383	0.0000	1.8409	0.7456	−0.1302
II	0	0.8971	−0.4780	1.2737	0.8012	−0.4909	1.1783	1.2059	−0.9483	0.2131
	1	2.1745	0.5282	−1.2958	1.3218	−2.5735	1.1783	1.9876	−0.2613	0.8658
	2	2.4619	−1.1172	0.0221	−0.5610	−0.0594	−2.3565	1.8409	0.7456	−0.1302
III	0	2.2012	1.0168	0.0000	0.0000	−2.9770	0.0000	0.4852	0.1242	0.1269
	1	1.1684	−0.4771	0.0000	0.0000	0.1469	0.0000	2.3564	−0.9864	−0.6866
	2	1.6305	0.5273	0.0000	0.0000	5.9540	0.0000	2.1584	0.5355	1.5084
IV	0	1.4619	0.4824	1.2737	−1.3525	−0.4463	−1.1783	0.4852	0.1242	0.1269
	1	2.4619	0.3300	−2.1007	−1.3524	2.6776	−1.1783	2.3564	−0.9864	−0.6866
	2	1.0761	0.2546	0.8270	2.7049	0.8925	2.3565	2.1584	0.5355	1.5084
VI	0	0.6410	0.9855	0.0663	0.5513	0.9372	0.0000	1.2089	−0.6064	−0.1319
	1	1.3636	0.1317	−0.0884	0.0306	−0.1041	0.0000	2.5272	−0.1109	0.1758
	2	2.4619	−1.1172	0.0221	−2.1438	−0.8332	0.0000	1.7830	0.7173	−0.0439
VII	0	0.6815	1.0168	0.0000	−0.4686	−1.1026	0.0000	1.2089	−0.6064	−0.1319
	1	1.3461	0.1631	0.0000	−0.9892	−2.1438	0.0000	2.5272	−0.1109	0.1758
	2	2.4389	−1.1800	0.0000	−0.1041	3.2464	0.0000	1.7830	0.7173	−0.0439
V*	0	0.8896	0.7203	0.0000	0.7967	0.7029	0.0000	1.0827	0.1487	0.5188
	1	1.3445	0.0800	0.0000	1.4996	1.4839	0.0000	2.5535	−0.1028	0.0000
	2	3.0060	0.0000	0.0000	−1.5935	0.1561	0.0000	1.4237	0.0057	0.0000
γ_1	0	1.0000	0.4619	0.0000	0.0000	−1.3525	0.0000	1.0000	−0.1414	−0.3734
	1	2.0000	0.4619	0.0000	0.0000	−1.3524	0.0000	2.0000	−0.1414	0.4978
	2	2.0000	− 0.9239	0.0000	0.0000	2.7049	0.0000	2.0000	0.2828	−0.1245
γ_2	0	1.0000	0.3300	0.8712	0.0000	0.0000	0.0000	1.0000	−0.1414	−0.3734
	1	2.0000	0.3300	−1.1616	0.0000	0.0000	0.0000	2.0000	−0.1414	0.4978
	2	2.0000	−0.6599	0.2904	0.0000	0.0000	0.0000	2.0000	0.2828	−0.1245

*In this case the expansion $W(\phi) = \Sigma_k a_k \cos k\phi$ is assumed.

TABLE IV

Legendre polynomial coefficients, $u_k^{\alpha}(abc\alpha L_1 L_1' L_2 L_2')$, of equation (18), for various cases and the spin sequence $abc = 320$. $L_2 = L_2' = 2$ for all entries

		L_1L_1'								
		11			12			22		
		k								
Case	α	0	2	4	0	2	4	0	2	4
I	0	0.3806	0.3070	0.0000	−0.3781	−1.5918	0.0000	0.9285	1.1584	−0.0107
	1	1.5283	−0.9801	0.0000	−0.9081	−0.1471	0.0000	1.6050	0.0123	0.4392
	2	2.3812	−0.0533	0.0000	−0.0974	0.0974	0.0000	1.3776	0.6802	−1.5950
	3	2.4966	1.1533	0.0000	−0.9542	6.3169	0.0000	2.4100	−0.3547	0.8345
II	0	1.1336	0.9731	−1.1198	0.7626	1.1856	0.6613	0.9285	1.1584	−0.0107
	1	2.1150	0.7736	0.7737	1.1244	2.1819	−2.3146	1.6050	0.0123	0.4392
	2	2.0000	−0.3049	0.6810	−0.7403	−0.3619	1.1022	1.3776	0.6802	−1.5950
	3	1.5381	−1.0150	−0.3350	−3.4843	1.6698	0.5511	2.4100	−0.3547	0.8345
III	0	1.0923	0.2110	0.0000	0.0000	−5.2189	0.0000	1.7854	0.5649	1.5288
	1	2.6467	−2.0312	0.0000	0.0000	−1.9835	0.0000	2.4158	−0.2197	−1.2513
	2	3.0164	1.2805	0.0000	0.0000	0.0000	0.0000	0.4754	−0.1524	−0.2367
	3	0.2446	0.1130	0.0000	0.0000	2.5270	0.0000	2.3234	−1.4122	−0.3729
IV	0	0.6304	0.2231	0.4498	−2.0242	−1.4312	−1.7635	1.7854	0.5649	1.5288
	1	1.4457	0.6700	−1.5001	−3.0362	−1.8129	2.8656	2.4158	−0.2197	−1.2513
	2	2.0000	0.6097	1.6872	0.0000	0.0000	0.0000	0.4754	−0.1524	−0.2367
	3	2.9239	−1.9295	−0.6368	5.0604	−1.4312	−1.1022	2.3234	−1.4122	−0.3729
VI	0	1.2360	0.3877	−0.6368	1.2616	0.2457	1.1022	1.2358	−0.5978	1.4382
	1	2.4394	0.9322	0.2908	1.9118	−0.3690	−0.5511	2.3604	0.2228	−0.5268
	2	2.0000	−0.3049	0.6810	0.7403	0.3619	−1.1022	1.4789	0.7298	−1.7459
	3	1.5381	−1.0150	−0.3350	−1.5760	−0.2385	0.5511	2.4100	−0.3547	0.8345

TABLE IV (*Concluded*)

Legendre polynomial coefficients, $u_k^i(abc\alpha L_1 L_1' L_2 L_2')$, of equation (18), for various cases and the spin sequence $abc = 320$. $L_2 = L_2' = 2$ for all entries

		L_1L_1'								
		11			12			22		
		k								
Case	α	0	2	4	0	2	4	0	2	4
VII	0	0.7648	−0.0772	0.0000	0.3781	−2.3479	0.0000	1.2358	−0.5978	1.4382
	1	1.5709	−1.0228	0.0000	0.9081	−1.9633	0.0000	2.3604	0.2228	−0.5268
	2	2.3811	−0.0533	0.0000	0.0973	−0.0973	0.0000	1.4789	0.7298	−1.7459
	3	2.4966	1.5133	0.0000	0.9542	4.4085	0.0000	2.4100	−0.3547	0.8345
V*	0	0.5229	−0.2881	0.0000	1.0207	−0.5671	0.0000	1.3870	−0.8644	−0.1816
	1	2.0534	−0.0320	0.0000	0.5729	−1.3621	0.0000	1.9097	−0.1440	0.0000
	2	2.3926	0.0000	0.0000	0.0000	−0.1460	0.0000	0.4711	−0.0100	0.0000
	3	1.9352	0.0000	0.0000	−2.6456	−1.4312	0.0000	2.9112	0.0000	0.0000
γ_1	0	1.0000	−0.3696	0.0000	0.0000	−2.0242	0.0000	1.0000	0.1320	0.6534
	1	2.0000	−0.5543	0.0000	0.0000	−3.0362	0.0000	2.0000	0.1980	0.2178
	2	2.0000	0.0000	0.0000	0.0000	0.0000	0.0000	2.0000	0.0000	−1.5246
	3	2.0000	0.9239	0.0000	0.0000	5.0604	0.0000	2.0000	−0.3300	0.6534
γ_2	0	1.0000	0.5279	−0.4356	0.0000	0.0000	0.0000	1.0000	0.1320	0.6534
	1	2.0000	0.7919	−0.1452	0.0000	0.0000	0.0000	2.0000	0.1980	0.2178
	2	2.0000	0.0000	1.0164	0.0000	0.0000	0.0000	2.0000	0.0000	−1.5246
	3	2.0000	−1.3198	−0.4356	0.0000	0.0000	0.0000	2.0000	−0.3300	0.6534

*In this case the expansion $W(\phi) = \Sigma_k a_k \cos k\phi$ is assumed.

the coefficients are identical. Under these conditions the correlations represented by these three pairs will be identical independently of the populations, $P(\alpha)$. This is an instance of a more general symmetry present if $L_1 = L_1' = L_2 = L_2' = b$ and $c = 0$. From equation (9) it is then readily found that

$$W(\theta_1,\theta_2,\phi) = W(\theta_2,\theta_1,\phi). \tag{19}$$

The nuclear parameters $P(\alpha)$, δ_1, and δ_2 are related to the Legendre polynomial coefficients, a_k^i, by equations (17) or (18). The problem is to obtain the best fit to the measured coefficients using these equations and every a priori admissible spin sequence, $a \to b \to c$. The nuclear parameters occur non-linearly and are rather more numerous than can be conveniently handled by hand computation. In some instances, prior knowledge of the system fixes some of the parameters, at least approximately. It may be possible to select certain measurements from which the remaining parameters can be found. In this way a number of data equal to the number of variables may be fitted more or less exactly. If the spin assignments are correct, then the remainder of the data also will probably be fitted reasonably well by these parameters. They will then constitute one solution to the problem which the limited experience with the method to date indicates will be probably unique. The considerable amount of numerical calculations associated with the analysis makes an electronic computer an almost necessary adjunct to the work. While solutions can be found by trial and error methods aided by physical insight as remarked above, there is no convincing assurance that less obvious ones, perhaps equally good or better, do not exist. The enormous capacity of an electronic computer can reduce this uncertainty to a negligible point.

If an electronic computer is available then it is feasible to analyze the measured data by the method of least squares. If a number of geometries described above have been measured, these can be analyzed first in terms of Legendre polynomials and then the resulting coefficients, a_k^i, treated as data for a further least squares fit in terms of the population parameters and multipole mixtures.* This procedure has the advantage of reducing the amount of data to be handled. It should be recognized that statistical correlations are normally present between the coefficients found from angular distribution analysis which are usually small enough to be ignored, but in some instances,† could be significant. The fits can be made using as data either the coefficients, a_k^i, together with adjustable normalization constants, N_i, introduced into equation (17), or the ratios a_k^i/a_0^i. The former approach leads to a slightly simpler program and was used in the analysis of Batchelor *et al.* (1960). It entails evidently more unknowns, but this is not generally of consequence to a computer.

*Broude and Gove (1960 and to be published) have studied a considerable number of correlations by this method, and have found that the convergence of the non-linear least squares fitting procedure is often unsatisfactory due to the presence of secondary minima in the fit and singular points for the normal equations. They have adopted a procedure in which different geometries were normalized so as to agree approximately at the common points. Linear least squares fits were then made having the $P(\alpha)$ as fitted variables for a series of values for the multipole mixtures. The best of these were then used as a first approximation for further refinement by the general program.

†For example, if the correlation were measured only over a small range of angles.

IV. AN EXAMPLE OF METHOD I, $Mg^{24}(pp'\gamma\gamma)Mg^{24}$

There have been several examples of the experimental study of gamma–gamma correlations from nuclei aligned by radiative capture reactions (Hoogenboom 1958; Litherland *et al.* 1959; and Broude *et al.* 1959 for example). However, since most of these experiments involved isolated resonances in the compound nucleus, the populations of the substates of the compound nucleus were not treated as unknowns to be determined by experiment. In other cases it is not possible to be sure that an isolated resonance is being studied and, consequently, there is considerable uncertainty in the interpretation of the results. For an example, consider the $Mg^{24}(pp'\gamma\gamma)Mg^{24}$ reaction at bombarding energies of greater than 5 Mev. Seward (1959) has shown that there are a number of broad overlapping resonances for the excitation of the 1.37-Mev state in Mg^{24} in this region, which makes it unlikely that a particular point on the yield curve can be used for an analysis of the gamma-ray angular correlations in terms of a single resonance in the compound nucleus. It is in this type of situation that analysis of the gamma-ray angular correlations in terms of an incoherent sum over the angular correlations from the magnetic substates of an isolated state in the residual nucleus becomes most useful. The energy stability of the particles initiating the reaction must, however, be adequate to ensure that the population parameters remain constant during an experiment because the population parameters can vary as rapidly as the yield of the reaction. The population parameters determined by experiment can then in principle be used to shed further light on the formation of the state in the residual nucleus formed by the reaction and in this respect the analysis represents a convenient two-step method of analysis of the results. The analysis in terms of population parameters also can be used when a single resonance in the compound nucleus is apparently being studied because there is then no lingering uncertainty due to the possibility that the resonance is not completely isolated.

Situations where the initial state, a, is unpolarized, or very nearly so, are unfavorable for the application of this method. This is because the correlation then reduces to a double one described by equation (1) and provides only a limited amount of information rather than the considerable amount we have been assuming on the basis of equation (2). The degree of alignment depends on the details of the nuclear reaction and a consideration of these enables some general conclusions concerning favorable and unfavorable situations to be drawn.

If the state a is unpolarized, then only the tensor parameter $\rho_{00}(aa)$ is non-zero. In the opposite situation, in which the populations of the magnetic substates differ strongly (but, of course, remain symmetric between positive and negative values), the higher terms $\rho_{20}(aa)$, $\rho_{40}(aa)$ . . . are non-zero. The cases in which these have magnitudes comparable to $\rho_{00}(aa)$ we can regard as particularly favorable ones. Selection rules which limit the order, k, of the tensor $\rho_{k0}(aa)$ are conveniently found from the Wigner $9-j$ coefficients

$$\begin{Bmatrix} x & \mathscr{L}_1 & y \\ x & \mathscr{L}_1' & y' \\ 0 & k & k \end{Bmatrix} \quad \text{and} \quad \begin{Bmatrix} y & \mathscr{L}_2 & a \\ y' & \mathscr{L}_2' & a \\ k & 0 & k \end{Bmatrix}$$

which are contained as factors in the formal expression for the tensors in terms of the parameters of the process $x \xrightarrow{\mathscr{L}_1} y \xrightarrow{\mathscr{L}_2} a$. The "triangle conditions" state that the three quantum numbers occurring in any row or column of a non-zero coefficient must be capable of forming a closed triangle. The zero in the first coefficient is due to the initial state, x, being unpolarized, and in the second, is due to the fact that the radiation $\mathscr{L}_2$ is unobserved. It is evident that k is limited by the triangles $(\mathscr{L}_1\mathscr{L}_1'k)$, $(yy'k)$, and (aak). Remembering that k is even, we see from the first two that only the $k = 0$ term will be present if either $\mathscr{L}_1$ and $\mathscr{L}_1'$, or y and y' are 0 or $\frac{1}{2}$. The third condition provides nothing new, being implied in the definition of $\rho_{kk}(aa)$. No limitation is imposed on k by $\mathscr{L}_2$ and $\mathscr{L}_2'$. Clearly high angular momentum of the incoming particle and high spin of the compound state are required for favorable cases.

In general, reactions which can be excited close to their thresholds will be favorable ones. In these the outgoing angular momentum, $\mathscr{L}_2$, will have small values because of the small outgoing energy, causing most of the angular momentum change between the states x and a to reside in $\mathscr{L}_1$. Thus, in conformity with the above requirement, $\mathscr{L}_1$ will be as large as is compatible with the various spins. Another and basically equivalent argument is to consider the magnetic substates of the state a. Since the incoming particle travels along the z-axis, the z component of its orbital momentum is zero. On the other hand, the outgoing orbital momentum, being unobserved, is analogous to an unpolarized spin and has all magnetic substates equally populated. The populated substates of the state a are derived from those of x, $\mathscr{L}_1$, and $\mathscr{L}_2$ and will be quite limited in the favorable cases considered now. This type of argument is the basis of method II and is discussed in detail in Section V. Consider, as an example, the reaction $Mg^{24}(pp'\gamma\gamma)Mg^{24}$; if the outgoing protons are s-waves, then only the $\alpha = 0$ and the $\alpha = \pm 1$ substates are populated, the latter arising from the flip of the proton spin. Thus for $a \geqslant 2$ the nuclear states are strongly aligned. The yield of gamma radiation from the excited state of interest may be low just above the threshold. Higher bombarding energies will then be necessary where the alignment of the nuclear state may be reduced if higher outgoing angular momenta become strong. A compromise may then be involved between the degree of alignment and the yield of the reaction.

At a resonance in the compound nucleus it may be advantageous to describe the alignment in terms of the statistical tensors rather than the population parameters. For example, if a $4+$ state in Mg^{24} is excited by the inelastic scattering of protons and the major contribution to the cross section comes from a $5/2+$ resonance in the compound nucleus Al^{25}, then all the $2j+1$ substates of the $4+$ state are populated and one is faced with the possibility of fitting an angular correlation with four population ratios. However, as mentioned in Section II, the alternative description of the alignment of the $4+$ state in terms of statistical tensors is simpler since the major contribution to the angular correlation comes from the terms containing the statistical tensors ρ_{00}, ρ_{20}, ρ_{40}. The other possible tensors ρ_{60} and ρ_{80} are small or zero. If

the resonance in Al^{25} is a pure 5/2+ resonance, this implies that ρ_{60} and ρ_{80} are identically zero because the tensor ρ_{k0} is proportional to $Z(2\,\frac{5}{2}\,2\,\frac{5}{2},\,\frac{1}{2}\,k)$ (cf. equation (14) of Section II) which arises from the $9-j$ symbol

$$\begin{Bmatrix} x & \mathscr{L}_1 & y \\ x & \mathscr{L}_1' & y' \\ 0 & k & k \end{Bmatrix} = \begin{Bmatrix} 1/2 & 2 & 5/2 \\ 1/2 & 2 & 5/2 \\ 0 & k & k \end{Bmatrix}.$$

Consequently, the populations $P(\alpha)$ of the 4+ state in Mg^{24} are not independent but are related by equations that can be derived from equation (3) of Section II. In general, some knowledge of the mode of formation of the axially symmetrical state in the residual nucleus is of great value since then one has a first approximation to the otherwise unknown ratios of the populations or alignment tensors. Modifications to these ratios can then be made to take into account the perturbing effects of other resonances in the compound nucleus.

The reaction $Mg^{24}(pp'\gamma\gamma)Mg^{24}$ has been studied by Batchelor *et al.* (1960), who exploited the ideas outlined above. The 4.24-Mev state in Mg^{24} was studied in the range of incident proton energies from 5.0 to 6.0 Mev. The two resonances shown in Fig. 3 were found and the angular distribution of

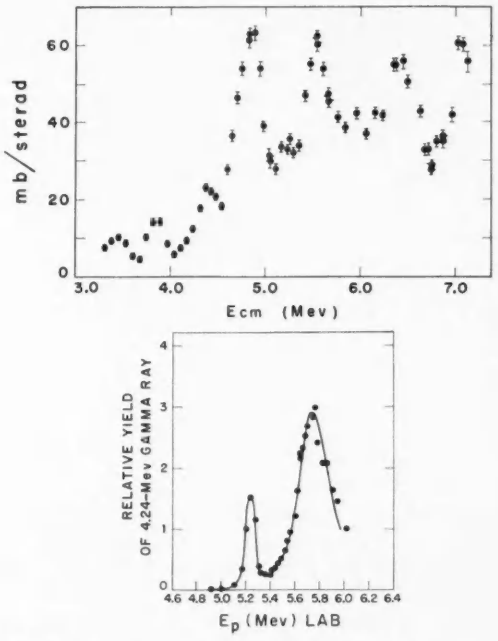

FIG. 3. Yield curve for the reactions $Mg^{24}(pp')Mg^{24*}$. The upper figure is taken from Seward (1959) and shows the yield of protons to the first excited state as a function of the center of mass energy. The lower one is taken from Batchelor *et al.* (1960) and shows the yield of 4.24-Mev gamma rays.

the gamma rays de-exciting the 4.24-Mev state in Mg^{24} are shown in Fig. 4. Since the angular distribution of the 4.24-Mev gamma ray at the 5.72-Mev resonance was stronger than that at the 5.24-Mev resonance, the 5.72-Mev resonance was chosen for study. The stronger angular distribution implies a

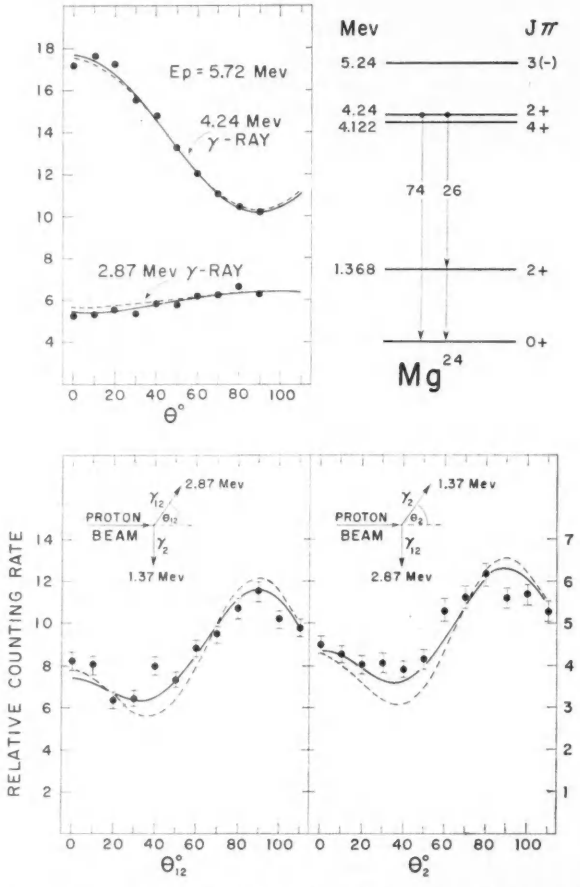

FIG. 4. Angular correlations for the 4.24 Mev–1.37 Mev ground-state cascade in the reaction $Mg^{24}(pp'\gamma\gamma)Mg^{24}$. The correlations shown are: the angular distributions of the 4.24-Mev and 2.87-Mev components and the correlations for cases I and II of Fig. 2. The solid lines are theoretical fits for the spin assignments 2, 2, and 0 for the 4.24 Mev, 1.37 Mev, and ground states. The dotted lines show the fits obtained if the corrections for finite counter aperture are omitted.

greater degree of alignment of the 4.24-Mev state at the 5.72-Mev resonance and the measured a_2/a_0 coefficient of approximately 0.42 implies that the 5.72-Mev resonance probably has angular momentum 3/2+ and that the

unobserved inelastic proton is predominantly s-wave. An isolated 3/2+ resonance in the reaction decaying to a 2+ state in Mg^{24} by the emission of an s-wave inelastic proton has a correlation coefficient $a_2/a_0 = +0.50$. The measured deviation from this value could be due to a d-wave admixture to the predominantly s-wave inelastic proton or it could be due to the 5.72-Mev resonance not being a single isolated resonance. However, as discussed above, the nature of the deviation is immaterial since the analysis of the angular correlation data is sufficiently general to take both possibilities into account.

The angular correlations taken at 5.72-Mev incident proton energy are shown in Fig. 4. Two geometrical arrangements of counters were used which correspond to the cases I and II of Fig. 2. Together with the angular distributions also shown in Fig. 4 these data were more than sufficient to determine the alignment parameters $T(s)$, discussed in Section III, and the multipole mixture of the 2.87-Mev radiation. The population parameters or the alignment parameters can be deduced from the $T(s)$ parameters with the help of equations (14) and (15) of Section II. These results are summarized in Table V and have been discussed by Batchelor *et al.* (1960). Table III gives

TABLE V

Comparison of measured and calculated angular distribution and angular correlation coefficients for the reaction $Mg^{24}(pp'\gamma\gamma)Mg^{24}$ through the excited states at 4.24 Mev and 1.37 Mev. The spins of the 4.24 Mev, 1.37 Mev, and ground states are 2, 2, and 0 respectively. The incident proton energy was 5.72 Mev. γ_0 designates the angular distribution of the gamma-ray transition from the 4.24-Mev level to the ground state. In the lower part of the table are given the $E2/M1$ amplitude mixing ratio, δ_1, for the primary gamma ray and the ratios $P(1)/P(0)$ and $P(2)/P(0)$ of the population parameters of the 4.24-Mev state

Case	Parameter	Experiment	Theory
I	a_2/a_0	$-.373\pm.035$	$-.442$
	a_4/a_0	$.278\pm.047$	$.292$
II	a_2/a_0	$-.285\pm.07$	$-.401$
	a_4/a_0	$.169\pm.09$	$.318$
γ_0	a_2/a_0	$.398\pm.014$	$.393$
	a_4/a_0	$-.013\pm.017$	$-.002$
γ_1	a_2/a_0	$-.147\pm.015$	$-.119$
	a_4/a_0	$.010\pm.010$	0
	δ_1		23
	$P(1)/P(0)$		$.77$
	$P(2)/P(0)$		$.09$

the theoretical correlations for the sequence of spins $2 \rightarrow 2 \rightarrow 0$ and for attenuation parameters Q_k appropriate for 5-in. diameter by 6-in. long NaI(Tl) crystals situated with their front faces 6.2 inches from the target.

Since the two angular correlations shown in Fig. 4 are nearly identical, the considerations outlined in Section III imply that the 2.87-Mev radiation is predominantly quadrupole radiation. This is a consequence of equation (19) of the previous section. Similar results have recently been obtained by Broude and Gove (1960) for a number of d-shell nuclei, for example, the 5.22-Mev state of Mg^{24}. The solid curves are a least squares fit to the data using the

parameters shown in Table V. The dotted curves are a similar fit except for the assumption that there is no attenuation of the correlations due to the finite size of the detectors. The fit shown in Fig. 4 was obtained using the Chalk River Datatron computer.[1] The parameters shown in Table V support the original conjecture that the 5.72-Mev resonance is predominantly a 3/2+ resonance decaying by the emission of predominantly *s*-wave protons to a 2+ state in Mg^{24}.

In the above discussion, aligned nuclear states were produced by reactions such as the $Mg^{24}(pp')Mg^{24*}$ reaction. The Mg^{24*} nuclei can be treated as aligned if the inelastic protons are not observed. Another very convenient method for producing aligned nuclear states is by Coulomb excitation. In this case the alignment parameters or populations of the substates can be calculated theoretically (Alder *et al.* 1956). The angular correlations of the cascade gamma rays from a state excited by Coulomb excitation are therefore determined by the spins and multipole mixtures of the final nuclear states. Alternatively the calculated alignment parameters can be regarded as a first approximation to the actual values, which are then determined more accurately by experiment. This is possible in principle because of the large number of experimentally determinable coefficients from a gamma-ray angular correlation measurement. From the experimental point of view angular correlations following Coulomb excitation of medium-weight and heavy nuclei should be as useful as the angular correlations following inelastic proton scattering in light nuclei.

V. METHOD II

If a nuclear state is formed by the absorption of an unpolarized particle in the direction of the quantization axis followed by the emission of a second particle which is detected along the axis, then the magnetic substates which can be populated do not exceed the sum of the spins of the target nucleus and the incident and emergent particles. This theorem arises basically from the fact that the orbital momenta contained in plane waves in the direction of the quantization axis have only zero projections on this axis. The system clearly has axial symmetry so that as discussed in Section II, the density matrix is diagonal in the magnetic quantum numbers, and further, is symmetric between positive and negative values. The state, which is assumed to have definite spin and parity, will then be described by a number of population parameters which will be limited by the spins of the target and the incident and emergent particles. The angular distribution of a gamma ray emitted from the state will be governed by these parameters and its multipole mixing ratio. The distribution will be of the form of equation (1) and the information obtainable will, in general, be the ratios a_2/a_0 and a_4/a_0. Thus, if no more than two arbitrary parameters describe the distribution, then the amount of information will be just sufficient or, in favorable cases, more than sufficient to determine them.

The determination of nuclear parameters based on these considerations we

[1]The computer program was written by one of the authors (A.J.F.).

term method II. It has evidently smaller applicability than method I but can be expected in suitable cases to yield multipole mixtures and spins. It is possible, in principle, to combine methods I and II by observing two gamma rays in coincidence with a particle detected by an axially symmetrical counter. This arrangement has the advantage of simplifying the gamma-ray spectrum because the energy selectivity of the particle counter can be used to ensure in many cases that only one state in the residual nucleus is studied at once. This point is discussed in more detail at the end of this section.

The mathematical formulation of the method is most simply carried out in terms of the density matrix. We shall assume that the state considered is the final one in the absorption and emission process described by

$$al_1s_1 \rightarrow b \rightarrow cl_2s_2.$$

Here, a, b, and c are the spins of the initial, intermediate, and final states and l_1, l_2, s_1, and s_2, are the orbital momenta and spins of the incident and emergent particles. We will use the channel spin coupling scheme:

$$\begin{aligned} \mathbf{S}_1 &= \mathbf{a}+\mathbf{s}_1, \\ \mathbf{b} &= \mathbf{S}_1+\mathbf{l}_1 = \mathbf{S}_2+\mathbf{l}_2, \\ \mathbf{S}_2 &= \mathbf{c}+\mathbf{s}_2. \end{aligned}$$

S_1 and S_2 are the incoming and outgoing channel spins. The density matrix for the intermediate state will be

$$\begin{aligned} (20) \qquad \langle b\beta|\rho|b'\beta\rangle = \sum_{\alpha\sigma_1} & (a\alpha,s_1\sigma_1|S_1\beta)^2(S_1\beta,l_10|b\beta) \\ & \times(S_1\beta,\, l_1'0|b'\beta)\,\langle a\alpha|\rho|a\alpha\rangle\,\langle s_1\sigma_1|\rho|s_1\sigma_1\rangle\,\langle l_10|\rho|l_1'0\rangle \\ & \times\langle S_1l_1||V||b\rangle^*\,\langle S_1l_1'||V||b'\rangle. \end{aligned}$$

The states a and s_1 are assumed unpolarized so that

$$\langle a\alpha|\rho|a\alpha\rangle = \frac{1}{\hat{a}^2},$$

$$\langle s_1\sigma_1|\rho|s_1\sigma_1\rangle = \frac{1}{\hat{s}_1^2}.$$

For a plane wave

$$\langle l_10|\rho|l_1'0\rangle = \hat{l}_1\hat{l}_1'.$$

Interference between different channel spin states is removed by the orthogonality of the Clebsch–Gordan coefficients. The factors $\langle S_1l_1||V||b\rangle$ and $\langle S_1l_1'||V||b'\rangle$ are the reduced matrix elements of the perturbing Hamiltonian for absorption causing the transition.

The feature of significance in equation (20) for the present considerations is that for each term of the sum, $\beta = \alpha+\sigma_1$. Thus, the largest β results from the largest α and σ_1, which cannot, respectively, exceed a and s_1.

The density matrix for the final state can be derived from that of the intermediate state. It is

$$(21)\quad \langle c\gamma s_2\sigma_2 l_2 0|\rho|c\gamma s_2\sigma_2 l_2' 0\rangle = \langle c\gamma|\rho|c\gamma\rangle\ \langle s_2\sigma_2|\rho|s_2\sigma_2\rangle\ \langle l_2 0|\rho|l_2' 0\rangle$$
$$= \sum\ (S_2\beta, l_2 0|b\beta)\ (S_2'\beta, l_2' 0|b\beta)\ (c\gamma, s_2\sigma_2|S_2\beta)$$
$$\times (c\gamma, s_2\sigma_2|S_2'\beta)\ \langle b\beta|\rho|b'\beta\rangle\ \langle S_2 l_2||V||b\rangle\ \langle S_2' l_2'||V||b'\rangle^*.$$

The summation here is over $b\ b'S_2$ and S_2'. The first line of this equation expresses the fact that the density matrix for the final state is the direct product of the density matrices of the component spins and orbital momenta. The factors $\langle S_2 l_2||V||b\rangle$, $\langle S_2' l_2'||V||b'\rangle$ are the reduced matrix elements for the emission of the emergent particles. The magnetic quantum numbers of the outgoing orbital momentum, λ_2 and λ_2', different from zero are omitted from equation (21) because we are considering only particles travelling in the direction of the quantization axis. For counters of finite size, which are considered later, this assumption is not justified.

From equation (21) it is evident that $\beta = \gamma + \sigma_2$. Polarization of the outgoing particle is not detected so that all values of σ_2 will occur. Finally, the maximum value of γ that will occur will be

$$(22)\qquad \gamma_{\max} = \max(\alpha+\sigma_1+\sigma_2) = a+s_1+s_2.$$

This conclusion is independent of the presence of interfering spins b or orbitals l_1', l_2' or indeed interfering final spins c'. The density matrix is also clearly diagonal in γ, as was inferred from the more general considerations of axial symmetry.

The angular distribution of a gamma ray in a transition from a state whose population parameters are $P(\gamma) = \langle c\gamma|\rho|c\gamma\rangle$ to a state of spin d is given by

$$(23)\quad W(\theta) = \sum_{\gamma k p} (-)^{f_6}\, P(\gamma)\delta^p(c\gamma, c-\gamma|k0)\ Z_1(LcL'c, dk)\ Q_k P_k(\cos\theta)$$

where L, L' are interfering multipolarities for the gamma ray, and δ is the multipole-mixing parameter as defined in equation (6). $f_6 = d+\gamma+L+L'+k/2$. $Z_1(LcL'c, dk)$ is the coefficient tabulated by Sharp *et al.* (1953). A factor 2 must be introduced into this formula for $L \neq L'$ corresponding to the 2^a of equation (9). As before $p = 0$, 1, or 2 for $(LL') = (11)$, (12), or (22) respectively. The quantities Q_k have been discussed in Section II. Equation (23) can be derived as a special case of equation (11).

The restriction $a+s_1+s_2 \leqslant 3/2$ or $\leqslant 1$ will lead to two population parameters $P(\gamma)$ corresponding to one unknown ratio. If, in this case, there is an additional unknown multipole mixture, and if the experiment yields the two observed quantities a_2/a_0 and a_4/a_0, then sufficient information is present to determine the unknowns. The above restriction is the one that is probably most generally applicable. If a multipole mixture is known to be absent, then the restriction can be relaxed. On the other hand, only the ratio a_2/a_0 may be obtainable from the experiment, in which case a closer restriction is needed. Clearly small spins of all the components of the reaction are required for the application of this method. In Section VI the application of these considerations to the reaction $Mg^{26}(\alpha n\gamma)Si^{29}$ is described.

The detector of the emergent particles can, in principle, detect either the

forward-emitted or the backward-emitted particles. Only the forward position allows the counter to be precisely on the beam axis, but in some circumstances, it might be convenient to keep this direction unobstructed and place the counter in the backward position. While it might be expected that if the counter is in the backward position and as close to the incident beam as possible, then the requirements of the method will be approximately satisfied, the axial symmetry of the system is lost, and the estimation of corrections is considerably complicated. The use of a counter symmetric about the beam axis, i.e. a circular counter with a hole in it, through which the beam passes restores the axial symmetry of the system and allows formulae for counter size corrections to be developed.

For a cluster of identical counters located symmetrically about the beam axis at angular intervals $2\pi/N$, the efficiency matrix $\epsilon_{k\kappa}(cc)$ will be zero unless $\kappa = 0, N, 2N, \ldots$. For the typical cases in the use of method II where k does not exceed 4, the requirements of the method are realized by choosing $N = 5$. In other words, with a cluster of five counters arranged symmetrically about the beam axis to detect the reaction particles, equation (23) describes the angular distribution of a gamma ray emitted by the resulting state provided terms with $k > 4$ are absent. A single counter may be used in a similar way by measuring the correlation at five equally spaced azimuthal angles and averaging the correlations over these positions. The five measurements may be reduced to three using the symmetry valid for method II

$$W(\phi) = W(-\phi)$$

and starting the measurements at $\phi = 0$. A form of the multiple counter scheme which might have value in the combination of methods I and II mentioned early in this section is to set the polar angle of each counter relative to the beam axis equal to $\pi/2$ radians. $\epsilon_{k\kappa}(cc)$ will then vanish unless $\kappa = 0, 2N, 4N, \ldots$.

Recalling that the correlation function is

$$W = \mathrm{Tr}(\rho\epsilon)$$

the effective density matrix involved in transitions from the state c in coincidence with the radiation l_2 will be

$$P(\gamma) = \sum_{l_2 l_2'\lambda_2\lambda_2'} \langle c\gamma|\rho|c\gamma\rangle \langle s_2\sigma_2|\rho|s_2\sigma_2\rangle \langle l_2\lambda_2|\rho|l_2'\lambda_2'\rangle\langle l_2'\lambda_2'|\epsilon|l_2\lambda_2\rangle. \tag{24}$$

For an ideal counter located on the beam axis

$$\langle l_2\lambda_2|\epsilon|l_2'\lambda_2'\rangle = \hat{l}_2\hat{l}_2'\delta_{\lambda_2 0}\delta_{\lambda_2' 0}.$$

The formula for a finite counter is readily found from the behavior of the efficiency matrix under co-ordinate axis rotations. The efficiency matrix for an ideal counter in an arbitrary position is

$$\langle l\lambda|\epsilon|l'\lambda'\rangle = D^l_{\lambda 0}(\mathscr{R}) \langle l0|\epsilon|l'0\rangle D^{l'*}_{\lambda' 0}(\mathscr{R}) \tag{25}$$

where $\langle l0|\epsilon|l'0\rangle$ is the efficiency matrix element for an ideal counter on the

z-axis and $\mathscr{R}$ is the rotation bringing the z-axis into the arbitrary direction. The efficiency matrix for a finite counter is obtained by interpreting $\langle l\lambda|\epsilon|l'\lambda'\rangle$ as the efficiency for an element of solid angle in the direction defined by $\mathscr{R}$, and integrating this over all directions. Thus putting

$$\mathscr{R} = (\phi,\theta,0),$$

$$D^{l}_{\lambda 0}(\mathscr{R}) = \frac{\sqrt{4\pi}}{\hat{l}} Y_l^{\lambda *}(\theta,\phi).$$

$\langle l0|\epsilon|l'0\rangle$ will be a function of the angles θ and ϕ in a finite counter, so that we may write

$$\langle l0|\epsilon|l'0\rangle = \hat{l}\hat{l}'\epsilon(\theta,\phi).$$

Then

$$\langle l\lambda|\epsilon|l'\lambda'\rangle = 4\pi \int \epsilon(\theta,\phi)\ Y_l^{\lambda *}(\theta,\phi)\ Y_{l'}^{\lambda'}(\theta,\phi) \sin\theta\, d\theta\, d\phi.$$

If the counter is axially symmetric, $\epsilon(\theta,\phi)$ is independent of ϕ and the integration over azimuth introduces the factor $\delta_{\lambda\lambda'}$. The spherical harmonics reduce to associated Legendre polynomials and we get

$$\langle l\lambda|\epsilon|l'\lambda\rangle = \hat{l}\hat{l}' \left[\frac{(l-|\lambda|)!\,(l'-|\lambda|)!}{(l+|\lambda|)!\,(l'+|\lambda|)!}\right]^{1/2} \int \epsilon(\theta) P_l^{|\lambda|}(\theta) P_{l'}^{|\lambda|}(\theta) \sin\theta\, d\theta. \tag{26}$$

By writing $P_l^{|\lambda|}(\theta)P_{l'}^{|\lambda|}(\theta)$ as a sum over k of the function $P_k^{|\lambda|}(\theta)$, $\langle l\lambda|\epsilon|l'\lambda\rangle$ can be expressed in terms of the Q_k defined in Section II. For the present discussion we will use a more compact expression obtained by taking the leading terms of a Taylor expansion in terms of the half-angle, ξ, subtended by the counter. Using the approximation that for θ small

$$P_l(\cos\theta) \simeq \frac{(l+\lambda)!}{2^\lambda \lambda!(l-\lambda)!} (1-\cos^2\theta)^{\lambda/2} \left[1 - \frac{(l-\lambda)(l+\lambda+1)}{2(\lambda+1)} (1-\cos\theta)\right]$$

and assuming that $\epsilon(\theta) = \text{const} = \epsilon$ for $0 \leqslant \theta \leqslant \xi$, and zero otherwise, we obtain

$$\langle l\lambda|\epsilon|l'\lambda\rangle \simeq \frac{\epsilon\xi^{2|\lambda|+2}\,\hat{l}\hat{l}'}{2^{2|\lambda|+1}(|\lambda|!)^2(|\lambda|+1)} \left[\frac{(l+|\lambda|)!(l'+|\lambda|)!}{(l-|\lambda|)!(l'-|\lambda|)!}\right]^{1/2} \times [1-\xi^2\{(l-|\lambda|)(l+|\lambda|+1)+(l'-|\lambda|)(l'+|\lambda|+1)\}/4(|\lambda|+2)]. \tag{27}$$

We can now obtain the effective density matrix for the state c by substituting equations (20), (21), and (27) in the expression (24), with the extension that we must include in equation (21) terms with $\lambda_2 \neq 0$. The effect of this will be to cause substates beyond $\gamma_{\max}$ to be populated; $\gamma_{\max}+1$ with a population proportional to ξ^4, $\gamma_{\max}+2$ with a population proportional to ξ^6, etc. In making the substitution noted above, it is convenient to introduce the coefficient defined by

$$(28)\quad A(\gamma l_2 l_2' \lambda_2) =$$
$$\sum \frac{\hat{l}_1 \hat{l}_1'}{\hat{a}^2 \hat{s}_1^2 \hat{s}_2^2} \frac{\hat{l}_2 \hat{l}_2'}{2^{2|\lambda_2|+1}(|\lambda_2|!)^2(|\lambda_2|+1)} \left[\frac{(l_2+|\lambda_2|)!(l_2'+|\lambda_2|)!}{(l_2-|\lambda_2|)!(l_2'-|\lambda_2|)!}\right]^{1/2}$$
$$\times (S_1\beta, l_1 0|b\beta)\ (S_1\beta, l_1' 0|b'\beta)$$
$$\times (S_2\Sigma_2, l_2\lambda_2|b\beta)\ (S_2'\Sigma_2, l_2'\lambda_2|b'\beta)\ (c\gamma, s_2\sigma_2|S_2\Sigma_2)(c\gamma, s_2\sigma_2|S_2'\Sigma_2)$$
$$\times \langle S_1 l_1||V||b\rangle^*\ \langle S_1 l_1'||V||b'\rangle\ \langle S_2 l_2||V||b\rangle\ \langle S_2' l_2'||V||b'\rangle^*$$

the summation being over $\beta, \Sigma_2, \sigma_2, b, b', l_1, l_1', S_1, S_2, S_2'$. Then to the order ξ^4 we can write for the population parameters

$$(29)\quad P(\gamma) = \xi^2 \epsilon \sum_{l_2\, l_2'} [A(\gamma l_2 l_2' 0) + \xi^2 \{A(\gamma l_2 l_2' 1)$$
$$+ A(\gamma l_2 l_2' -1) - (l_2(l_2+1) + l_2'(l_2'+1))\, A(\gamma l_2 l_2' 0)/8\}].$$

The factor ξ^2 outside the summation on the right-hand side of equation (29) reflects the fact that the response of the system is proportional to the approximate area of the counter $\pi\xi^2$. The first term within the square bracket, $A(\gamma l_2 l_2' 0)$, is that obtained with a particle counter of negligible size. The second term containing the factor ξ^2 is the leading correction term. In the summations of equations (28) and (29), as was noted also in the case of equation (7), interfering terms will be duplicated.

The complexity of the details of the formation of the state c is illustrated by equations (28) and (29), which are quoted here to show the form taken by the population parameters $P(\gamma)$. Cases can be found where b, l_1, l_2, and possibly less frequently S_1 and S_2, are sharp so that the $A(\gamma l_2 l_2' \lambda_2)$ can be written in terms of a small number of reduced matrix elements. However, such cases are amenable to a more general triple correlation analysis in which the emergent particle is observed at angles other than 0° or 180°, and this analysis will yield the large amount of information which is also a feature of method I. The terms of equation (28) with $\lambda_2 = 0$ are those obtained with an ideal counter and are zero for $\gamma > \gamma_{max}$. Those with $\lambda_2 \neq 0$ modify all of the populations, $P(\gamma)$, up to $\gamma = \gamma_{max} + \lambda_2$ in increasing orders of ξ^2. The magnitudes of the correction terms depend on a generally large number of reduced matrix elements and cannot be predicted. However, the coefficients $A(\gamma l_2 l_2' \lambda_2)$ can be expected to be of the same order of magnitude. Thus the corrections arising from λ_2 different from zero will be of the order of magnitude $\xi^{2|\lambda_2|}$. The practical application of these conclusions will be discussed in Section VI.

The combination of methods I and II, mentioned at the beginning of this section, in which two cascade gamma rays are observed in coincidence with an axially symmetrical particle counter, is necessary when the gamma-ray spectrum from a nuclear reaction becomes complicated, such as in the case of deuteron-induced reactions. This simplifies the gamma-ray pulse spectrum in a NaI(Tl) crystal to the point where a study of the individual gamma rays is possible. The theoretical formulae required here are identical with

those for method I. The measurement of a triple coincidence between a particle and two gamma rays is normally highly inefficient. However, in deuteron-stripping reactions and some other direct interaction types of reaction, a large portion of the cross section for a particular particle group usually appears in a narrow cone in the forward direction. A counter situated at 0° to the beam and subtending about 30° at the target can consequently have an enhanced efficiency. In favorable cases, such as s-wave and p-wave stripping patterns with low Q, the effective geometrical efficiency can be as high as 50%. Also the alignment tensors ρ_{k0} of the resulting state in the residual nucleus are strongly limited by the stripping mechanism. In the case of an $l = 1$ transition only the tensors ρ_{00} and ρ_{20} are to a first approximation significant even though, for example, the tensors ρ_{40} and ρ_{60} can be allowed by the total angular momentum of the state in the residual nucleus. The $B^{10}(d,n)C^{11*}$ reaction leaving C^{11} in the 6.50-Mev state is a case in point. The total angular momentum of this state is probably 7/2.

VI. APPLICATIONS OF METHOD II

Section V contained a theoretical discussion of the selection of aligned nuclear states, from a nuclear reaction $X(h_1,h_2)Y^*$, by the observation of the particle h_2 in an axially symmetrical counter at 0° or 180° to the beam. It was pointed out in Section V that under these conditions the maximum value of the magnetic substate of the residual nucleus Y^* is limited to the maximum value of the sum of the spins of the particles X, h_1, and h_2. In the case where the maximum value of this sum is 0 or ½ the angular correlation of the gamma rays de-exciting the nucleus Y^* is independent of the details of the formation. Consequently such reactions can be used when the yield of the reaction shows complex resonance structure.

In this section the reaction $Mg^{26}(He^4,n\gamma)Si^{29}$ will be discussed as an example of the use of method II. The $Mg^{26}(He^4,n\gamma)Si^{29}$ reaction was studied by Litherland and McCallum (1960) to provide an illustration of method II and in addition to measure magnetic dipole – electric quadrupole mixing amplitudes for the 1.28-Mev and 2.43-Mev gamma rays from Si^{29}. Equation (23) of Section V gives the full theoretical expression for the interpretation of such measurements.

Many other reactions which are as simple to interpret as the $Mg^{26}(He^4,n\gamma)Si^{29}$ reaction can be used to study the properties of the excited states of even–odd and odd–even nuclei. However, odd–odd nuclei cannot be studied in this way and reactions such as the $O^{16}(He^3,p\gamma)F^{18}$ and $Ne^{20}(d,He^4\gamma)F^{18}$ have to be used. In these cases the residual F^{18} states have their $\alpha = 0, \pm 1$ substates populated. Consequently, unless the details of the formation and decay of the compound state are specified, the observation of the proton or the alpha particle at 0° or 180° to the incident beam introduces an unknown parameter into equation (23). This parameter is the ratio of the populations of the $\alpha = \pm 1$ substates to the $\alpha = 0$ substate and it must be determined by experiment. The measurement of the angular correlation of the gamma rays from an excited state in an odd–odd nucleus is therefore unlikely to give an

unambiguous answer to, for example, the $M1$–$E2$ amplitude mixture. If both a_2/a_0 and a_4/a_0 coefficients are observed, this situation is altered since there are then two unquantized parameters to determine and two measured quantities. Further information can be obtained by measuring the linear polarization of the gamma rays in coincidence with the particles and in favorable cases a linear polarization measurement also determines the parity change. Also if more than one gamma ray is emitted in coincidence with the particle then it may be possible to use the extra information obtained to determine the unknown population parameters.

Method II can be reliably used only if the effects of the finite size of the counter, detecting the heavy particle at 0° or 180° to the beam, are corrected for. These effects have been considered in a general way in Section V. It was shown that for a small counter of half-angle ξ situated at 0° or 180° to the beam there were extra terms introduced into equation (23). Again taking the $Mg^{26}(He^4,n\gamma)Si^{29}$ reaction as an example, the effect on the angular correlation of the gamma rays is to multiply the correlation from the $\alpha = \pm\frac{1}{2}$ substates by a factor $1+A\xi^2$ and to introduce a contribution from the $\alpha = \pm 3/2$ substate which was multiplied by a factor $B\xi^2$. The quantities A and B cannot be calculated unless the details of the reaction leading to the state c in the residual nucleus are specified (see equations (28) and (29)). Figure 5 shows the results of some calculations for a particular case which is relevant to the results of the experiment on the $Mg^{26}(He^4,n\gamma)Si^{29}$ discussed by Litherland and McCallum (1960). A 2+ resonance in Si^{30} is formed by the capture of d-wave alpha particles by Mg^{26}. This compound state decays by emitting $s_{1/2}$ or $d_{3/2}$ neutrons to a 5/2+ state in Si^{29} which in turn decays by emitting an electric quadrupole quantum to the 1/2+ ground state of Si^{29}. The neutrons are detected by an axially symmetrical counter of half-angle ξ. The effect of varying the half-angle ξ is shown for both the a_2/a_0 and a_4/a_0 coefficients. The approach to the theoretical values of $+4/7$ and $-4/7$ as ξ is reduced illustrates the necessity for a careful measurement of the variation of the a_2/a_0 and a_4/a_0 coefficients with the angle ξ.

When the angle ξ is small, it is possible to show for the case shown in Fig. 5 that the coefficients A and B defined above are given by equations (30) and (31).

$$A = -\frac{3}{4}\frac{2\sqrt{\frac{2}{7}}\delta+\frac{1}{7}\delta^2}{1+2\sqrt{\frac{2}{7}}\delta+\frac{2}{7}\delta^2} \tag{30}$$

$$B = \frac{3}{4}\frac{\frac{6}{7}\delta^2}{1+2\sqrt{\frac{2}{7}}\delta+\frac{2}{7}\delta^2} \tag{31}$$

These equations illustrate the important role played by the $s_{1/2}$–$d_{3/2}$ interference term δ in the correction for the finite solid angle of the neutron counter.

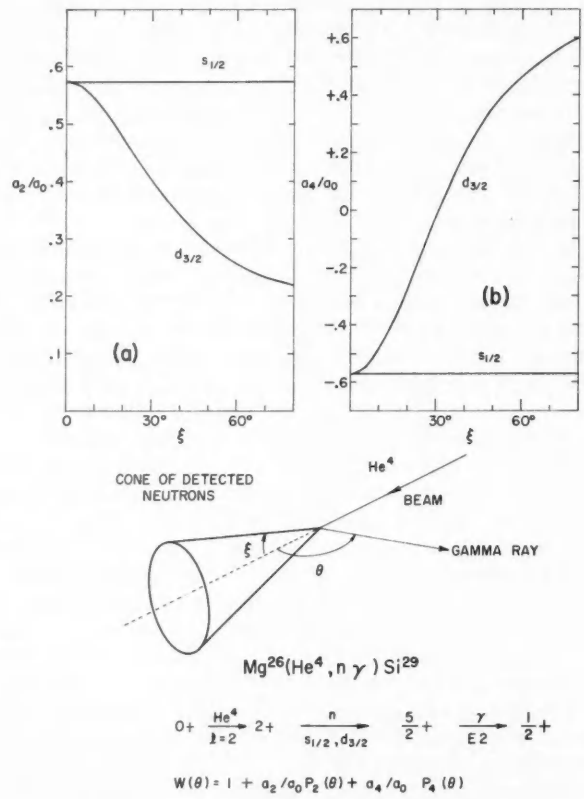

FIG. 5. Corrections to the angular distributions resulting from the finite aperture of the particle counter in the reaction $Mg^{26}(\alpha n\gamma)Si^{29}$. As the size of the counter increases, the corrections become increasingly dependent on the $d_{3/2}$:$s_{1/2}$ mixture of the outgoing neutrons. Graph (*a*) shows the behavior of the a_2/a_0 term, graph (*b*) the behavior of the a_4/a_0 term for both $s_{1/2}$ and $d_{3/2}$ neutrons as functions of the half-angle, ξ, subtended by the counter at the target.

The quantity δ is the amplitude of the $d_{3/2}$ neutron wave divided by the amplitude of the $s_{1/2}$ neutron wave. Equations (30) and (31) can be obtained from equations (28) and (29) with the coupling scheme for outgoing particles changed to the one used above or alternatively from expressions given by Sharp *et al.* (1953).

The correction for the finite solid angle of the gamma-ray counter is easier to apply in the case of method II than in the case of method I. It can be seen from equation (1) that the measured angular correlation coefficients are actually $(Q_2/Q_0)a_2/a_0$ and $(Q_4/Q_0)a_4/a_0$. Since the quantities Q_k can be calculated or obtained from tables (Gove and Rutledge 1958 and Rutledge 1959), the coefficients a_2/a_0 and a_4/a_0 can readily be obtained. Figure 6 shows

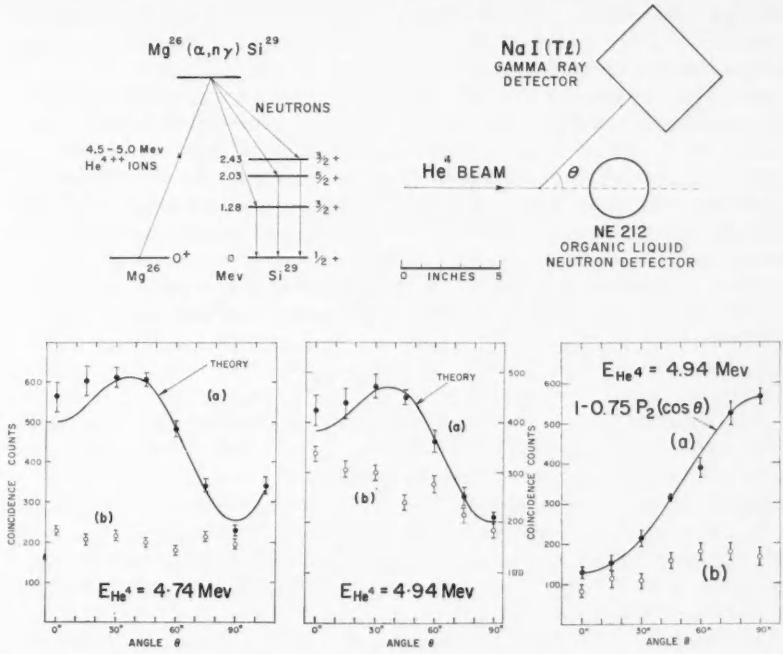

FIG. 6. Angular correlations obtained by method II. The left-hand and center lower graphs are the correlations of the 2.03-Mev gamma ray at two different bombarding energies. The solid line is the theoretical correlation for a $5/2+ \rightarrow 1/2+$ transition. The right-hand graph is the correlation of the 2.43-Mev gamma ray together with the theoretical correlation for a $3/2+ \rightarrow 1/2+$ transition. The open circles marked (*b*) in the lower parts of all three graphs are the correlations obtained with the neutron counter at 90° relative to the beam direction.

some experimental results obtained by Litherland and McCallum from the $Mg^{26}(He^4,n\gamma)Si^{29}$ reaction. The geometrical arrangement of the counters used is also shown. The angular correlation measurements were made with the neutron counter at 0° and at 90°. These two cases are labelled (*a*) and (*b*) in Fig. 6. The theoretical curves shown include only the effect of the finite solid angle of the gamma-ray counter. In Table VI the results of a least

TABLE VI

Measured and theoretical coefficients for the angular correlations shown in Fig. 6 analyzed according to method II. The reaction is $Mg^{26}(\alpha n\gamma)Si^{29}$ and the gamma rays studied are the 2.03-Mev and 2.43-Mev transitions to the ground state. In the case of the 2.43-Mev gamma ray, the $E2/M1$ amplitude ratio, δ, has two values, -0.26 and -1.10, which give agreement with the measured a_2/a_0 coefficient

Bombarding energy (Mev)	Gamma ray (Mev)	a_2/a_0		a_4/a_0	
		Measured	Theory	Measured	Theory
4.74	2.03	$+0.62\pm0.06$	0.53	-0.43 ± 0.06	-0.43
4.94	2.03	$+0.55\pm0.06$	0.53	-0.34 ± 0.06	-0.43
4.94	2.43	-0.75 ± 0.07	-0.75	—	0

squares analysis of the data are compared with theory. As discussed by Litherland and McCallum, the agreement between theory and experiment is good when only the correction for the finite size of the gamma-ray counters is made. The fact that no correction for neutron counter size is needed implies that the neutrons are predominantly *s*-wave, a conclusion which is supported by the measurement in one case of the angular distribution of the 2.03-Mev gamma rays with the neutrons unobserved. However, the measurement of the correlations with the neutron counter at 90° to the beam (marked (*b*) in Fig. 6) shows clearly the effect of the small admixture of *d*-wave neutrons to the predominantly *s*-wave neutrons.

The experiment reported by Litherland and McCallum was of a preliminary nature but serves to illustrate the simplifications possible by the use of method II.

VII. CONCLUSIONS

It is apparent that the method I, typified by the reaction $Mg^{24}(pp'\gamma\gamma)Mg^{24}$, has considerable advantages over method II, typified by the reaction $Mg^{26}(He^4,n\gamma)Si^{29}$. In method I, a measurement of the angular correlation of the gamma rays gives a possible total of 18 measurable ratios if both gamma rays contain a quadrupole component. These are the ratios $a^{\kappa}_{k_1k_2}/a^{0}_{00}$ for k_1, $k_2 = 0$, 2, or 4 and for $\kappa = 0$, 1, 2, 3, and 4. For an even–even nucleus there are at the most a unknown alignment parameters and two unknown multipole mixtures. As discussed in Section IV the number of unknown alignment parameters is usually less than a if a is large. In contrast the angular correlation measurements of method II yield at the most two measurable parameters a_2/a_0 and a_4/a_0 if the gamma radiation is limited to quadrupole radiation. As discussed in the previous subsection, these measured quantities are usually only just sufficient in favorable cases to permit the measurements to be interpreted.

The advantage of method II lies in the comparative simplicity of the gamma-ray pulse spectra obtained from the sodium iodide gamma-ray spectrometer. Since it is possible to use energy analysis on the pulses from the counter detecting the particles at 0° or 180° to the beam the number of gamma rays producing pulse spectra can often be drastically limited. This is in contrast with method I where the only simplification that is possible lies in the specification that gamma rays in coincidence are studied. To take an extreme example, it would be very difficult to study the gamma rays from the reaction $Mg^{26}(He^4,p\gamma)Al^{29}$ by method I but it would be relatively straightforward by method II since the gamma rays from the competing reaction $Mg^{26}(He^4,n\gamma)Si^{29}$ would be eliminated by the requirement that they be in coincidence with protons.

This discussion leads naturally to a synthesis of methods I and II. The weaknesses of method I can be removed by observing the outgoing heavy particles in an energy-sensitive detector in coincidence with the gamma rays. This detector would have to be of large solid angle to obtain an adequate triple coincidence counting rate but, provided it was axially symmetrical with

respect to the incident beam, the analysis procedure of method I will still apply. As discussed in Section V, the strongly peaked deuteron-stripping angular distribution of the neutrons or protons contains a large part of the cross section leading to a particular excited state. Consequently a relatively small particle counter on the beam axis can be efficiently used to specify that a certain excited state has been formed.

In conclusion the types of the triple-angular correlation measurements discussed in this paper have been shown to be potentially powerful methods of determining nuclear spectroscopic data from nuclear reactions. The full exploitation of angular correlations of method I probably requires the use of an electronic computer, as in the example quoted in Section V, because the data obtained experimentally have to be analyzed by least squares to obtain several parameters. This analysis has then to be repeated for various values of the spins of the nuclear states involved. In contrast the data obtained by method II can be analyzed quite easily though as discussed above, the method is limited in its applicability.

ACKNOWLEDGMENTS

We wish to acknowledge the great interest and co-operation of Drs. R. Batchelor, C. Broude, H. E. Gove, G. J. McCallum, and W. T. Sharp in this work. We are indebted to Dr. F. D. Seward for permission to use the $Mg^{24}(pp')$ yield curve from his paper.

REFERENCES

ALDER, K., BOHR, A., HUUS, T., MOTTELSON, B., and WINTHER, A. 1956. Revs. Modern Phys. **28**, 432.

BATCHELOR, R., FERGUSON, A. J., GOVE, H. E., and LITHERLAND, A. E. 1960. Nuclear Phys. **16**, 38.

BIEDENHARN, L. C. 1960. Nuclear spectroscopy, *edited by* F. Ajzenberg-Selove (The Academic Press, New York and London).

BIEDENHARN, L. C. and ROSE, M. E. 1953. Revs. Modern Phys. **25**, 729.

BLATT, J. M. and BIEDENHARN, L. C. 1952. Revs. Modern Phys. **24**, 258.

BLIN-STOYLE, R. J. and GRACE, M. A. 1957. Encyclopedia of Physics (Julius Springer, Berlin), **42**, 555.

BROUDE, C. and GOVE, H. E. 1960. Private communication.

——— 1960. Proceedings of the International Conference on Nuclear Structure, Kingston, Canada, 1960, *edited by* D. A. Bromley and E. W. Vogt (University of Toronto Press, Toronto and the North-Holland Publishing Company, Amsterdam). See also BROUDE, C. and GOVE, H. E. 1960. Bull. Am. Phys. Soc. Series II, Vol. **5**, 248, and GOVE, H. E. 1960. Proceedings of the Second Accelerator Conference, Amsterdam (to be published in Nuclear Instr.).

BROUDE, C., GREEN, L. L., and WILLMOTT, J. C. 1959. Proc. Phys. Soc. (London), **72**, 1097.

CONDON, E. U. and SHORTLEY, G. H. 1951. Theory of atomic spectra (Cambridge University Press).

DEVONS, S. and GOLDFARB, L. J. B. 1957. Encyclopedia of Physics (Julius Springer, Berlin), **42**, 362.

FANO, U. and RACAH, G. 1959. Irreducible tensorial sets (Academic Press Inc., New York).

FERENTZ, M. and ROSENZWEIG, N. 1955. Table of F Coefficients, ANL-5324, Office of Technical Services, Dept. of Commerce, Washington 25, D.C., U.S.A.

FERGUSON, A. J. 1961. Can. J. Phys. **39**. To be published.

FERGUSON, A. J. and LITHERLAND, A. E. 1955. Phys. Rev. **99**, 1654 (A).

FERGUSON, A. J. and RUTLEDGE, A. R. 1957. Coefficients for Triple Angular Correlation Analysis in Nuclear Bombardment Experiments, Atomic Energy of Canada Report AECL-420.

GOVE, H. E. and RUTLEDGE, A. R. 1958. Finite Geometry Corrections to Gamma-Ray Angular Correlations Measured with 5 in. Diameter by 4 in. Long NaI(Tl) Crystals, Atomic Energy of Canada Report CRP-755.

GIBBS, R. C. and WAY, K. 1958. A Directory to Nuclear Data Tabulations, National Academy of Sciences, National Research Council, Washington, D.C., U.S.A.

HOOGENBOOM, A. M. 1958. Thesis, Utrecht.

LITHERLAND, A. E. 1959. Bull. Am. Phys. Soc. II, **4**, 58.

LITHERLAND, A. E. and MCCALLUM, G. J. 1960. Can. J. Phys. **38**, 927.

LITHERLAND, A. E., PAUL, E. B., BARTHOLOMEW, G. A., and GOVE, H. E. 1959. Can. J. Phys. **37**, 53.

OFER, S. 1959. Phys. Rev. **114**, 870.

ROSE, M. E. 1953. Phys. Rev. **91**, 610.

——— 1958. Triple Correlations, ORNL-2516, Office of Technical Services, U.S. Dept. of Commerce, Washington, D.C.

RUTLEDGE, A. R. 1959. Finite Geometry Corrections to Gamma-Ray Angular Correlations Measured with 5 in. Diameter by 6 in. Long NaI(Tl) Crystals and with 3 in. Diameter by 3 in. Long NaI(Tl) Crystals, Atomic Energy of Canada Report CRP-851.

SEWARD, F. D. 1959. Phys. Rev. **114**, 514.

SHARP, W. J., KENNEDY, J. M., SEARS, B. J., and HOYLE, M. G. 1953. Tables of Coefficients for Angular Distribution Analysis, Atomic Energy of Canada Report 97, CRT-556.

SIMON, A. 1954. ORNL-1718.

SIMON, A., VANDER SLUIS, J. H., and BIEDENHARN, L. C. 1954. Tables of the Racah Coefficients, ORNL-1679.

SMITH, K. 1958. ANL-5860, supplement to ANL-5776, in two parts.

SMITH, K. and STEVENSON, J. W. 1957. A Table of Wigner $9-j$ Coefficients for Integral and Half-Integral Values of the Parameters, ANL-5776.

WAPSTRA, A. H., NIJGH, G. J., and VAN LIESHOUT, R. 1959. Nuclear spectroscopy tables (North-Holland Publishing Company, Amsterdam).

WARBURTON, E. K. and ROSE, H. J. 1958. Phys. Rev. **109**, 1199.

WAY, K. 1959. 1959 Nuclear Data Tables, National Academy of Sciences, National Research Council, Washington, D.C., U.S.A.

A PSYCHROMETER TABLE FOR HEAVY WATER HUMIDITIES[1]

C. D. NIVEN

ABSTRACT

A psychrometer table for use in atmospheres humidified with heavy water has been constructed by calculation from data on the vapor pressure and latent heat of vaporization of heavy water, between 10° and 40° C. The relative humidity is quite markedly lower in the low temperature end of this range when heavy water is used instead of ordinary water, for the same wet and dry bulb readings.

INTRODUCTION

A search for a psychrometer table converting wet and dry bulb readings to percentage relative humidity figures when heavy water vapor humidified air, indicated that such a table had not been published. For work in which hydrogen atoms must be replaced by deuterium atoms, it is sometimes useful to know the relative humidity of the abient atmosphere, humidified with heavy water vapor, and this can be calculated from the wet and dry bulb temperatures provided certain properties of heavy water are known. Hougen and Watson (1936) have given the method: Whalley (1957) has assembled pertinent data: therefore the construction of the table is feasible.

This has been undertaken by the writer in the range 10°–40° C dry bulb temperature and 9°–39° C wet bulb temperature and figures are presented below in Table II. Sufficient details of the method of calculation have been given in order that an experimenter requiring figures beyond the extremes which the table provides for, can extend it, if desired, without too much trouble.

DETAILS OF THE METHOD

Hougen and Watson give the formula

$$t = \frac{(H_w - H)L_v}{6.95 + 8.4H} + t_w$$

where t and t_w are dry and wet bulb centigrade temperatures respectively,

H is the molal humidity and is what has to be calculated,

H_w is the saturation molal humidity at wet bulb temperature t_w, and

L_v is the molal heat of vaporization at t_w.

For convenience we introduce the depression D, which is $t - t_w$. Accordingly $D(6.95+8.4H) = (H_w - H)L_v$ or

$$\text{(A)} \qquad H = \frac{L_v H_w - 6.95D}{L_v + 8.4D}.$$

[1]Manuscript received March 8, 1961.
Contribution from the Division of Applied Physics, National Research Council, Ottawa, Canada.
Issued as N.R.C. No. 6301.

The constants 6.95 and 8.4 are the molal heat capacities of air and of water vapor respectively and, according to Hougen and Watson, they can be taken as constants. In taking the molal heat capacity of *heavy* water vapor at 8.4 we are admittedly assuming that the heat capacity of heavy water vapor differs negligibly from that of ordinary water vapor. In the range of calculations we are considering, the effect of an error introduced by this assumption is going to be greatest when $D = 10$, that is to say, when the amount added to the value of L_v is 84. Since L_v runs from 11,039 at $t_w = 9$ to 10,674 at $t_w = 39$, one may regard any error introduced in assuming 8.4 for the heat capacity constant to be of mere academic interest.

The work then reduces itself to (*a*) the interpolation of tabulated values for L_v, (*b*) the interpolation of tabulated values of vapor pressure and the calculation of H_w therefrom, and (*c*) the computation of H and hence the computation of percentage relative humidity.

(a) Tabulation of L_v Values Between 9° C and 39° C

Using some amended values for molal enthalpy change during vaporization, which Dr. Whalley kindly supplied, the writer noted that L_v was a linear function of the temperature between 20° and 50° C. So by subtracting the value of L_v at 50° from that at 20°, it was possible to get the increment per degree to great accuracy. The interpolated values thus obtained have to be multiplied by 1000 and divided by 4.186 in order to convert kilojoules to calories for use in expression (A). These values are tabulated in Table I for

TABLE I

°C	L_v (calories)	P_D (bars)	H_w	°C	L_v (calories)	P_D (bars)	H_w
9	11,039	0.00958	0.009545	25	10,843	0.02732	0.027710
10	11,027	0.01030	0.010270	26	10,831	0.02890	0.029359
11	11,013	0.01110	0.011076	27	10,820	0.03080	0.031350
12	11,001	0.01191	0.011894	28	10,808	0.03285	0.033507
13	10,989	0.01275	0.012744	29	10,796	0.03500	0.035778
14	10,977	0.01362	0.013625	30	10,784	0.03728	0.03820
15	10,965	0.01453	0.014549	31	10,772	0.03966	0.04074
16	10,953	0.01559	0.015627	32	10,760	0.04217	0.04343
17	10,941	0.01661	0.016666	33	10,748	0.04474	0.04619
18	10,927	0.01770	0.017779	34	10,734	0.04745	0.04913
19	10,915	0.01886	0.018966	35	10,721	0.05026	0.05219
20	10,903	0.02011	0.020249	36	10,709	0.05318	0.05539
21	10,891	0.02146	0.021638	37	10,698	0.05621	0.05873
22	10,879	0.02285	0.023071	38	10,686	0.05935	0.06222
23	10,867	0.02429	0.024561	39	10,674	0.06260	0.06585
24	10,855	0.02578	0.026107	40	10,662	0.06596	0.06963

the range 9° to 39° C. In passing it may be of interest to mention that the use of the amended values in place of the values originally tabulated did not affect the relative humidity results.

(b) Tabulation of H_w Values Between 9° C and 39° C

$$H_w = \frac{P_D}{\text{pressure of 1 atmosphere} - P_D}$$

where P_D is the vapor pressure of heavy water at some particular temperature: so if P_D is measured in bars

$$H_w = \frac{P_D}{1.01325 - P_D}.$$

Whalley's table gives P_D in bars for various values of temperature but the relation between P_D and temperature is unfortunately far from linear; accordingly the task of interpolating P_D is not quite so easy as it was for L_v. In Table I are given the interpolated values chosen, along with the values of H_w calculated from them.

(c) Computation

The next step is to lay out the data given in Table I in such a way that a professional computer has merely to fill in the figures after each computation on the machine. To do this, part of a wide sheet of paper sufficiently large to take 10 rows of figures must be allotted to each dry bulb temperature: this must then be ruled to provide 14 vertical columns. The first two of these can be narrow but most of the others must be wide enough to take 6- or 7-figure numbers. In the first column t_w, the wet bulb temperature, is entered: in the second depression D is entered: in the third values for L_v taken from Table I are entered (corresponding of course to temperature t_w): in the fourth corresponding values for H_w are entered. The values in columns 3 and 4 are then multiplied together and the products entered in column 5. In the sixth column the values 6.95 D are entered; this is the same for all sheets. Column 6 is then subtracted from column 5 and the differences entered in column 7: this gives the numerator of expression (A). In column 8 the values of 8.4 D are entered; this is the same for all sheets. Column 8 is added to column 3 and the sum is entered in column 9: this gives the denominator of expression (A). Column 7 is then divided by column 9 and the quotient entered in column 10: this is H. The rest of the columns are used for $H+1$, $H/(H+1)$, 1 bar/P_D, and $[H/(H+1)]\times(1\text{ bar}/P_D)\times 100$, which is the relative humidity in per cent, where P_D is the vapor pressure at dry bulb temperature.

RESULTS

In order to smooth out any slight error introduced by interpolation and exaggerated in the calculation, the calculated relative humidities were plotted against dry bulb temperature for each value of the depression. A smooth curve was then drawn through the points and values read off to half of one per cent relative humidity. These values were then cross-checked by plotting them against depression for each dry bulb temperature. The figures are tabulated in Table II: the accuracy attempted is to the nearest one-half per cent.

In order to show the type of change introduced in the psychrometer table by using heavy instead of ordinary water for humidifying, the curves relating percentage relative humidity with dry bulb temperature at depressions of 5° and 10° C are shown in Fig. 1 along with the corresponding relative humidity values for ordinary water plotted at intervals of 5° C dry bulb temperature.

TABLE II

Psychrometer table for atmospheres humidified with heavy water vapor

Dry bulb, °C	Depression									
	1	2	3	4	5	6	7	8	9	10
10	87									
11	87.5	75								
12	88	76	64.5							
13	88.5	77	66	55.5						
14	89	78	67.5	57	47					
15	89.5	78.5	68.5	59	49	40				
16	89.5	79.5	70	60	51	42	33			
17	90	80	71	61.5	52.5	44	35.5	27		
18	90	81	72	62.5	54	46	37.5	29.5	22	
19	90.5	81.5	72.5	63.5	55.5	47.5	39.5	32	24.5	17
20	90.5	82	73	65	56.5	49	41	34	27	20
21	90.5	82.5	74	65.5	58	50	43	36	29	22
22	91	82.5	74.5	66.5	59	51.5	44.5	37.5	31	24
23	91.5	83	75.5	67.5	60	53	46	39	33	26
24	91.5	83.5	76	68	61	54	47	40.5	34.5	28
25	92	84	76.5	69	62	55	48.5	42	36	30
26	92	84	77	69.5	62.5	56	49.5	43.5	37.5	31.5
27	92	84.5	77.5	70.5	63	57	50.5	44.5	39	33
28	92	85	77.5	71	63.5	57.5	51	45	40	34.5
29	92.5	85	78	71.5	64.5	58	52	46	41	36
30	92.5	85.5	78.5	72	65	59	53	47	42	37
31	92.5	85.5	79	72.5	65.5	59.5	54	48	43	38
32	93	86	79.5	73	66	60	54.5	49	44	39
33	93	86	79.5	73.5	67	61	55.5	50	45	40
34	93	86.5	80	74	67.5	62	56	50.5	46	41
35	93	86.5	80.5	74.5	68	62.5	57	51.5	47	42
36	93	87	80.5	75	69	63	58	52.5	48	43
37	93.5	87.5	81	75.5	69.5	64	58.5	53.5	49	44
38	93.5	87.5	81.5	76	70	64.5	59.5	54.5	50	45
39	94	88	82	76.5	70.5	65.5	60.5	55.5	51	46
40	94	88	82.5	77	71	66	61	56.5	52	47

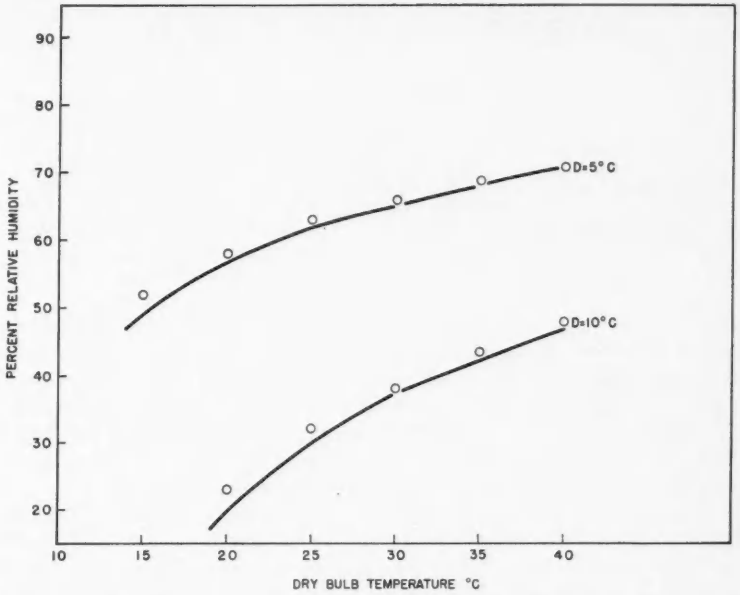

FIG. 1. Comparison between relative humidity values in per cent for heavy water and those for ordinary water. Full lines, heavy water; O, ordinary water.

Clearly the effect of using heavy water for humidifying is not very great at the higher temperatures and smaller depressions (high humidities); but at temperatures around 20° C it amounts to as much as 3% in relative humidity value for a depression of 10° C, which corresponds to an error of 3 on 23 or about 13%.

ACKNOWLEDGMENTS

The author expresses his thanks to Dr. E. Whalley for valuable assistance in applying the method of calculation and to Miss C. M. De Chantigny and to Mrs. N. M. Thomas, both of the Division of Applied Physics, National Research Council, Ottawa, for the calculations.

REFERENCES

HOUGEN, O. A. and WATSON, K. M. 1936. Industrial chemical calculations, 2nd. ed. (John Wiley & Sons, Inc., New York), p. 148.

WHALLEY, E. 1957. The Thermodynamic and Transport Properties of Heavy Water, N.R.C. No. 4469 (reprinted from the Proc. of the Joint Conference on Thermodynamic and Transport Properties of Fluids, pp. 15–26).

REPRESENTATIONS OF SPACE GROUPS[1]

I. V. V. RAGHAVACHARYULU

ABSTRACT

The construction of the irreducible representations of space groups by the little-group method making use of their solvability property is discussed. As an example the two-dimensional space group $p4g$ is considered and all the allowable representations for the groups $G^{\mathbf{k}}$'s of typical wave vectors $\mathbf{k}$ of the group $p4g$ are obtained.

INTRODUCTION

The symmetry groups of crystals are space groups. Seitz (1936) initiated a study of the representations of space groups. He showed that all space groups are solvable, and their irreducible representations could be obtained from the general theory given for such groups by Frobenius and Schur. Later, following Seitz (1936), Bouckaert, Smoluchowski, and Wigner (1936) and Herring (1942) pointed out that all the irreducible representations of a space group G could be induced by a set of representations of its subgroups $G^{\mathbf{k}}$'s. These representations are called allowable or small representations of $G^{\mathbf{k}}$'s. They are obtained from those of the groups $G^{\mathbf{k}}/T^{\mathbf{k}}$'s, reduced by the usual algebraic process, by picking out all those representations of $G^{\mathbf{k}}/T^{\mathbf{k}}$ which subduce in the group T a multiple of the representation of T associated with the wave vector $\mathbf{k}$. This method is very elegantly explained and illustrated in a recent monograph by Lomont (1959).

In this paper the problem of constructing all the irreducible representations of space groups is studied by the little-group method making use of their solvability property. This method not only avoids the tedious algebraic process used to reduce $G^{\mathbf{k}}/T^{\mathbf{k}}$ but also weeds out all other representations of $G^{\mathbf{k}}/T^{\mathbf{k}}$ and directly gives us all its allowable representations.

First of all let us quickly review the little-group method. In doing this we will follow very closely Lomont's presentation and terminology (Lomont 1959). Incidentally we develop some theorems which can be used as checks in the implementation of the method to construct irreducible representations of space groups.

MONOMIAL REPRESENTATIONS

Let $G = (A)$ be a group of finite order g, $H = (B)$ a subgroup of G of order h, and $G = \sum_{i=1}^{g/h} A_i H$ a coset decomposition of G. Every element A of G could be written as $A_r B$ for some r. Consider $A\,A_i$. It is an element of G and could be written as $A_j B'$. Now construct a matrix M_A of degree g/h corresponding to A whose ith row jth column element is B' and all the other elements in the ith row are zeros. It is easily verified that $A \rightarrow M_A$ is a repre-

[1]Manuscript received November 4, 1959.
Contribution from the Department of Physics, Annamalai University, South India.
Can. J. Phys. Vol. 39 (1961)

sentation of G in terms of the elements of H. This is called a monomial representation of G. (See Zassenhaus (1949) where much more general monomial representations are discussed.)

For future use let us set up monomial representations of a group G in a particular case.

Let G be a group, H a normal subgroup, and G/H an Abelian group generated by a single element A. Let $G = H+AH+\ldots+A^{m-1}H$ be a coset decomposition of G where m is the smallest integer such that $A^m = B'$ an element of H. Now in the monomial representation of G for the above coset decomposition of it we have

$$A \to M_A = \begin{bmatrix} 0 & E & 0 \ldots 0 \\ 0 & 0 & E \ldots 0 \\ \ldots\ldots\ldots\ldots \\ 0 & 0 & 0 \ldots E \\ B' & 0 & 0 \ldots 0 \end{bmatrix} \quad B \to M_B = \begin{bmatrix} B & 0 & \ldots & 0 \\ 0 & ABA^{-1} & \ldots & 0 \\ & & & \\ \ldots\ldots\ldots\ldots & & & \\ 0 & 0 & \ldots & A^{m-1}BA^{1-m} \end{bmatrix}$$

where E is the identity element of G.

The following theorem regarding monomial representations can be easily proved.

THEOREM: *The monomial representation of G that can be obtained by taking different sets of elements A_i in the coset decomposition of G with respect to H or a different subgroup H' conjugate to H are all equivalent.*

Let Δ be a representation of H, $A \to M_A$ a monomial representation of G. Substituting for the elements of H in M_A their corresponding matrices in Δ we obtain the induced representation Δ^t of G. From the above theorem we see that Δ^t's, obtained for different choices of the elements A_i in the coset decomposition of G with respect to the subgroup H, are all equivalent.

LITTLE GROUPS

Let $G = (A)$ be a group and E its identity element, $H = (B)$ a normal subgroup of G, Δ an irreducible representation of H in which the matrix $D^\Delta(B)$ corresponds to the element B, and Δ^A the irreducible representation of H which is conjugate to $\Delta = \Delta^E$ and defined by $B \to D^\Delta(ABA^{-1})$.

In general the representations Δ^A and Δ^E of H need not be equivalent ($\cdot\equiv\cdot$).

THEOREM: *All the elements A of G such that $\Delta^A \cdot\equiv\cdot \Delta^E$ form a group $L^{II}(\Delta)$ called the little group of second kind relative to G, H, and Δ.*

$L^{II}(\Delta)$ contains the group H as a normal subgroup and $L^{I}(\Delta) = L^{II}(\Delta)/H$ is called the little group of first kind relative to G, H, and Δ.

Further, let $G = \sum A_i L^{II}(\Delta)$ be a coset decomposition of G.

THEOREM: *For any two elements A and A' of G $\Delta^A \cdot\equiv\cdot \Delta^{A'}$ if and only if A and A' belong to the same coset of G with respect to the group $L^{II}(\Delta)$.*

This theorem suggests a way of grouping the irreducible representations of H with respect to the group G. This is done by introducing the idea of orbits.

Definition.—An *orbit* of a normal subgroup H of G is defined as a maximal set of inequivalent irreducible representations of H which are mutually conjugate to each other with respect to the elements of G. The number of such representations (in an orbit) is called the *order of the orbit.*

THEOREM: *Making use of the above notation, let G be a group and H a normal subgroup of G then*

(1) the order of an orbit containing Δ *is equal to the index of the group* $L^{II}(\Delta)$ *in G;*

(2) the groups $L^{II}(\Delta), L^{II}(\Delta') \ldots$ *etc. which correspond to different representations* Δ, Δ' *etc. of H in the same orbit* $\{\Delta\}$ *are conjugate subgroups of G.*

ALLOWABLE REPRESENTATIONS OF $L^{II}(\Delta)$

Let $L(\Delta)$ be a subgroup of $L^{II}(\Delta)$, not necessarily a proper subgroup, containing H, and ν an irreducible representation of it.

Definition.—ν will be called an allowable or small representation of $L(\Delta)$ relative to G, H, and Δ if it subduces a multiple of Δ in H, i.e. $\nu^s \cdot \equiv \cdot m\Delta$ in H. It is to be noted here that usually allowable representations of the group $L^{II}(\Delta)$ are defined but not those of the subgroups of it containing H. We have extended the definition as it is useful in the construction of the representations of space groups.

THEOREM: *With the above notation let G be a group and H a normal subgroup of it then*

(1) the allowable representations of $L(\Delta)$ *are contained in the induced representation* Δ^L *of* $L(\Delta)$ *from* Δ *of H as many times as they subduce the representation* Δ *in H;*

(2) all the irreducible representations of $L(\Delta)$ *which are obtained by reducing the induced representation* Δ^L *are allowable representations of* $L(\Delta)$*;*

(3) if $\nu_1, \nu_2, \ldots \nu_r$ *are a complete set of allowable representations of* $L(\Delta)$ *which subduce* $m_1, m_2, \ldots m_r$ *times the irreducible representation* Δ *in H then*

$$\sum_{i=1}^{r} m_i^2 = N(L(\Delta)/H) \tag{1}$$

which is the order of the group $L(\Delta)/H$.

The important relation (1) in the above theorem will be called *completeness relation* of the allowable representations. It can be used as a check when allowable representations are constructed to see whether all of them are obtained or not.

Now we state the central theorem of the reduction of groups with respect to normal subgroups by the little-group method.

THEOREM: *With the above notation let G be a group and H a normal subgroup of it then*

(1) the representation γ^t of G induced by the allowable representation γ of $L^{II}(\Delta)$ is an irreducible representation of G;

(2) if only one little group $L^{II}(\Delta)$ per orbit $\{\Delta\}$ is used to induce the irreducible representations of G then each irreducible representation of G is obtained once and only once and all the irreducible representations of G can be obtained in this way.

CONSTRUCTION OF ALLOWABLE REPRESENTATIONS OF $L^{II}(\Delta)$ WHEN G IS SOLVABLE

From the preceding theorem we see that if we construct the allowable representations ν of the groups $L^{II}(\Delta)$ for one irreducible representation Δ of each orbit $\{\Delta\}$ of H then all the irreducible representations of G can be simply induced by them. These allowable representations ν of $L^{II}(\Delta)$ can be very easily constructed when G is a solvable group. To show this suppose G is a solvable group. $H, L^{II}(\Delta)$, and $L(\Delta)$ are also solvable as they are subgroups of G. Let

$$L(\Delta) = L_0(\Delta) \supset L_1(\Delta) \supset L_2(\Delta) \ldots . \supset L_r(\Delta) \supset H$$

be a composition series of $L(\Delta)$ containing the group H. Then all the factor groups $L_i(\Delta)/L_{i+1}(\Delta)$ are cyclic groups of prime order α_i, say. Supposing from the representation Δ of H we have constructed the allowable representations of $L_r(\Delta)$ and making use of them all the allowable representations of $L_{r-1}(\Delta)$ and so on, we can ultimately obtain the required allowable representations of $L(\Delta)$. So we set up a method of obtaining the allowable representations of $L_i(\Delta)$ from that of $L_{i+1}(\Delta)$.

As $L_{i+1}(\Delta)$ is a normal subgroup of $L_i(\Delta)$ the allowable representations γ of $L_{i+1}(\Delta)$ can be classified into orbits with respect to $L_i(\Delta)$. As the group $L_i(\Delta)/L_{i+1}(\Delta)$ is of prime order α_i the order of the orbit $\{\nu\}$ is either α_i or 1.

In the case when the order of $\{\gamma\}$ is α_i the induced representation γ^t of $L_i(\Delta)$ from γ of $L_{i+1}(\Delta)$ is an allowable representation of $L_i(\Delta)$. More explicitly, if A is an element of $L_i(\Delta)$ but not in $L_{i+1}(\Delta)$ such that $A^{\alpha_i} = B'$ an element in $L_{i+1}(\Delta)$ then the allowable representation γ^t of $L_i(\Delta)$ is given with respect to the coset decomposition

$$L_i(\Delta) = L_{i+1}(\Delta) + A\,L_{i+1}(\Delta) + \ldots + A^{\alpha_i - 1} L_{i+1}(\Delta)$$

by

$$A \to \begin{bmatrix} 0 & I & 0 \ldots 0 \\ 0 & 0 & I \ldots 0 \\ \ldots & \ldots & \ldots \\ 0 & 0 & 0 \ldots I \\ \gamma(B') & 0 & 0 \ldots 0 \end{bmatrix} \qquad B \to \begin{bmatrix} \gamma(B) & 0 & \ldots & 0 \\ 0 & \gamma(ABA^{-1}) & \ldots & 0 \\ \ldots & \ldots & \ldots & \ldots \\ 0 & 0 & \ldots & \gamma(A^{\alpha_i - 1} B A^{1-\alpha_i}) \end{bmatrix}$$

where B is a general element of $L_{i+1}(\Delta)$ and I is the unit matrix.

In the case when the orbit $\{\gamma\}$ is of order one $\gamma(B) \cdot \equiv \cdot \gamma(ABA^{-1})$. So a matrix M exists such that $\gamma(ABA^{-1}) = M\gamma(B)M^{-1}$. By Schur's well-known theorem M is determined but for a scalar constant λ. Now choose λ such that

$(\lambda M)^{\alpha_i} = D^{\gamma}(B')$. Obviously if λ is a value which satisfies the equation then $\omega\lambda$ also satisfies it where ω is an α_ith root of unity. So, corresponding to the allowable representation γ of $L_{i+1}(\Delta)$ there are α_i allowable representations of $L_i(\Delta)$ which are given by $A \rightarrow \omega\lambda M$ and $B \rightarrow D^{\gamma}(B)$ where ω is an α_ith root of unity.

In this way all the allowable representations of $L_i^{II}(\Delta)$ can be obtained from that of $L_{i+1}^{II}(\Delta)$.

Moreover, it is interesting to note that if the allowable representations of $L_{i+1}^{II}(\Delta)$ satisfy the completeness relation, it can be proved that all the allowable representations of $L_i^{II}(\Delta)$ constructed from that of L_i^{II} (Δ) also satisfy the completeness relation. As the completeness relation is obviously satisfied for the representation Δ of H by induction it follows that the allowable representations of $L^{II}(\Delta)$ also satisfy the completeness relation. So all the allowable representations of $L^{II}(\Delta)$ are obtained by this process in the case of solvable groups.

SPACE GROUPS

The symmetry groups of crystals are space groups which are solvable groups. They consist of pure translations, rotations, and rotation-reflections, and combinations of these operations. Among the combinations we have certain types of symmetry operations which are called screws and glides. A screw is a rotation followed by a translation in the direction of the rotation axis and a glide is a reflection followed by a translation in the reflection plane. The translational part in a screw or a glide is by itself not a symmetry operation of the crystal and is called fractional translation.

The set of all pure translational symmetry operations of a space group G form a normal Abelian subgroup T of G called the translational group of G. Space groups which do not contain screws or glides are called point space groups or symmorphic groups. In a space group which contains screws or glides, if we set the fractional part of the translations of them arbitrarily zero we obtain the associated or underlying point space group of the original group. For example, the underlying point space group of O_h^7, the symmetry group of diamond, is given by O_h^5.

All space groups belong to one or other of the 14 Bravais lattices. These Bravais lattices are of four types: primitive, side-centered, face-centered, and body-centered. The reciprocal lattices of them are primitive, side-centered, body-centered, and face-centered lattices respectively.

If x, y, z are the co-ordinates of a point of a crystal referred to some suitable axes and x', y', z' are the co-ordinates of the point into which x, y, z are transformed by a symmetry operation of the space group of the crystal, the symmetry operation may be defined by a linear inhomogeneous transformation

$$\begin{bmatrix} x' \\ y' \\ z' \end{bmatrix} = \begin{bmatrix} a_{11} & a_{12} & a_{13} \\ a_{21} & a_{22} & a_{23} \\ a_{31} & a_{32} & a_{33} \end{bmatrix} \begin{bmatrix} x \\ y \\ z \end{bmatrix} + \begin{bmatrix} t_1 \\ t_2 \\ t_3 \end{bmatrix} \tag{2}$$

which can be written in the form $X' = aX + t$ in the matrix notation, where

a is an orthogonal matrix. Now, using the notation of Seitz the symmetry operation can also be written in a convenient form as $(a|t)$. The identity transformation is $(I|\mathbf{0})$ and a pure translation $(I|t)$. The product of any two symmetry operations $(a_2|t_2)$ and $(a_1|t_1)$ is given by

$$(a_1|t_1)\ (a_2|t_2) = (a_1a_2|a_1t_2+t_1).$$

The inverse transformation of $(a|t)$ is $(a^{-1}|-a^{-1}t)$.

Two points x, y, z and x', y', z' of a crystal are called equivalent points if one can be transformed into the other by an operation of the space group of the crystal. In the *International Tables for X-ray Crystallography* (1952) the basic equivalent points for all the space groups of crystals are specified.

ORBITS OF SPACE GROUPS

Let G be a space group referred to Bravais axes and T its translational normal Abelian subgroup. It can very easily be proved that the bounded irreducible representations $\Delta(\mathbf{k})$ of T are given by $(I|t) \rightarrow \exp 2\pi i\mathbf{k}.\mathbf{t}$ where $\mathbf{k}$ is a wave vector in the reciprocal point space group of G. Moreover, two wave vectors $\mathbf{k}$ and $\mathbf{k}'$ which differ by a complete translation in the reciprocal space of G define the same irreducible representations of T. Two such wave vectors are called equivalent wave vectors.

Consider an orbit $\{\Delta(\mathbf{k})\}$ of the representations of T with respect to G. We can associate with it a set of inequivalent wave vectors $\{\mathbf{k}\}$ which correspond to different irreducible representations of T in $\{\Delta(\mathbf{k})\}$. This inequivalent set of wave vectors $\mathbf{k}$ is called a star of G.

To see how to obtain the stars of a space group G consider a representation $\Delta(\mathbf{k})$ of T, and elements $(a|t')$ and $(I|t)$ of G and T respectively. As

$$(a|t')(I|t)(a^{-1}|-a^{-1}t') = (I|at) \tag{3}$$

the representation conjugate to $\Delta(\mathbf{k})$ of T with respect to the element $(a|t')$ is given by $\Delta(a\mathbf{k})$. If $\Delta(\mathbf{k}) \cdot\equiv\cdot \Delta(a\mathbf{k})$ then $\mathbf{k}$ and $a\mathbf{k}$ should differ by a complete translation vector in the reciprocal point space of G. So the star of a wave vector $\mathbf{k}$ is constructed by finding the inequivalent wave vectors which are obtained by multiplying $\mathbf{k}$ by the matrices a of the underlying point space group operations of the space group G. Since the relation (3) is independent of t' in $(a|t')$ all space groups which have the same underlying point space group have the same set of stars. Moreover, if we write $\mathbf{k} = (\mathbf{k}_x, \mathbf{k}_y, \mathbf{k}_z)$ as (x, y, z) dropping $\mathbf{k}$, $a\mathbf{k}$ becomes (x', y', z') for the point space group operation $(a|0)$ in relation (2). Hence, we have the following important theorem.

THEOREM: *The stars of a space group G are given by the equivalent points in the reciprocal space group of the underlying point space group of G*

For example, in the case of the space group O_h^7 its underlying point space group is O_h^5 whose reciprocal space group is O_h^9 in the notation adopted in the International Tables. So the stars of the space group O_h^7 are given by the equivalent points of O_h^9.

Here it may be noted that the specification of inequivalent wave vectors with respect to the 14 Bravais lattices (see Koster 1956) is incomplete as different space groups G which belong to the same Bravais lattice may have different sets of wave vectors as stars. In fact for the 230 space groups their stars are given by the equivalent points of one or the other of 73 point space groups.

REPRESENTATIONS OF SPACE GROUPS

In the little-group theory the prescription for deriving the irreducible representations of a space group G making use of its solvability property is as follows:

(1) find the underlying point space group G' of G and the reciprocal space group G'' of G'; then the stars $\{\mathbf{k}\}$ of the group G are the equivalent points of G'';

(2) find the little groups $G^{\mathbf{k}}$'s of the second kind corresponding to the representative wave vectors $\mathbf{k}$ of the stars $\{\mathbf{k}\}$ of G;

(3) find a composition series for each of the groups $G^{\mathbf{k}}$'s containing the translational group T;

(4) obtain the allowable representations of each of the $G^{\mathbf{k}}$'s from the allowable representation $\Delta(\mathbf{k})$ of T;

(5) with these allowable representations of $G^{\mathbf{k}}$'s induce the irreducible representations of the space group G.

Example.—Let us consider the two-dimensional space group $p4g$ whose basic symmetry operations can be taken as

$$E \quad xy \quad C_4 \quad y\bar{x} \quad C_y \quad \tfrac{1}{2}-x \quad \tfrac{1}{2}+y \quad C_2 \quad \tfrac{1}{2}-y \quad \tfrac{1}{2}-x$$
$$i \quad \bar{x}\bar{y} \quad C_4^3 \quad \bar{y}x \quad C_x \quad \tfrac{1}{2}+x \quad \tfrac{1}{2}-y \quad C_2' \quad \tfrac{1}{2}+y \quad \tfrac{1}{2}+x,$$

apart from translations ($t_x \rightarrow (1, 0)$, $t_y \rightarrow (0, 1)$) and their products with these basic operations. The description of these operations is quite simple.

The underlying point space group of $p4g$ is $p4m$ and the reciprocal point space group of $p4m$ is $p4m$ itself as it belongs to primitive Bravais lattice. So the stars of $p4g$ are the equivalent points of $p4m$ and are described as below in the *International Tables for X-ray Crystallography.*

a	$4mm$	00				
b	$4mm$	$\frac{1}{2}\frac{1}{2}$				
c	mm	$\frac{1}{2}0$	$0\frac{1}{2}$			
d	m	$x0$	$\bar{x}0$	$0x$	$0\bar{x}$	
e	m	$x\frac{1}{2}$	$\bar{x}\frac{1}{2}$	$\frac{1}{2}x$	$\frac{1}{2}\bar{x}$	
f	m	xx	$\bar{x}\bar{x}$	$\bar{x}x$	$x\bar{x}$	
g	1	xy	$\bar{x}\bar{y}$	$\bar{y}x$	$y\bar{x}$	
		$\bar{x}y$	$x\bar{y}$	yx	$\bar{y}\bar{x}$	

Let us find the $G^{\mathbf{k}}$'s of the first wave vectors of each of the above stars and construct their allowable representations.

Star a (b)

The $G^{\mathbf{k}}$'s in the case of these stars a and b are identical with the space group itself. Let the translational group T of G be augmented by C_x, C_y, and C_4 successively, then we get the groups G_2, G_1, and G, say. A composition series for G is given by

$$G \supset G_1 \supset G_2 \supset T \qquad \text{containing the group } T.$$

The representation of T for the wave vector 00 $(\frac{1}{2}\frac{1}{2})$ is given by $t_x \to 1$, $t_y \to 1$ $(t_x \to -1,\ t_y \to -1)$. C_x transforms a (b) into itself. So the representation $\Delta(00)(\Delta(\frac{1}{2}\frac{1}{2}))$ of T forms a nondegenerate orbit of G_2. As $C_x^2 = t_x$ there are two allowable representations of G_2.

Now, as $\Delta(00)(\Delta(\frac{1}{2}\frac{1}{2}))$ is a one-dimensional representation the matrix M corresponding to C_x which transforms $\Delta(00)(\Delta(\frac{1}{2}\frac{1}{2}))$ into itself can be taken as $M = \lambda$. Since $C_x^2 \to 1 (C_x^2 \to -1)$ in $\Delta(00)(\Delta(\frac{1}{2}\frac{1}{2}))$ is given by $\lambda^2 = 1$ $(\lambda^2 = -1)$. So the two allowable representations of G_2 are

	(00)		$(\frac{1}{2}\frac{1}{2})$	
	C_x	t_y	C_x	t_y
$\Gamma+$	1	1	i	-1
$\Gamma-$	-1	1	$-i$	-1

when specified with respect to the generating elements C_x and t_y of G_2.

G_2 is a normal subgroup of G_1. Since $C_yC_xC_y^{-1} = t_x^{-1}t_yC_x$ the orbits of allowable representations of G_2 in G_1 are $\{\Gamma+\}$ and $\{\Gamma-\}$. As $C_y^2 = t_y$ there are two allowable representations of G_1 for each of these orbits. Proceeding as in the case of the group G_2 we obtain the four following allowable representations of G_1

	(00)		$(\frac{1}{2}\frac{1}{2})$	
	C_x	C_y	C_x	C_y
Δ_1	1	1	i	$-i$
Δ_2	-1	-1	$-i$	i
Δ_3	-1	1	i	i
Δ_4	1	-1	$-i$	$-i$

which are specified with respect to the generating elements C_x and C_y of G_1.

G_1 is a normal subgroup of G. Since $C_4C_xC_4^3 = t_y^{-1}C_y$ and $C_4C_yC_4^3 = t_y^{-1}C_x$ the orbits of allowable representations of G_1 in G are $\{\Delta_1\}$, $\{\Delta_2\}$, and $\{\Delta_3, \Delta_4\}$.

In the case of the nondegenerate orbits $\{\Delta_1\}$ and $\{\Delta_2\}$, proceeding as in the group G_2 and making use of $C_4^2 = i$ we obtain the four following allowable representations of G

(00), G		$(\frac{1}{2}\frac{1}{2})$, G	
C_4	C_x	C_4	C_x
± 1	± 1	$\pm i$	$\pm i$

which are specified with respect to the generating elements C_4 and C_x of G.

In the case of the degenerate orbit $\{\Delta_3, \Delta_4\}$, Δ_3^4 of G from Δ_3 of G_1 is the allowable representation of G. For the coset decomposition $G = G_1 + C_4G_1$ of G and from $C_4^2 = i$, Δ_3^4 is given as shown below.

(00), G^a		(½½), G^b	
C_x	C_4	C_x	C_4
$\begin{bmatrix} 1 & 0 \\ 0 & -1 \end{bmatrix}$	$\begin{bmatrix} 0 & 1 \\ -1 & 0 \end{bmatrix}$	$\begin{bmatrix} i & 0 \\ 0 & -i \end{bmatrix}$	$\begin{bmatrix} 0 & 1 \\ -1 & 0 \end{bmatrix}$

Star c

The first wave vector of the star c is $\frac{1}{2}0$. The little group G^c of the second kind of the wave vector $\frac{1}{2}0$ is given by the basic operations C_x, C_y translations and their products. Let the translational group T be augmented by C_x and C_y successively, then we get the groups G_1^c and G^c, say.

The representation $\Delta(\frac{1}{2}0)$ of T is $t_x \rightarrow -1$, $t_y \rightarrow 1$.

T is a normal subgroup of G_1^c and as C_x transforms the wave vector $\frac{1}{2}0$ into itself $\{\Delta(\frac{1}{2}0)\}$ is the only orbit of allowable representation of T in G_1^c. Proceeding as in the case of the group G_2 in stars a and b and making use of $C_x^2 = t_x$ we obtain the following two allowable representations of G_1^c

	($\frac{1}{2}0$)	
	C_x	t_y
Γ_+	i	1
Γ_-	$-i$	1

which are specified with respect to the generating elements C_x and t_y of G_1^c.

G_1^c is a normal subgroup of G^c. Since $C_yC_xC_y^{-1} = t_x^{-1}t_yC_x$ $\{\Gamma_+, \Gamma_-\}$ is the only orbit of the allowable representations of $G_1{}^c$ in G^c. In the case of this degenerate orbit $\Gamma_+{}^4$ of G^c from Γ_+ of $G_1{}^c$ is the allowable representation of G^c. For the coset decomposition $G^c = G_1^c + C_yG_1^c$ of G^c and from $C_y^2 = t_y$, $\Gamma_+{}^4$ is given by

($\frac{1}{2}0$), G^c	
C_x	C_y
$\begin{bmatrix} i & 0 \\ 0 & -i \end{bmatrix}$	$\begin{bmatrix} 0 & 1 \\ 1 & 0 \end{bmatrix}$

when specified with respect to the generating elements C_x and C_y of G^c.

Stars d and e

The first wave vectors in the case of these two stars are given by $x0$ and $x\frac{1}{2}$ respectively. The groups G^d and G^e of the second kind of these two wave vectors are identical, and are given by the basic operation C_x, translations, and their products.

The representations $\Delta(x0)$ and $\Delta(x\frac{1}{2})$ of T are given by $t_z \rightarrow \exp 2\pi ix$, $t_y \rightarrow 1$, and $t_z \rightarrow \exp 2\pi ix$, $t_y \rightarrow -1$ respectively.

T is a normal subgroup of both G^d and G^e. As C_x transforms the two wave vectors $(x0)$ and $(x\frac{1}{2})$ into themselves $\{\Delta(x0)\}$ and $\{\Delta(x\frac{1}{2})\}$ are the orbits of the allowable representations of T in G^d and G^e respectively. Proceeding as in the case of the group G_2 in the stars a and b and making use of $C_x^2 = t_x$ we obtain the following pairs of allowable representations of G^d and G^e

$(x0)$, G^d		$(x\frac{1}{2})$, G^e	
C_x	t_y	C_x	t_y
$\pm\exp \pi ix$	1	$\pm\exp \pi ix$	-1

when specified with respect to the generating elements C_x and t_y of both the groups G^d and G^e.

Star f

The first wave vector of the star f is xx. The group G^f for the wave vector xx is given by the basic operation C_2', translations, and their products.

The representation $\Delta(xx)$ of T with respect to the wave vector xx is $t_x \rightarrow \exp 2\pi ix$, $t_y \rightarrow \exp 2\pi ix$.

T is a normal subgroup of G^f and as C_2' transforms the wave vector xx into itself $\{\Delta(xx)\}$ is the only orbit of T. Proceeding as in the case of the group G_2 in the stars a and b and making use of $C_2'^2 = t_x t_y$ we obtain the following two allowable representations of G^f

(xx), G^f	
C_2'	t_x
$\pm\exp 2\pi ix$	$\exp 2\pi ix$

when specified with respect to the generating elements C_2' and t_x of G^f.

Star g

The first wave vector of the star g is xy. The group G^g of this wave vector is given by the translational group T itself. So the allowable representation of this group is

(xy), G^g	
t_x	t_y
$\exp 2\pi ix$	$\exp 2\pi iy$

when specified with respect to the generating elements t_x and t_y of T.

Moreover, it is easily verified in the case of all the above allowable representations of the different groups G^k's that they satisfy the completeness relation.

ACKNOWLEDGMENTS

The author expresses his grateful thanks to Prof. K. Venkateswarlu, Professor and Head of the Department of Physics, Annamalai University, and Prof. T. Venkatarayudu, Professor in Mathematical Physics Department, Andhra University, for their keen interest in this work.

REFERENCES

BOUCKAERT, L., SMOLUCHOWSKI, R., and WIGNER, E. 1936. Phys. Rev. **50**, 58.
HENRY, NORMAN F. M. and LONSDALE, KATHLEEN. 1952. International tables for X-ray crystallography.
HERRING, C. 1942. J. Franklin Inst. **233**, 525.
KOSTER, G. F. 1957. Solid State Physics, Vol. 5, 173.
LOMONT, J. S. 1959. Applications of finite groups (Academic Press, New York).
SEITZ, F. 1936. Ann. Math. **37**, 17.
ZASSENHAUS, H. 1949. Theory of groups (Chelsea Pub. Co.).

THE KNIGHT SHIFT OF CADMIUM IN SOME ALLOYS WITH GROUP IB AND IIB METALS[1]

R. F. GRANT[2] AND W. G. HENRY

ABSTRACT

The Knight shift of the Cd^{111} and the Cd^{113} resonance in the primary solid solutions of silver, gold, magnesium, zinc, and mercury in cadmium has been investigated. The effect of the solute metal on the Knight shift of the solvent is discussed in terms of the charge displacements.

1. INTRODUCTION

It has been suggested by Townes, Herring, and Knight (1950) that the Knight shift may be represented by

$$\frac{\Delta\nu}{\nu} = \frac{8\pi}{3}\chi_p M\langle|\psi_F(0)|^2\rangle_{Av} \tag{1.1}$$

where ν and $\nu+\Delta\nu$ are the resonance frequencies in the non-metal and metal respectively; χ_p is the spin paramagnetism of the conduction electrons per gram, M is the gram atomic weight, and $\langle|\psi_F(0)|^2\rangle_{Av}$ is the probability density at the nucleus, of a given species, for all electronic states on the Fermi surface. Blandin and Daniel (1959) presented an explanation of the Knight shift in monovalent–polyvalent solid solutions which appears to give a reasonable numerical agreement for these systems. It is, however, not applicable to systems with metals of the same valency. An alternative approach, which appears to give a satisfactory explanation for both monovalent–polyvalent and monovalent–monovalent systems, was suggested by Henry (1960). The experimental work presented here is a further test of the applicability of the last-mentioned approach to divalent–divalent and divalent–monovalent systems. The results suggest that certain modifications to the original idea are required.

2. METHOD

The nuclear magnetic resonance spectrometer employed a marginal oscillator of the Pound–Knight–Watkins' type (1950), followed by a phase sensitive detector (Schuster 1951) with an output time constant of 60 seconds. The magnet was a Newport Type A with 10 cm diameter pole faces and a 3-cm gap. Well-regulated current was supplied to the magnet by a transistorized power supply (Garwin 1958). The magnetic field was held constant and was modulated at 30 cycles/sec by means of coils taped to the pole faces. The spectrometer frequency was swept at about 2 kc/sec per hour and was measured

[1]Manuscript received February 8, 1961.
Contribution from the Division of Applied Chemistry, National Research Council, Ottawa, Canada.
Issued as N.R.C. No. 6308.
[2]Present address: British Columbia Research Council, Vancouver, Canada.

with a BC 221 frequency meter. The magnetic field was set at 4000 gauss and the maximum absorption frequency of the metal resonance was compared to that of Na^{23} in NaOH solution after each measurement.

The alloys were prepared by melting and chill-casting the constituents in a vacuum induction furnace (Craw and Henry 1956). The purity of all the materials was 99.99% or better. The alloys were annealed for several days close to the melting point and were either air-cooled or quenched. The homogeneity was checked by spectrographic analyses; the presence of another phase was checked for by X-ray analyses. A portion of each alloy was analyzed chemically. Each alloy was ground by a method suggested by Drain (1959), to pass 325 mesh and the powder was cast in a paraffin wax cylinder which could be placed directly in the spectrometer sample coil.

3. RESULTS

The Knight shift for Cd^{111} and Cd^{113} in the various alloys are given in Table I. Each result is the mean of at least four measurements. The Knight

TABLE I

Atomic per cent solute	Knight shift of Cd^{111} in per cent	Knight shift of Cd^{113} in per cent
None	0.402±.002	0.405±.004
5.03±0.05 Ag	0.419±.004	0.420±.004
3.11±0.05 Au	0.406±.003	0.410±.003
4.69±0.05 Hg	0.426±.002	0.426±.004
10.00±0.05 Hg	0.443±.002	0.448±.004
14.32±0.05 Hg	0.471±.003	0.472±.005
4.71±0.05 Mg	0.398±.002	0.400±.003
10.20±0.05 Mg	0.394±.002	0.396±.002
4.44±0.05 Zn	0.397±.002	0.398±.003

shift was calculated on the basis of the published frequency for cadmium in the non-metallic state (Pake 1956). At 4000 gauss this is 3611.2 kc/sec for Cd^{111} and 3777.6 kc/sec for Cd^{113}.

The Knight shifts for Cd^{111} and Cd^{113} in the pure metal are in reasonable agreement with the values reported by Knight (1956), Rowland (1956), and Drain (1959) which have a range from 0.39 to 0.41_5. The change in the Knight shift of the solvent seems to be linear in the cadmium–mercury and cadmium–magnesium systems and the straight lines pass through the value for pure cadmium. The cadmium–silver alloy was found to contain a small amount, of the order of a few per cent, of a second phase; the Knight shift reported, which agrees well with a result obtained by Drain (1959) on extrapolation from a two-phase region, probably corresponds to the saturated solution. In the cadmium–gold and cadmium–zinc systems, the alloys measured are close to the limit of solubility. The results are shown in Fig. 1.

4. DISCUSSION

In monovalent metal-based alloys, it was suggested (Henry 1960) that the decrease in the observed Knight shift might be associated with the decrease

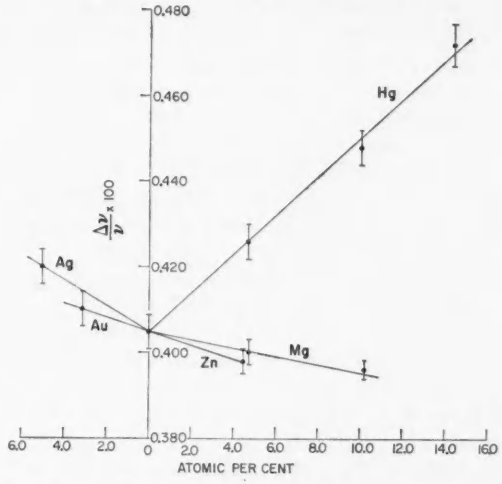

FIG. 1. The Knight shift of Cd^{113} in per cent for the solutes: Ag, Au, Mg, Zn, and Hg in Cd.

in the local charge density at the solvent atoms which may occur on the addition of a polyvalent solute. For divalent metals a decrease in the local charge density at the solvent site may have an opposite effect. In a divalent metal solid solution, if one electron is partially removed from a solvent atom by the larger effective nuclear charge of neighboring solute atoms, then the effective nuclear charge on the remaining electron is increased. In addition, there is a tendency away from a "$^1S_0$-like state" to a "$^2S_{1/2}$-like state". This together with the increased probability of the electron being at the nucleus would cause an increase in the Knight shift. The result of an increase in the charge density at the solvent site of a divalent metal may depend on the character of the state which the charge occupies.

An indication of the charge transfer may be obtained from the experimentally determined heats of solution. The means of the first two ionization energies of the series magnesium, zinc, cadmium, and mercury are approximately 11.3, 13.6, 12.9, and 14.5 ev respectively. According to a simple model (Henry 1958), the relative heats of solution of magnesium, zinc, and mercury in cadmium should vary approximately as the square of the differences between the means of the first two ionization energies of the metals and the mean of the first two ionization energies of cadmium; that is, as 1:0.20:1. It is found that the infinite heat of solution of magnesium (Trumbore, Wallace, and Craig 1954) and mercury (Kubaschewski and Evans 1951) in cadmium are about equal in the solid state and have a value of about -2.0 kcal per mole. The heat of solution of zinc in cadmium (Kubaschewski and Evans 1951) is positive. These results are in reasonable agreement with the simple model and are to be interpreted on the basis of this model as indicating a charge transfer from magnesium to cadmium in the cadmium–magnesium system

and a charge transfer of the same order of magnitude from cadmium to mercury in the cadmium–mercury system. In the cadmium–zinc system little or no charge transfer is to be expected.

Kleppa (1956) measured the heats of formation of the liquid cadmium rich alloys in the cadmium–silver and cadmium–gold systems; the infinite heats of solution when corrected for the latent heat of fusion of the noble metals in the solid alloys are approximately −5.8 and −13.8 kcal per mole respectively. The simple theory referred to above would suggest, on the basis of the measured heats of solution, that in these two systems charge is transferred from the solute to the solvent and that more charge is transferred in the cadmium–gold system than in the cadmium–silver system. It should be pointed out that this conclusion is not in accord with the idea that the amount of charge transferred should be proportional to the differences between the ionization energies of gold and silver, which are 9.2 and 7.5 ev respectively, and the mean of the first two ionization energies of cadmium. That the heat of solution should be large and negative is in accord with the theory but the order of magnitudes is reversed.

It is therefore suggested that the increase in the Knight shift observed on the cadmium–mercury system is associated with the transfer of charge from the solvent sites to the solute. In the cadmium–zinc system the relatively small change in the Knight shift may be associated with the relatively small charge transfer. In the cadmium–magnesium system and in the cadmium–noble metal systems on the other hand, where it is thought that the transfer of charge is from the solute to the solvent, the Knight shift is decreased in the magnesium system and increased in the noble metal systems. It should be noted, however, that the donors are of different valency, which may determine the character of the state of the donated charge. It should be further noted that the increase in the Knight shift in the cadmium–gold system is less than in the cadmium–silver system, which is in keeping with the suggestion that the amount of charge transferred in the cadmium–gold system is less.

ACKNOWLEDGMENTS

The authors wish to thank Mr. D. S. Russell and Dr. L. D. Calvert for the chemical and X-ray analyses respectively.

REFERENCES

BLANDIN, A. and DANIEL, E. 1959. Phys. Chem. Solids, **10**, 126.
CRAW, D. A. and HENRY, W. G. 1956. J. Sci. Instr. **33**, 22.
DRAIN, L. E. 1959. Phil. Mag. **4**, 484.
GARWIN, R. L. 1958. Rev. Sci. Instr. **29**, 223.
HENRY, W. G. 1958. Can. J. Phys. **36**, 611.
——— 1960. Proc. Phys. Soc. **76**, 989.
KLEPPA, O. J. 1956. J. Phys. Chem. **60**, 846, 858.
KNIGHT, W. D. 1956. Solid state physics, Vol. 2 (The Academic Press, New York), p. 122.
KUBASCHEWSKI, O. and EVANS, E. LL. 1951. Metallurgical thermochemistry (Butterworth–Springer Ltd., London), p. 310.
PAKE, G. E. 1956. Solid state physics, Vol. 2 (The Academic Press, New York), p. 4.
POUND, R. V. and KNIGHT, W. D. 1950. Rev. Sci. Instr. **21**, 219.
ROWLAND, T. J. 1956. Phys. Rev. **103**, 1670.
SCHUSTER, N. A. 1951. Rev. Sci. Instr. **22**, 254.
TOWNES, C. H., HERRING, C., and KNIGHT, W. D. 1950. Phys. Rev. **77**, 852.
TRUMBORE, F. A., WALLACE, W. E., and CRAIG, R. S. 1954. J.A.C.S. **76**, 6417.

NUCLEAR SPIN RELAXATION IN GASES AND LIQUIDS

I. CORRELATION FUNCTIONS[1]

IRWIN OPPENHEIM[2] AND MYER BLOOM[3]

ABSTRACT

Calculation of nuclear spin–lattice relaxation times T_1 in liquids and gases involves the correlation functions of the matrix elements between different spin states of the interaction coupling the nuclear spin to other degrees of freedom of the system. The correlation functions are expressed in terms of a time-dependent pair-distribution function (TDPDF) for the system. The TDPDF is evaluated using the Wigner distribution function to describe the equilibrium ensemble of the gas or liquid. A time expansion of the dynamics of the system to a constant acceleration approximation and use of the symmetry properties of the TDPDF leads to an expression of the form

$$g(\mathbf{R}^2, \mathbf{R'}^2, t) = [g(R)]^{1/2}\,[g(R')]^{1/2}\,P(\mathbf{R}^2, \mathbf{R'}^2, t).$$

This form for the TDPDF is derived for the high temperature dilute gas, for the dilute gas with first quantum correction, and for classical liquids in which the molecular dynamics can be described by the Langevin equation. The quantity $g(R)$ is the radial distribution function appropriate to each case. The quantity $P(\mathbf{R}^2, \mathbf{R'}^2, t)$ is the free particle TDPDF for the classical gas; it is the classical free particle TDPDF at an effective temperature for the quantum gas; it is the product of solutions to the diffusion equation for the liquid multiplied by the (density)^2.

1. INTRODUCTION

One of the quantities measurable in nuclear magnetic resonance experiments is the rate at which thermal equilibrium is established among the nuclear spin energy levels. The mechanism for the attainment of equilibrium involves a coupling of the spin degrees of freedom with other degrees of freedom in the material. The rate at which thermal equilibrium is established is often expressible in terms of a single parameter T_1 called the spin–lattice relaxation time. Since T_1 is a measure of the rate at which energy is exchanged between the nuclear spin system and the other degrees of freedom in the material in which the spins are located, measurements of T_1 are capable of giving detailed information about the molecular properties of matter. Measurements and interpretations of T_1 have been made on a variety of interesting systems and general theories of T_1, valid for a wide class of systems, have been formulated (Bloembergen, Purcell, and Pound 1948; Redfield 1957; Bloch 1957; Kubo and Tomita 1954).

In this paper we investigate the interpretation of T_1 measurements in gases and liquids in terms of their fundamental statistical mechanical properties. A considerable background of theory applicable to gases and liquids is already

[1]Manuscript received February 14, 1961.
Contribution from the Department of Physics, University of British Columbia, Vancouver, B.C.
[2]Physics Section, Convair, San Diego. A portion of this research was carried out at the Heat Division, National Bureau of Standards, Washington, D.C., and was supported by the U.S.A.E.C., Division of Research.
[3]Research supported by the National Research Council of Canada.

available. The general formulae for T_1 previously derived may be applied to systems in which the coupling between the nuclear spin system and the "lattice" ("lattice" here refers to all degrees of freedom of the gas or liquid, other than the spin system) satisfies the following properties: (1) the coupling is "weak" in the sense that time-dependent perturbation theory may be used, (2) there is only a negligible reaction of the spin system on the "lattice". The "lattice" may be described by a Boltzmann distribution with modulus T. When the above conditions are satisfied, the transition probability per unit time W between nuclear spin states differing by energy $\hbar\omega_0$, is proportional to the amplitude at the angular frequency ω_0 of the Fourier transform of the correlation function of $a(t)$, the matrix element coupling the two spin states (Bloembergen *et al.* 1948), i.e.

$$W \propto J(\omega_0) = \int_{-\infty}^{\infty} e^{i\omega_0 t} k(t)\, dt. \tag{1}$$

The correlation function $k(t) = (N-1)\langle a(t')a^*(t'+t)\rangle$ is the ensemble average of the product of the matrix element at two different times t' and $t'+t$ and in the equilibrium ensemble depends only on $|t|$.

In Section 2 we present a brief survey of the forms of $a(t)$ for monatomic gases and for diatomic hydrogen molecules. We remark that only in special cases can the spin relaxation be described in terms of a single parameter. More generally, one has to deal with a relaxation matrix (Redfield 1957; Bloch 1957) which involves transition probabilities between various pairs of spin states. In such cases, one must measure all the terms which appear in the relaxation matrix to describe the relaxation completely. Each term in the matrix will, however, involve expressions similar to (1), and hence each measurable parameter can be related to specific correlation functions if the complete Hamiltonian for spin–lattice coupling is known.

Approximate formulae for T_1 for monatomic and diatomic gases have been derived using simple collision models (Bloembergen *et al.* 1948). These formulae, although suitable for order of magnitude calculations at high temperatures do not allow a detailed interpretation of T_1 in terms of the appropriate molecular properties of the gas. In this paper we calculate the correlation functions appearing in T_1 from first principles using the Wigner distribution function (Wigner 1932) to compute the ensemble averages. It will be shown in Section 3 that the correlation functions can be calculated in terms of a time-dependent pair-distribution function (TDPDF) similar to, but not identical with, that introduced by van Hove (1954) to describe inelastic neutron diffraction.

Section 4 deals with the evaluation of the TDPDF for high temperature gases, first in the limit of the dilute gas where only binary collisions are important. The calculation is then extended to higher densities at which three-body collisions may be important, corresponding to the region in which the third virial coefficient plays a role in the equation of state. The calculation involves a time expansion of the dynamics of the system, to an approximation which we call the constant acceleration approximation, and also makes use

of the symmetry properties of the TDPDF. The approximations utilized yield expressions for the TDPDF which have the same functional dependence on the pair distribution function for the denser gas and for the dilute gas. Furthermore, in Section 5, in which the first quantum correction for the dilute gas is calculated from the previously derived expansion of the Wigner distribution function in powers of $\hbar$ (Wigner 1932), the expression for the TDPDF is expressed in the same form as for the classical case. In the quantum expression, the temperature T is replaced by an effective temperature T_e, defined by the relation

$$\frac{3}{2}kT_e(R) = \left\langle \frac{p^2}{2m} \right\rangle. \tag{2}$$

In eq. (2), p and m refer, respectively, to the momentum and mass of a gas molecule and the average is over an ensemble in which a pair of molecules are separated by a fixed distance R.

In Section 6 we derive the form of the TDPDF in classical dense gases and liquids. We assume that the particle dynamics can be described in terms of generalized Langevin equations. The constant acceleration approximation is made. The functional dependence of the TDPDF on the pair-distribution function is the same as that for the classical and quantum dilute gas. The time-dependent term is, however, quite different.

In Section 7 we compare our results with those of previous theories for some special cases. Detailed comparison with experiment will be reported in a subsequent paper.

2. THE FORM OF THE MATRIX ELEMENTS

In this section we present the explicit forms for the matrix elements for systems of monatomic and diatomic molecules. We also discuss the relationship of these matrix elements to T_1. It is necessary to distinguish between monatomic and polyatomic molecules because of the rotational degrees of freedom available to the latter.

The simplest case is that of a system of N identical monatomic atoms with nuclei of spin $\frac{1}{2}$. In this case, the only important interaction coupling the nuclear spin system to the translational degrees of freedom is the magnetic dipole–dipole interaction between pairs of nuclear spins. The Hamiltonian for this interaction is written as

$$\mathcal{H}_{\text{dip-dip}} = \gamma^2\hbar^2 \sum_{i>j}^{N} \left[\frac{\mathbf{I}_i \cdot \mathbf{I}_j}{R_{ij}^3} - \frac{3(\mathbf{I}_i \cdot \mathbf{R}_{ij})(\mathbf{I}_j \cdot \mathbf{R}_{ij})}{R_{ij}^5} \right] \tag{3}$$

where γ is the nuclear gyromagnetic ratio,

$\mathbf{R}_{ij}$ is the vector joining the ith and jth nuclei with polar co-ordinates R_{ij}, θ_{ij}, ϕ_{ij}, and

$\mathbf{I}_i$ is the angular momentum operator for the ith nucleus.

The well-known expression for T_1 due to this interaction is (Bloembergen *et al.* 1948; Kubo and Tomita 1954)

$$\frac{1}{T_1} = \frac{3}{2}\gamma^4\hbar^2 I(I+1)[J_1(\omega_0)+J_2(2\omega_0)] \tag{4}$$

where ω_0 is the Larmor frequency of the nuclei and

$$J_m(\omega) = \int_{-\infty}^{\infty} e^{i\omega t} k_m(t)\, dt, \qquad m = 1, 2. \tag{5}$$

In liquids and gases the correlation functions $k_m(t)$ are defined to be of the form

$$k_m(t) = \left\langle \sum_{j \neq i} a_m^{ij}(t') a_m^{*ij}(t'+t) \right\rangle = (N-1)\langle a_m(t') a_m^*(t'+t)\rangle \tag{6}$$

where

$$a_1(t) = \left(\frac{8\pi}{15}\right)^{1/2} \frac{Y_{21}(\theta,\phi)}{R^3},$$

$$a_2(t) = \left(\frac{32\pi}{15}\right)^{1/2} \frac{Y_{22}(\theta,\phi)}{R^3}, \tag{7}$$

and $Y_{21}(\theta,\phi)$ and $Y_{22}(\theta,\phi)$ are spherical harmonics.

In relating T_1 to correlation functions of the form given in eq. (6), the assumption was made (Bloembergen *et al.* 1948) that only pair spin correlations are of importance. In more general formulations of the theory, 3- and 4-spin particle correlations are also required, since the rate of change of the density matrix for the spin system involves terms of the form (Redfield 1957)

$$\langle a_m^{ij}(t') a_m^{kl*}(t'+t)\rangle. \tag{8}$$

In this paper we restrict ourselves to cases in which only pair correlation functions are of importance, which corresponds to neglecting off-diagonal terms in the spin density matrix. The methods used here could be extended, however, to include 3- and 4-spin correlations.

The matrix elements $a_1(t)$ and $a_2(t)$ are implicit functions of time because of their dependence on $\mathbf{R}(t)$. In the following sections we shall evaluate these correlation functions explicitly, calculating $\mathbf{R}(t)$ to a certain approximation from the equations of motion of the molecules.

An additional contribution to T_1 is present in systems of monatomic gases having nuclei with $I > \frac{1}{2}$ due to coupling between the nuclear electric quadrupole moments and electric field gradients induced at the nuclei during collisions. The form of the correlation functions in this case is similar to the above and has been derived by Adrian (1955).

The mechanisms for spin–lattice relaxation described above are present in systems of diatomic molecules such as H_2, HD, etc. but are usually negligible compared with the effects of intramolecular interactions. In H_2 (Bloembergen *et al.* 1948; Bloom 1957), the two protons interact with each other by dipole–dipole interaction and also interact with the magnetic field produced by the magnetic moment of the molecule itself. In this case T_1 can be expressed in

terms of correlation functions of $\mathbf{J}$, the rotational angular momentum of the molecule. This quantity is time dependent because of collisions between molecules which cause molecular reorientations. At low temperatures all of the ortho-H_2 molecules are in their lowest rotational state ($J = 1$) and the time dependence of $\mathbf{J}$ is due to collisions between molecules which cause transitions between the $m_J = 1, 0, -1$ states of the molecules. The intermolecular interactions which produce these transitions are anisotropic forces which depend on the relative orientations of pairs of molecules. If $\mathcal{H}_R$ is the Hamiltonian for these interactions, $\mathbf{J}(t)$ can be written in the form

$$\mathbf{J}(t) = \exp[it\mathcal{H}_R/\hbar]\mathbf{J}\exp[-it\mathcal{H}_R/\hbar]. \tag{9}$$

A detailed discussion of the exact relationship between T_1 and correlation functions of $\mathbf{J}(t)$ has been given for solid, liquid, and gaseous H_2 (Moriya and Motizuki 1957; Moriya 1957; Oppenheim and Bloom 1959; Bloom 1960). We do not reproduce the explicit relationship between T_1 and $\langle \mathbf{J}(t')\mathbf{J}(t'+t)\rangle$ because of its complexity. In evaluating these correlation functions, $\mathcal{H}_R$ is written in terms of $\mathbf{R}_{ij}(t)$ as well as $\mathbf{J}_i$ and $\mathbf{J}_j$. Again, $\mathbf{R}_{ij}(t)$ is calculated from the equations of motion for the system and the final result is found by averaging over all the m_J states. The general form of the correlation functions to be evaluated is similar to eq. (6), but involves a sum of terms of the form $a \sim Y_{lm}(\theta,\phi)/R^n$, with $n \geqslant 5$.

3. CORRELATION FUNCTIONS

In this section we derive general expressions for the correlation functions that appear in calculations of T_1. We make use of the Wigner distribution function in order to unify the treatments of quantum and classical systems.

We consider systems which consist of N identical molecules. We assume that the Hamiltonian of the system can be written in the form $H = H_0 + U$, where H_0 is the Hamiltonian for the system of N interacting structureless particles and U includes all of the interactions which produce spin transitions. The Hamiltonian H_0 is given by

$$H_0 = \frac{\mathbf{p}^N \cdot \mathbf{p}^N}{2m} + V(\mathbf{R}^N) \tag{10}$$

where

$$\mathbf{p}^N \cdot \mathbf{p}^N = \sum_{i=1}^{N} \mathbf{p}_i \cdot \mathbf{p}_i \tag{11}$$

and $\mathbf{p}_i$ is the momentum of the center of mass of the ith particle. The notation $V(\mathbf{R}^N)$ implies that V is a function of the $3N$ co-ordinates $\mathbf{R}_1, \ldots, \mathbf{R}_N$ where $\mathbf{R}_i$ is the vector position of the center of mass of the ith particle. The quantity $V(\mathbf{R}^N)$ is that part of the potential energy of the system which depends only on the positions of the center of masses of the particles of the system. In the systems treated here

$$V(\mathbf{R}^N) = \sum_{\substack{i<j \\ 1}}^{N} V_{ij} \tag{12}$$

where

$$V_{ij} = V(\mathbf{R}_i, \mathbf{R}_j).$$

V_{ij} is that part of the interaction between the ith and the jth particle which depends only on the positions of their centers of mass. We make the additional assumption that

$$V_{ij} = V(|\mathbf{R}_{ij}|) \tag{13}$$

where $\mathbf{R}_{ij} = \mathbf{R}_i - \mathbf{R}_j$. Thus V_{ij} depends only on the scalar distance between particles i and j. For most systems, the form of V_{ij} is that of the Lennard–Jones potential. The interaction U is assumed to be small compared to V and is of the form

$$U = \sum_{\substack{i<j \\ 1}}^{N} U_{ij}$$

where U_{ij} depends on the configurations of the ith and jth molecules.

The correlation functions that are of interest are of the form

$$k(t) = (N-1)\langle a(t')a^*(t+t')\rangle. \tag{14}$$

The matrix elements $a(t)$ have been discussed in Section 2. They are non zero because of the existence of the interaction U. As discussed in Section 2, the matrix elements can be written more explicitly as

$$\begin{aligned} a(t') &= a(\mathbf{R}^2(t')) \\ a(t+t') &= a(\mathbf{R}^2(t+t'), t). \end{aligned} \tag{15}$$

The notation $\langle G\rangle$ stands for the ensemble average of G. The ensemble over which G is averaged is that characterized by the Hamiltonian H_0, which is the Hamiltonian for the lattice degrees of freedom. Since U is small the lattice remains undisturbed and the average is over an equilibrium ensemble.

An explicit expression for the correlation function for a classical system is

$$k(t) = (N-1)\int f_{\mathrm{cl}}^N(\mathbf{R}^N,\mathbf{p}^N)a_{\mathrm{cl}}^*(\mathbf{R}^2(t+t'),t)a_{\mathrm{cl}}(\mathbf{R}^2(t'))d\mathbf{R}^N d\mathbf{p}^N \tag{16}$$

where f_{cl}^N is the classical equilibrium ensemble distribution function. The quantity $a_{\mathrm{cl}}(\mathbf{R}^2(t+t'),t)$ is a classical dynamical quantity. The notation $\mathbf{R}^2(t+t')$ represents the functional dependence of the configurations of particles 1 and 2 at time $t+t'$ on the set of variables $\mathbf{R}^N$ and $\mathbf{p}^N$ at time t'. This dependence is determined by the classical equations of motion.

The correlation function for many quantum systems can be written in terms of the density matrix, ρ, in the form

$$k(t) = (N-1)\mathrm{Tr}\{\tfrac{1}{2}(a(t')a^*(t+t')+a(t+t')a^*(t'))\rho\} \tag{17}$$

where

$$a(t+t') = \exp[iH_0t/\hbar]a(\mathbf{R}^2(t'),t)\exp[-iH_0t/\hbar]. \tag{18}$$

In the following, we present a unified discussion of the quantum and classical correlation functions in terms of the Wigner distribution function.

The Wigner distribution function (WDF) (Wigner 1932) is denoted by $f^N(\mathbf{R}^N,\mathbf{p}^N)$ for a system of N identical particles having $3N$ position co-ordinates $\mathbf{R}^N = (\mathbf{R}_1, \mathbf{R}_2, \ldots, \mathbf{R}_N)$ and $3N$ momentum co-ordinates $\mathbf{p}^N$. This distribution function has the property that the average of some quantum mechanical observable G which is related to a classical dynamical quantity $G_{\mathrm{W}}(\mathbf{R}^N,\mathbf{p}^N)$ by means of the Weyl correspondence is given by

$$\langle G\rangle = \mathrm{Tr}\{G\rho\} = \int f^N(\mathbf{R}^N,\mathbf{p}^N)G_{\mathrm{W}}(\mathbf{R}^N,\mathbf{p}^N)d\mathbf{R}^N d\mathbf{p}^N. \tag{19}$$

The WDF is related to the density matrix by the expression

$$f^N(\mathbf{R}^N,\mathbf{p}^N) = \left(\frac{1}{\pi\hbar}\right)^{2N}\int \exp[(2i/\hbar)\mathbf{p}^N\cdot\mathbf{Y}^N]\rho(\mathbf{R}^N+\mathbf{Y}^N,\mathbf{R}^N-\mathbf{Y}^N)d\mathbf{Y}^N. \tag{20}$$

It cannot be interpreted as being a phase space probability function since it can be negative. The reason for this is the fact that $\mathbf{R}^N$ and $\mathbf{p}^N$ cannot all be specified in a quantum mechanical system. However, the integral of the WDF over momentum space yields

$$n(\mathbf{R}^N) = \int f^N(\mathbf{R}^N,\mathbf{p}^N)d\mathbf{p}^N \tag{21}$$

where $n(\mathbf{R}^N)$ is the probability distribution function in configuration space. The advantages of the WDF formalism are that quantum mechanical averages can be obtained by using classical dynamical quantities and that the WDF becomes the classical phase space distribution function in the classical limit.

We may rewrite the correlation function in terms of the WDF in the form

$$k(t) = (N-1)\int f^N(\mathbf{R}^N,\mathbf{p}^N)[a(\mathbf{R}^2_{t'}(\mathbf{R}^N,\mathbf{p}^N))\, a^*(\mathbf{R}^2_{t'+t}(\mathbf{R}^N,\mathbf{p}^N),t)]_{\mathrm{W}}\, d\mathbf{R}^N d\mathbf{p}^N \tag{22}$$

where we have written $\mathbf{R}^2(t') = \mathbf{R}^2_{t'}(\mathbf{R}^N,\mathbf{p}^N)$, etc. to indicate that the vector $\mathbf{R}^2(t')$ is completely specified in terms of the $6N$ co-ordinates $\mathbf{R}^N, \mathbf{p}^N$ at the time t_0. The WDF for the system is $f^N(\mathbf{R}^N,\mathbf{p}^N)$ at the time t_0. The quantity $[a(\mathbf{R}^2_{t'})a^*(\mathbf{R}^2_{t+t'}, t)]_{\mathrm{W}}$ is the classical dynamical quantity related to the quantum mechanical operator $a(t')a^*(t+t')$ by the Weyl correspondence. For a system in thermodynamic equilibrium eq. (22) is independent of t_0 and also of t'. We may therefore put $t_0 = t' = 0$ and rewrite (22) in the form

$$k(t) = (N-1)\int f^N(\mathbf{R}^N,\mathbf{p}^N)[a(\mathbf{R}^2)a^*(\mathbf{R}^2_t(\mathbf{R}^N,\mathbf{p}^N),t)]_{\mathrm{W}}\, d\mathbf{R}^N\, d\mathbf{p}^N. \tag{23}$$

In the following we restrict ourselves to temperature and density regions in which the particles obey Maxwell–Boltzmann statistics but in which quantum mechanics may be important. The theory can be generalized to include very low temperatures when the system obeys quantum statistics (Bose–Einstein

or Fermi–Dirac), since it is possible to make a formal separation of the problem of statistics from that of quantum dynamics (Oppenheim and Ross 1957), but we restrict ourselves here to a consideration of quantum dynamics.

Equation (23) can now be rewritten in a more convenient form when we introduce new variables $(\mathbf{R}'_1,\mathbf{R}'_2) = \mathbf{R}'^2$ and write

$$k(t) = \frac{1}{N}\int [a(\mathbf{R}^2)a^*(\mathbf{R}'^2, t)]_{\mathrm{W}}\, g(\mathbf{R}^2,\mathbf{R}'^2, t)\, d\mathbf{R}^2 d\mathbf{R}'^2 \tag{24}$$

where

$$g(\mathbf{R}^2,\mathbf{R}'^2,t) = N(N-1)\int f^N(\mathbf{R}^N,\mathbf{p}^N)\delta(\mathbf{R}'^2-\mathbf{R}_t{}^2(\mathbf{R}^N,\mathbf{p}^N))d\mathbf{R}^{N-2}d\mathbf{p}^N \tag{25}$$

and $\delta(\mathbf{R}'^2-\mathbf{R}_t{}^2(\mathbf{R}^N, \mathbf{p}^N))$ is shorthand notation for the product of six Dirac delta functions. The quantity $g(\mathbf{R}^2,\mathbf{R}'^2,t)$ is the simultaneous probability per (unit volume)[4] that two particles have position co-ordinates between $\mathbf{R}_1$, $\mathbf{R}_1+d\mathbf{R}_1$, and $\mathbf{R}_2$, $\mathbf{R}_2+d\mathbf{R}_2$ at $t = 0$ and between $\mathbf{R}'_1$, $\mathbf{R}'_1+d\mathbf{R}'_1$ and $\mathbf{R}'_2$, $\mathbf{R}'_2+d\mathbf{R}'_2$ at a time t. It is the time-dependent pair-distribution function (TDPDF) of Section 1. At time 0 it reduces to the static pair co-ordinate space distribution function times $\delta(\mathbf{R}'^2-\mathbf{R}^2)$. $g(\mathbf{R}^2, \mathbf{R}'^2, t)$ is symmetric with respect to interchange of $\mathbf{R}^2$, $\mathbf{R}'^2$.

The problem in calculating $\langle a(t')a^*(t'+t)\rangle$ is now reduced to a calculation of the TDPDF (25), which we now proceed to do for several systems of interest. Then expressions for the correlation functions will be obtained by evaluating (24).

4. THE TIME-DEPENDENT PAIR-DISTRIBUTION FUNCTION FOR THE CLASSICAL GAS

In a classical system the WDF is identical with the classical distribution function, which can be written in the form

$$f^N_{\mathrm{cl}}(\mathbf{R}^N, \mathbf{p}^N) = A^{(N)} \exp[-\beta H^N_{\mathrm{cl}}] \tag{26}$$

where $\beta = 1/kT$, $A^{(N)}$ is a normalization factor, and H^N_{cl} is the classical Hamiltonian for the N particle system, which is assumed to have the form

$$H^N_{\mathrm{cl}} = \frac{\mathbf{p}^N\cdot\mathbf{p}^N}{2m} + V(\mathbf{R}^N). \tag{27}$$

The N-particle distribution function is normalized such that

$$\int f^N(\mathbf{R}^N,\mathbf{p}^N)d\mathbf{R}^N d\mathbf{p}^N = 1. \tag{28}$$

Thus, the normalization factor $A^{(N)}$ is given by

$$A^{(N)} = \left(\frac{\beta}{2\pi m}\right)^{3N/2}\left\{\int \exp[-\beta V(\mathbf{R}^N)]\, d\mathbf{R}^N\right\}^{-1} \tag{29}$$

where the co-ordinate integrations extend over the volume V of the system. Reduced distribution functions $f^{(n/N)}(\mathbf{R}^n, \mathbf{p}^n)$ are defined by the relations

$$f^{(n/N)} = \frac{N!}{(N-n)!}\int f^N(\mathbf{R}^N,\mathbf{p}^N)\, d\mathbf{R}^{N-n}\, d\mathbf{p}^{N-n}. \tag{30}$$

In particular, for fluid systems

$$f^{(0/N)} = 1 \tag{31}$$

$$f_{\mathrm{cl}}^{(1/N)}(\mathbf{R}_1,\mathbf{p}_1) = \frac{N}{V}\left(\frac{\beta}{2\pi m}\right)^{3/2} \exp[-\beta p_1^2/2m] \tag{32}$$

and

$$f_{\mathrm{cl}}^{(2/N)}(\mathbf{R}^2,\mathbf{p}^2) = \frac{(N)(N-1)}{V^2}\left(\frac{\beta}{2\pi m}\right)^3 \exp\left[-\frac{\beta}{2m}(p_1^2+p_2^2)\right] g_{\mathrm{cl}}(\mathbf{R}^2) \tag{33}$$

where $g_{\mathrm{cl}}(\mathbf{R}^2)$ the radial distribution function is given by

$$g_{\mathrm{cl}}(\mathbf{R}^2) = V^2\left\{\int \exp[-\beta V(\mathbf{R}^N)]d\mathbf{R}^{N-2}\right\}\left\{\int \exp[-\beta V(\mathbf{R}^N)]d\mathbf{R}^N\right\}^{-1}. \tag{34}$$

We first derive the form of the TDPDF in the limit of zero density and then extend this result to obtain the first density correction. In the zero density limit the trajectory of a pair of particles depends only on the interactions between that pair. Thus, $\mathbf{R}_t^2(\mathbf{R}^N,\mathbf{p}^N) = \mathbf{R}_t^2(\mathbf{R}^2,\mathbf{p}^2)$ and eq. (25) can be immediately integrated over $3(N-2)$ configuration co-ordinates and $3(N-2)$ momentum co-ordinates to yield

$$g_{\mathrm{cl}}(\mathbf{R}^2,\mathbf{R}'^2,t) = \int f_{\mathrm{cl}}^{(2/N)}(\mathbf{R}^2,\mathbf{p}^2)\,\delta(\mathbf{R}'^2-\mathbf{R}_t^2(\mathbf{R}^2,\mathbf{p}^2))\, d\mathbf{p}^2. \tag{35}$$

In the zero density limit the radial distribution function, eq. (34), becomes

$$g_{\mathrm{cl}}(\mathbf{R}^2) = \exp[-\beta V(R)] \tag{36}$$

where $R = |\mathbf{R}| = |\mathbf{R}_1-\mathbf{R}_2|$. Substitution of eqs. (33) and (36) into eq. (35) yields

$$g_{\mathrm{cl}}(\mathbf{R}^2,\mathbf{R}'^2,t) = \rho^2\left(\frac{\beta}{2\pi m}\right)^3 \int \exp\left[-\frac{\beta}{2m}(p_1^2+p_2^2)\right]\exp[-\beta V(R)] \times \delta(\mathbf{R}'^2-\mathbf{R}_t^2(\mathbf{R}^2,\mathbf{p}^2))\, d\mathbf{p}^2 \tag{37}$$

for the zero density limit for the TDPDF. The quantity $\rho = N/V$ is the number density of the system.

It is convenient in describing the two-body problem to introduce center of mass and relative co-ordinates and momenta by the expressions

$$\begin{aligned} \mathbf{R}(t) &= \mathbf{R}_1(t)-\mathbf{R}_2(t) & \mathbf{p}(t) &= \frac{\mathbf{p}_1(t)+\mathbf{p}_2(t)}{2} \\ \mathbf{R}_c(t) &= \frac{\mathbf{R}_1(t)+\mathbf{R}_2(t)}{2} & \mathbf{p}_c(t) &= \mathbf{p}_1(t)+\mathbf{p}_2(t). \end{aligned} \tag{38}$$

We also introduce the notation $M = 2m$ for the total mass and $\mu = m/2$ for the reduced mass. In this notation, eq. (37) becomes

$$(39)\quad g_{\mathrm{cl}}(\mathbf{R}^2,\mathbf{R}'^2,t) = g_{\mathrm{cl}}(\mathbf{R},\mathbf{R}_c,\mathbf{R}',\mathbf{R}_c',t)$$
$$= \rho^2\left(\frac{\beta}{2\pi m}\right)^3 \int \exp\left[-\beta\left\{\frac{p_c^2}{2M}+\frac{p^2}{2\mu}+V(R)\right\}\right]$$
$$\times\delta(\mathbf{R}_c'-\mathbf{R}_c(t))\,\delta(\mathbf{R}'-\mathbf{R}(t))\,d\mathbf{p}d\mathbf{p}_c$$

where

$$(40)\quad \mathbf{R}_c(t) = \mathbf{R}_c+\frac{\mathbf{p}_c}{M}t, \qquad \mathbf{p}_c(t) = \mathbf{p}_c = \text{constant}$$
$$\mathbf{R}(t) = \mathbf{R}+\int_0^t \frac{\mathbf{p}(t')}{\mu}\,dt', \qquad \mathbf{p}(t) = \mathbf{p}-\int_0^t \nabla_{\mathbf{R}(t')}V(\mathbf{R}(t'))\,dt'.$$

The problem of calculating $g(\mathbf{R}^2, \mathbf{R}'^2, t)$ can be solved exactly for $V(R) = 0$ (free particle approximation). This approximation is not useful for computational purposes because the integral in (24) will diverge for the most common expressions for $a(\mathbf{R})$. However, it will later be useful to refer to the free particle approximation as a limiting case of the "constant acceleration" approximation. In the free particle approximation

$$(41)\quad g_{\mathrm{cl}}^{(0)}(\mathbf{R},\mathbf{R}_c,\mathbf{R}',\mathbf{R}_c',t) = g_{\mathrm{cl}}^{(0)}(\mathbf{R},\mathbf{R}',t)\,g_{\mathrm{cl}}^{(0)}(\mathbf{R}_c,\mathbf{R}_c',t)$$

where

$$(42)\quad g_{\mathrm{cl}}^{(0)}(\mathbf{R},\mathbf{R}',t) = \rho\left(\frac{\beta}{2\pi\mu}\right)^{3/2}\left(\frac{\mu}{t}\right)^3 \exp\left[-\frac{\beta\mu}{2t^2}(\mathbf{R}'-\mathbf{R})^2\right]$$

and

$$(43)\quad g_{\mathrm{cl}}^{(0)}(\mathbf{R},\mathbf{R}_c',t) = \rho\left(\frac{\beta}{2\pi M}\right)^{3/2}\left(\frac{M}{t}\right)^3 \exp\left[-\frac{\beta M}{2t^2}(\mathbf{R}_c'-\mathbf{R}_c)^2\right].$$

We now turn our attention to a calculation of the TDPDF in the very dilute gas in which there is interaction between the particles. We consider an expansion of $\nabla_{\mathbf{R}(t)}V(\mathbf{R}(t))$ in a power series in t of the form

$$(44)\quad \nabla_{\mathbf{R}(t)}V(\mathbf{R}(t)) = \nabla_{\mathbf{R}}V(\mathbf{R})+\nabla_{\mathbf{R}}\nabla_{\mathbf{R}}V(\mathbf{R})\cdot\frac{\mathbf{p}}{\mu}t+O(t^2).$$

Substitution of eq. (44) into the expression for $\mathbf{p}(t)$ yields

$$(45)\quad \mathbf{p}(t) = \mathbf{p}-\nabla_{\mathbf{R}}V(\mathbf{R})t-\nabla_{\mathbf{R}}\nabla_{\mathbf{R}}V(\mathbf{R})\cdot\frac{\mathbf{p}}{\mu}\frac{t^2}{2}+O(t^3).$$

Finally substitution of eq. (45) into the expression for $\mathbf{R}(t)$ results in

$$(46)\quad \mathbf{R}(t) = \mathbf{R}+\frac{\mathbf{p}t}{\mu}-\frac{\nabla_{\mathbf{R}}V(\mathbf{R})}{\mu}\cdot\frac{t^2}{2}+O(t^3).$$

In the constant acceleration approximation that is used here, the force $\nabla_{\mathbf{R}(t)}V(\mathbf{R}(t))$ is assumed to be independent of time. This corresponds to neglecting terms of $O(t^3)$ in the time expansion of $\mathbf{R}(t)$. The justification for the constant acceleration approximation is a heuristic one and will be pre-

sented below. We believe that it is valid over a wider range than is immediately apparent because of the ad hoc reasons discussed and because of the a posteriori reason that the results obtained using it are eminently reasonable.

Substitution of eqs. (40) and (46) into eq. (37) results in

$$g_{\rm cl}(\mathbf{R},\mathbf{R}_c,\mathbf{R}',\mathbf{R}'_c,t) = g^{(0)}_{\rm cl}(\mathbf{R}_c,\mathbf{R}'_c,t)\, g_{\rm cl}(\mathbf{R},\mathbf{R}',t) \tag{47}$$

where

$$g_{\rm cl}(\mathbf{R},\mathbf{R}',t) = \rho\left(\frac{\beta}{2\pi\mu}\right)^{3/2}\left(\frac{\mu}{t}\right)^{3}\exp\left[-\frac{\beta\mu}{2t^2}(\mathbf{R}'-\mathbf{R})^2\right] \times[g_{\rm cl}(R)]^{1/2}[g_{\rm cl}(R')]^{1/2}. \tag{48}$$

The expression $g^{(0)}_{\rm cl}(\mathbf{R}_c,\mathbf{R}'_c,t)$ has been defined by eq. (43) and $g_{\rm cl}(R) = \exp[-\beta V(R)]$ is the radial distribution function for the very dilute gas.

In the integration over $\mathbf{p}$ we have only kept terms consistent with our approximation (46). Furthermore, we have made use of the Taylor expansion of $V(R)$

$$V(R') \cong V(R)+(\mathbf{R}'-\mathbf{R})\cdot\nabla_{\mathbf{R}}V(R)+\ldots \tag{49}$$

to obtain an expression for $g(\mathbf{R}^2,\mathbf{R}^2,t)$ consistent with the expected symmetry requirements. Equation (49) effectively replaces the force $\nabla_{\mathbf{R}}V(R)$ in the time expansion (46) with the average force $[V(R')-V(R)]/|\mathbf{R}'-\mathbf{R}|$.

The TDPDF for the dilute gas as written in eq. (47) is expressed in terms of two terms $g^{(0)}_{\rm cl}(\mathbf{R}_c,\mathbf{R}'_c,t)$ and $g_{\rm cl}(\mathbf{R},\mathbf{R}',t)$, which are, respectively, the joint probabilities (of the type defined in eq. (25)) for a free particle of mass M, and to first order, for particles of mass μ moving in a potential $V(R)$. It is easy to derive the terms $[g(R)]^{1/2}[g(R')]^{1/2}$ in terms of a model in which all molecules which go from $\mathbf{R}$ to $\mathbf{R}'$ are assumed to move in a straight line with constant acceleration.

It is well to anticipate objections to our use of an expansion in time (46), valid only for short times, to derive a correlation function in whose low-frequency components we are primarily interested. However, the result (47) may be much better than this expansion would indicate, partly because the symmetrization involved in the use of (49) and discussed above improves the approximation *insofar as computing correlation functions is concerned*, and partly because the terms $a(\mathbf{R})$ in (24) vary inversely as R^3 for dipole–dipole interactions (7) and as R^n $(n \geqslant 5)$ for polyatomic systems, so that the greatest contribution to $k(t)$ is made during the very short time in which the particles are close together.

It is difficult to justify the above remarks rigorously and experiment must eventually judge the usefulness of the "constant acceleration" approximation. It is possible to think of it intuitively in terms of all possible trajectories which take a molecule from a separation $\mathbf{R}$ from another molecule to a separation $\mathbf{R}'$ in a time t, and to consider the fraction of those trajectories which our approximation does not describe reasonably well, in terms of averages over a Maxwell–Boltzmann distribution; that is, for molecules at large $\mathbf{R}$,

most of the contributions to (24) will be from $\mathbf{R}'$, also fairly large, for which $g(\mathbf{R}^2, \mathbf{R}'^2, t)$ correctly reduces to the free particle TDPDF $g^{(0)}(\mathbf{R}^2,\mathbf{R}'^2, t)$. A type of contribution not described well by our expansion is that of two molecules colliding head on. Such contributions may be too few to contribute appreciably to the correlation functions. In conclusion we call attention to the similarity between the constant acceleration approximation used here and the concept of linear trajectories introduced by Kirkwood (1946) into calculations of transport coefficients in fluids.

We shall now extend the calculations described above to include the influence of the other molecules in the system on the dynamics of the two particles under consideration and on the form of the distribution functions to first order in powers of the density. To take into account the influence of other molecules, eqs. (40) must be modified as follows:

$$\begin{aligned} \mathbf{R}_c(t) &= \mathbf{R}_c+\frac{1}{M}\int_0^t \mathbf{p}_c(t')\,dt', \qquad \mathbf{p}_c(t) = \mathbf{p}_c-\int_0^t \boldsymbol{\Delta}^+(t')\,dt' \\ \mathbf{R}(t) &= \mathbf{R}+\frac{1}{\mu}\int_0^t \mathbf{p}(t')\,dt', \qquad \mathbf{p}(t) = \mathbf{p}-\int_0^t \boldsymbol{\nabla}_{\mathbf{R}(t')} V(R(t'))\,dt' \\ &\qquad\qquad -\frac{1}{2}\int_0^t \boldsymbol{\Delta}^-(t')\,dt' \end{aligned} \tag{50}$$

where

$$\boldsymbol{\Delta}^{\pm}(t) = \sum_{i=3}^{N} [\boldsymbol{\nabla}_{\mathbf{R}_1(t)} V(R_{1i}(t)) \pm \boldsymbol{\nabla}_{\mathbf{R}_2(t)} V(R_{2i}(t))] \tag{51}$$

and we use the notation $\boldsymbol{\Delta}^{\pm}(0) = \boldsymbol{\Delta}^{\pm}$.

In the "constant acceleration" approximation eq. (25) becomes

$$g_{cl}(\mathbf{R}^2,\mathbf{R}'^2,t) = N(N-1)\int f_{cl}^N(\mathbf{R}^N,\mathbf{p}^N)\,\delta\left(\mathbf{B}_1+\frac{t^2}{4\mu}\boldsymbol{\Delta}^-\right) \delta\left(\mathbf{B}_2+\frac{t^2}{2M}\boldsymbol{\Delta}^+\right) d\mathbf{R}^{N-2}\,d\mathbf{p}^{N-2}\,d\mathbf{p}\,d\mathbf{p}_c \tag{52}$$

where

$$\begin{aligned} \mathbf{B}_1 &= \mathbf{R}'-\mathbf{R}-\frac{t}{\mu}\mathbf{p}+\frac{t^2}{2\mu}\boldsymbol{\nabla}_{\mathbf{R}} V(R) \\ \mathbf{B}_2 &= \mathbf{R}'_c-\mathbf{R}_c-\frac{t}{M}\mathbf{p}_c \end{aligned} \tag{53}$$

and we have used eqs. (50) in the "constant acceleration" approximation. It is consistent with this approximation to make a Taylor expansion of the delta functions in the form

$$\begin{aligned} \delta\left(\mathbf{B}_1+\frac{t^2}{4\mu}\boldsymbol{\Delta}^-\right) &= \delta(\mathbf{B}_1)+\frac{t^2}{4\mu}\boldsymbol{\Delta}^-\cdot\frac{\partial}{\partial\mathbf{B}_1}[\delta(\mathbf{B}_1)]+\ldots \\ \text{and}\qquad \delta\left(\mathbf{B}_2+\frac{t^2}{2M}\boldsymbol{\Delta}^+\right) &= \delta(\mathbf{B}_2)+\frac{t^2}{2M}\boldsymbol{\Delta}^+\cdot\frac{\partial}{\partial\mathbf{B}_2}[\delta(\mathbf{B}_2)]+\ldots. \end{aligned} \tag{54}$$

Substitution of eqs. (54) into eq. (52) and use of eq. (30) yields

$$(55)\quad g_{\rm cl}(\mathbf{R}^2,\mathbf{R}'^2,t) = \int f_{\rm cl}^{(2/n)}(\mathbf{R}^2,\mathbf{p}^2)\,\delta(\mathbf{B}_1)\,\delta(\mathbf{B}_2)\,d\mathbf{p}^2$$
$$+\frac{t^2}{4\mu}\int f_{\rm cl}^{(3/N)}(\mathbf{R}^3,\mathbf{p}^3)\{\nabla_{\mathbf{R}_1}V_{13}-\nabla_{\mathbf{R}_2}V_{23}\}\cdot\frac{\partial\delta(\mathbf{B}_1)}{\partial\mathbf{B}_1}\,\delta(\mathbf{B}_2)d\mathbf{R}_3d\mathbf{p}^3$$
$$+\frac{t^2}{2M}\int f_{\rm cl}^{(3/N)}(\mathbf{R}^3,\mathbf{p}^3)\{\nabla_{\mathbf{R}_1}V_{13}+\nabla_{\mathbf{R}_2}V_{23}\}\cdot\frac{\partial\delta(\mathbf{B}_2)}{\partial\mathbf{B}_2}\,\delta(\mathbf{B}_1)d\mathbf{R}_3d\mathbf{p}^3$$
$$+\ldots\,.$$

In order to obtain terms of order ρ^3 in eq. (55) we write the pair-distribution function in the form

$$(56)\quad f_{\rm cl}^{(2/N)} = \rho^2\left(\frac{\beta}{2\pi m}\right)^3\exp\left[-\frac{\beta}{2m}\,(p_1{}^2+p_2{}^2)\right]g_{\rm cl}(R)$$

where

$$(57)\quad g_{\rm cl}(R) = \exp[-\beta V(R)]\{1+\rho\gamma(R)\}$$

and (Oppenheim and Mazur 1957)

$$(58)\quad \gamma(R) = \int(\exp[-\beta(V_{13}+V_{23})]-1)d\mathbf{R}_3-2\int(\exp[-\beta V_{12}]-1)d\mathbf{R}_2.$$

To terms of order ρ^3 the triplet-distribution function is

$$(59)\quad f_{\rm cl}^{(3/N)}(\mathbf{R}^3,\mathbf{p}^3) = \rho^3\left(\frac{\beta}{2\pi m}\right)^{9/2}\exp\left[-\frac{\beta}{2m}\,(p_1{}^2+p_2{}^2+p_3{}^2)\right]$$
$$\times\exp[-\beta(V_{12}+V_{13}+V_{23})].$$

Substitution of eqs. (56–58) into the first term on the right-hand side of eq. (55) yields the expression

$$(60)\quad g_{\rm cl}^{(0)}(\mathbf{R}_c,\mathbf{R}_c',t)\,g_{\rm cl}^{(0)}(\mathbf{R},\mathbf{R}',t)\exp\int-\frac{\beta}{2}\,[V(R)+V(R')](1+\rho\gamma(R))$$

where we have used the approximation of eq. (49). Substitution of eq. (59) into the second term on the right-hand side of eq. (55) and use of eq. (49) results in

$$(61)\quad \rho g_{\rm cl}^{(0)}(\mathbf{R}_c,\mathbf{R}_c',t)\,g_{\rm cl}^{(0)}(\mathbf{R},\mathbf{R}',t)\exp\left[-\frac{\beta}{2}\,(V(R)+V(R'))\right]$$
$$\times(\tfrac{1}{2})(\mathbf{R}'-\mathbf{R})\cdot\frac{\partial}{\partial\mathbf{R}}\,(\gamma(R)).$$

Substitution of eq. (59) into the third term on the right-hand side of eq. (55) yields 0. Use of the Taylor's series expansion

$$(62)\quad \gamma(R') = \gamma(R)+(\mathbf{R}'-\mathbf{R})\cdot\frac{\partial}{\partial\mathbf{R}}\,(\gamma(R))+\ldots$$

together with the expansion

$$[g(R)\,g(R')]^{1/2} = \exp\left[-\frac{\beta}{2}(V(R)+V(R'))\right] \times\left\{1+\rho\left(\frac{\gamma(R)+\gamma(R')}{2}\right)+O(\rho^2)\right\} \tag{63}$$

enables us to write eq. (55) as

$$g_{cl}(\mathbf{R}^2,\mathbf{R}'^2,t) = g_{cl}^{(0)}(\mathbf{R}_c,\mathbf{R}_c',t)\,g_{cl}^{(0)}(\mathbf{R},\mathbf{R}',t)[g(R)]^{1/2}\,[g(R')]^{1/2} \tag{64}$$

where we have made use of eqs. (60) and (61). Equation (64) is the expression for the TDPDF retaining first order density corrections. It is of the same form as eq. (48) for the very dilute gas, but $g_{cl}(R)$ is given here by eq. (57).

5. THE TIME-DEPENDENT PAIR-DISTRIBUTION FUNCTION FOR THE QUANTUM GAS

From the discussion of the previous section, one may well expect to obtain an expression for the TDPDF for the quantum gas which is similar to that given by eqs. (47) and (48), with the static radial distribution function $g(R)$ appropriate to the quantum gas. We shall see that a result consistent with this is obtained within the scope of the "constant acceleration" approximation. Another modification also appears due to the fact that the momentum distribution of the quantum gas differs from the Maxwell–Boltzmann distribution. In fact, unlike the classical gas, the momentum distribution depends on the spatial configuration of the molecules, a manifestation of the fact that position and momentum operators do not commute in quantum mechanics.

The expression for the quantum mechanical correlation function in terms of the WDF, $f^N(\mathbf{R}^N,\mathbf{p}^N)$, is given by eq. (23) in the form

$$k(t) = (N-1)\int f^N(\mathbf{R}^N,\mathbf{p}^N)[a(0)a^*(t)]_W\,d\mathbf{R}^N d\mathbf{p}^N. \tag{65}$$

Equation (65) differs from the classical correlation function in two ways. First, the average is taken over the WDF instead of the classical distribution function. In this section, we use a power series expansion of the WDF in powers of $\hbar^2$, retaining terms of order $\hbar^2$. This expansion is valid for intermediate temperatures and provides important corrections to the classical distribution function. The second difference between eq. (65) and the classical expression is due to the difference in temporal development of the classical and quantum quantities $a(t)$. In other words, the function $[a(0)a^*(t)]_W$ of the classical variables $\mathbf{R}^N$ and $\mathbf{p}^N$, which is related to the quantum mechanical operator $a(0)a^*(t)$ by the Weyl correspondence, need not be the same as the classical quantity $a_{cl}(\mathbf{R}^2)a_{cl}^*(\mathbf{R}_t^2(\mathbf{R}^N,\mathbf{p}^N))$, which is used in the previous sections. We shall neglect this difference here. With this modification eq. (65) becomes

$$\begin{aligned} k(t) &= (N-1)\int f^N(\mathbf{R}^N,\mathbf{p}^N)\,a(\mathbf{R}^2)\,a(\mathbf{R}_t^2(\mathbf{R}^N,\mathbf{p}^N))\,d\mathbf{R}^N d\mathbf{p}^N \\ &= \frac{1}{N}\int a(\mathbf{R}^2)\,a(\mathbf{R}'^2)\,g(\mathbf{R}^2,\mathbf{R}'^2,t)\,d\mathbf{R}^2 d\mathbf{R}'^2 \end{aligned} \tag{66}$$

where $g(\mathbf{R}^2,\mathbf{R}'^2, t)$ is given by eq. (25) in the form

$$g(\mathbf{R}^2,\mathbf{R}'^2,t) = N(N-1)\int f^N(\mathbf{R}^N,\mathbf{p}^N)\delta(\mathbf{R}'^2-\mathbf{R}_t^2(\mathbf{R}^N,\mathbf{p}^N))d\mathbf{R}^{N-2}d\mathbf{p}^N. \tag{67}$$

The quantity $\mathbf{R}_t^2(\mathbf{R}^N,\mathbf{p}^N)$ is determined by classical dynamics and all quantum effects now reside in the WDF.

For the very dilute quantum gas $\mathbf{R}_t^2 = \mathbf{R}_t^2(\mathbf{R}^2,\mathbf{p}^2)$ and we can rewrite eq. (67) as

$$g(\mathbf{R}^2,\mathbf{R}'^2,t) = \int f^{(2/N)}(\mathbf{R}^2,\mathbf{p}^2)\delta(\mathbf{R}'^2-\mathbf{R}_t^2(\mathbf{R}^2,\mathbf{p}^2))d\mathbf{p}^2. \tag{68}$$

In the very dilute quantum gas $f^{(2/N)}$ is given to first order in $\hbar^2$ by

$$f^{2/N}(\mathbf{R}^N,\mathbf{p}^N) = \rho^2\left(\frac{\beta}{2\pi m}\right)^3 \exp[-\beta V(R)]\exp\left[-\beta\left(\frac{p_c^2}{2M}+\frac{p^2}{2\mu}\right)\right] \times\{1+\hbar^2\chi(\mathbf{R},\mathbf{p},\beta)\} \tag{69}$$

where

$$\chi(\mathbf{R},\mathbf{p},\beta) = -\frac{\beta^2}{8\mu}\nabla_{\mathbf{R}}{}^2V(R)+\frac{\beta^3}{24\mu}[\nabla_{\mathbf{R}}V(R)]^2 +\frac{\beta^3}{24\mu^2}\left\{p^2+(\mathbf{R}\cdot\mathbf{p})^2\frac{1}{R}\frac{d}{dR}\right\}\frac{1}{R}\frac{dV(R)}{dR}. \tag{70}$$

The last term in (70) has been written for convenience in a different form than usual (Wigner 1932; Oppenheim and Ross 1957).

It is useful to define a function $T_e(\mathbf{R})$ by

$$\frac{3}{2}kT_e(\mathbf{R}) = \frac{3}{2\beta_e(\mathbf{R})} = \frac{\int\frac{p^2}{2\mu}f^{(2/N)}(\mathbf{R}^2,\mathbf{p}^2)d\mathbf{p}\,d\mathbf{p}_c}{\int f^{(2/N)}(\mathbf{R}^2,\mathbf{p}^2)\,d\mathbf{p}\,d\mathbf{p}_c}. \tag{71}$$

For a classical gas $\beta_e(\mathbf{R}) \equiv \beta$ independent of $\mathbf{R}$, but for $f^{(2/N)}$ given by (69), one obtains from (71), assuming $\hbar^2\chi \ll 1$

$$\beta_e(\mathbf{R}) \cong \beta\left[1-\frac{\beta^2\hbar^2}{36\mu}\nabla_{\mathbf{R}}^2V(R)\right]. \tag{72}$$

Turning now to the calculation of the TDPDF, it is only necessary to repeat the steps of Section 3 in evaluating (35) using $f^{(2/N)}$ given by (69). Equations (38), (40), and (46) may be used as they stand, though as mentioned earlier, this use of classical position and momentum co-ordinates should not be interpreted as implying knowledge of molecular trajectories. The integration of (35) is straightforward and we obtain:

$$g(\mathbf{R}^2,\mathbf{R}'^2, t) = g(\mathbf{R}^2,\mathbf{R}'^2, t)_{el}[1+\hbar^2\{D_1(\mathbf{R},\mathbf{R}', t)+D_2(\mathbf{R},\mathbf{R}')\}] \tag{73}$$

where

$$(74)\qquad D_1(\mathbf{R},\mathbf{R}',t) = \frac{\beta^3}{24t^2}\left[(\mathbf{R}'-\mathbf{R})^2+\{\mathbf{R}\cdot(\mathbf{R}'-\mathbf{R})\}^2\frac{1}{R}\frac{d}{dR}\right]\frac{1}{R}\frac{dV(R)}{dR}$$

and

$$(75)\quad D_2(\mathbf{R},\mathbf{R}') = -\frac{\beta^2}{8\mu}\nabla_{\mathbf{R}}^2V(R)+\frac{\beta^3}{24\mu}[\nabla_{\mathbf{R}}V(R)]^2$$
$$+\frac{\beta^3}{24\mu}\left[(\mathbf{R}'-\mathbf{R})\cdot\nabla_{\mathbf{R}}V(R)+\{\mathbf{R}\cdot(\mathbf{R}'-\mathbf{R})\}\{\mathbf{R}\cdot\nabla_{\mathbf{R}}V(R)\}\frac{1}{R}\frac{d}{dR}\right]\frac{1}{R}\frac{dV(R)}{dR}.$$

The quantum mechanical corrections to the TDPDF have been separated into time-dependent and time-independent contributions. To simplify the calculations we *approximate* the effect of D_1 by replacing it with its average over all orientations of $\mathbf{R}$, keeping $\mathbf{R}'-\mathbf{R}$ fixed.

$$(76)\qquad \hbar^2\langle D_1\rangle = \frac{\beta^3\hbar^2(\mathbf{R}'-\mathbf{R})^2}{72t^2}\nabla_{\mathbf{R}}{}^2V(R).$$

Since the expansion of $f^{(2/N)}$ in powers of $\hbar^2$ is only valid if the quantum correction is not too large

$$\exp[\hbar^2\langle D_1\rangle] \cong 1+\hbar^2\langle D_1\rangle$$

and the effect of the term D_1 is accounted for by replacing β in the time-dependent part of (48) with $\beta_e(\mathbf{R})$ for a particle of mass 2μ as defined in (72). Because of the symmetry properties of $g(\mathbf{R}^2,\mathbf{R}'^2,t)$, we replace $\beta_e(\mathbf{R})$ by its symmetric form $\beta_e(\mathbf{R},\mathbf{R}') = [\beta_e(\mathbf{R})+\beta_e(\mathbf{R}')]/2$.

Examination of the time-independent terms shows that

$$(77)\quad D_2 = -\frac{\beta^2}{8\mu}\nabla_{\mathbf{R}}^2V(R)+\frac{\beta^3}{24\mu}[\nabla_{\mathbf{R}}V(R)]^2+\frac{\beta^3}{24\mu}(\mathbf{R}'-\mathbf{R})\cdot\nabla_{\mathbf{R}}V(R)\frac{d^2V(R)}{dR^2}$$
$$\cong -\frac{\beta^2}{8\mu}\nabla_{\mathbf{R}}^2V(R)+\frac{\beta^3}{48\mu}\{[\nabla_{\mathbf{R}}V(R)]^2+[\nabla_{\mathbf{R}'}V(R')]^2\}$$

where we have used the Taylor expansion of $[\nabla_{\mathbf{R}}V(R')]^2$. The radial distribution functions for the dilute quantum gas of molecules of mass 2μ is to first order in $\hbar^2$ (Wigner 1932; Oppenheim 1957)

$$(78)\qquad g(R) = e^{-\beta V(R)}\left[1+\hbar^2\left\{-\frac{\beta^2}{12\mu}\nabla_{\mathbf{R}}^2V(R)+\frac{\beta^3}{24\mu}[\nabla_{\mathbf{R}}V(R)]^2\right\}\right].$$

We see that the anticipated form of $g(R)$ in (48) is only realized for terms involving $\nabla_{\mathbf{R}}V(R)$ and not $\nabla_{\mathbf{R}}^2V(R)$. This result is consistent with the "constant acceleration" approximation since our treatment of the molecular dynamics has only been carried out to first order terms in the gradient operator. Without further ado, we replace

$$-\frac{\beta^2}{8\mu}\nabla_{\mathbf{R}}{}^2V(R)$$

in (77) by

$$-\frac{\beta^2}{24\mu}\left[\nabla_{\mathbf{R}}^2 V(R)+\nabla_{\mathbf{R}'}^2 V(R')\right]$$

for purposes of calculation. This step is not inconsistent with anything we have done but its justification is mainly intuitive at this time. It symmetrizes $g(\mathbf{R}^2, \mathbf{R}'^2, t)$ just as replacement of $\beta_e(\mathbf{R})$ with $\beta_e(\mathbf{R}, \mathbf{R}')$ did in the time-dependent term.

Summing up: for the very dilute quantum gas, $g(\mathbf{R}^2, \mathbf{R}'^2, t)$ to first order in $\hbar^2$ has a form similar to that of (47), (48), (43), where $g(R)$ is here given by (78) and β in (48) is replaced by $\beta_e(\mathbf{R}, \mathbf{R}') = [\beta_e(\mathbf{R})+\beta_e(\mathbf{R}')]/2$.

6. THE TDPDF FOR CLASSICAL DENSE FLUIDS

In the previous sections we have considered the form of the TDPDF for dilute gases. We have obtained expressions for the TDPDF which are suitable for the calculation of correlation functions of the type of eq. (14). The functions $a(\mathbf{R})$ tend to zero rapidly as R, the distance between the two particles under consideration, increases. Thus, contributions to the correlation function will come only from those regions in phase space in which both R and R_t are small. We have made the implicit assumption that the variables R and R_t will both be small only when t is of the order of or shorter than the time between collisions and is very short compared to the characteristic spin relaxation time. The time between collisions of a single pair of molecules is taken to be very long compared to either the Larmor period or the characteristic spin relaxation time. If the time between collisions of a single pair is long compared to the Larmor period the contribution from correlations between successive collisions will be down by $(\omega_0 t)^{-2}$. If the time is long compared to the spin relaxation time there will be no contribution to the spin relaxation. In a dilute gas, the situation in which R and R_t are both small when t is longer than the time between collisions and less than the Larmor period is extremely unlikely. Thus, in the dilute gas we have considered only those configurations in which R and R_t will be small when t is short. Under these conditions the assumption that the motions of the two particles are either unaffected by the other particles in the system or affected by the other particles as described in eq. (50) is justified and we may use Newton's laws of motion in a straightforward fashion.

In a dense fluid, however, the situation is quite different. The particles of interest interact with many other particles while interacting with each other. They may remain within each other's field of force for comparatively long times while executing complicated motions. In this section we shall make use of generalized Langevin equations to describe the motions of the particles of interest. Equations of this type have been used by Kirkwood and collaborators to describe the transport properties of dense fluids. We shall also make use of the constant acceleration approximation and again mention the similarity between this approximation and the straight path approximation used by Kirkwood (1946) to calculate friction constants and other transport properties.

We shall not present a detailed exposition of the derivation of the equations of motion utilized here since many subtle points regarding coarse graining must be included. This exposition will appear in a paper by one of us (I.O.). The exact equation of motion for particle 1 in the N particle system is given by

$$m\ddot{\mathbf{R}}_1(t) = \mathbf{F}_1(t) = \sum_{i=2}^{N} \mathbf{F}_{1i}(\mathbf{R}_{1i}(t)) \tag{79}$$

where $\ddot{\mathbf{R}}_1(t)$ is the acceleration of particle 1 at time t, $\mathbf{F}_1$ is the total force acting on particle 1, and $\mathbf{F}_{1i}$ is the force exerted on particle 1 by particle i at vector distance $\mathbf{R}_{1i}(t)$. When eq. (79) is averaged over all particles except 1 in the equilibrium ensemble at time $t = 0$ we obtain

$$m\langle\ddot{\mathbf{R}}_1(t)\rangle^{N-1} = -\alpha\langle\dot{\mathbf{R}}_1(t)\rangle^{N-1} + \mathbf{A}(t) \tag{80}$$

where α is a constant, the term $-\alpha\langle\dot{\mathbf{R}}_1(t)\rangle^{N-1}$ is a systematic force acting on particle 1, and $\mathbf{A}(t)$ is a fluctuating force. The notation $\langle G(\mathbf{R}_1(t), \dot{\mathbf{R}}_1(t))\rangle^{N-m}$ implies

$$\langle G(\mathbf{R}_1(t),\dot{\mathbf{R}}_1(t))\rangle^{N-m} = \frac{\int G(\mathbf{R}_1(t),\dot{\mathbf{R}}_1(t)) f_{\mathrm{el}}^N(\mathbf{R}^N,\mathbf{p}^N,0) d\mathbf{R}^{N-m} d\mathbf{p}^{N-m}}{\int f_{\mathrm{el}}^N(\mathbf{R}^N, \mathbf{p}^N,0) d\mathbf{R}^{N-m} d\mathbf{p}^{N-m}}. \tag{81}$$

The quantities $\mathbf{R}^m(0)$ and $\dot{\mathbf{R}}^m(0)$ are fixed in the averaging process in eq. (81). Equation (80) is the Langevin equation and the fluctuating force $\mathbf{A}(t)$ has the usual properties (Chandrasekhar 1943).

When eq. (79) is averaged over all particles except 1 and 2 in the equilibrium ensemble at $t = 0$ we obtain

$$m\langle\ddot{\mathbf{R}}_1(t)\rangle^{N-2} = -\alpha\langle\dot{\mathbf{R}}_1(t)\rangle^{N-2} - \nabla_{\mathbf{R}_1(t)} W(\mathbf{R}_1(t), \mathbf{R}_2(t)) + \mathbf{A}(t) \tag{82}$$

where α and $\mathbf{A}$ have the same significance as in eq. (80) and $W(\mathbf{R}_1, \mathbf{R}_2)$ is the potential of mean force between particles 1 and 2 and is defined by the equation

$$\nabla_{\mathbf{R}_1} W(\mathbf{R}_1, \mathbf{R}_2) = -\langle\mathbf{F}_1\rangle^{N-2}. \tag{83}$$

The potential of mean force is related to the radial distribution function by the relation

$$g_{\mathrm{el}}(R) = \exp[-\beta W(R)] \tag{84}$$

and depends only on the scalar distance between particles 1 and 2. Equation (82) provides the dynamical basis for our treatment of the TDPDF in dense fluids. For notational simplicity, we rewrite eq. (82) in the form

$$m\ddot{\mathbf{R}}_1(t) = -\alpha\dot{\mathbf{R}}_1(t) - \nabla_{\mathbf{R}_1(t)} W(\mathbf{R}(t)) + \mathbf{A}(t), \tag{85}$$

though we must remember that the quantities $\ddot{\mathbf{R}}_1(t)$ and $\dot{\mathbf{R}}_1(t)$ are averages of the type defined in eq. (81).

Combination of eq. (82) and a similar equation for particle 2 yields

$$M\ddot{\mathbf{R}}_c(t) = -2\alpha\dot{\mathbf{R}}_c(t)+\mathbf{A}(t) \tag{86}$$

and

$$m\ddot{\mathbf{R}}(t) = -\alpha\dot{\mathbf{R}}(t)-2\nabla_{\mathbf{R}(t)}W(\mathbf{R}(t))+\mathbf{A}(t) \tag{87}$$

where we have used the definitions of eqs. (38) and the fact that the fluctuating forces appearing in eq. (82) and the corresponding equation for particle 2 are uncorrelated. Multiplication of eq. (86) by $\exp[2\alpha t/M]$ and integration over time from 0 to t results in

$$M\dot{\mathbf{R}}_c(t) = M\dot{\mathbf{R}}_c \exp\left[-\frac{2\alpha t}{M}\right]+\exp\left[-\frac{2\alpha t}{M}\right]\int_0^t \mathbf{A}(s)\exp\left[\frac{2\alpha s}{M}\right]ds. \tag{88}$$

Equation (88) is easily integrated to yield

$$M(\mathbf{R}_c(t)-\mathbf{R}_c) = M\dot{\mathbf{R}}_c\left(\frac{M}{2\alpha}\right)\left(1-\exp\left[-\frac{2\alpha t}{M}\right]\right) +\frac{M}{2\alpha}\int_0^t\left(1-\exp\left[-\frac{2\alpha(t-s)}{M}\right]\right)\mathbf{A}(s)ds. \tag{89}$$

In a similar fashion, eq. (87) can be integrated in the form

$$m(\mathbf{R}(t)-\mathbf{R}) = m\dot{\mathbf{R}}\left(\frac{m}{\alpha}\right)\left(1-\exp\left[-\frac{\alpha t}{m}\right]\right) +\frac{m}{\alpha}\int_0^t\left(1-\exp\left[-\frac{\alpha(t-s)}{m}\right]\right)\left(-2\nabla_{\mathbf{R}(s)}W(\mathbf{R}(s))+\mathbf{A}(s)\right)ds. \tag{90}$$

If we assume that $\nabla_{\mathbf{R}(s)}W(\mathbf{R}(s))$ can be adequately represented by $\nabla_{\mathbf{R}}W(\mathbf{R})$ during the times of interest (cf. constant acceleration approximation of the previous sections and the Kirkwood linear trajectory hypothesis (1946)), eq. (90) becomes

$$\begin{aligned} m(\mathbf{R}(t)-\mathbf{R}) &= m\dot{\mathbf{R}}\left(\frac{m}{\alpha}\right)\left(1-\exp\left[-\frac{\alpha t}{m}\right]\right)-\frac{2m}{\alpha}\nabla_{\mathbf{R}}W(\mathbf{R})\left(t-\frac{m}{\alpha}\left(1-\exp\left[-\frac{\alpha t}{m}\right]\right)\right) \\ &\quad +\frac{m}{\alpha}\int_0^t\left(1-\exp\left[-\frac{\alpha(t-s)}{m}\right]\right)\mathbf{A}(s)ds. \end{aligned} \tag{91}$$

Equations (89) and (91) may be averaged over the initial momenta of particles 1 and 2 in the equilibrium ensemble at time 0 to obtain

$$\mathbf{R}_c(t)-\mathbf{R}_c = \frac{1}{2\alpha}\int_0^t\left(1-\exp\left[-\frac{2\alpha(t-s)}{M}\right]\right)\mathbf{A}(s)ds \tag{92}$$

and

$$\mathbf{R}(t)-\mathbf{R} = -\frac{2}{\alpha}\nabla_{\mathbf{R}}W(\mathbf{R})\left(t-\frac{m}{\alpha}\left(1-\exp\left[-\frac{\alpha t}{m}\right]\right)\right) +\frac{1}{\alpha}\int_0^t\left(1-\exp\left[-\frac{\alpha(t-s)}{m}\right]\right)\mathbf{A}(s)ds \tag{93}$$

where we have made use of the facts that the average values of $\dot{\mathbf{R}}$ and $\dot{\mathbf{R}}_c$ in the equilibrium ensemble are zero.

The solution of the stochastic eq. (92) yields a form for the conditional probability density function $P(\mathbf{R}_c(t),\, t/\mathbf{R}_c,\, 0)$. The quantity $P(\mathbf{R}_c(t),t/\mathbf{R}_c,0)$ $d\mathbf{R}_c(t)$ is the probability that if the random variable $\mathbf{R}_c(\tau)$ had the value $\mathbf{R}_c$ at $\tau = 0$ it lies in the range between $\mathbf{R}_c(t)$ and $\mathbf{R}_c(t)+d\mathbf{R}_c(t)$ at time $\tau = t$. We recall that the random variable $\mathbf{R}_c(\tau)$ is the mean value of the center of mass co-ordinate of particles 1 and 2 averaged over the initial co-ordinates of the $N-2$ other particles of the system and over all initial momenta. Equation (92) can be solved by standard techniques (Chandrasekhar 1943) to yield

$$(94)\qquad P(\mathbf{R}_c(t),t/\mathbf{R}_c,0) = \{\pi\, Q_c\}^{-3/2} \exp\left[-\frac{|\mathbf{R}_c(t)-\mathbf{R}_c|^2}{Q_c}\right]$$

where

$$Q_c = 4\left(\frac{D}{2}\right)\left[t-\frac{M}{\alpha}\left(1-\exp\left[-\frac{2\alpha t}{M}\right]\right)+\frac{M}{4\alpha}\left(1-\exp\left[-\frac{4\alpha t}{M}\right]\right)\right].$$

$D = kT/\alpha$ is the diffusion constant for a particle of mass m. Equation (94) reduces to a solution of the diffusion equation

$$(95)\qquad P(\mathbf{R}_c(t),t/\mathbf{R}_c,0) = \left(4\pi\frac{D}{2}t\right)^{-3/2} \exp\left[-\frac{|\mathbf{R}_c(t)-\mathbf{R}_c|^2}{4\dfrac{D}{2}t}\right]$$

when $\alpha t/m \gg 1$. The quantity $D/2$ is the diffusion constant for a particle of mass $M = 2m$.

In an analogous fashion, the stochastic eq. (93) can be solved to yield

$$(96)\quad P(\mathbf{R}(t),t/\mathbf{R},0) = \{\pi Q\}^{-3/2} \exp\left[-\frac{1}{Q}\left\{\mathbf{R}(t)-\mathbf{R}+\frac{2}{\alpha}\nabla_{\mathbf{R}}W(\mathbf{R})\left(t-\frac{m}{\alpha}\left(1-\exp\left[-\frac{\alpha t}{m}\right]\right)\right)\right\}^2\right]$$

where

$$Q = 4(2D)\left[t-\frac{2m}{\alpha}\left(1-\exp\left[-\frac{\alpha t}{m}\right]\right)+\frac{m}{2\alpha}\left(1-\exp\left[-\frac{2\alpha t}{m}\right]\right)\right].$$

Equation (96) reduces to

$$(97)\quad P(\mathbf{R}(t),t/\mathbf{R},0) = \{4\pi(2D)t\}^{-3/2} \exp\left[-\frac{\left\{\mathbf{R}(t)-\mathbf{R}+\dfrac{2}{\alpha}\nabla_{\mathbf{R}}W(\mathbf{R})t\right\}^2}{4(2D)t}\right]$$

when $\alpha t/m \gg 1$. The quantity $2D$ is the diffusion constant for a particle of mass $\mu = m/2$. Equation (97) can be rewritten in the form

$$(98)\quad P(\mathbf{R}(t),t/\mathbf{R},0) = \{4\pi(2D)t\}^{-3/2} \exp\left[-\frac{|\mathbf{R}(t)-\mathbf{R}|^2}{4(2D)t}\right] \times \exp\left[-\frac{(\mathbf{R}(t)-\mathbf{R})\cdot\nabla_{\mathbf{R}}W(\mathbf{R})}{2kT}\right] \exp\left[-\frac{(\nabla_{\mathbf{R}}W(\mathbf{R}))^2 t}{2\alpha kT}\right].$$

The first two terms in the product on the right-hand side of eq. (98) are a solution to the diffusion equation for a particle of mass μ. The third term will contribute to a symmetrization of the distribution function. The fourth term may be replaced by unity consistent with the approximation introduced into eq. (91).

The classical TDPDF is defined by eq. (25) to be

$$g(\mathbf{R}^2,\mathbf{R}'^2,t) = N(N-1)\int f_{\mathrm{cl}}^N(\mathbf{R}^N,\mathbf{p}^N)\delta(\mathbf{R}'^2-\mathbf{R}^2(t))d\mathbf{R}^{N-2}d\mathbf{p}^N . \tag{99}$$

Equation (99) may be rewritten in the form

$$g(\mathbf{R}^2,\mathbf{R}'^2,t) = \rho_{\mathrm{cl}}^{2/N}(\mathbf{R}^2)\,\langle\delta(\mathbf{R}'-\mathbf{R}(t))\delta(\mathbf{R}'_c-\mathbf{R}_c(t))\rangle^{N-2,N} \tag{100}$$

where the notation $\langle G\rangle^{N-2,N}$ implies

$$\langle G\rangle^{N-2,N} = \frac{\int f_{\mathrm{cl}}^N(\mathbf{R}^N,\mathbf{p}^N)G\,d\mathbf{R}^{N-2}d\mathbf{p}^N}{\frac{1}{N(N-1)}\rho_{\mathrm{cl}}^{2/N}(\mathbf{R}^2)} \tag{101}$$

and $\rho_{\mathrm{cl}}^{2/N}(\mathbf{R}^2)$ is the classical pair configuration space distribution function, which can be written in terms of the radial distribution function as

$$\rho_{\mathrm{cl}}^{2/N}(\mathbf{R}^2) = \rho^2 g_{\mathrm{cl}}(R) = \rho^2\exp[-\beta\,W(R)] \tag{102}$$

where we have used eq. (84). The averaging process defined by eq. (101) is identical with the averaging process utilized to arrive at the stochastic eqs. (92) and (93). The stochastic variables $\mathbf{R}_c(t)$ and $\mathbf{R}(t)$ are independent. Thus eq. (100) becomes

$$g(\mathbf{R}^2,\mathbf{R}'^2,t) = \rho^2\exp[-\beta\,W(R)]\,P(\mathbf{R}',t/\mathbf{R},0)P(\mathbf{R}'_c,t/\mathbf{R}_c,0) \tag{103}$$

where the P's are defined by eqs. (94) and (96). A particularly simple form for the TDPDF is obtained when $\alpha t/m \gg 1$ and eq. (95) and the approximation to eq. (98) can be utilized to yield

$$\begin{aligned} g(\mathbf{R}^2,\mathbf{R}'^2,t) &= \rho^2\exp[-\beta\,W(R)]\exp\left[-\frac{\beta}{2}(\mathbf{R}'-\mathbf{R})\cdot\nabla_{\mathbf{R}}W(R)\right] \\ &\qquad P^0(\mathbf{R}'_c,t/\mathbf{R}_c,0)P^0(\mathbf{R}',t/\mathbf{R},0) \\ &= \rho^2\exp\left[-\frac{\beta}{2}W(R)\right]\exp\left[-\frac{\beta}{2}W(R')\right]P^0(\mathbf{R}'_c,t/\mathbf{R}_c,0) \\ &\qquad P^0(\mathbf{R}',t/\mathbf{R},0) \\ &= \rho^2[g(R)g(R')]^{\frac{1}{2}}\,P^0(\mathbf{R}'_c,t/\mathbf{R}_c,0)P^0(\mathbf{R}',t/\mathbf{R},0) \end{aligned} \tag{104}$$

where $P^0(\mathbf{R}'_c,\,t/\mathbf{R}_c,\,0)$ is a solution to the diffusion equation for a particle of mass M (see eq. (95)) and $P^0(\mathbf{R}',\,t/\mathbf{R},\,0)$ is a solution to the diffusion equation for a particle of mass μ (see first two terms of eq. (98)). The form of eq. (104) is similar to the form of the TDPDF for the dilute gas.

7. APPLICATION OF THE THEORY

In order to interpret T_1 in terms of our theory the expression for $k(t)$ must be evaluated using the TDPDF appropriate to the system under consideration. If the interaction between molecules is taken to be the Lennard–Jones potential as is customary, the integrations involved in calculating $k(t)$ must be done numerically. Results of such calculations shall be discussed in a subsequent publication. It may be worth while, however, to work out one special case here to illustrate the use of the theory. Consider, therefore, a system in which $a(\mathbf{R})$ is assumed to have the form associated with the dipole–dipole interaction.

$$a_m(\mathbf{R}) = \frac{C_m Y_{2m}(\theta, \phi)}{R^3} \tag{105}$$

where

$$C_1 = \left(\frac{8\pi}{15}\right)^{1/2}; \qquad C_2 = \left(\frac{32\pi}{15}\right)^{1/2}.$$

We must calculate $k_m(t)$ as defined by eqs. (6) and (24). The expressions for $g(\mathbf{R}^2, \mathbf{R}'^2, t)$ have been expressed in terms of the center of mass co-ordinates $\mathbf{R}_c$, $\mathbf{R}'_c$ and the relative co-ordinates $\mathbf{R}$, $\mathbf{R}'$ for all the systems considered. Since $a_m(\mathbf{R})$ is independent of the center of mass co-ordinates, the integrations over $\mathbf{R}_c$ and $\mathbf{R}'_c$ in eq. (24) can be performed at once. When this is done, one obtains for the two cases to be considered here, the classical gas and the classical liquid respectively.

$$k_m(t) = \int a(\mathbf{R}) a^*(\mathbf{R}') [g(R)]^{1/2} [g(R')]^{1/2} g^{(0)}(\mathbf{R}, \mathbf{R}', t) d\mathbf{R} d\mathbf{R}', \qquad \text{gas,} \tag{106}$$

$$k_m(t) = \rho \int a(\mathbf{R}) a^*(\mathbf{R}') [g(R)]^{1/2} [g(R')]^{1/2} P^0(\mathbf{R}', t/\mathbf{R}, 0) d\mathbf{R} d\mathbf{R}', \qquad \text{liquid,} \tag{107}$$

where $g^{(0)}(\mathbf{R}, \mathbf{R}', t)$ is the TDPDF for a free particle of mass μ as defined by eq. (42) and $P^0(\mathbf{R}', t/\mathbf{R}, 0)$ is the solution to the diffusion equation for a particle of mass μ as defined by the first two terms of eq. (98). $g(R)$ is the radial distribution for the system.

The integrals appearing in eqs. (106) and (107) are identical with those considered by Torrey (1953). Following this procedure, we obtain

$$k_m(t) = \rho \int_0^\infty u f(u, t) E_m(u) du \tag{108}$$

where

$$E_m(u) = C_m^2 \left[\int_0^\infty \frac{[g(R)]^{1/2} J_{5/2}(uR)}{R^{3/2}} dR \right]^2 \tag{109}$$

$$f(u, t) = e^{-[t^2 u^2 / 2\beta\mu]}, \qquad \text{gas,} \tag{110}$$

$$f(u, t) = e^{-[2Dtu^2]}, \qquad \text{liquid.} \tag{111}$$

The Fourier transforms of the $k_m(t)$ appearing in the expressions for T_1 in eq. (4) may now be evaluated. We express the results for T_1 in terms of a characteristic length, a, of the intermolecular interaction and write the integrals in terms of the dimensionless quantities x, y.

$$x = R/a, \qquad y = ua. \tag{112}$$

The Larmor frequencies of the nuclei are much smaller than the characteristic frequencies for the molecular motions in gases and liquids for most cases of interest, i.e.

$$\omega_0^2(2\beta\mu a^2) \ll 1, \qquad \text{gas}, \tag{113}$$

$$\omega_0^2\left(\frac{a^2}{2D}\right)^2 \ll 1, \qquad \text{liquid}. \tag{114}$$

For this low-frequency limit the expressions for T_1 for a system of identical spins interacting via dipole–dipole interactions is given by eq. (4) to be

$$\frac{1}{T_1} = \frac{4\pi\gamma^4\hbar^2 I(I+1)(\pi\beta m)^{1/2}\rho}{a^2}\int_0^\infty F(y)dy, \qquad \text{gas}, \tag{115}$$

$$\frac{1}{T_1} = \frac{4\pi\gamma^4\hbar^2 I(I+1)\rho}{Da}\int_0^\infty \frac{F(y)}{y}\,dy, \qquad \text{liquid}, \tag{116}$$

where

$$F(y) = \left[\int_0^\infty \frac{[g(x)]^{1/2}J_{5/2}(xy)}{x^{3/2}}\,dx\right]^2. \tag{117}$$

Hard Sphere Approximation

In the hard sphere approximation, a is taken to be the diameter of the molecules and the radial distribution function for the very dilute gas is given by

$$\begin{aligned} g(x) &= 0 \qquad x < 1 \\ g(x) &= 1 \qquad x > 1. \end{aligned} \tag{118}$$

Then

$$\int_0^\infty F(y)dy = \frac{1}{2\pi}. \tag{119}$$

Previous theoretical treatments of the liquid have also assumed a uniform $g(x)$ as given by (118). For this case, one obtains

$$\int_0^\infty \frac{F(y)}{y}\,dy = \frac{2}{15}. \tag{120}$$

For the hard sphere gas, substitution of (119) into (115) gives $T_1\rho \propto T^{\frac{1}{2}}$ as obtained by Bloembergen (1948) using a cruder approach. The numerical coefficients are different, however. No experiments have yet been made on dilute monatomic gases having nuclei of spin $\frac{1}{2}$ because of the very long relaxation times predicted (Bloembergen 1948).

Probably the simplest experiment to check eq. (115) would be to measure T_1 for He^3 gas in the presence of accurately known amounts of a paramagnetic impurity such as O_2 gas. It is simple to generalize eq. (115) to include interactions between dissimilar molecules. It should be noted that a deviation from $T_{1\rho} \propto T^{\frac{1}{2}}$ for the dilute gas should be observed due to the temperature dependence of the integral in eq. (115) if one assumes a more realistic interaction between molecules than that given by the hard sphere approximation.

For the liquid with $g(x)$ given by (118), substitution of (120) into eq. (116) gives the usual Bloembergen, Purcell, and Pound formula (1948), which has been applied, for example, by Romer (1960) and others to interpret T_1 in He^3 liquid. Ideally, we would like to evaluate the integral in (116) using the experimental values for the radial distribution function, but no experimental values of $g(x)$ are available as yet for He^3. In the absence of such data, we have performed numerical integrations using $g(x)$ evaluated for the liquid assuming a Lennard–Jones potential and Kirkwood's superposition principle (Kirkwood *et al.* 1952). Quite good agreement is obtained for $g(x)$ for He^4 if an "effective temperature" T_{eff} for the liquid is used instead of the true temperature (Mazo and Kirkwood 1955). For He^3, $T_{\text{eff}}(1^\circ\text{K})/T_{\text{eff}}(3^\circ\text{K}) = 1.42$.

Values of the integral $\int_0^\infty F(y)/y\, dy$ are presented in Table I as a function of $\beta\epsilon$ and density (described by Kirkwood *et al.* (1952), in terms of the parameter λ). ϵ is the Lennard–Jones parameter. For He^3 $\epsilon/k = 10.42^\circ$ K, $a = 2.56 \times 10^{-8}$ cm.

TABLE I

$\int_0^\infty \frac{F(y)}{y}\, dy$ as a function of temperature ($\beta\epsilon$) and density (λ)

	$\beta\epsilon$					
λ	0.2	0.4	0.6	0.8	1.0	1.2
5	0.156	0.152	0.151	0.152	0.154	0.157
10	0.161	0.154	0.151	0.150	0.150	0.150
20	0.168	0.159	0.154	0.152	0.150	0.149
27.4	0.172	0.162	0.157	0.154	0.151	0.150

The results show that the integral is remarkably insensitive to density and temperature and that the values of T_1 for He^3 in equilibrium with its vapor are predicted to be about 15% lower than that given by $g(x)$ according to eq. (118). We have discussed this point earlier (Oppenheim and Bloom 1959). Agreement between experiment and theory is improved and it will be interesting to use experimental values of $g(x)$ in evaluating $\int_0^\infty F(y)/y\, dy$ when they become available.

REFERENCES

ADRIAN, F. J. 1955. Thesis, Cornell University.
BLOCH, F. 1957. Phys. Rev. **105**, 1206.
BLOEMBERGEN, N., PURCELL, E. M., and POUND, R. V. 1948. Phys. Rev. **73**, 679.
BLOOM, M. 1957. Physica, **23**, 237.
——— 1960. Proceedings of the 7th Int. Low Temperature Conf. (Toronto).

CHANDRASEKHAR, S. 1943. Revs. Modern Phys. **15**, 1.
KIRKWOOD, J. G. 1946. J. Chem. Phys. **14**, 180.
KIRKWOOD, J. G., LEWINSON, V. A., and ALDER, B. J. 1952. J. Chem. Phys. **20**, 929.
KUBO, R. and TOMITA, K. 1954. J. Phys. Soc. Japan, **9**, 888.
MAZO, R. M. and KIRKWOOD, J. G. 1955. Proc. Natl. Acad. Sci. **41**, 204.
MORIYA, T. 1957. Progr. Theoret. Phys. **18**, 567.
MORIYA, T. and MOTIZUKI, K. 1957. Progr. Theoret. Phys. **18**, 183.
OPPENHEIM, I. 1957. Thesis, Yale University.
OPPENHEIM, I. and BLOOM, M. 1959. Can. J. Phys. **37**, 1324.
OPPENHEIM, I. and MAZUR, P. 1957. Physica, **23**, 197.
OPPENHEIM, I. and ROSS, J. 1957. Phys. Rev. **107**, 28.
REDFIELD, A. G. 1957. I.B.M. J. Research and Develop. **1**, 19.
ROMER, R. H. 1960. Phys. Rev. **117**, 1183.
TORREY, H. C. 1953. Phys. Rev. **92**, 962.
VAN HOVE, L. 1954. Phys. Rev. **95**, 249.
WIGNER, E. 1932. Phys. Rev. **40**, 749.

ON THE NUCLEAR SPIN RELAXATION IN HYDROGEN GAS[1]

G. T. NEEDLER[2] AND W. OPECHOWSKI

ABSTRACT

The Schwinger formula for the relaxation time T_1 of nuclear spins in hydrogen gas is valid only for sufficiently low temperatures. In this paper an approximate theory of T_1 is developed valid for any temperature. An explicit expression is given for T_1 valid for temperatures up to room temperature; this expression reduces to the Schwinger formula for sufficiently low temperatures.

1. INTRODUCTION

A simple theory of nuclear spin relaxation in gaseous hydrogen at low temperatures has been developed by Schwinger, and published by Bloembergen (1948) and by Bloembergen, Purcell, and Pound (1948). The theory is based on the assumptions (*a*) that the relaxation is due to *intra*molecular interactions involving the nuclear spins and the rotational angular momentum of the molecule, and (*b*) that the effect of intermolecular interactions can be taken into account by letting the rotational angular momentum of the hydrogen molecules undergo random changes.

However, in the derivation of the formula for the relaxation time T_1, Schwinger introduced an additional assumption, which restricts the validity of the formula to the case in which all orthohydrogen molecules are in rotational states corresponding to a fixed value of quantum number j. This means that the formula can be used only for low temperatures at which practically all orthohydrogen molecules are in the rotational states $j = 1, m_j = +1, 0, -1$ (parahydrogen molecules are of no interest as their nuclear spin is zero).

Recent measurements of T_1, by Lipsicas and Bloom (1961) for hydrogen over a temperature range up to 300° K have made it desirable to derive a formula for T_1 valid for arbitrary temperatures. On Dr. Bloom's suggestion we have done this, and our derivation is given in the present paper. Questions closely related to this derivation are also discussed in Oppenheim and Bloom (1961).

In our calculation we accept the basic physical assumptions of Schwinger's theory without any essential modification. Hence, from the physical point of view our theory is no better than his (or perhaps we should rather say "is as crude as his"). However, we do not assume that the random process does not affect the magnitude of the rotational angular momentum of the molecule so that our formula for T_1 is valid for arbitrary temperatures.

In Section 2 we set up a "master equation" which takes into account the random effects which simulate the intermolecular interactions. Although we have in mind, of course, the problem of nuclear spin relaxation of hydrogen gas, we obtain the master equation for a much more general problem. The

[1]Manuscript received February 14, 1961.
Contribution from the Department of Physics, University of British Columbia, Vancouver.
[2]Present address: Department of Mathematics, McGill University, Montreal.

formal procedure we follow is different from that used by Schwinger. In Section 3 we specialize the master equation to the case of nuclear spin relaxation in hydrogen. In Section 4 we obtain from this equation a generalized Schwinger formula for T_1 for this case.

2. GENERAL TREATMENT OF THE RANDOM PROCESS AND THE MASTER EQUATION

We consider a macroscopic assembly of interacting atomic systems. We assume that the properties of the assembly which we are interested in are approximately the same as those of a suitably chosen statistical ensemble of these atomic systems, the eigenstates of each system being subjected to random changes which simulate the effect of interactions between the systems. In our case the assembly of atomic systems will be the hydrogen gas; and the interactions of an orthohydrogen molecule with other hydrogen molecules will be simulated by a random process affecting the rotational states of the orthohydrogen molecule.

We assume that the Hamiltonian $\mathscr{H}$ of each system does not depend on time explicitly, and that it can be split up into two terms $\mathscr{H}_0$ and Ω,

$$\mathscr{H} = \mathscr{H}_0 + \Omega, \tag{2.1}$$

such that the random process affects the average occupation numbers of the eigenstates of $\mathscr{H}$ in the ensemble only because of the presence of Ω; in other words, if Ω were zero these occupation numbers would be time independent. It must be emphasized that Ω depends only on the dynamical variables of the system itself; it does not contain any dynamical variables pertaining to other systems of the ensemble. For example, in the case of hydrogen gas, the "system" is an isolated orthohydrogen molecule in the presence of a constant magnetic field, and Ω stands for *intra*molecular interactions.

We first disregard the presence of the random process; in other words, we consider an isolated system. We treat then Ω as a weak perturbation, and expand the solution of the Schroedinger equation which corresponds to the Hamiltonian $\mathscr{H}$ into time-dependent eigenstates $|n\rangle e^{-iE_n t/\hbar}$ of $\mathscr{H}_0$. The coefficients $a_n(t)$ of $|n\rangle e^{-iE_n t/\hbar}$ in this expansion (that is, the probability amplitudes of the eigenstates of $\mathscr{H}_0$) satisfy, as is well known, the equations:

$$a_n(t) = a_n(0) + \frac{1}{i\hbar} \sum_{n'} \int_0^t dt'\, \Omega_{nn'}(t') a_{n'}(t'), \tag{2.2}$$

where

$$\Omega_{nn'}(t) = \Omega_{nn'} e^{i\omega_{nn'} t}, \tag{2.3}$$

$$\hbar\omega_{nn'} = E_n - E_{n'}, \tag{2.4}$$

$$\Omega_{nn'} = (n|\Omega|n'), \tag{2.5}$$

and we assume

$$\Omega_{nn} = 0. \tag{2.6}$$

We next consider the solution of equation (2.2) in the usual form of an infinite expansion into powers of the perturbation operator. Neglecting the terms of the order of Ω^3 and higher, the solution is:

$$(2.7)\qquad a_n(t) = a_n(0) + \frac{1}{i\hbar}\sum_{n_1}\int_0^t dt_1\Omega_{nn_1}(t_1)a_{n_1}(0) + \frac{1}{(i\hbar)^2}\sum_{n_1}\sum_{n_2}\int_0^t dt_1\int_0^{t_1} dt_2\Omega_{nn_1}(t_1)\Omega_{n_1n_2}(t_2)a_{n_2}(0).$$

Of course, the constants $a_{n_k}(0)$ could have been written to the left of the integrals in equation (2.7). It will become clear in a moment why we have not done so.

The presence of the random process which simulates interactions with other systems (collisions with other molecules in the case of orthohydrogen gas) will now be taken into account.

The presence of such a random process will be interpreted as meaning that the probability amplitudes $a_n(t)$ become random functions $A_n(t)$ of time. Consequently, we shall now have to deal with a statistical ensemble of systems rather than one single isolated system. The question which arises immediately is this: how does the random character of the time dependence of the probability amplitudes influence the effect of the perturbation? We answer this question by assuming that this influence can be taken into account by replacing, in the integrands of the integrals in equation (2.7),

$$(2.8)\qquad \Omega_{n_{k-1}n_k}(t_k)a_{n_k}(0) \quad \text{by} \quad \Omega_{n_{k-1}n_k}(t_k)A_{n_k}(t_k).$$

To put it more physically, the random process is assumed to affect the influence of the perturbation on the system at each time at which the n_k state ($k = 1, 2, 3, \ldots$) is involved in the transition caused by the perturbation, that is at the time t_k.

Equation (2.7) is then replaced by

$$(2.9)\qquad A_n(t) = A_n(0) + \frac{1}{i\hbar}\sum_{n_1}\int_0^t dt_1\Omega_{nn_1}(t_1)A_{n_1}(t_1) + \frac{1}{(i\hbar)^2}\sum_{n_1}\sum_{n_2}\int_0^t dt_1\int_0^{t_1} dt_2\Omega_{nn_1}(t_1)\Omega_{n_1n_2}(t_2)A_{n_2}(t_2).$$

From this equation we can immediately obtain the expression for the elements $A^*_{n'}(t)A_n(t)$ of the corresponding density matrix. In particular, by forming the product of the amplitudes $A_n(t)$ and $A^*_n(t)$ as given by this equation and its complex conjugate, we obtain the following expression for the diagonal elements of the density matrix:

$$
\begin{aligned}
(2.10)\quad A_n^*(t)A_n(t) &= A_n^*(0)A_n(0) \\
&+\frac{1}{i\hbar}\sum_{n_1}\int_0^t dt_1\Omega_{nn_1}(t_1)A_n^*(0)A_{n_1}(t_1) \\
&-\frac{1}{i\hbar}\sum_{n_1}\int_0^t dt_1\Omega_{nn_1}^*(t_1)A_n(0)A_{n_1}^*(t_1) \\
&+\frac{1}{\hbar^2}\sum_{n_1}\sum_{n_2}\int_0^t dt_1\int_0^t dt_2\Omega_{nn_1}^*(t_1)\Omega_{nn_2}(t_2)A_{n_1}^*(t_1)A_{n_2}(t_2) \\
&-\frac{1}{\hbar^2}\sum_{n_1}\sum_{n_2}\int_0^t dt_1\int_0^{t_1} dt_2\Omega_{nn_1}(t_1)\Omega_{n_1n_2}(t_2)A_n^*(0)A_{n_2}(t_2) \\
&-\frac{1}{\hbar^2}\sum_{n_1}\sum_{n_2}\int_0^t dt_1\int_0^{t_1} dt_2\Omega_{nn_1}^*(t_1)\Omega_{n_1n_2}^*(t_2)A_n(0)A_{n_2}^*(t_2).
\end{aligned}
$$

Next, we replace $A_n^*(0)$ and $A_n(0)$ by $A_n^*(t_1)$ and $A_n(t_1)$ in the fifth and sixth term on the right-hand side of equation (2.10). This is permissible, because the difference $A_n(t_1)-A_n(0)$ is of the order of Ω (see equation (2.9)); hence, this replacement adds to equation (2.10) terms of the order of Ω^3, which we neglect anyway.

Finally, we take the ensemble average, denoted by $\langle \ldots \rangle$, of both sides of the so-modified equation (2.10). We obtain:

$$
\begin{aligned}
(2.11)\quad \langle A_n^*(t)A_n(t)\rangle &= \langle A_n^*(0)A_n(0)\rangle \\
&+\frac{1}{i\hbar}\sum_{n_1}\int_0^t dt_1\Omega_{nn_1}(t_1)\langle A_n^*(0)A_{n_1}(t_1)\rangle \\
&-\frac{1}{i\hbar}\sum_{n_1}\int_0^t dt_1\Omega_{nn_1}^*(t_1)\langle A_n(0)A_{n_1}^*(t_1)\rangle \\
&+\frac{1}{\hbar^2}\sum_{n_1}\sum_{n_2}\int_0^t dt_1\int_0^t dt_2\Omega_{nn_1}^*(t_1)\Omega_{nn_2}(t_2)\langle A_{n_1}^*(t_1)A_{n_2}(t_2)\rangle \\
&-\frac{1}{\hbar^2}\sum_{n_1}\sum_{n_2}\int_0^t dt_1\int_0^{t_1} dt_2\Omega_{nn_1}(t_1)\Omega_{n_1n_2}(t_2)\langle A_n^*(t_1)A_{n_2}(t_2)\rangle \\
&-\frac{1}{\hbar^2}\sum_{n_1}\sum_{n_2}\int_0^t dt_1\int_0^{t_1} dt_2\Omega_{nn_1}^*(t_1)\Omega_{n_1n_2}^*(t_2)\langle A_n(t_1)A_{n_2}^*(t_2)\rangle.
\end{aligned}
$$

We shall call, as is usual, the ensemble-averaged elements of the density matrix the "correlation functions" of the probability amplitudes.

We have not yet introduced any specific assumptions about the random process. We will do this now.

First, assume that the random process is stationary. This means that the correlation functions $\langle A_{n'}^*(t')A_{n''}(t'')\rangle$ depend only on the time difference $t'-t''$.

We assume that the random functions $A_n(t)$ are uncorrelated: $\langle A_{n'}^*(t')A_{n''}(t'')\rangle = 0$ for $n'\neq n''$.

It is this neglecting of the off-diagonal elements of the density matrix which makes the theory presented in this paper rather crude, even apart from the additional simplifying assumptions to be introduced later.

Finally, we assume more specifically that

$$\langle A_n^*(t)A_{n'}(t')\rangle = \delta_{nn'}\langle|A_n(t'')|^2\rangle f_n(t-t'), \tag{2.12}$$

where $f_n(t-t')$ is an even function which rapidly decreases from $f_n(0) = 1$ to $f_n(\infty) = 0$; t'' is any time instant in the time interval between t and t'. In other words, $\langle|A_n(t'')|^2\rangle$ is assumed to be a slowly varying function over the time interval for which $f_n(t-t')$ is appreciably different from zero. For simplicity, we introduce the notation:

$$\rho_n(t) = \langle|A_n(t)|^2\rangle. \tag{2.13}$$

Later on each "autocorrelation function" $f_n(t-t')$ will be characterized by a "correlation time". If the time variation of $\rho_n(t)$ is similarly characterized by a "relaxation time", then the above assumption can be expressed by saying that the correlation times are assumed to be much shorter than the relaxation times.

Using (2.6), (2.12), and (2.13), we obtain from equation (2.11):

$$\begin{aligned}\rho_n(t)-\rho_n(0) &= \frac{1}{\hbar^2}\sum_{n_1}|\Omega_{nn_1}|^2\int_0^t dt_1\int_0^t dt_2\rho_{n_1}\left(\frac{t_1+t_2}{2}\right)f_{n_1}(t_1-t_2)e^{-i\omega_{nn_1}(t_1-t_2)}\\ &-\frac{1}{\hbar^2}\sum_{n_1}|\Omega_{nn_1}|^2\int_0^t dt_1\int_0^{t_1} dt_2\rho_n\left(\frac{t_1+t_2}{2}\right)f_n(t_1-t_2)e^{i\omega_{nn_1}(t_1-t_2)}\\ &-\frac{1}{\hbar^2}\sum_{n_1}|\Omega_{nn_1}|^2\int_0^t dt_1\int_0^{t_1} dt_2\rho_n\left(\frac{t_1+t_2}{2}\right)f_n(t_1-t_2)\,e^{-i\omega_{nn_1}(t_1-t_2)}.\end{aligned} \tag{2.14}$$

Next we transform the double integrals in this equation by introducing*

$$t' = t_1-t_2 \qquad \text{and} \qquad t'' = (1/2)(t_1+t_2)$$

as the new integration variables. Since the autocorrelation functions $f_n(t')$ have been assumed to decrease rapidly as t' increases, the integration with respect to t' can be extended from $-\infty$ to $+\infty$. After some simple rearrangements we finally obtain the "master equation",

$$\frac{d\rho_n}{dt} = \sum_{n_1} W_{n_1n}\rho_{n_1} - \sum_{n_1} W_{nn_1}\rho_n, \tag{2.15}$$

where W_{nn_1} are the transition probabilities given by

$$W_{nn_1} = \hbar^{-2}|\Omega_{nn_1}|^2\int_{-\infty}^{+\infty} f_n(t)e^{i\omega_{nn_1}t}\,dt. \tag{2.16}$$

The first term on the right-hand side of equation (2.15) arises from the first term on the right-hand side of equation (2.14); the second term on the right-hand side of (2.15) arises from the second and third terms on the right-hand side of (2.14).

*Compare a similar transformation in Van Hove (1955), p. 523. We may emphasize in passing that the approach-to-equilibrium problem treated in Van Hove's paper is physically different from that treated in the present paper despite some obvious similarities (quite apart from the elegance and mathematical rigor of his theory as compared with the crudity of our approximations).

3. MASTER EQUATION FOR THE SPIN SYSTEM IN HYDROGEN GAS

In the case of an orthohydrogen molecule the two parts of the Hamiltonian (2.1) are given by:

$$\mathcal{H}_0 = B\mathbf{J}^2+\hbar\omega_J J_z+\hbar\omega_I I_z+A \tag{3.1}$$

and

$$\Omega = \Omega_0-A \tag{3.2}$$

where

$$\Omega_0 = c(\mathbf{I}^{(1)}+\mathbf{I}^{(2)})\cdot\mathbf{J}+5d[\mathbf{I}^{(1)}\cdot\mathbf{I}^{(2)}-3(\mathbf{I}^{(1)}\cdot\mathbf{u})(\mathbf{I}^{(2)}\cdot\mathbf{u})]. \tag{3.3}$$

The meaning of the symbols in these equations is as follows:

$\mathbf{J}$ (eigenvalues: j) is the rotational angular momentum of the molecule;

J_z (eigenvalues: m_j) its z component, the z-axis being taken parallel to the direction of the external, homogeneous magnetic field H;

$B\mathbf{J}^2$ is the rotational energy of the molecule;

$\mathbf{I}^{(1)}$ and $\mathbf{I}^{(2)}$ are the nuclear spins of the two protons;

$\mathbf{I} = \mathbf{I}^{(1)}+\mathbf{I}^{(2)}$ is the resultant nuclear spin of the molecules (which, in the case of orthohydrogen molecule, has a unique eigenvalue $I = 1$);

I_z (eigenvalues $\alpha = +1, 0, -1$) its z component;

$\omega_J = \mu_j H/j\hbar$ and $\omega_I = \mu H/I\hbar = \mu H/\hbar$, where μ_j is the magnitude of the rotational magnetic moment, and μ the magnitude of the total nuclear magnetic moment of the molecule;

$\mathbf{u}$ is the unit vector along the direction of the line joining the two protons of the molecule;

c and d will here be treated as constants, although, strictly speaking, their matrix elements are slowly varying functions of j. The numerical values of these constants are (Ramsey 1956):

$$-ch^{-1} = 113.9 \text{ kc/sec},$$

$$dh^{-1} = 57.7 \text{ kc/sec}.$$

The eigenstates of $(\mathcal{H}_0-A)$, that is the eigenstates of the orthohydrogen molecule when the interaction Ω is neglected, will be labeled by the three quantum numbers just defined: α, j, m_j (for simplicity, we shall write m instead of m_j). The quantity A is that part of the Ω_0 which has only diagonal elements in the representation in which Ω_0-A is diagonal, i.e. in the α, j, m_j representation just defined. The difference between the eigenstates of $\mathcal{H}_0$ and $\mathcal{H}_0+A$ is easily shown to be negligible for our purposes, and we will disregard it in what follows. The only reason for subtracting and adding A in equations (3.1) and (3.2) is to obtain an interaction operator which satisfies condition (2.6.).

We now specialize equations (2.15) and (2.16) to the nuclear spin relaxation problem in hydrogen gas. We assume that, if one disregards the nuclear spins, the gas is in thermal equilibrium at any time. Therefore we replace in equation (2.15)

$$\rho_n(t) \qquad \text{by} \qquad \rho_\alpha(t)\rho_{jm},$$

where

$$\rho_{jm} = e^{-E_{jm}/kT}\left(\sum_{jm} e^{-E_{jm}/kT}\right)^{-1} \tag{3.4}$$

and $E_{jm} = E_j + E_m$ are eigenvalues of $BJ^2 + \hbar\omega_J J_z$. Next, we replace in equation (2.16)

$$f_n(t) \qquad \text{by} \qquad f_{jm}(t);$$

the independence of $f_{jm}(t)$ from α corresponds to the fact that collisions directly affect only the rotational states of the molecule. In this way we obtain from equation (2.16) an equation which, when summed over all values of j and m, gives:

$$\frac{d\rho_\alpha}{dt} = \sum_{\alpha'} [W_{\alpha'\alpha}\rho_{\alpha'} - W_{\alpha\alpha'}\rho_\alpha], \tag{3.5}$$

where

$$W_{\alpha'\alpha} = \hbar^{-2} \sum_{jm} \sum_{j'm'} \rho_{j'm'} |\Omega_{\alpha' j'm';\alpha jm}|^2 \int_{-\infty}^{+\infty} f_{j'm'}(t) e^{it(E_{\alpha' j'm'} - E_{\alpha jm})/\hbar} dt \tag{3.6}$$

and

$$E_{\alpha jm} = E_{jm} + E_\alpha.$$

It is customary to assume (see, for example, Bloembergen 1948) that the transition probabilities $W_{\alpha'\alpha}$ satisfy the relations

$$\frac{W_{\alpha'\alpha}}{W_{\alpha\alpha'}} = e^{(E_{\alpha'} - E_\alpha)/kT} \approx 1 + \frac{E_{\alpha'} - E_\alpha}{kT}. \tag{3.7}$$

These relations have been used and derived for various models and approximations by many authors. We are going to assume their validity in our case. By doing this we impose certain restrictions on the autocorrelation functions $f_{jm}(t)$. We will not discuss here these restrictions, although we have derived them. They are not very illuminating. In any case, they are not necessarily violated by the explicit form of $f_{jm}(t)$ introduced in Section 4.

4. EXPRESSION FOR T_1 IN HYDROGEN GAS

It is well known that under certain conditions the master equation (3.5) has an approximate solution which can be interpreted as meaning that the nuclear spin system has a well-defined spin temperature T_s.* In other words, there exists an approximate solution of the form

$$\rho_\alpha = e^{-E_\alpha/kT_s} Z^{-1}, \qquad Z = \sum_\alpha e^{-E_\alpha/kT_s} \tag{4.1}$$

where T_s is a function of time. These conditions are: the validity of equation (3.7), provided

*For a recent discussion of this point, see Sher and Primakoff (1960).

(4.2) $$|E_\alpha - E_{\alpha'}| \ll kT_s \quad \text{and} \quad |E_\alpha - E_{\alpha'}| \ll kT,$$

and the validity of certain relations between the $W_{\alpha\beta}$'s, which we will now derive (see equation (4.5) below).

Using equations (4.2) and (3.7), the master equation (3.5) can be rewritten as

(4.3) $$\frac{d}{dt}\left(\frac{1}{T_s}\right) = B_{\alpha\beta}\left(\frac{1}{T}-\frac{1}{T_s}\right),$$

where

(4.4) $$B_{\alpha\beta} = W_{\alpha\beta}+W_{\beta\alpha}+\frac{1}{2}\sum_{\gamma\neq\alpha,\beta}\left[\frac{E_\gamma-E_\alpha}{E_\beta-E_\alpha}(W_{\gamma\alpha}+W_{\alpha\gamma})+\frac{E_\gamma-E_\beta}{E_\alpha-E_\beta}(W_{\gamma\beta}+W_{\beta\gamma})\right].$$

If T_s is to be interpreted as the nuclear spin temperature it must obviously be independent of α and β. This implies that all the $B_{\alpha\beta}$'s must have the same value.

From now on we assume that $I = 1$ (the case of an orthohydrogen molecule), and that the nuclear Zeeman energy levels are equidistant. A simple calculation shows then that $B_{\alpha\beta}$'s will have the same value if and only if

(4.5) $$W_{10}+W_{01} = W_{-10}+W_{0-1}.$$

Then

(4.6) $$B_{\alpha\beta} = W_1+2W_2 \qquad \text{(for any } \alpha \text{ and } \beta\text{)},$$

where

(4.7) $$W_1 = \tfrac{1}{2}(W_{10}+W_{01}), \qquad W_2 = \tfrac{1}{2}(W_{1-1}+W_{-11}).$$

Thus, if equations (3.7), (4.2), and (4.5) are valid, the master equation (3.5) has a solution of the form (4.1), where the time dependence of T_s is obtained from (4.3); or more explicitly:

(4.8) $$\frac{1}{T_s} = \left(\frac{1}{T_s^0}-\frac{1}{T}\right)e^{-t/T_1}+\frac{1}{T},$$

where the relaxation time T_1 is given by

(4.9) $$1/T_1 = W_1+2W_2.$$

Next we show that, if the autocorrelation functions $f_{jm}(t)$ are independent of m, the $W_{\alpha\beta}$ for the orthohydrogen nuclear spin system do satisfy the condition (4.5) to the same approximation as that which is used in obtaining the solution of the form given by (4.1) and (4.8). To this end we shall first replace equation (3.6) for $W_{\alpha\beta}$ by a simpler approximate expression. It should be remembered that each $f_{jm}(t)$ is an unknown quantity which depends on the temperature. Thus, if expression (3.6) for $W_{\alpha\beta}$ is used and only those terms for which $j = 1$ or 3 are important, the relaxation time T_1 is given in terms of 10 unknown quantities at each temperature; if only those terms for which $j = 1$ are important, T_1 is given in terms of three unknown quantities. The Schwinger formula, which is valid for $j = 1$, has only one unknown

quantity. The expression with which we replace (3.6) is both simpler in form and has fewer unknown quantities. In addition, the simplified expression satisfies condition (4.5) which, as mentioned before, is necessary if the master equation is to have a solution of the form (4.1).

We first consider ρ_{jm}, which is given by equation (3.4). For commonly used values of the static magnetic field (several thousand gauss) $E_m \approx 10^{-19}$ ergs, while, on the other hand, $E_j = 1.2j(j+1)10^{-14}$ ergs. Thus we may rewrite (3.4) approximately as

$$\rho_{jm} \approx \rho_j/(2j+1), \tag{4.10}$$

where ρ_j is the average fraction of the total number of orthohydrogen molecules with rotational angular momentum j. For orthohydrogen, although j takes all odd integer values, ρ_j is negligible up to room temperature for $j \geqq 5$.

Now consider the autocorrelation functions $f_{jm}(t)$. As is usual (Bloembergen 1948), we will assume an exponential form for the autocorrelation functions, that is

$$f_{jm}(t) = e^{-|t|/\tau_{jm}}. \tag{4.11}$$

The correlation time τ_{jm} may be interpreted as being the mean time spent by a molecule in the rotational state j, m before a collision with another molecule causes a transition to another rotational state. Using (4.11) we have

$$\int_{-\infty}^{+\infty} f_{jm}(t) e^{i(E_{\alpha jm} - E_{\alpha' j' m'})t/\hbar} dt = \frac{2\tau_{jm}}{1+[(E_{\alpha jm} - E_{\alpha' j' m'})\tau_{jm}/\hbar]^2}. \tag{4.12}$$

If the correlation times τ_{jm} are longer than 10^{-13} seconds, all expressions of the form (4.12) for which $j' \neq j$ are negligible compared to those for which $j' = j$. We omit the terms for which $j' \neq j$ thus limiting the theory to temperatures and pressures for which $\tau_{jm} \geqq 10^{-13}$ seconds. Using the Schwinger formula, which is valid at low temperatures, it has been found that the correlation time for collisions which change the rotational state of a molecule is of the order of 10^{-10} seconds. It seems that the above condition for τ_{jm} will be satisfied at least for temperatures up to room temperature and pressures up to 200 atmospheres. We assume this is in fact the case.

Next we assume that we may write

$$\tau_{jm} = \tau_j \tag{4.13}$$

for all m. This assumption is an extension of an assumption implicit in the original Schwinger theory where $j = 1$.

For a hydrogen molecule the nuclear spin and rotational Zeeman levels are both equidistant. We introduce the notation

$$E_{\alpha jm} - E_{\alpha-1,j,m+1} = \hbar\omega_j. \tag{4.14}$$

If we now substitute (4.10), (4.12), (4.13), and (4.14) into (3.6) and calculate the matrix elements of Ω as defined by equations (3.2) and (3.3), we obtain

$$(4.15)\quad W_{10} = W_{01} = W_{-10} = W_{0-1} = \frac{1}{\hbar^2}\left[\rho_1\left(\frac{3}{2}d^2+\frac{2}{3}c^2\right)\frac{2\tau_1}{1+(\omega_1\tau_1)^2}+\rho_3(d^2+4c^2)\frac{2\tau_3}{1+(\omega_3\tau_3)^2}\right].$$

$$(4.16)\quad W_{1-1} = W_{-11} = \frac{1}{\hbar^2}\left[\rho_1 3d^2\frac{2\tau_1}{1+(2\omega_1\tau_1)^2}+\rho_2 2d^2\frac{2\tau_3}{1+(2\omega_3\tau_3)^2}\right].$$

We will now use the simplified expressions (4.15) and (4.16) for the transition probabilities to calculate the relaxation time T_1. It was shown at the beginning of this section that, if the transition probabilities satisfy conditions (3.7), (4.2), and (4.5), the master equation has an approximate solution of the form (4.1) and the relaxation time is given by (4.9). The simple approximate expressions (4.15) satisfy (4.5) but they do not satisfy (3.7). However, since the relaxation time is given in terms of the transition probabilities only to the first order in $|E_\alpha - E_{\alpha'}|/kT$ and $|E_\alpha - E_{\alpha'}|/kT_s$, it does not matter for the calculation of the relaxation time if the simplified expressions for the transition probabilities violate condition (3.7) to the same order. Since this is indeed the case, we use the simplified expressions for the transition probabilities to calculate T_1 from (4.9). We obtain for temperatures up to room temperature

$$(4.17)\quad \frac{1}{T_1} = \frac{\rho_1}{\hbar^2}\left[\left(\frac{3}{2}d^2+\frac{2}{3}c^2\right)\frac{2\tau_1}{1+(\omega_1\tau_1)^2}+3d^2\frac{4\tau_1}{1+(2\omega_1\tau_1)^2}\right] + \frac{\rho_3}{\hbar^2}\left[(d^2+4c^2)\frac{2\tau_3}{1+(\omega_3\tau_3)^2}+2d^2\frac{4\tau_3}{1+(2\omega_3\tau_3)^2}\right],$$

where ρ_1, ρ_3, τ_1, and τ_3 are all temperature dependent. At low temperatures where $\rho_3 \to 0$ and $\rho_1 \to 1$, we have

$$(4.18)\quad \frac{1}{T_1} \approx \frac{1}{\hbar^2}\left(\frac{3}{2}d^2+\frac{2}{3}c^2\right)\frac{2\tau_1}{1+(\omega_1\tau_1)^2}+\frac{1}{\hbar^2}3d^2\frac{4\tau_1}{1+(2\omega_1\tau_1)^2}.$$

Expression (4.18) for the relaxation time at low temperatures and the Schwinger formula are identical with one exception. Where we have $\hbar\omega_1 = E_{\alpha 1m} - E_{\alpha-1,1,m+1}$, the Schwinger formula has $\hbar\omega = E_\alpha - E_{\alpha-1}$; that is, the Schwinger formula does not take into account the rotational Zeeman energy splitting. So far as we know, the Schwinger formula has only been checked experimentally for $\omega_1\tau_1 \ll 1$. In this case our expression and the Schwinger formula agree. For the case that $\omega_1\tau_1 \approx 1$, which occurs at low temperatures and low pressures, we believe a more correct result is (4.18). Since the rotational Zeeman energy is approximately one-fifth of the nuclear Zeeman energy for $j = 1$, it should be possible to check this point experimentally.

If one neglects the denominators containing the frequency in equation (4.17) the contribution of one j-state agrees of course with the Schwinger formula for an arbitrary j as given for example in Bloom (1957), equation (1), provided one puts $c = \gamma\hbar H'$ and $5d = 2\gamma\hbar H''$.

For an application of equation (4.17) to a discussion of experimental data, see Lipsicas and Bloom (1961).

ACKNOWLEDGMENTS

We are indebted to Mr. Kyoji Nishikawa for a discussion which led to the present improved version of Section 2. One of us (G.T.N.) would like to acknowledge the financial help from the National Research Council of Canada in the form of a scholarship.

REFERENCES

BLOEMBERGEN, N. 1948. Thesis, University of Leiden.
BLOEMBERGEN, N., PURCELL, E. N., and POUND, R. V. 1948. Phys. Rev. **73**, 679.
BLOOM, M. 1957. Physica, **23**, 237.
LIPSICAS, M. and BLOOM, M. 1961. Can. J. Phys. **39**. This issue.
OPPENHEIM, I. and BLOOM, M. 1961. Can. J. Phys. **39**. This issue.
RAMSEY, N. F. 1956. Molecular beams (Clarendon Press, Oxford).
SHER, A. and PRIMAKOFF, H. 1960. Phys. Rev. **119**, 178.
VAN HOVE, L. 1955. Physica, **21**, 517.

NUCLEAR MAGNETIC RESONANCE MEASUREMENTS IN HYDROGEN GAS[1]

M. LIPSICAS[2] AND M. BLOOM

ABSTRACT

The proton spin–lattice relaxation time T_1 has been measured for H_2 gas using pulse techniques over the temperature range 39° K to 300° K and at pressures up to 150 atmospheres. T_1 is proportional to density, ρ, at low densities and constant temperature, over the entire temperature range studied. Deviations from linearity due to three-body collisions are observed at densities of the order of 500 Amagats. T_1/ρ for the dilute gas is approximately constant from about 100° K to 300° K but increases sharply at lower temperatures. The spin–spin relaxation time T_2 was measured at 78° K and found to be proportional to ρ but shorter than T_1. The diffusion constant D was measured, using the properties of the spin echo, at 78° K in the dilute gas. $D\rho$ was found to be constant. An analysis of the temperature dependence of T_1/ρ using the theory of Needler and Opechowski shows that the excited rotational states of ortho-H_2 probably play no role in the spin–lattice relaxation below 300° K. The T_1 results are interpreted in terms of the theory of Oppenheim and Bloom to give information on the anisotropic H_2–H_2 interactions. The constancy of T_1/ρ at high temperatures cannot be understood in terms of the classical properties of the gas. Quantum mechanical diffraction effects play an extremely important role in the spin–lattice relaxation even at high temperatures because of the very short range nature of the anisotropic interactions.

1. INTRODUCTION

In this paper we report a nuclear magnetic resonance (n.m.r.) investigation of hydrogen gas over a wide range of temperatures and pressures. In the field of solid state physics, the usefulness of n.m.r. studies is now well recognized and important contributions have been made to the understanding of metals, semiconductors, etc. However, little systematic work on gases has been reported hitherto, earlier measurements on H_2 gas having been made only below 20° K and at pressures up to 1 atmosphere (Bloom 1957). These measurements of the proton spin–lattice relaxation time T_1 confirmed that the mechanism for the exchange of energy between the proton spin system and the heat reservoir represented by the translational degrees of freedom of the gas molecules was that predicted by Schwinger, and first investigated by Bloembergen, Purcell, and Pound (1948). The rate of relaxation was found to be determined by those collisions between molecules which cause ortho-H_2 molecules to undergo transitions between the three magnetic substates of the $J = 1$ rotational state. The interactions which couple the protons in H_2 to the rotational angular momentum have been known for some time from molecular beam measurements (Ramsey 1956). Therefore, it was possible to relate T_1 to the mean lifetime τ_1 of the molecules in the three magnetic substates of the $J = 1$ state at low temperatures where all the ortho-H_2 molecules

[1]Manuscript received February 14, 1961.
Contribution from the Department of Physics, University of British Columbia, Vancouver, B.C. This research was supported by the National Research Council of Canada.
[2]Present address: Department of Physics, Rutgers University, New Brunswick, N.J.

are in the $J = 1$ state. Schwinger's formula, valid for the region where $\tau_1 \ll$ Larmor period of the protons in the external magnetic field, is

$$\frac{1}{T_1} = \left(\frac{4}{3}c^2+15d^2\right)\frac{\tau_1}{\hbar^2} = 2.7\times10^{12}\tau_1. \tag{1}$$

$c/h = 113.9$ kc/sec and $d/h = 57.67$ kc/sec are parameters associated with the intramolecular interactions.

Thus, the n.m.r. technique is capable, in principle, of yielding detailed information on the very weak anisotropic interactions between H_2 molecules which produce molecular reorientation. Most other transport properties of H_2 are affected only slightly by these weak interactions whereas the T_1 measurements are primarily determined by them.

The previous measurements of T_1 were all made at low densities, where only binary collisions between molecules are important, and it was found that $T_1 \propto \rho$, the number of molecules per cm^3. This was to be expected from equation (1), since one can define a cross section σ for collisions which cause transitions between the magnetic substates, such that

$$\frac{1}{\tau_1} = \rho\langle\sigma V\rangle \tag{2}$$

where V is the relative velocity of a pair of molecules and $\langle\sigma V\rangle$ represents an average over the velocity distribution at the temperature of the gas.

The present experimental study extends the measurements of T_1 in normal H_2 (75% ortho and 25% para) to the temperature range 39° K to 300° K and up to pressures of about 150 atmospheres. The experimental techniques required for this study are discussed in Section 2.

At high densities, where three-body and higher order collisions become important, one expects a deviation from the linear relationship between T_1 and ρ. As may be seen from the experimental results presented in Section 3, one requires a more general expansion in powers of ρ to interpret the experiments.

$$T_1 = A_1\rho+A_2\rho^2+A_3\rho^3+\ldots \tag{3}$$

In order to interpret T_1 at high temperatures, a generalization of Schwinger's theory to include the thermal excitation of higher rotational states is required. This has been carried out by Needler and Opechowski (1961) and we make use of their results in discussing our measurements in Section 4.

The extension of measurements to high temperatures also represents a bridging of the gap between the classical gas at high temperatures and the quantum gas at low temperatures where the average de Broglie wavelength of the molecules becomes larger than the size of the molecules. Oppenheim and Bloom (1960, 1961) have developed a theory which relates T_1 to the molecular properties of the gas. This enables one to evaluate T_1 quantitatively in the quantum and classical regions, and also to obtain expressions for A_1, A_2, etc. in equation (3). The interpretation of our measurements in terms of this theory is quite complicated, as is any problem involving details of molecular interactions, and is discussed at length in Section 5.

Although the major part of the work reported here is concerned with T_1 measurements, we also report some measurements of the spin–spin relaxation

time T_2 and of the self-diffusion coefficient of hydrogen gas at 78° K in Section 3. A more complete study of diffusion in hydrogen is now being carried out by one of us (M.L.) and will be reported at a later date.

2. EXPERIMENTAL TECHNIQUE AND APPARATUS

The basic equipment required for this work comprised:

(*a*) a pulsed nuclear magnetic resonance spectrometer,

(*b*) a low temperature system capable of maintaining the gas sample at any temperature between 35° K and room temperature,

(*c*) a high pressure system, including the sample "bomb" itself, designed for operation up to maximum pressures of order 200 atmospheres.

Each of these three major items of equipment was specially constructed for this work, but, where possible, considerable flexibility was allowed for in the design to make the equipment suitable for other nuclear magnetic resonance work in the future. A detailed description of the apparatus and electronic circuits may be found in Lipsicas' Ph.D. thesis (1960).

The magnet used in this work was a 7000-gauss permanent magnet and the proton resonance was observed near 30 Mc/sec.

(a) Radio-frequency Technique

All the measurements reported here were made using the pulse technique (Hahn 1950). T_1 was measured using either (*a*) a $\pi,\pi/2$ pulse sequence or (*b*) a $\pi/2,\pi/2$ pulse sequence. In either case, the first pulse disturbs the system from equilibrium, in (*a*) by inverting the nuclear magnetization ($\mathbf{M} = -\mathbf{M}_0$) and in (*b*) by making the magnetization wholly transverse ($M_z = 0$). The second pulse, applied at time τ after the first pulse, is a searching pulse, the amplitude $A(\tau)$ of its induction tail being a measure of the recovery of the z component of magnetization. T_1 is determined from the slope of the plot of $\log A[A = A(\infty) - A(\tau)]$ as a function of τ. The T_1 values for hydrogen gas were found to lie in the experimentally convenient range of approximately 10 milliseconds to 140 milliseconds.

The Spectrometer

A block diagram of the spectrometer is given in Fig. 1. The timing unit employs a time mark generator, Burroughs beam switching tube counters, and coincidence circuits which provide a double channel sequence of timing pulses. The circuitry is similar in principle to that described by Schwartz (1957). The particular timing sequence desired (time separation and mark of pulses in each pulse train, repetition rate of the pulse train) is selected by setting a number of decade selector switches appropriately. This preset timing facility of the spectrometer coupled with the use of printed log sheets for data recording was of great value in reducing to a minimum the period of time necessary for a measurement. The timing pulses trigger two Tektronix 163 pulse generators, which, in turn switch a 30-Mc oscillator on and off. The oscillator provides an output r-f. pulse of approximately 400 volt peak to peak, and a "$\pi/2$ pulse" corresponds to a pulse duration of approximately 9 microseconds. The sample coil is tuned to the resonance frequency with the aid of an air capacitor coupled to the coil through a half-wave line and the

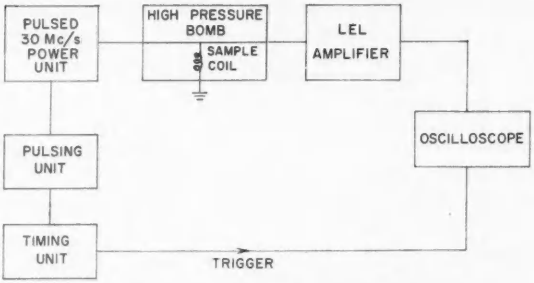

FIG. 1. Block diagram of the radio-frequency pulse spectrometer.

resonance signal is amplified by a LEL Inc. model 21BS amplifier and detected by a IN295 diode. The signal-to-noise ratio was improved considerably (by a factor of order 5) by a simple RC filter at the input to the oscilloscope. This was particularly useful for measurements on the echo signal (for example, as used in the measurement of the spin–spin relaxation time described below) since the latter is usually weaker than $\pi/2$ induction tail and yet the frequency bandwidth required for the echo is much less than that required for the induction tail, in particular because the amplifier is overdriven by the pulse.

(b) The Low Temperature System

A "blow cryostat" system was used in this work, i.e. cold helium gas obtained by boiling off helium at 4.2° K in a storage Dewar was circulated in a jacket surrounding the sample "bomb". It was not found possible to maintain the bomb temperature sufficiently constant by regulating the gas flow and, consequently, the procedure adopted in all the measurements below 50° K was first to cool the bomb down to about 30° K and then to shut off the gas flow completely and take measurements during the slow "warm-up" cycle of the bomb. The maximum temperature rise during a T_1 measurement was 1.5 Kelvin degrees at 36° K, and improved to about 0.8 Kelvin degree at 50° K. The temperature was measured by means of a platinum resistance thermometer and the difference between true gas temperature and thermometer reading due to thermal lag was calculated to be less than 0.3 Kelvin degree. The thermometer was calibrated *in situ* against the vapor pressure of hydrogen and other gases. Above 50° K, liquid nitrogen and other coolants (for example, acetone–CO_2 mixture) were used. A new low temperature system is now in the course of construction; this system employs a metal Dewar and a variable heat leak in the form of a heated steel rod connecting the bomb to the liquid helium container of the Dewar.

(c) The High Pressure System

The experiments envisaged when designing this equipment were expected to require maximum gas pressures of order 200 atmospheres. The problems involved in designing a high pressure system for nuclear magnetic resonance work at these pressures are essentially twofold:

(1) Restrictions imposed by the magnetic field. The spatial limitation here is not too serious; however, the use of non-magnetic materials does complicate matters somewhat.

(2) Difficulties due to the fact that the high pressure system has to withstand very large temperature changes.

High pressure systems and techniques suitable for the range of temperatures encountered in this work have been discussed (Paul *et al.* 1959). In the present work it was decided to make the sample chamber ("bomb") out of copper in preference to stainless steel. This decision was based on the following factors:

(1) It was desired to have a non-magnetic bomb and this would have necessitated the use of type 321 stainless steel, which is somewhat difficult to machine.

(2) It was important that the bomb should be at a uniform temperature during measurements and that the thermal time constant of the bomb should be small. The high thermal conductivity of copper is very advantageous in this respect.

The final design evolved is shown in Fig. 2. The sample coil, wound on a thin glass former, is normally "immersed" in the gas being studied. One side of the coil is anchored (and grounded) to a copper plate held in position by the pressure screw P. The seam between P and the bomb casing is sealed by a fillet of soft solder. The other end of the coil is brought out through a Kovar glass seal soft-soldered to the bomb casing. Initial attempts to seal this end of the bomb with a commercial high pressure cone joint fitting were barely satisfactory at room temperature. At low temperatures, however, it was found impossible to make such a fitting leaktight, even after Dow Corning silicone fluid had been applied. The Kovar seal, on the other hand, has been found to be very satisfactory up to pressures of order 200 atmospheres. For measurements of the diffusion constant of gases, a smaller, spatially well-defined, gas sample must be used. In this case, the interior of the bomb is filled with a teflon plug which confines the gas to the volume enclosed in the glass former. The teflon is suitably shaped to allow the gas to leak into this volume (Fig. 2). The bomb casing has been considerably overdesigned, with a very large factor of safety. The inner diameter is approximately one half of the outer diameter, which corresponds to a bursting pressure of 18,000 p.s.i. Some additional protection is also provided by the teflon cap placed over the Kovar seal as a precaution against the glass of the seal shattering. Commercial stainless steel pressure tubing and Ermeto-type high pressure fittings and valves were used for the gas transfer and handling system connecting the gas cylinder to the bomb. Sample pressures in excess of the maximum gas cylinder pressure were obtained by first liquefying a sample in the bomb at low temperatures. The gas pressure in the bomb was measured on a 6-in. diameter Budenberg Bourdon-type gauge calibrated against a Barnett dead weight tester. A new high pressure system is now being assembled using a copper–beryllium bomb designed for 1000 atmospheres working pressure, a h.i.p. 1000-atmosphere compressor, and a Heiss pressure gauge.

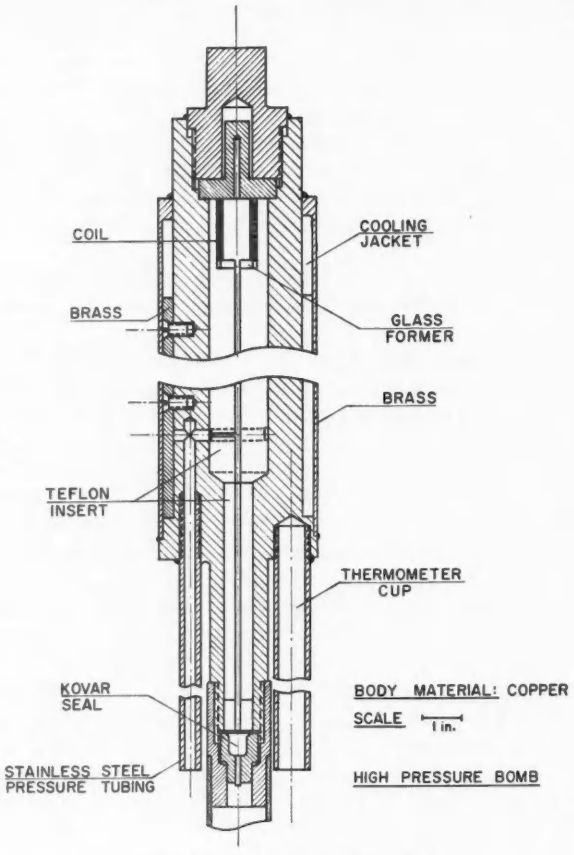

Fig. 2. The high pressure bomb.

3. EXPERIMENTAL RESULTS

(1) Spin–Lattice Relaxation

Measurements of T_1 were carried out over a range of densities up to 750 Amagats and temperatures between 37° K and 300° K.

Figures 3 through 9 are plots of the measured values of T_1 as a function of density for the nominal temperatures 37° K, 39° K, 41° K, 43° K, 45° K, 47° K, and 49° K. The density has been calculated on the basis of the *mean* temperature and pressure over each measurement, and all measurements have been grouped according to the respective mean temperature in 2-degree steps; for example, the 37° K plot shows all T_1 values corresponding to a mean temperature of between 36° K and 38° K. The solid curves drawn are the apparent best fit, as drawn by eye. Each of these plots confirms equation

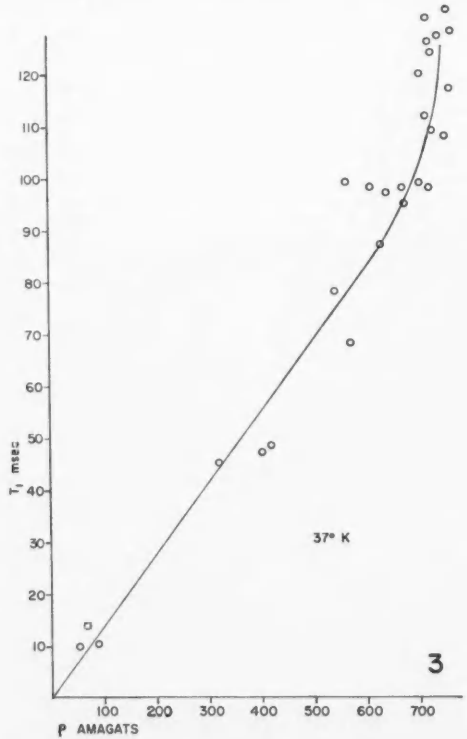

FIG. 3. Plot of $\frac{1}{2}T_1$ versus H_2 gas density, expressed in Amagats, at 37° K. One Amagat is the number density at NTP and corresponds to 2.69×10^{19} molecules/cm³.

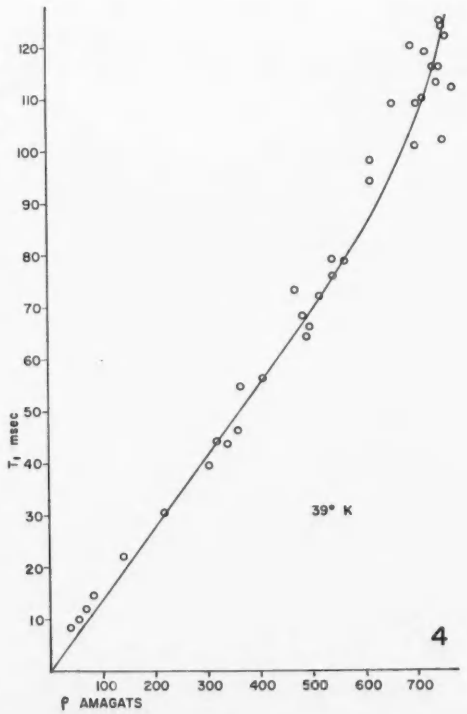

FIG. 4. Plot of T_1 versus density at 39° K.

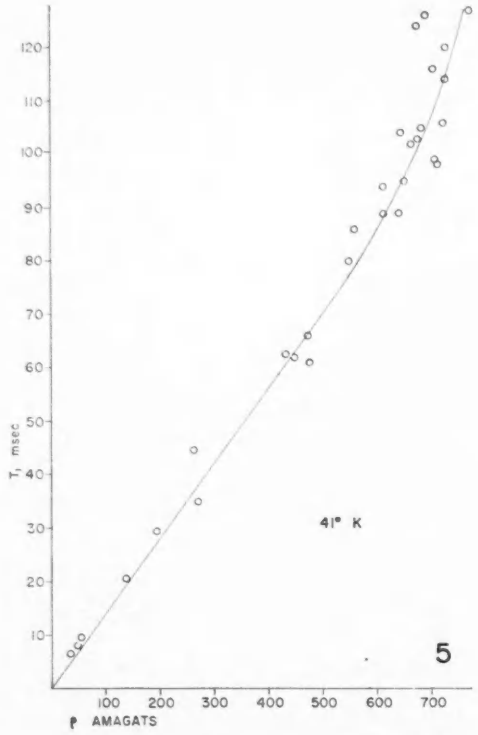

FIG. 5. Plot of T_1 versus density at 41° K.

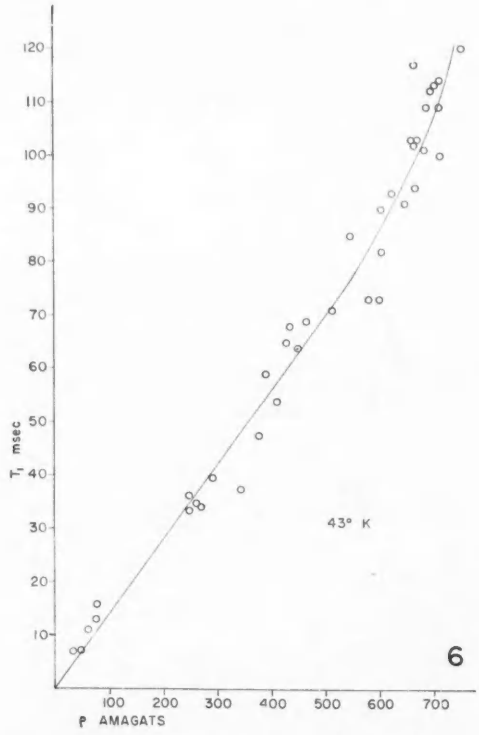

FIG. 6. Plot of T_1 versus density at 43° K.

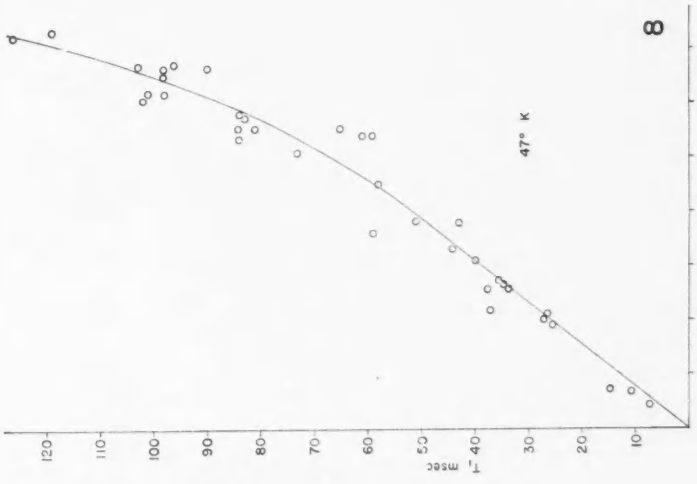

FIG. 8. Plot of T_1 versus density at 47° K.

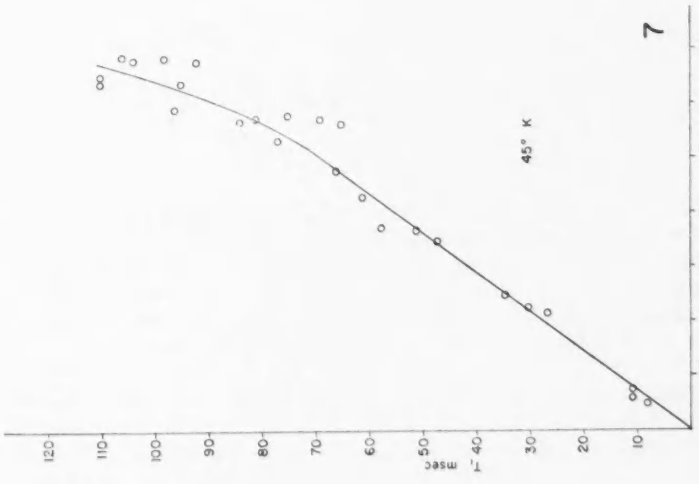

FIG. 7. Plot of T_1 versus density at 45° K.

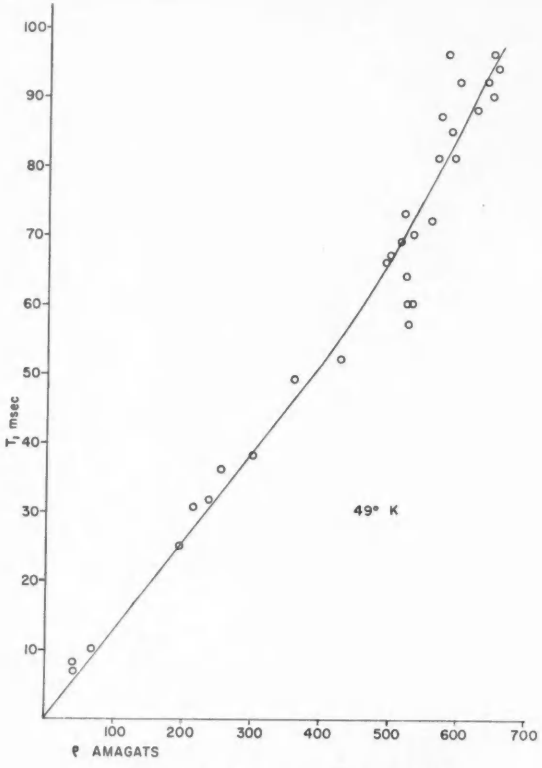

FIG. 9. Plot of T_1 versus density at 49° K.

(3) above, that at constant temperature in the "dilute" gas (low density) T_1 is proportional to the density while at high densities T_1 is seen to increase more rapidly with density. The coefficient of the ρ^2 term in (3) is positive in all cases. However, in this "dense" gas region, a very small change in density corresponds to a large change in pressure as indicated in Fig. 10, which is a plot of the variation of T_1 with pressure in the temperature range 38°–40° K.

In Fig. 11 we plot the temperature dependence of T_1/ρ for the dilute gas between 35° K and 300° K. The T_1/ρ values are obtained from the slope of the linear portion of the T_1 versus ρ plot for each temperature. The most striking features of Fig. 11 are:

(i) the sharp increase in T_1/ρ as the temperature is lowered below 80° K,

(ii) the relative independence of T_1/ρ on temperature above about 80° K.

The extrapolated experimental T_1/ρ curve at 20.4° K is found to be in good agreement with Bloom's data (Bloom 1957).

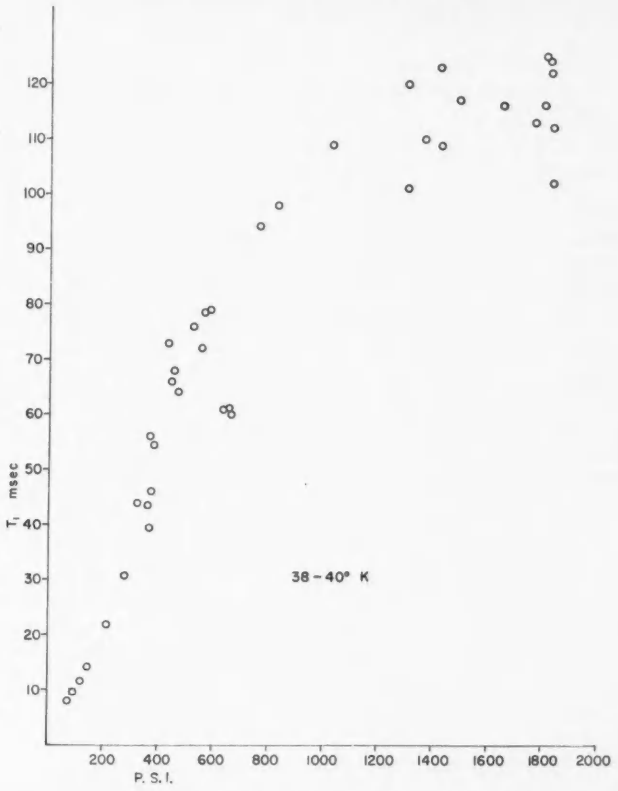

FIG. 10. Plot of T_1 versus gas pressure at 39° K.

Some measurements of T_1 were made on an approximately 50% ortho–para sample of H_2 at a number of temperatures between 35° K and 78° K in the dilute gas region. At all temperatures it was found that, at constant temperature,

$$(T_1)50\%\ \text{ortho–}H_2 < (T_1)\text{normal } H_2.$$

The results shown in Fig. 12 for 43° K and 78° K, which are only of a preliminary nature, indicate that the temperature dependence of the contributions to T_1 from ortho–ortho and ortho–para interactions may be quite different and a more detailed study of T_1/ρ as a function of ortho–para concentration at different temperatures is expected to give valuable information on these interactions.

(2) Spin–Spin Relaxation

Measurements have been made at 78° K on the decay rate of the "echo" produced in a two-pulse experiment, with a view to determining both the

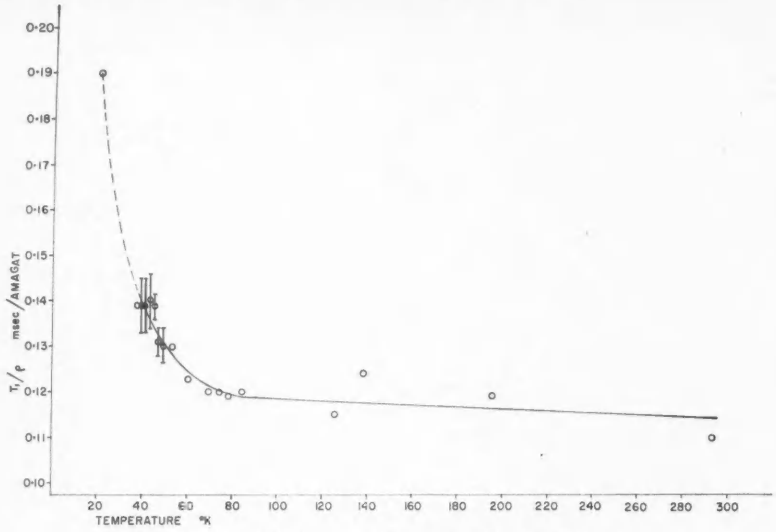

FIG. 11. Plot of T_1/ρ versus temperature for the dilute gas.

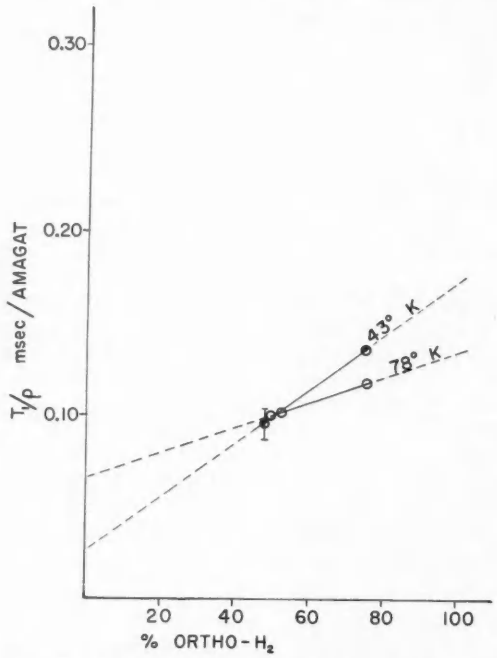

FIG. 12. Plot of T_1/ρ versus ortho-H_2 concentration at 78° K and 43° K.

spin–spin relaxation time T_2 for hydrogen gas and the translation diffusion constant of the gas D as functions of density.

If the magnetic field at a position x in the sample is of the form $H(x) = H_0+Gx$, the amplitude of the spin echo signal in a two-pulse experiment is given by (Muller and Bloom 1960)

$$A(2\tau) \propto \sin\theta_1 \sin^2\theta_2 \exp\left[\frac{-2\tau}{T_2}-\frac{2}{3}\gamma^2G^2D\tau^3\right] \tag{4}$$

where θ_1 and θ_2 are the angles through which the first and second pulses respectively rotate the nuclear magnetization vectors, τ is the time separation of the two pulses, and γ is the nuclear gyromagnetic ratio. The magnetic field gradient G is assumed to be constant over the sample. Carr and Purcell (1954) have shown that, by using a multipulse train, the effect of the diffusion term on this equation for the echo decay with time may be made negligibly small. In our experimental determination of T_2 a Carr–Purcell-type sequence of pulses was applied, consisting of an initial $\pi/2$ pulse followed by about 15 π pulses per relaxation period. Our experimental accuracy in the determination of T_2 is $\pm 10\%$ and to this accuracy we find:

(i) $T_2 = 0.8T_1$,

(ii) T_2/ρ is a constant, over the range of density studied.

In Fig. 13 we plot both T_1 and T_2 as functions of ρ at 78° K. The linear dependence of T_2 on density in the "dilute" gas is to be expected from similar considerations to the T_1 dependence on density. However, the fact that $T_1 > T_2$ is unexpected (Pines and Slichter 1955) and further theoretical examination of the hydrogen spin system must be made to account for this result.

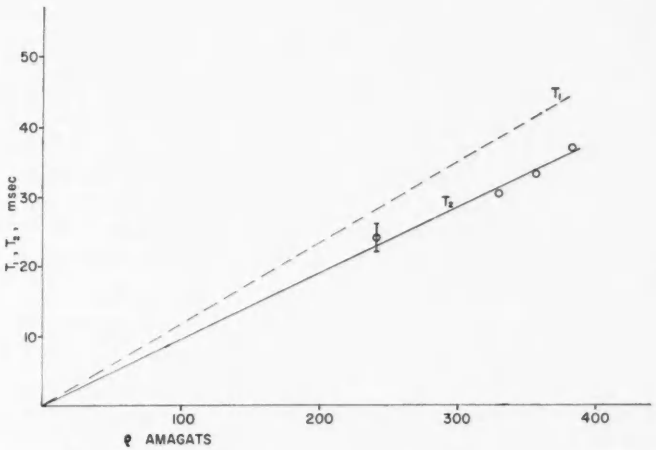

FIG. 13. Plots of T_1 and T_2 versus density for H_2 gas at 78° K.

(3) Diffusion Measurements

All measurements of diffusion depend on finding a suitable unambiguous method of "labelling" molecules. The n.m.r. technique allows one to label the molecules without making any changes at all in the composition or physical conditions of the molecule, and it thus offers a considerable advantage over all other methods of studying diffusion, in that true self-diffusion measurements *are* possible, in principle. However, in diatomic and polyatomic gases the molecules are not completely indistinguishable, because of the fact that they exist in the several modifications ortho, para, and meta, in contradistinction to monatomic gases where the molecules are completely indistinguishable. Thus the n.m.r. technique would be capable of measuring true self-diffusion in He^3, but in the gas samples used in the present work, the diffusion constant, D, measured is really that of a "binary mixture" of ortho- and para-hydrogen gases. An ortho molecule in the $J = 1$, $I = 1$ state has, in fact, 9 quantum states and so, in an ortho–ortho collision there are $9^2 = 81$ possible internal states for the system. The effect of the multiplicity of quantum states on the transport properties of gases has been treated in detail by several authors (Cohen *et al.* 1956, 1958; Buckingham *et al.* 1958), taking into account symmetry effects which are the result of the necessary symmetrization of the wave function for a system of identical particles. Cohen *et al.* (1956) find that the theoretical self-diffusion coefficients for 100% parahydrogen and for 100% orthohydrogen are equal to all intents and purposes, but that there will be a strong temperature and ortho–para concentration dependence for H_2 gas at low temperatures. The measurement of D in hydrogen gas as a function of both temperature and ortho–para concentration is thus a very worth while project. The only measurements of diffusion in hydrogen reported in the literature are those of Harteck and Schmidt (1933) for para-H_2 diffusing into ortho-H_2 at 273° K, 85° K, and 20.4° K at 1 atmosphere pressure.

The measurements to be discussed here are in the nature of preliminary measurements for a detailed study of diffusion in gases as a function of density and temperature. In addition to interest in experimental values of D for their own sake, it would be of interest to measure the diffusion coefficient in the dense gas region to aid in the interpretation of the T_1 results in this region. The scope of the present measurements was to examine the feasibility of doing diffusion measurements with the present apparatus and to examine the density dependence of D in the "dilute" normal hydrogen gas at liquid N_2 temperature. Further measurements are now in progress.

For the dilute gas, a rigorous relation exists between self-diffusion and viscosity, which may be written:

$$D = f\frac{\eta}{\rho m} \tag{5}$$

where η is the coefficient of viscosity for the gas,
ρm is the mass density of the gas,
f is a constant of order unity.

The exact value of f depends on the choice of gas model and intermolecular potential employed in the theory. For H_2, the calculations based on a Lennard–Jones potential (Hirschfelder *et al.* 1954) give $f = 1.37$.

Since the viscosity of a gas at fixed temperature is independent of its density over a wide range of densities (see, for example, Coremans and Beenakker 1960) one would expect to find:

$$D = \frac{\text{constant}}{\rho}. \tag{6}$$

Our technique for determining D is to examine the decay of the echo amplitude in a two-pulse $(\pi/2,\pi)$ experiment and correct for the T_2 term in equation (4), using measured values of T_2. A small correction to the observed echo amplitudes must, however, be made to allow for non-linearity in the diode detection. A calibration experiment was made in which the induction tail amplitude for a single, $\pi/2$ pulse was measured as a function of the gas density at fixed temperature. Multiplying (4) by $e^{+2\tau/T_2}$ one obtains:

$$\begin{aligned} A^*(2\tau) &= A_0 \exp[-\tfrac{2}{3}\gamma^2 G^2 D\tau^3] \\ &= A_0 \exp[-k\tau^3]. \end{aligned} \tag{7}$$

The slope of the plot of $\log A^*(2\tau)$ versus τ^3 is k and, if the value of the gradient G is known, one may immediately derive the value of D. The experimental results to be discussed here were restricted to measurements of "relative D", i.e. to measurements of k. The accuracy of these measurements is of order 10%. Unfortunately, the natural inhomogeneity of the magnet used for this work was so large ($\simeq 1.5$ gauss/cm) as to make it extremely difficult to establish a known uniform gradient in H_0. A further point which had to be considered was the effect of any inhomogeneity of the r-f. field and departure from $\pi/2,\pi$ conditions on the echo decay. A theoretical analysis (Muller and Bloom 1960) shows that the rate of the echo decay is independent of the angles through which the magnetization is rotated by the r-f. pulses, and is independent of the intensity and homogeneity of the r-f. field and the duration of the r-f. pulse. The effect of a non-constant gradient in the external magnetic field may be examined by use of Muller and Bloom's equation (20).

For a one-dimensional gradient of form $G(x) = g_1 + xg_2$, where the deviation from a constant gradient is small so that $xg_2 \ll g_1$, we find that the rate of the echo decay is of the form

$$A^*(2\tau) = A_0 \exp[-k_1\tau^3] \frac{\sinh(k_2\tau^3)}{k_2\tau^3} \tag{8}$$

where $k_1 = \frac{2}{3}\gamma^2 g_1^2 D$,

$k_2 = \frac{4}{3}\gamma^2 g_1 g_2 d D$,

d = length of the sample.

Examination of equation (8) shows that for $k_2\tau^3 \gg 1$,

$$\log A^*(2\tau) \simeq \text{constant} - (k_1 - k_2)\tau^3. \tag{9}$$

This is exactly the same form as obtained using equation (7). Since k_1 and k_2 are each proportional to D, the slopes of $\log A^*(2\tau)$ versus τ^3 curves at large values of τ^3 may thus be used to measure relative values of D in spite of the fact that G is not constant over the sample. The only condition which must be satisfied is that $G(x)$ be the same for all measurements, a condition normally satisfied in experiments involving a permanent magnet.

The approximations made in deriving (8) and (9) seem to be borne out in our experiments since we obtain a linear relationship between $\log A^*(2\tau)$ and τ^3 for large values of τ^3 while the deviation from linearity at small values of τ^3 is consistent with equation (8).

Our experimental values for relative values of $1/D$, which we plot in Fig. 14 as a function of the gas density ρ, show that $D\rho$ is a constant at this tempera-

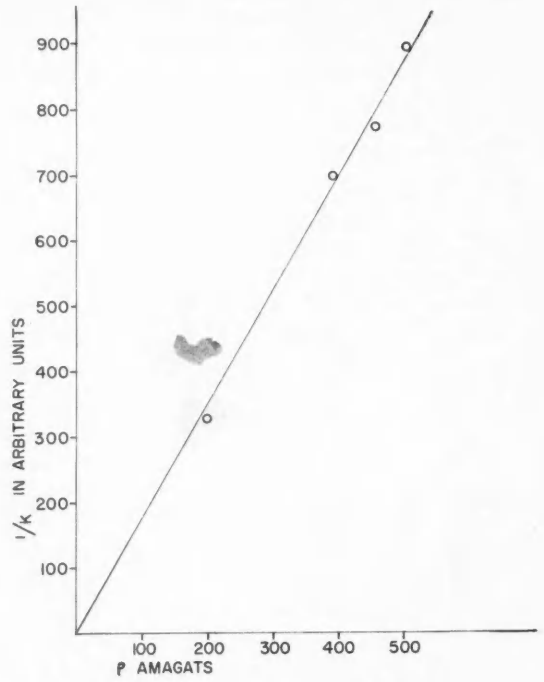

FIG. 14. Plot of $1/k$ versus density for H_2 gas at 78° K. This graph demonstrates that $D\rho$ is constant at fixed temperature for the dilute gas.

ture over the range of densities studied as demanded by equation (5). Some of our more recent measurements at 42° K show that in the dense gas $D\rho$ decreases with ρ. This decrease in $D\rho$ becomes evident in the same range of density over which T_1 ceases to be a linear function of ρ.

4. INFLUENCE OF THE HIGHER ROTATIONAL STATES

In this section we use the results of Needler and Opechowski (1961) to show that even at temperatures up to 300° K, the influence of the higher rotational states ($J = 3, 5$, etc.) of the ortho-H_2 molecules on the proton spin–lattice relaxation is probably negligible.

At temperatures below 300° K only the $J = 1, 3$ states need be considered. If f_1 and f_3 are the fractional populations of the $J = 1$ and $J = 3$ states respectively, then

$$\frac{f_3}{f_1} = \frac{7}{3}\exp[-848/T] \tag{10}$$

$$\simeq 0.14 \text{ at } T = 300^\circ \text{K}.$$

For this case the following expression for T_1 is given by Needler and Opechowski (1961) in equation (4:17) of their paper

$$\frac{1}{T_1} = \frac{f_1\tau_1}{\hbar^2}\left(\frac{4}{3}c^2+15d^2\right)+\frac{f_3\tau_3}{\hbar^2}\left(8c^2+10d^2\right) \tag{11}$$

where τ_1, τ_3 are the mean lifetimes of the ortho-H_2 molecules in the 3 substates of the $J = 1$ state and the 5 substates of the $J = 3$ state respectively.

The low temperature limiting case corresponds to $f_3 \to 0$, $f_1 \to 1$, in which case equation (11) reduces to the Schwinger formula given in equation (1).

The main experimental result to be discussed is that within the accuracy of the experiments ($\simeq 10\%$), T_1/ρ is independent of temperature between about 100° K and 300° K, the highest temperature studied (Fig. 11).

Equations (10) and (11) show that the influence of the $J = 3$ state will only be large if $\tau_3 \gg \tau_1$. Since f_3/f_1 varies very strongly with temperature between 100° K and 300° K it is very unlikely that the temperature dependence of τ_1 and τ_3 would be such that the temperature dependences of $f_1\tau_1$ and $f_3\tau_3$ would be the same over the entire temperature range as required by the constancy of T_1/ρ.

Indeed, it is much more likely that $\tau_3 < \tau_1$ in which case the second term in (11) would contribute less than 10% and may be neglected insofar as our experiments are concerned. One would expect the probability of transition from one magnetic substate to another to be roughly the same for the $J = 1$ and $J = 3$ states. On the other hand transitions between the $J = 1$ and $J = 3$ states are also possible, but the transition $1 \to 3$ is much less frequent than the inverse transition because of the large amount of rotational energy required. We therefore conclude that equation (1) may be used to interpret all the experimental values of T_1 below 300° K.

5. RELATIONSHIP OF T_1 TO MOLECULAR PROPERTIES OF HYDROGEN

In this section we discuss the relationship of T_1 to the molecular properties of H_2. The interaction between pairs of H_2 molecules separated by a distance r is expressed in terms of an isotropic potential energy $V(r)$ which is the same

for ortho–ortho as for ortho–para pairs and a much smaller anisotropic term which is different for ortho–ortho and ortho–para pairs. A direct relationship between T_1 and the intermolecular interactions valid for the following conditions has been discussed for the gas (Oppenheim and Bloom 1960, 1961; Bloom 1960); similar formulae for the liquid and solid cases have also been previously introduced (Oppenheim and Bloom 1959; Moriya 1957; Moriya and Motizuki 1957).

(1) The effect of the small anisotropic interactions on the dynamical motions of the molecules is assumed negligible.

(2) All the ortho-H_2 molecules are assumed to be in the $J = 1$ states. The validity of this approximation insofar as spin–lattice relaxation is concerned has been discussed in the previous section.

Of the various terms in the H_2–H_2 interaction, the ones which have been studied experimentally the least are the anisotropic terms and we examine here the extent to which the T_1 measurements reported in this paper give experimental information about them. We first examine in detail one of the theoretical expressions previously derived for the anisotropic H_2–H_2 interaction. Our considerations of the relationship of T_1 to these interactions will be limited to order of magnitude considerations, however, as will be evident later.

A theoretical expression for the anisotropic interaction Hamiltonian $\mathscr{H}_R$ has been derived by de Boer (1940) and written in the following form by Moriya and Motizuki (1957), whom we now quote in detail.

$$\mathscr{H}_R = \sum_i \mathscr{H}_i + \sum_{j>k} \mathscr{H}_{jk} \tag{12}$$

where the first term, common to ortho–para and ortho–ortho interactions, comes from the valence force and dispersion force, and the second term, which is proper to ortho–ortho interactions, includes the quadrupole–quadrupole interaction as a main part as well as the valence and dispersion forces. The radial dependence of the valence terms varies as $\exp[-1.87r/a_0]$, where a_0 is the Bohr radius, the dispersion terms as r^{-6}, and the quadrupole–quadrupole terms as r^{-5}.

$$\begin{aligned} \mathscr{H}_i &= -A \sum_k \sum_m p_m \mathscr{D}_{m0}^{(i,k)} K_m^{(i)} \\ \mathscr{H}_{ik} &= \frac{2}{25} \sum_{mm'} a_{mm'}^{(i,k)} K_m^{(i)} K_{m'}^{(k)} \end{aligned} \tag{13}$$

where

$$\begin{aligned} a_{mm'}^{(i,k)} = p_m p_{m'} \{ & B \mathscr{D}_{m0}^{(i,k)} \mathscr{D}_{m'0}^{(i,k)} + C(\mathscr{D}_{m1}^{(i,k)} \mathscr{D}_{m'-1}^{(i,k)} + \mathscr{D}_{m-1}^{(i,k)} \mathscr{D}_{m'1}^{(i,k)}) \\ & + D(\mathscr{D}_{m2}^{(i,k)} \mathscr{D}_{m'-2}^{(i,k)} + \mathscr{D}_{m-2}^{(i,k)} \mathscr{D}_{m'2}^{(i,k)}) \} \end{aligned} \tag{14}$$

$$p_0 = 2/3, \qquad p_{\pm 1} = \mp 1, \qquad p_{\pm 2} = 1,$$

$$K_0 = 3J_z^2 - 2, \qquad K_{\pm 1} = J_z J_{\pm 1} + J_{\pm} J_z, \qquad K_{\pm 2} = J_{\pm}^2,$$

$\mathcal{D}_{mm'}^{(i,k)}$ are the matrix elements of the five-dimensional irreducible representation of the rotation which rotates the z-axis (direction of the applied magnetic field, say) into the direction of the line joining the ith molecule to the jth molecule.

The terms A, B, C, and D are complicated functions of r. Instead of giving the analytic expressions for these terms it will serve our purposes to represent each of them graphically, in Fig. 15. It is interesting to notice that the A term predominates at separations near or smaller than $r = a$, where $a = 2.93 \times 10^{-8}$ is one of the Lennard–Jones parameters for H_2. Near $r = a$, $A \cong r^{-13}$, being dominated by the valence term. For $r \gtrsim 1.2a$, A is negligible and B, C, and D all vary approximately as r^{-5}.

A general formula for T_1 may now be written in terms of the correlation functions of $\mathcal{H}_i$, $\mathcal{H}_{ik}$. Instead of writing out the general expression for T_1 in all its complexity we can find which terms in $\mathcal{H}_R$ are important by replacing (12) and (13) by an $\mathcal{H}_R^{\text{eff}}$ which is identical for all pairs. We assume for the moment

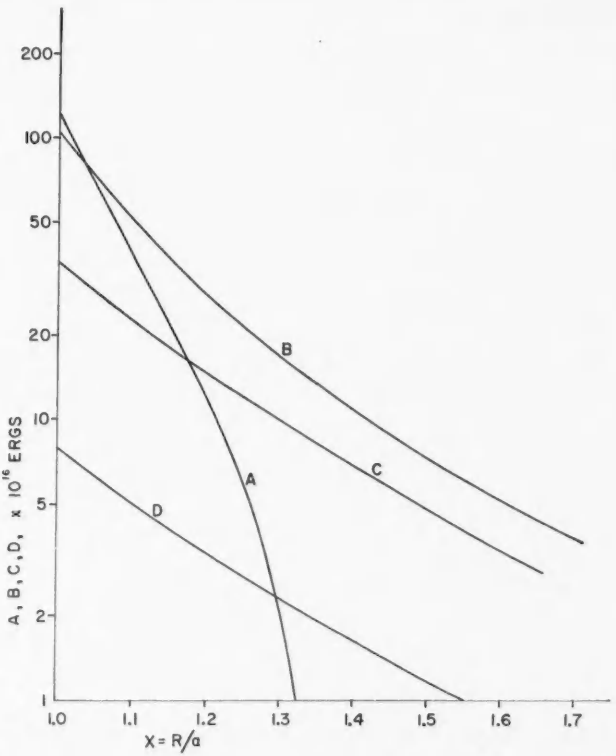

FIG. 15. Dependences of the terms A, B, C, and D, which appear in equations (13) and (14) for the anisotropic H_2–H_2 interactions, on the separation of a pair of molecules. The separation is expressed in terms of the reduced variable $x = r/a$, where $a = 2.93 \times 10^{-8}$ cm.

$$\mathcal{H}_R^{\text{ett}} = E_a \sum_{i,k} \sum_{m} \frac{Y_{lq}(\theta_{ik}, \phi_{ik})}{x_{ik}^{p}} K_m^i \tag{15}$$

where $x = r/a$ is the separation of a pair of molecules in units of a; θ_{ik}, ϕ_{ik} are the polar and azimuthal angles of the vector joining molecule i to molecule k; $Y_{lq}(\theta,\phi)$ is a spherical harmonic, p and l are treated as parameters to be determined from experiment. E_a is the strength of the anisotropic interaction at $r = a$.

The resulting expression for T_1 is as follows (Oppenheim and Bloom 1960, 1961; Bloom 1960):

$$T_1 = \frac{3.7\times10^{-13}\rho a^4}{\hbar^2}\left(\frac{M}{kT}\right)^{1/2} E_a^2 C \int_0^\infty F(y)dy \tag{16}$$

where

$$F(y) = \left[\int_0^\infty \frac{[g(x)]^{1/2} J_{l+1/2}(xy)}{x^{p-(3/2)}} dx\right]^2, \tag{17}$$

M is the mass of the H_2 molecule,

C is a number of order unity arising from matrix elements of the K_m operators,

$J_{l+1/2}(xy)$ is the Bessel function of order $l+1/2$,

$g(x)$ is the radial distribution function for the gas.

For the *dilute gas*

$$g(x) = \exp[-\beta V(x)] \tag{18}$$

where

$\beta = 1/kT$

$V(x)$ is the isotropic part of the intermolecular potential expressed in terms of the reduced co-ordinate $x = r/a$.

The *first density correction* for T_1 (the term A_2 in equation (3)) is obtained from the expansion of $g(x)$ in powers of ρ

$$g(x) = \exp[-\beta V(x)]\{1+\rho\gamma(x)+\text{higher order terms}\} \tag{19}$$

where (de Boer 1948; Oppenheim and Mazur 1957)

$$\gamma(x) = \int\{\exp[-\beta V(r_{13})-\beta V(r_{23})]-1\}d\mathbf{r}_3 - 2\int\{\exp[-\beta V(r)]-1\}d\mathbf{r}, \tag{20}$$

$\mathbf{r}$ is the vector joining molecules 1 and 2 ($r = xa$),

$\mathbf{r}_{13}$, $\mathbf{r}_{23}$ are vectors joining molecules 1 and 2 respectively to 3. The integrations are over the volume elements $d\mathbf{r}_3$ and $d\mathbf{r}$.

At intermediate temperatures, one can expand $g(x)$ in powers of $\hbar^2$. The *first quantum correction* for T_1 is obtained from the coefficient of the term in $\hbar^2$ (de Boer 1948; Oppenheim and Bloom 1961).

$$g(x) = \exp[-\beta V(x)]\{1+\chi(x)\hbar^2+\text{higher order terms}\} \tag{21}$$

where

$$\chi(x) = \frac{\beta^2}{6Ma^2}\left(\frac{d^2V(x)}{dx^2} + \frac{2}{x}\frac{dV(x)}{dx}\right) + \frac{\beta^3}{12Ma^2}\left(\frac{dV(x)}{dx}\right)^2. \tag{22}$$

Thus we see that the temperature dependence of T_1 as given by equation (16) has two types of contributions. For a hard sphere gas $T_1 \propto T^{-1/2}$, but for a more realistic description of the isotropic interactions, an additional temperature dependence results from integrals of the anisotropic interactions over $[g(x)]^{1/2}$ as expressed by equations (16) and (17).

Physical Interpretation of Equation (16)

The physical meaning of these two contributions can be understood as follows in terms of a simplified picture of the relaxation process. If we consider the relationship between T_1 and τ_1 given by equation (1) and assume that the probability of a molecular transition between magnetic substates in a single collision is small, then the expression for τ_1 in equation (2) can be calculated approximately in a manner similar to Bloembergen's treatment of nuclear spin relaxation in a monatomic gas (Bloembergen *et al.* 1948). If the anisotropic interaction energy is $E(r)$ for two molecules separated by a distance r

$$\frac{1}{\tau_1} = \rho\langle\sigma v\rangle \cong \rho\left\langle\frac{\pi a^2}{2}\left(\frac{E(r)}{\hbar}\frac{a}{v}\right)^2 v\right\rangle \approx \frac{\rho a^4}{\hbar^2}\left(\frac{M}{kT}\right)^{1/2}\langle E(r)^2\rangle. \tag{23}$$

We see that the terms outside the integral in equation (16) are all accounted for by this crude picture. The relationship $T_1 \propto T^{-1/2}$ is due to the fact that the collisions between slower molecules are favored because the probability for a change of molecular orientation per collision is proportional to v^{-2}.

The presence of an attractive potential $V(r)$ would increase the time spent by the molecules in the vicinity of one another thus increasing the transition probability for a molecular reorientation. The integral appearing in equation (16) expresses this fact quantitatively and we can identify $\langle E(r)^2\rangle$ in (23) with $E_a^2\int F(y)dy$ in (16).

A. Hard Sphere Approximation

In the hard sphere approximation

$$\begin{aligned} V(x) &= \infty, & x &< 1 \\ V(x) &= 0, & x &> 1 \end{aligned} \tag{24}$$

and hence equation (17) becomes

$$F(y) = \left[\int_1^\infty \frac{J_{l+1/2}(xy)}{x^{p-(3/2)}}dx\right]^2. \tag{25}$$

Thus the theory gives $T_1/\rho \propto T^{-1/2}$ in this approximation regardless of p and l. Figure 16 shows the comparison of a $T_1/\rho \propto T^{-1/2}$ temperature dependence with experiment. We see that between 100° K and 300° K the experimental values for T_1/ρ are roughly constant and the agreement is poor.

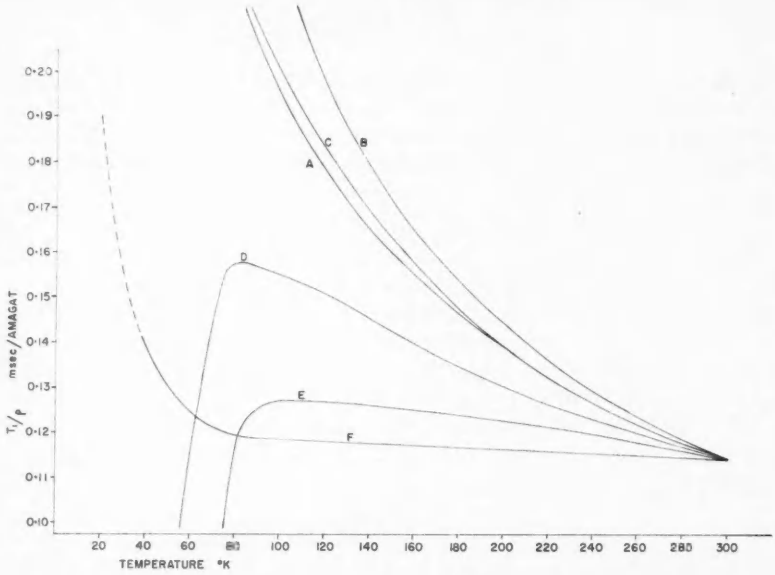

FIG. 16. Comparison of the experimental values for the temperature dependence of T_1/ρ in H_2 gas at low density with theory. Curves A, B, C, D, and E are theoretical curves while F is the curve drawn to fit the experimental points in Fig. 11. The theoretical curves are for the following cases: A: Hard sphere model for the isotropic H_2–H_2 interaction. B: Square well model where the parameter p in equation (15) is assumed large and the radial distribution function is that given by equation (18) for the classical gas. C: Quantum mechanical values given by the approximate formula (36) for $p = 5$. D: Same as C for $p = 11$. E: Same as C for $p = 17$. All the theoretical curves are normalized to fit the experimental curve at $T = 300°$ K.

Still, it is interesting to find the value of E_a which is required to fit T_1 at the highest temperature studied where the hard sphere approximation may have some validity. The integral in (25) can be evaluated simply for the case $p = l+1$, in which case we obtain

$$\int_0^\infty F(y)dy = \frac{1}{\pi(p-1)(p-2)}. \tag{26}$$

It would be interesting to evaluate this integral for many values of l and p but this is tedious and has not yet been done. The interesting values of l are expected to be close to $l = 2$ while, judging from Fig. 15, the intermolecular interaction is expected to contain terms corresponding to the range $p = 5$ to $p = 13$, or even higher at high temperatures where the average distance of closest approach is less than a. We have evaluated numerically the case $p = 4$, $l = 2$, and obtain $\int_0^\infty F(y)dy = 0.0675$. Formula (26) gives 0.058 for $p = 4$, $l = 3$, and 0.159 for $p = 3$, $l = 2$. This indicates that the integral is much less sensitive to variations in l than p and we shall therefore neglect the dependence on l in using equation (26) to evaluate $\int_0^\infty F(y)dy$ in order to arrive at an order of magnitude estimate for E_a.

If, in equation (16), we put $T_1 = 0.11$ msec for $\rho = 1$ Amagat $= 2.69\times10^{19}$ molecules/cm^3, $a = 2.93\times10^{-8}$, $M = 3.32\times10^{-24}$ g, $T = 300°$ K and if C is taken to be unity, we obtain:

$$E_a \simeq 2.4\times10^{-15}\sqrt{[(p-1)(p-2)]}\text{ ergs.} \tag{27}$$

The dominant term in the theoretical expression for the intermolecular interactions is A, which, from Fig. 15, is seen to have a value of approximately 10^{-14} ergs at $x = 1$. Considering the simplifying approximations made in deriving equation (27) and the approximate nature of the theoretical expressions used for the anisotropic interaction, this is in good agreement with the order of magnitude of E_a obtained from T_1 measurements. For $p = 13$, equation (27) gives $E_a \simeq 2.7\times10^{-14}$ ergs.

The *first density correction* can be made within the scope of the hard sphere approximation by using the $\gamma(x)$ in (20) appropriate to this case (de Boer 1948).

$$\begin{aligned} &\gamma(x) = 0, && x < 1,\ x \geqslant 2 \\ &\gamma(x) = \frac{4\pi}{3}a^3\left(1-\frac{3}{4}x+\frac{1}{16}x^3\right), && 1 < x \leqslant 2 \end{aligned} \tag{28}$$

Using (28) and (19) in evaluating (17) to first order in ρ, we obtain for the first density correction in (3)

$$\frac{A_2}{A_1} < 2.84\times10^{-3}\ (\text{Amagat})^{-1} \tag{29}$$

where the upper bound would hold if only the leading term were present. A detailed comparison of the first density correction with experiment cannot be made as yet since we have only observed departures from linearity in T_1 versus ρ at low temperatures where quantum mechanical effects should play an important role.

Figure 17 shows the T_1 versus ρ plot at 41° K compared with $T_1 = A_1\rho+A_2\rho^2$ for several values of A_2/A_1 to show that the results in the quantum region are consistent with the inequality in (29).

B. Square Well Model

As discussed earlier, the temperature dependence of T_1 according to equation (16) has two types of contributions. The $T^{-1/2}$ term has been discussed above. The integral in (16), (17) over $[g(x)]^{1/2}$ is also temperature dependent and one would like to perform these integrations over a "realistic" potential such as a Lennard–Jones potential. Numerical integrations using a Lennard–Jones potential will be presented in a future publication, but in the meantime, one can gain some insight into the temperature dependence of the integral by using a square well potential using parameters which give best fit to Second Virial Coefficient data (Hirschfelder *et al.* 1954)

$$\begin{aligned} &V(x) = \infty, && x < 1 \\ &V(x) = -0.56\epsilon, && 1 < x < 1.8 \\ &V(x) = 0, && x > 1.8 \end{aligned} \tag{30}$$

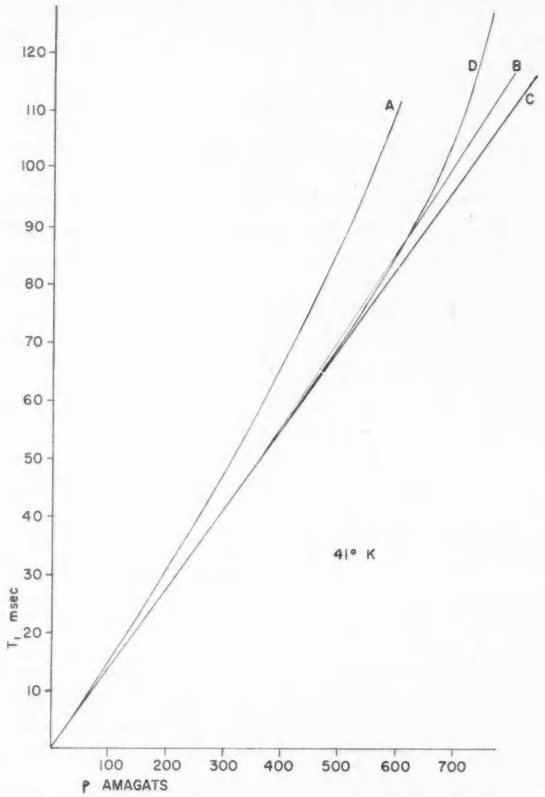

FIG. 17. Comparison of experimental values for density dependence of T_1 at 41° K with theoretical curves obtained from the first density correction according to equation (3) for several values of A_2/A_1. Curves A, B, and C are theoretical curves while curve D is the line drawn through the experimental values of Fig. 5. The theoretical curves correspond to A: $A_2/A_1 = 2.50\times10^{-4}$ (Amagat)$^{-1}$; B: $A_2/A_1 = 2.50\times10^{-5}$ (Amagat)$^{-1}$; C: $A_2/A_1 = 0$.

ϵ is the Lennard–Jones parameter which is given by $\epsilon/k = 37°$ K for H_2. Calculations have been performed using (30) in (16) and (17). It is found that for large values of p, most of the contributions come from the smallest values of x and that within the scope of the approximations made in deriving (26) one obtains

$$\int_0^\infty F(y)dy \cong \frac{\exp[+0.56\beta\epsilon]}{\pi(p-1)(p-2)}. \tag{31}$$

The effect of the attractive potential is thus to increase the theoretical temperature dependence of T_1/ρ for the classical gas over that given by the hard sphere approximations. This is shown in Fig. 16. The effect of the

attractive part of the isotropic intermolecular potential is to increase the collision time for a pair of molecules and hence increase the probability per collision that a molecule is reoriented.

Thus, the classical theory fails completely to explain the temperature dependence of T_1/ρ even at temperatures above 100° K. We see below that it is necessary to include quantum mechanical effects even at high temperatures in order to understand the experimental results.

C. Quantum Mechanical Effects

The quantum mechanical effects which we discuss here are due to diffraction effects associated with the finite de Broglie wavelengths of the molecules. Quantum mechanical effects associated with other transport properties have been discussed elsewhere (Cohen *et al.* 1956). These effects should become large when the ratio of the average de Broglie wavelength to the size of the molecules becomes appreciable. This ratio is given by

$$\frac{h}{a(MkT)^{1/2}} = \Lambda^* T^{*-1/2} \tag{32}$$

where

$$\Lambda^* = \frac{h}{a(M\epsilon)^{1/2}} = 1.73 \text{ for } H_2, \qquad T^* = \frac{T}{37° \text{ K}} \text{ for } H_2.$$

Thus one normally expects quantum effects to become observable at temperatures below 100° K for H_2. It would appear from our discussion below that the T_1 measurements are much more sensitive to quantum effects than other transport properties of H_2 and that we have possibly been observing quantum effects even at several hundred degrees Kelvin corresponding to values of T^* as large as 8!.

In our first attempts to understand the temperature dependence of T_1/ρ in Fig. 11 (Lipsicas 1960; Lipsicas and Bloom 1960) we surmised that the constancy of T_1/ρ above 100° K could be understood in terms of the properties of the classical gas, while the sharp increase below 100° K was a manifestation of the increased cross section due to the increased average de Broglie wavelengths of the molecules. We now believe that this interpretation is completely incorrect. Instead, it seems that the temperature dependence predicted by the classical gas would be much stronger than that observed, and that the larger effective size of the molecules tends to *decrease* the cross section of reorientational collisions rather than increase it.

The reason for this apparent paradox is that the anisotropic interactions are very short range. The larger average effective size of the molecules in the quantum region means that in a collision the molecules do not approach each other as closely on the average as in the classical gas. Thus, the anisotropic interaction is not as effective in reorienting the molecules. A recent discussion of the sign of the quantum mechanical contributions to the cross sections for transport coefficients (Choi and Ross 1960) seems closely related to our findings.

Calculations of T_1 using the radial distribution function for the dilute quantum gas given in equation (21) will be made using a Lennard–Jones potential.

$$V(x) = 4\epsilon(x^{-12}-x^{-6}) \tag{33}$$

and the results reported in a subsequent publication.

In the meantime, an order of magnitude calculation can be made by estimating the fractional change in the effective size of the molecules due to quantum mechanical effects from the value of x at which $g(x) = 1$ if one uses equations (21), (22), and $V(x)$ given by equation (33).

Solving for

$$\ln g(x_0) = 0, \qquad x_0 = 1+\delta(T^*) \tag{34}$$

to first order in δ one obtains a result valid for $T \gtrsim 60°$ K

$$\delta(T^*) = \frac{5.1T^*-3.6}{247T^{*2}+81T^*-136}. \tag{35}$$

Then, if we estimate T_1 approximately by replacing the lower limit of integration in equation (25) by $1+\delta(T^*)$ we obtain

$$\frac{T_1}{\rho} \propto \frac{\exp[-0.56/T^*]}{T^{*1/2}[1+\delta(T^*)]^{2p-4}}. \tag{36}$$

The term $[1+\delta(T^*)]^{2p-4}$ gives a crude measure of the quantum effect and we see that for large values of p, the T_1 measurements are very sensitive to even small values of $\delta(T^*)$. The effect of this quantum term for several values of p is shown in Fig. 16.

It may be seen from Fig. 16 that the very slow dependence of T_1/ρ versus temperature between 100° K and 300° K may be understood if the effective anisotropic interaction given by equation (15) involves large values of p at high temperature, i.e. if the A term in equation (13), which is plotted in Fig. 15, predominates. This is expected at high temperatures since the molecules can approach quite closely to one another. Thus, the short range anisotropic intermolecular interactions act as a fine probe for very small changes in the $g(x)$ introduced by quantum mechanical effects even at quite high temperatures.

At low temperatures the very short range term A should become much less effective than the long range $1/r^5$ terms and T_1/ρ should increase as indicated by Fig. 16. It should be noted, however, that the long range terms are only present in the ortho–ortho interaction. Thus, T_1/ρ for ortho-H_2 in H_2 with a *very large percentage of para-H_2* should *decrease* as the temperature is lowered. This is consistent with the results of Fig. 12 which shows that the slope of T_1/ρ versus ortho-H_2 concentration increases with decreasing temperature. We would predict that the slope of T_1/ρ versus ortho-H_2 concentration at 20° K should be steeper than that measured previously by Bloom (1957). Judging from the more accurate results of Hass, Seidel, and Poulis (1960), in liquid H_2, this is indeed the case. In fact, after examining the data of

Hass *et al.* it now appears that the only discrepancy between their results and those of Bloom (1957) was probably in the measured value of ortho-H_2 concentration for the "5% ortho-H_2" sample. Since the same sample was used for the gas measurements, correction of this measurement leads to a slope of T_1/ρ versus ortho-H_2 concentration at 20° K much steeper than previously reported (Bloom 1957) and also much steeper than the high temperature values shown in Fig. 12.

ACKNOWLEDGMENTS

We wish to thank Dr. W. Opechowski and Dr. I. Oppenheim for helpful discussions and Dr. B. H. Muller for help with some of the measurements.

REFERENCES

BLOEMBERGEN, N., PURCELL, E. M., and POUND, R. V. 1948. Phys. Rev. **73**, 679.
BLOOM, M. 1957. Physica, **23**, 237, 378.
——— 1960. Proceedings of the 7th International Low Temperature Conference (Toronto).
BUCKINGHAM, R. A., DAVIES, A. R., and GILLES, D. C. 1958. Proc. Phys. Soc. **71**, 457.
CARR, H. Y. and PURCELL, E. M. 1954. Phys. Rev. **94**, 630.
CHOI, S. and ROSS, J. 1960. J. Chem. Phys. **33**, 1324.
COHEN, E. G. D. and OFFERHAUS, M. J. 1958. Physica, **24**, 742.
COHEN, E. G. D., OFFERHAUS, M. J., VAN LEEUVEN, J. M. J., ROOS, B. W., and DE BOER, J. 1956. Physica, **22**, 791.
COREMANS, J. M. J. and BEENAKKER, J. J. M. 1960. Physica, **26**, 653.
DE BOER, J. 1940. Thesis, Amsterdam.
——— 1948. Repts. Progr. in Phys. **12**, 305.
HAHN, E. L. 1950. Phys. Rev. **80**, 980.
HARTECK, P. and SCHMIDT, H. W. 1933. Z. physik. Chem. B, **21**, 447.
HASS, W. P. A., SEIDEL, G., and POULIS, N. J. 1960. Physica, **26**, 834.
HIRSCHFELDER, J. O., CURTISS, C. F., and BIRD, R. B. 1954. Molecular theory of gases and liquids (John Wiley & Sons, Inc.).
LIPSICAS, M. 1960. Thesis, University of British Columbia.
LIPSICAS, M. and BLOOM, M. 1960. Proceedings of the 7th International Low Temperature Conference (Toronto).
MORIYA, T. 1957. Progr. Theoret. Phys. **18**, 567.
MORIYA, T. and MOTIZUKI, K. 1957. Progr. Theoret. Phys. **18**, 183.
MULLER, B. and BLOOM, M. 1960. Can. J. Phys. **38**, 1318.
NEEDLER, G. T. and OPECHOWSKI, W. 1961. Can. J. Phys. **39**. This issue.
OPPENHEIM, I. and BLOOM, M. 1959. Can. J. Phys. **37**, 1324.
——— 1960. Proceedings of the 7th International Low Temperature Conference (Toronto).
——— 1961. Can. J. Phys. **39**. This issue.
OPPENHEIM, I. and MAZUR, P. 1957. Physica, **23**, 197.
PAUL, W., BENEDEK, G. D., and WARSCHAUER, D. M. 1959. Rev. Sci. Instr. **30**, 874.
PINES, D. and SLICHTER, C. P. 1955. Phys. Rev. **100**, 1014.
RAMSEY, N. F. 1956. Molecular beams (Oxford, Clarendon Press).
SCHWARTZ, J. 1957. Rev. Sci. Instr. **28**, 780.

A $^1\Sigma^-$–$^3\Pi_r$ SPECTRUM OF SiO[1]

R. D. VERMA AND R. S. MULLIKEN

ABSTRACT

A new $^1\Sigma^-$–$^3\Pi_r$ (case *a*) spectrum is identified in the region 4200–4300 Å for the SiO molecule. The rotational analysis of the spectrum gives the following constants for the lower and upper states in cm^{-1}.

$B_0' = 0.6801_2$ $\quad D_0' = 1.7\times10^{-6}$

$B_0'' = 0.6765_6$ $\quad D_0'' = 1.4\times10^{-6}$ $\quad A = 72.55\pm0.015$

A discussion of electron configurations is given.

INTRODUCTION

A complex spectrum in the region 4200–4300 Å was observed by Pankhurst (1940) in a heavy current discharge through a quartz capillary containing hydrogen. Later Woods (1943) also observed the same spectrum in a similar kind of discharge but in a helium atmosphere. However, these investigators could not photograph the spectrum at high resolution because of its low intensity. From the complexity of the spectrum and the experimental conditions, they suspected the emitter of these bands to be SiO_2. Recently, while looking for the SiCl spectrum, we observed the afore-mentioned spectrum emitted strongly in the high-frequency discharge through very low pressures (see the following) of flowing $SiCl_4$. To study this spectrum in detail, a high resolution photograph was obtained; the results, discussed in this paper, indicate that the spectrum is an intercombination transition of SiO.

EXPERIMENTAL

The experimental arrangement for excitation of the spectrum was the same as that described recently (Verma and Mulliken 1961; Verma 1961) in the case of CCl and CCl^+. Silicon tetrachloride was frozen at dry ice temperature without removing the dissolved air and moisture in the liquid. It was noticed that the removal of dissolved air weakens the spectrum. The spectrum was photographed in the first and second orders of the 30-ft grating Paschen spectrograph with a 30,000 lines/in. grating. A practical resolving power of about 210,000 was obtained. A hollow-cathode iron spectrum was used as the reference standard. The hollow-cathode iron wavelengths were obtained from the recent interferometric measurements of Crosswhite (1958). Eastman photographic plates of type 103*a*-0 were used; exposure times ranged from 3 to 12 hours. Measurements were made on the photoelectric comparator developed by Tomkins and Fred (1951) at the Argonne National Laboratory. The accuracy of measurement was estimated to be ±0.002 Å (equivalent to

[1]Manuscript received February 7, 1961.

Contribution from the Laboratory of Molecular Structure and Spectra, Department of Physics, University of Chicago, Chicago 37, Illinois. This work was assisted by the Geophysics Research Directorate of the Air Force Cambridge Research Center with the University of Chicago.

± 0.011 cm^{-1}). Vacuum wavenumbers were then obtained from the "Tables of Wavenumbers" (NBS monograph 3) of the National Bureau of Standards, Washington, D.C.

ROTATIONAL ANALYSIS

The observed spectrum consists of three intense bands with strongest heads at 23642, 23569, and 23498 cm^{-1} (see Fig. 1). There are also a few weaker bands, some of which extend into the region of the strong bands, obscuring a few of their lines. However, they are not discussed in this paper because they could not be photographed with sufficient intensity and because the strong bands masked them. Each of the three strong bands has three branches, P, Q, and R. No head formation is observed in the P or R branches. Each Q branch shows a head at the beginning of the branch. This branch of the middle band, seen at 23569 cm^{-1} in Fig. 1, is strong but not at all resolved. The Q branches of the bands at 23642 and 23569 cm^{-1} are shaded toward short wavelength and that of the band at 23498 is shaded toward long wavelength.

These bands were analyzed by standard methods using well-known combination relations. The band at 23498 cm^{-1} does not show any 'combination defect' whereas that at 23642 cm^{-1} has an appreciable Λ-splitting. For the middle band the presence or absence of Λ-doubling could not be ascertained since the Q branch could not be resolved. It was found that these three bands have a single common upper electronic state, as is shown in Table II by the very good agreement in the $\Delta_2F'(J)$ values. The separation of the middle band from each of the other two was found to be about 72 cm^{-1}. This triplet multiplicity then suggests that the spectrum is probably of the type of $^3\Sigma$–$^3\Pi$ (case a). A search, however, for satellite branches expected in this type of transition did not succeed. The Λ-splitting, the effective B'' values for the three bands, and their relation to the spin splitting constant A show definitely that the lower state is a regular case a $^3\Pi$. It was thought that the complex overlapping and a fine background due to other weak bands might obscure the expected satellite branches. However, during a careful search for satellites at the expected positions, there were noticed a number of points where a line, if it were there, should have been recorded. This gave rise to the suspicion that the upper state may not be $^3\Sigma$. Very strong evidence against $^3\Sigma$ came from the following observations.

The analysis of the data as shown in Table I is consistent with the well-known combination relations. Since the $^3\Pi$ state is close to ideal case a, the quantum number J is used in the numbering of the branches. The absolute J value for each band was determined by plotting $\Delta_2F''(J)$ values versus J for tentative choices of J and requiring the straight line formed by Δ_2F'' to pass through $J = -\frac{1}{2}$. Figure 2 shows this kind of straight line for the band at 23642 cm^{-1}. Similar straight lines were obtained for the other two bands. For all three bands, this numbering agrees with one determined by recognizing the coincidence of the zero gap in the PR series with the Q head. Having fixed J in this manner, we noticed that the following relations hold good within the experimental error.

TABLE I

J	R_1	Q_1	P_1	R_2	P_2	R_3	Q_3	P_3
1	23644.63	23641.73	—	23571.95	23568.02			
2	46.05	41.87	23639.28	73.30	66.70			
3	47.56	42.03	38.02	74.63	65.26	23503.35	—	23493.92
4	48.96	42.22	36.76	76.05	63.80	04.71	23497.96	92.48
5	50.53	42.45	35.57	77.59	62.44	05.98	97.85	90.96
6	52.07	42.71	34.40	78.82	61.15	07.24	97.73	89.51
7	53.66	43.00	33.26	80.26	59.86	08.44	97.59	88.06
8	55.26	43.31	32.16	81.69	58.52	09.66	97.41	86.57
9	56.89	43.68	31.09	83.10	57.25	10.85	97.26	84.94
10	58.56	44.06	30.05	84.54	55.97	12.04	97.07	83.47
11	60.27	44.48	29.01	85.98	54.70	13.18	96.88	81.98
12	62.00	44.92	28.04	87.42	53.44	14.31	96.66	80.33
13	63.76	45.39	27.08	88.88	52.17	15.43	96.41	78.77
14	65.54	45.90	26.15	90.32	50.91	16.52	96.15	77.13
15	67.38	46.43	25.28	91.81	49.68	17.61	95.88	75.49
16	69.20	46.98	24.40	93.25	48.43	18.63	95.59	73.87
17	71.07	47.56	23.56	94.76	47.20	19.72	95.30	72.20
18	72.96	48.19	22.75	96.24	45.97	20.74	94.96	70.54
19	74.89	48.84	21.98	97.74	44.76	21.75	94.63	68.83
20	76.85	49.49	21.21	99.23	43.55	22.79	94.28	67.15
21	78.82	50.18	20.48	600.76	42.36	23.73	93.92	65.38
22	80.81	50.90	19.89	02.24	41.16	24.71	93.52	63.69
23	82.84	51.64	19.11	03.76	39.96	25.66	93.13	61.97
24	84.89	52.39	18.45	05.27	38.78	26.60	92.72	60.16
25	86.96	53.18	17.81	06.79	37.59	27.52	92.31	58.40
26	89.05	53.99	17.21	08.28	36.47	28.42	91.85	56.65
27	91.17	54.83	16.63	09.85	35.25	29.33	91.41	54.83
28	93.31	55.68	16.05	11.37	34.12	30.22	90.96	53.05
29	95.45	56.59	15.53	12.76	32.96	31.08	90.47	51.21
30	97.63	57.49	15.10	14.50	31.93	31.93	89.99	49.37
31	99.83	58.39	14.50	16.05	31.08	32.79	89.51	47.55
32	702.02	59.33	14.04	17.59	30.22	33.60	88.98	45.67
33	04.25	60.27	13.59	19.11	29.35	34.41	88.45	43.82
34	06.51	61.23	13.13	20.63	28.42	35.25	87.94	41.95
35	08.74	62.20	12.76	22.24	27.52	36.02	87.39	40.15
36	11.04	63.29	12.33	23.79	26.60	36.81	86.83	38.18
37	13.33	64.31	11.97			37.59	86.29	36.37
38	15.62	65.37	11.70			38.36	85.67	34.39
39	17.94	66.43	11.37			39.08	—	32.45
40	20.26	67.50	11.03			39.80	84.64	30.50
41	22.60	68.63				40.53	83.95	
42		69.76				41.16	—	
43		70.91				41.94	82.72	
44		72.07				42.60	81.98	
45		73.24				43.31		
46		74.51				43.98		
47		75.73				44.58		
48		77.00				45.23		

$$R_1(J)-P_1(J) = R_2(J)-P_2(J) = R_3(J)-P_3(J) \tag{1}$$

where the suffixes 1, 2, and 3 refer to $^3\Pi_0$, $^3\Pi_1$, and $^3\Pi_2$ respectively.

If the transition were $^3\Sigma$–$^3\Pi$, the three equations in (1) would become

$$\begin{aligned} R_{11}(J)-P_{11}(J) &= F_1'(J+1)-F_1'(J-1) = \Delta_2F_1'(J) = \Delta_2F'(N-1), \\ R_{22}(J)-P_{22}(J) &= F_2'(J+1)-F_2'(J-1) = \Delta_2F_2'(J) = \Delta_2F'(N), \\ R_{33}(J)-P_{33}(J) &= F_3'(J+1)-F_3'(J-1) = \Delta_2F_3'(J) = \Delta_2F'(N+1). \end{aligned} \tag{2}$$

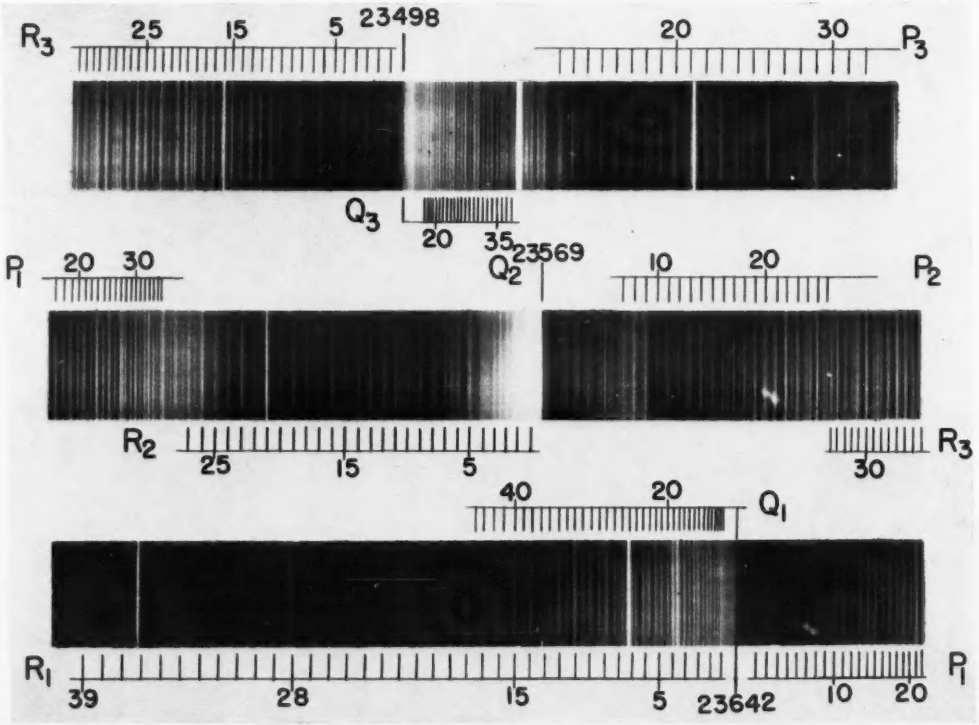

FIG. 1. Rotational structure of (0,0) band of $^1\Sigma^- - {}^3\Pi$ (case *a*) of SiO.

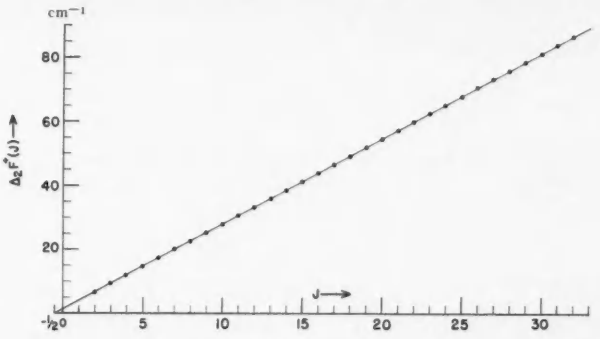

FIG. 2. A graph showing $\Delta_2F''(J)$ versus J for the subband at 23642 cm^{-1}.

However, it is obvious that for a $^3\Sigma$ state one must have $\Delta_2F'(N-1) \neq \Delta_2F'(N) \neq \Delta_2F'(N+1)$. On the other hand if we assume that the upper state is $^1\Sigma$, the relations in (1) are just what should hold, since each of the three expressions in (1) should be equal to the same quantity $\Delta_2F'(J)$. In a $^3\Sigma$–$^3\Pi$ transition, neglecting the spin splitting in $^3\Sigma$, one would expect, instead of equations (1),

$$(3) \quad R_{11}(J+1)-P_{11}(J+1) = R_{22}(J)-P_{22}(J) = R_{33}(J-1)-P_{33}(J-1),$$

with each of the three expressions equal to $\Delta_2F'(N)$.

These observations apparently rule out the possibility that the upper state is $^3\Sigma$ in type. However, if we assume $^1\Sigma$ for the upper state, all the difficulties mentioned above are removed and the whole analysis is in harmony with well-known facts regarding diatomic spectra. There is, of course, the objection that according to the selection rule $\Delta\Omega = 0, \pm1$, we do not expect a $^1\Sigma$–$^3\Pi_2$ subband, while in the $^1\Sigma$–$^3\Pi_0$ subband only P and R branches are expected, as was observed by Sharma (1951) in the $a^3\Pi$–$X^1\Sigma^+$ transition of AlCl. In the Cameron bands (Gero *et al.* 1937) of CO ($a^3\Pi_r$–$X^1\Sigma^+$) however, where the $^3\Pi_r$ state is case a, all three subbands, each with three branches, are observed with almost equal intensity, in emission as well as in absorption. In the SiO bands described here, the intensity for the various branches in all three subbands reaches a maximum for J values in about the range 15 to 25. It is interesting to note that the A/B values for CO, SiO, and AlCl are in the ratio 26:115:260, i.e. 1:4:10, yet the intensity of the three subbands for SiO is almost like those of CO, whereas in AlCl, the selection rule $\Delta\Omega = 0, \pm1$ apparently holds strictly. One would then be inclined to expect that the intensities for SiO would have shown a behavior intermediate between those of CO and AlCl, and somewhat nearer the latter; but the facts indicate otherwise.

CALCULATION OF CONSTANTS

Having established the type of transition as $^1\Sigma$–$^3\Pi$ (case a) the constants of the upper and lower states were calculated as described below.

For $^1\Sigma$

The rotational constants B' and D' of $^1\Sigma$ were calculated graphically by using the relation

$$\Delta_2F'(J) = 4B'(J+\tfrac{1}{2}) - 8D'(J+\tfrac{1}{2})^3. \tag{4}$$

Three sets of $\Delta_2F'(J)$ values were obtained as shown in Table II from the three subbands. The average of these three sets of $\Delta_2F'(J)$ values was used for the calculation of B' and D'. The values obtained are shown in Table III.

TABLE II

J	23642 $\Delta_2F'(J)$	23569 $\Delta_2F'(J)$	23498 $\Delta_2F'(J)$	$\Delta_2F_1''(J)$	$\Delta_2F_2''(J)$	$\Delta_2F_3''(J)$
1		3.93				
2	6.77	6.60		6.61	6.69	
3	9.54	9.37	9.43	9.29	9.50	
4	12.20	12.25	12.23	11.99	12.19	12.39
5	14.96	15.15	15.02	14.56	14.90	15.20
6	17.67	17.67	17.73	17.27	17.73	17.92
7	20.40	20.40	20.38	19.91	20.30	20.67
8	23.10	23.17	23.09	22.57	23.01	23.50
9	25.80	25.85	25.91	25.21	25.72	26.19
10	28.51	28.57	28.57	27.88	28.40	28.87
11	31.26	31.28	31.20	30.52	31.10	31.71
12	33.96	33.98	33.98	33.19	33.81	34.41
13	36.68	36.71	36.66	35.85	36.51	37.18
14	39.39	39.41	39.39	38.48	39.20	39.94
15	42.10	42.13	42.12	41.14	41.89	42.65
16	44.80	44.82	44.76	43.82	44.61	45.41
17	47.51	47.56	47.52	46.45	47.28	48.09
18	50.21	50.27	50.20	49.09	50.00	50.89
19	52.91	52.98	52.92	51.75	52.69	53.59
20	55.64	55.68	55.64	54.41	55.38	56.37
21	58.34	58.40	58.35	56.96	58.07	59.10
22	60.92	61.08	61.02	59.71	60.80	61.76
23	63.73	63.80	63.69	62.36	63.46	64.55
24	66.44	66.49	66.44	65.03	66.17	67.26
25	69.15	69.20	69.12	67.68	68.80	69.95
26	71.84	71.81	71.77	70.33	71.54	72.69
27	74.54	74.60	74.52	73.00	74.16	75.37
28	77.26	77.25	77.17	75.64	76.89	78.14
29	79.92	79.80	79.87	78.21	79.44	80.85
30	82.53	82.57	82.56	80.95	81.68	83.53
31	85.33	84.97*	85.24	83.59	84.28*	86.26
32	87.98	87.37*	87.93	86.24	86.70*	88.97
33	90.66	89.76*	90.59	88.89	89.17*	91.65
34	93.38	92.21*	93.30	91.49	91.59*	94.26
35	95.98	94.72*	95.87	94.18	94.03*	97.07
36	98.71	97.19*	98.63	96.77		99.65
37	101.36		101.22	99.34		102.42
38	103.92		103.97	101.96		105.14
39	106.57		106.63	104.59		107.86
40	109.23		109.30			

*NOTE: The experimental error is more in the values marked * because R_2 and P_2 lines were obscured for high J values by the strong lines of other bands.

For $^3\Pi$

(1) Constants B'' and D''

According to Gilbert (1936) we have

$$\sum_i \Delta_2 F_i/3(J+\tfrac{1}{2}) = (4B+16D)+8D\,J(J+1) \tag{5}$$

where $$\sum_i \Delta_2 F_i = \Delta_2 F_1(J)+\Delta_2 F_2(J)+\Delta_2 F_3(J).$$

The determination of B'' and D'' was performed graphically by using equation (5). The $\Delta_2 F_i''(J)$ values used in obtaining $\sum_i \Delta_2 F_i$ are shown in Table II. The constants thus calculated are given in Table III.

TABLE III

$B_0' = 0.6801_2$		$A = 72.55 \pm 0.015$
$D_0' = 1.7\times10^{-6}$		$B_0'' = 0.6765_6$
		$D_0'' = 1.4\times10^{-6}$
	$\nu_{00}^{(1)} = 23641.91\ \text{cm}^{-1}$	
	$\nu_{00}^{(2)} = 23569.18\ \text{cm}^{-1}$	
	$\nu_{00}^{(3)} = 23498.06\ \text{cm}^{-1}$	

(2) Constant A

Using Gilbert's expression one obtains

$$[F_3(J)-F_1(J)]^2+1/3[\{F_3(J)-F_2(J)\}-\{F_2(J)-F_1(J)\}]^2 \tag{6}$$
$$= [4A(A-4B)+16/3\ B^2-16A\cdot D]+[16B^2+32A\cdot D-32B\cdot D]J(J+1)$$
$$-64B\cdot D\cdot J^2(J+1)^2$$

where B and D are the true values of the rotational constants for the $^3\Pi$ state obtained as described in the preceding paragraph. The terms on the left-hand side of (6) were calculated as follows:

$$\begin{aligned} F_3''(J)-F_1''(J) &= R_1(J)-R_3(J) = P_1(J)-P_3(J), \\ F_2''(J)-F_1''(J) &= R_1(J)-R_2(J) = P_1(J)-P_2(J), \\ F_3''(J)-F_2''(J) &= R_2(J)-R_3(J) = P_2(J)-P_3(J). \end{aligned} \tag{7}$$

The average values obtained from R and P branches were used in (6). The last term on the right in (6) is very small and was calculated by using the constants already calculated. Transferring this term to the left, eq. (6) becomes

$$[F_3(J)-F_1(J)]^2+1/3[\{F_3(J)-F_2(J)\}-\{F_2(J)-F_1(J)\}]^2 \tag{6'}$$
$$+64B\cdot DJ^2(J+1)^2 = [4A(A-4B)+16/3\ B^2-16A\cdot D]$$
$$+[16B^2+32A\cdot D-32B\cdot D]J(J+1).$$

A graph $X(J)-YJ(J+1)$ versus $J(J+1)$ was plotted as shown in Fig. 3, where X is equal to the left-hand side of (6′) and Y is an approximate value of the coefficient of $J(J+1)$. As is evident from the figure a very good straight line was obtained from $J = 3$ to 38. The slope of the line gave a correction to Y and the intercept with the ordinate gave a quantity from which the constant A could be calculated. This value of A is shown in Table III.

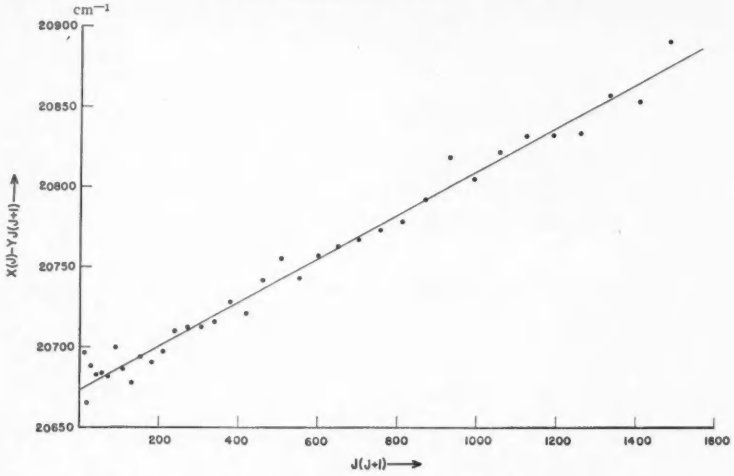

FIG. 3. A graph showing $X(J)-YJ(J+1)$ versus $J(J+1)$ from which the constant A was calculated.

(3) Λ-Splitting

As mentioned earlier no 'combination defect' was observed in the subband $^1\Sigma$–$^3\Pi_2$ within experimental error. From theory also it is expected to be very small. Since the Q_2 branch is not resolved, there is no way of knowing the Λ-splitting in $^3\Pi_1$. The Λ-splitting in $^3\Pi_0$ was calculated by the following relation

$$\epsilon = [R_1(J)-Q_1(J)]-[Q_1(J+1)-P_1(J+1)] \tag{8}$$

where ϵ is the sum of the Λ-splittings in two successive levels. This splitting is plotted against $J(J+1)$ as shown in Fig. 4, where a comparison with the Λ-splitting of the $a^3\Pi_0$ of CO is also shown. From Van Vleck's theory (1932) we expect the Λ-splitting in $^3\Pi_0$ to be almost independent of J in ideal case *a*. However, in an intermediate case to which most of the observed $^3\Pi$ states belong, Hebb (1936) has shown a typical variation of Λ-splitting in $^3\Pi$ with J. The present case of $^3\Pi_0$ shows a case of Λ-splitting which is quite analogous to that of $^3\Pi_0$ of the PH molecule as shown by Gilbert (1936). It is not certain whether the sign of the Λ-splitting for SiO should be as shown by the plotted points in Fig. 4, or by the dotted curve.

(4) Band Origins

The band origins of the three subbands were calculated by the method described by Herzberg (1950) and the values obtained are included in Table III.

Since the B values in the lower and upper states differ very slightly, the two electronic states probably have more or less equal vibrational frequencies and it seems fairly certain that the band discussed in this paper is the (0,0) band.

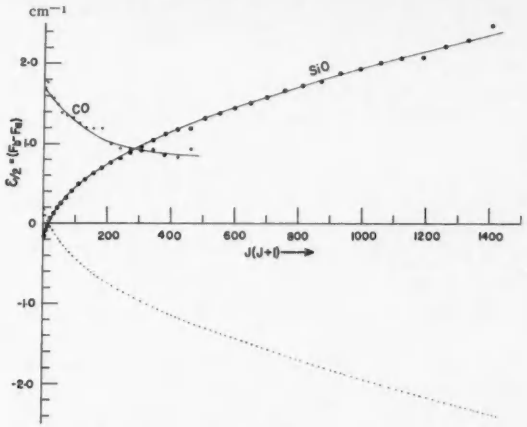

FIG. 4. Λ-Splitting of $^3\Pi_0$ plotted against $J(J+1)$. The dotted curve shows the alternative sign for Λ-splitting. Λ-Splitting of $^3\Pi_0$ of the CO molecule is also shown for comparison.

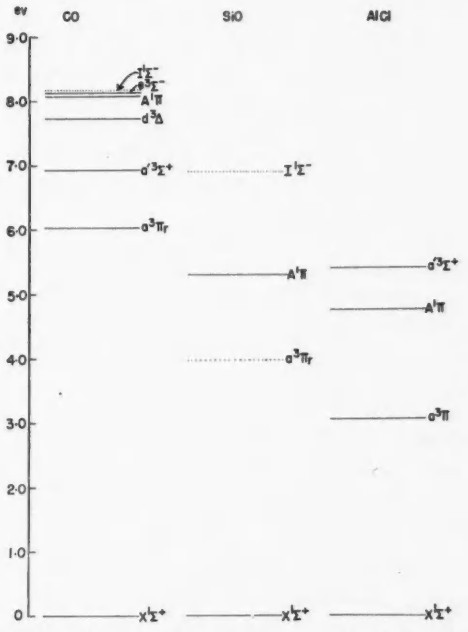

FIG. 5. A comparison of low-lying electronic states of CO, SiO, and AlCl. The dotted lines are the estimated positions of the indicated electronic states. The *d* state of CO has been interpreted as $^3\Delta$ by Mulliken (1958), who has pointed out objections to its being considered $^3\Pi$.

ELECTRON CONFIGURATION

The ground electron configuration of SiO may be described, in analogy to that of CO, as $w\pi^4x\sigma^2$. The low excited electronic states of CO have been discussed recently by Mulliken (1958). The SiO molecule is expected to have low excited levels rather similar to those of CO. Thus it is very probable that the lower state $^3\Pi_r$ of the present system is the lowest $w\pi^4x\sigma v\pi$, $^3\Pi_r$ state of SiO analogous to the $a^3\Pi_r$ state of CO. If one compares low-lying electronic states of CO, SiO, and AlCl as shown in Fig. 5, it seems rather probable that the upper state of the present system is $^1\Sigma^-$ analogous to $I^1\Sigma^-$ of CO with electron configuration (Mulliken 1958) $w\pi^3x\sigma^2v\pi$. This $^1\Sigma^-$ state is expected to be metastable and hence may account for the fairly high intensity of the present bands.

It is, however, strange that B' and B'' for the above-mentioned two electronic states of SiO are almost equal, in sharp contrast to those of analogous states of CO and N_2, where B is considerably smaller for the $^1\Sigma^-$ state than for the $^3\Pi$ state.

If the suggested assignment of the electronic states to configurations is correct, one might expect that the $a^3\Pi_r$–$X^1\Sigma^+$ transition in SiO would show considerable intensity, in fact stronger intensity than do the Cameron bands of CO. However, an earlier effort (Herzberg 1952) in this direction did not prove successful. On the other hand a spectrum analogous to the present one is expected in the case of CO.

ACKNOWLEDGMENTS

The authors extend their thanks to Drs. F. S. Tomkins and M. Fred for their permission to use the photoelectric comparator.

REFERENCES

Crosswhite, H. M. 1958. John Hopkins Spectroscopic Report No. 13, The John Hopkins University, Department of Physics, Baltimore, Md.
Gero, L., Herzberg, G., and Schmid, R. 1937. Phys. Rev. **52**, 467.
Gilbert, C. 1936. Phys. Rev. **49**, 619.
Hebb, M. H. 1936. Phys. Rev. **49**, 610.
Herzberg, G. 1950. Spectra of diatomic molecules (D. Van Nostrand Company, New York).
——— 1952. Trans. Roy. Soc. Canada, **146**, 1.
Mulliken, R. S. 1958. Can. J. Chem. **36**, 10.
Pankhurst, R. C. 1940. Proc. Phys. Soc. **52**, 707.
Sharma, D. 1951. Astrophys. J. **113**, 210.
Tomkins, F. S. and Fred, M. 1951. J. Opt. Soc. Am. **41**, 641.
Van Vleck, J. H. 1932. Phys. Rev. **40**, 544.
Verma, R. D. 1961. J. Mol. Spectroscopy. In press.
Verma, R. D. and Mulliken, R. S. 1961. J. Mol. Spectroscopy. In press.
Woods, L. H. 1943. Phys. Rev. **63**, 426.

LOW-LYING ENERGY LEVELS IN Cl-35[1]

R. S. STOREY[2] AND L. W. OLEKSIUK

ABSTRACT

The reaction $Cl^{35}(p,p'\gamma)Cl^{35}$ has been observed by the gamma radiation arising from the first two excited levels of chlorine-35. Excitation functions for these radiations were measured for a range of proton energies from 2.3 to 3.25 Mev. Many sharp resonances are observed, of which a dozen are prominent. Angular distributions of the gamma rays from the 1.22-Mev and the 1.76-Mev excited levels of Cl^{35} have been measured over six resonances. The distribution functions, together with additional measurements by other investigators, yield spin assignments of 1/2 and 5/2 for the levels at 1.22 and 1.76 Mev respectively.

INTRODUCTION

Sufficient experimental information is now available about the properties of nuclei in the $2s$ $1d$ shell to permit systematic features to be detected (Gove 1960). The nuclei near the high A limit of the shell have, however, been only slightly investigated, and in particular little is known about the energy levels of the chlorine isotopes. An intensive study of the levels of Cl^{35} and Cl^{37} is now being carried out in this laboratory. This paper describes the determination of the spins of the two lowest excited states of Cl^{35}.

The most accurate values of the energies of these two excited states have been obtained by Endt, Paris, Sperduto, and Buechner (1956) and Schiffer, Gossett, Phillips, and Young (1956) using magnetic analysis of inelastically scattered protons. These values are 1.220 and 1.763 Mev. Similarly in Cl^{37}, Endt and his colleagues found 0.837 and 1.723 Mev for the energies of the first two excited states, though Schiffer did not detect the former.

Kistner, Schwarzschild, and Rustad (1956) have shown that beta decay branches of argon-35 to the first three excited states of Cl^{35} are allowed transitions, and that these states have therefore positive parity with spins $\leqslant 5/2$. Excitation curves for the capture of protons in Cl^{35} up to about 2.5 Mev in proton energy have been reported by Brostrøm, Madsen, and Madsen (1951), who used the (p,γ) reaction and Almqvist, Clarke, and Paul (1960), who used the (p,α) reaction. In the work reported here, the low-lying states of Cl^{35} have been further investigated by measurements of the angular distributions of the gamma radiations arising from the reaction $Cl^{35}(p,p'\gamma)Cl^{35}$. These distributions were measured at six of the prominent resonances in the excitation functions of the radiations, and together with additional existing observations, spin assignments with small likelihood of error could be made.

Accurate measurements of the gamma-ray spectra at these resonances were carried out so that the 1.72-Mev radiation from the reaction $Cl^{37}(p,p'\gamma)Cl^{37}$ would be recognized. No radiation of this energy was observed at the resonances

[1]Manuscript received January 25, 1961.
Contribution from the Department of Physics, University of Toronto, Toronto, Ontario.
[2]Now at the National Research Council, Ottawa, Canada.

at which angular distributions of the 1.76-Mev Cl^{35} radiation were observed, so that the distributions measured were definitely those of radiations arising from the Cl^{35} isotope.

APPARATUS

A commercial model 3-Mev electrostatic generator was used to accelerate protons to energies ranging from 2.3 Mev to 3.25 Mev. Voltage stabilization was obtained by means of a feedback system utilizing an error signal that arose from the beam striking a pair of centering slits after passing through an analyzing magnet: the signal so obtained regulated the corona load of the generator. The analyzing magnet was current-stabilized, and provided a deflection of 25 degrees in the horizontal plane. Measurements of beam energy were made by means of a Harvey-Wells nuclear magnetic resonance gaussmeter used to measure the flux density of the deflecting field. The magnetometer allowed the energy measurements to be transcribed into a measurement of a radio frequency, the error in this measurement being much less than the drift inherent in the magnet itself. These energy measurements were found to be accurate to within ±5 kilovolts in the proton energy range of 2.3 Mev to 3.25 Mev. The number of protons incident on the target was measured by means of a commercial current integrator.

The target which the beam bombarded consisted of a gold (.005 in.) or tantalum (.02 in.) backing on which was deposited a thin film of AgCl. Both isotopically enriched and natural salts were used; the enriched target of 88.5% Cl^{35} was obtained from A.E.R.E. Harwell, while the natural targets were produced at the University of Toronto. The angular distribution table and target chamber were modified versions of ones constructed at Chalk River.

The gamma radiation under investigation was measured by a 5 in. diameter by 4 in. long NaI(Tl) crystal and a $1\frac{3}{4}$ in. diameter by 2 in. long NaI(Tl) crystal. The resulting pulse spectra were analyzed and recorded with single channel analyzers and scalers, and a 100-channel pulse-height analyzer for detailed spectrum analysis.

EXCITATION STUDIES

The energy scale for the excitation studies was obtained by calibrating the generator using a narrow resonance in the reaction $F^{19}(p,\alpha\gamma)O^{16}$, given to be 873.5±.9 kev (Herb, Snowdon, and Sala 1949) by the electrostatic deflection method. Both proton and H_2^+ beams were used for calibration, with the result that the deflecting magnetic field was calibrated for protons at 873.5 kev and at four times this energy, that is, at 3.494 Mev. The excitation studies were carried out in two phases. The first consisted of determining the excitation curve for the 1.22-Mev gamma ray from the first excited state of Cl^{35}. When the Harwell isotopically enriched target was used, the yield of the 1.22-Mev radiation was measured by means of a single channel analyzer gated to count the photopeak region of the pulse spectrum. The energy of the proton beam was varied from 2.3 Mev to 3.05 Mev in steps of 2 kev. The

excitation function obtained with this target is shown in Fig. 1. Since no compensation was made for Compton interference from higher energy gamma peaks in the pulse spectrum, some of the smaller resonances may, in fact, be due to excitation of levels which decay by the emission of 1.7-Mev radiation.

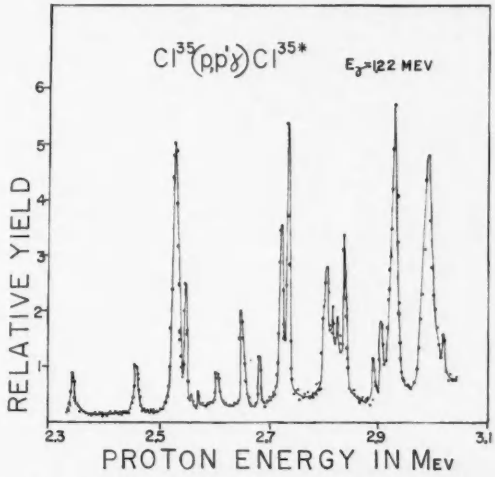

FIG. 1. Excitation of $Cl^{35}(p,p'\gamma)Cl^{35}$ for proton energies of 2.3–3.05 Mev.

Comparison of this excitation function to that for the reaction $Cl^{35}(p,\alpha\gamma)S^{32}$ obtained by Almqvist *et al.* (1960) shows good correspondence. In both cases about 20 resonances are observed in the proton energy range of 2.3 Mev to 3.05 Mev of which 12 correspond to within 10 kev. The present data and those obtained by Almqvist are tabulated in Table I, along with approximate width values for the resonances in kev. These values have not been corrected for target thickness and beam spread, the sum of which was shown to be less than 3 kev by detailed study of some of the narrow resonances.

The second phase of the excitation studies consisted of measuring the excitation of both excited levels of Cl^{35}, for the proton energies between 2.95 to 3.25 Mev, in an experiment using a non-enriched AgCl target so that any Cl^{37} excitation might also be observed. This target was measured to be about 2.2 kev thick at $E_p = 2.45$ Mev. The entire gamma-energy spectrum of interest was recorded during this excitation study, with the 100-channel pulse-height analyzer set to record all gamma pulses corresponding to the gamma-energy range of 0.55 Mev to 3.0 Mev. Frequent background level checks were made by rotating the target through 180°. The 5-in. spectrometer used in the study was placed at 90° to the beam direction.

The analysis of the spectra separated the contributions of four possible gamma energies. Two of these arose from Cl^{35} levels, at 1.22 and 1.76 Mev and the two other radiations expected were at 2.1 Mev and 0.84 Mev. No

TABLE I

Comparison of the resonances in the reactions $Cl^{35}(p,p'\gamma)Cl^{35}$ and $Cl^{35}(p,\alpha)S^{32}$ (resonance energies given in Mev and widths in kev)

Almqvist *et al.* (1960) p,α (E_p)	Present work $p,p'\gamma$ (E_p)	Present work Γ	Almqvist *et al.* (1960) p,α (E_p)	Present work $p,p'\gamma$ (E_p)	Present work Γ
2.307	—		2.830	2.826	—
2.325	—		—	2.838	5
—	2.345	6	2.867	—	
2.400	—		2.892	2.892	5
2.450	2.460	8	2.910	2.907	10
2.505	—		—	2.921	
—	2.530	11	—	2.933	~5
2.545	2.545	6	2.978	2.980*	8
—	2.560	~7		2.993	~9
2.572	2.572	<3	3.03	3.020	5
2.602	2.606	8		3.065*	9
	2.650	7		3.093*	14
2.682	2.683	<4		3.115*	~4
2.718	2.724	~4		3.135*	~4
2.730	2.733	<3		3.154	23
2.757	—			3.159*	—
2.772	—			3.182	<10
2.800	2.807	8		3.205*	<8
—	2.818	—		3.225	<12

*Indicates strong 1.7-Mev γ-ray.

evidence for a 0.84-Mev radiation was found in the spectra. This radiation had been previously observed (Endt, Paris, Sperduto, and Buechner 1956) and was thought to be evidence of a level in Cl^{37}. The 2.1-Mev radiation can arise from both (p,α) and (p,γ) reactions in Cl^{35} and Cl^{37}, but was found to be very weak. Excitation curves for the 1.22- and 1.76-Mev gamma ray are shown in Fig. 2.

Because of the presence of approximately 25% Cl^{37} in the natural target, the possibility existed that some of the resonances in the 1.7-Mev excitation curve were from this isotope. For this reason careful measurements of the gamma energy were performed for the three prominent resonances in the 1.7-Mev excitation curve at proton energies of 3.093, 3.115, and 3.135 Mev. In order to determine which isotope was excited at these resonances it was necessary to distinguish between the Cl^{37} gamma energy of $1.728\pm.005$ Mev and the $1.763\pm.005$ Mev radiation from Cl^{35}.

A sodium-24 source was used in order to give clear calibration points at 1.368 Mev and the "two-escape" peak of the 2.76-Mev transition (Kinsey and Bartholomew 1953). The latter energy (1.73 Mev) was particularly suitable as it lay between the two energies to be resolved. Using a 1-in. NaI crystal (coupled to a 2-in. photomultiplier tube) so that the small crystal size would increase the probability of both the positron annihilation quanta escaping and thus yield a prominent 1.732-Mev peak, we compared the Na^{24} spectrum to the gamma spectrum from the natural chlorine target at all three resonances. As a check on the calibration, the 1.22-Mev gamma photopeak was also used, for its value is well known. Care was taken to avoid

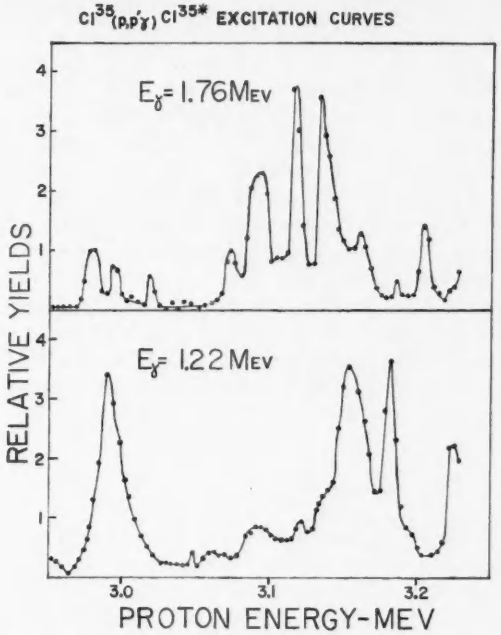

FIG. 2. Excitation of $Cl^{35}(p,p'\gamma)Cl^{35}$ for proton energies 2.95–3.25 Mev.

any saturation effects in the amplification of the pulses. The results obtained for the three resonances were: 1.767, 1.762, and 1.763 (all ±.008) Mev. Thus the activity at these resonances could be definitely ascribed to the Cl^{35} isotope.

The possibility of the 1.22-Mev radiation arising from the cascade transition from the 1.76-Mev levels was examined. It was found that in all the 1.76-Mev resonances, the amount of cascade transitions was less than 10% of the number of crossover transitions. At the 1.22-Mev gamma resonances where angular distributions were measured, the yield of the 1.76-Mev radiation was always less than 20% of the 1.22-Mev yield. Thus it was deduced that the contribution of any cascade 1.22-Mev radiation was less than 2% in the angular distributions measured, and so would have negligible effect on the angular distributions of these gamma rays.

THE ANGULAR DISTRIBUTIONS

The angular distributions of the gamma rays from Cl^{35*} were measured at several resonance energies. In all cases the 5-in. crystal was used as the movable detector, and a collimator used to improve the total absorption peak fraction. The 100-channel pulse-height analyzer was used to record the resulting spectra. A 2-in. NaI crystal assembly mounted at 105° to the proton beam served as a monitor. The monitor pulses were selected by a single

channel analyzer, set to accept pulses corresponding to the photopeak of the gamma ray under investigation. The target was placed at 45° to the beam so that backing absorption would not contribute to the 0°/90° anisotropy.

Background measurements were of great importance because of the small yields resulting from the use of thin targets necessary for good resonance definition. Backgrounds in the 5-in. crystal assembly were found with the target turned through 180°, that is, with the beam incident on the backing alone, and were measured at detection angles of 0°, 30°, 60°, and 90°. In the case of the monitor crystal, continuous observation of a portion of the gamma-ray spectrum immediately above the photopeak of interest was maintained for monitor background corrections.

The pulse spectra from the 5-in. crystal were analyzed in such a manner that the areas of the photopeak of the 1.22- and 1.76-Mev radiations could be separated. We made appropriate corrections for background and for Compton pulses from other radiations by using photofractions obtained by subsidiary measurements with standard sources and identical crystal geometries.

RESULTS

Table II shows the results of the measurements of the angular distributions at several resonances, for both 1.22-Mev and 1.76-Mev gamma radiation. The

TABLE II

Angular distribution fitting functions obtained at several resonances in the reaction $Cl^{35}(p,p'\gamma)Cl^{35}$ for the two gamma radiations investigated

E_p(Mev)	E_γ(Mev)	Fitting function
3.12	1.76	$1-(.141\pm.013)P_2+(.107\pm.016)P_4$
3.135	1.76	$1-(.049\pm.012)P_2-(.036\pm.014)P_4$
2.84	1.76	$1-(.225\pm.029)P_2+(.083\pm.035)P_4$
3.154	1.22	$1+(.031\pm.016)P_2-(.014\pm.020)P_4$
2.99	1.22	$1-(.012\pm.022)P_2-(.002\pm.030)P_4$
2.84	1.22	$1-(.009\pm.014)P_2+(.014\pm.006)P_4$

Legendre expressions given are the least squares fit to the distributions obtained, the fitting function being of the form:

$$1+A_2P_2(\cos\theta)+A_4P_4(\cos\theta)$$

where θ is the angle between the beam direction and the 5-in. scintillator axis. The root mean square fitting error is given after each coefficient. Thus, a fitting error that is approximately equal to or greater than the corresponding coefficient indicates that the coefficient is not significantly different from zero.

Plots of several of the fitting functions and the observed points are given in Figs. 3 and 4.

INTERPRETATION

Because the distributions were measured on sharp resonances in the reaction, it is assumed that the reaction proceeds through sharp states in the compound

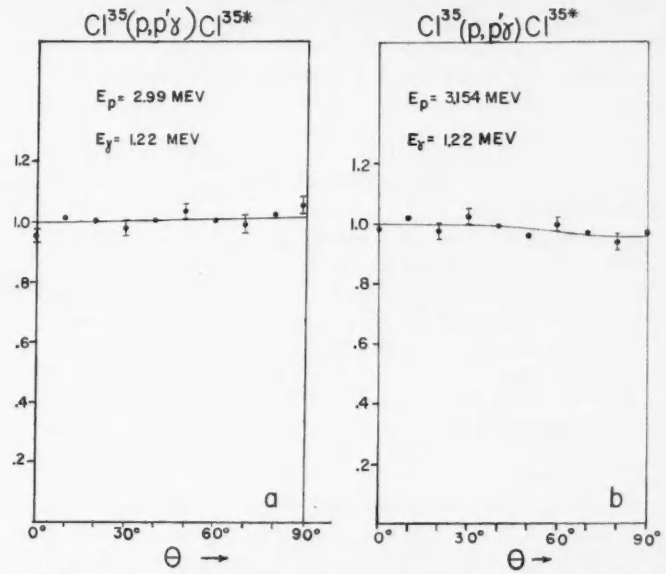

FIG. 3. The angular distribution of the 1.22-Mev gamma ray with respect to the proton beam at resonances $E_p = 2.99$ Mev and $E_p = 3.154$ Mev. Standard deviations are shown by error flags on representative points.

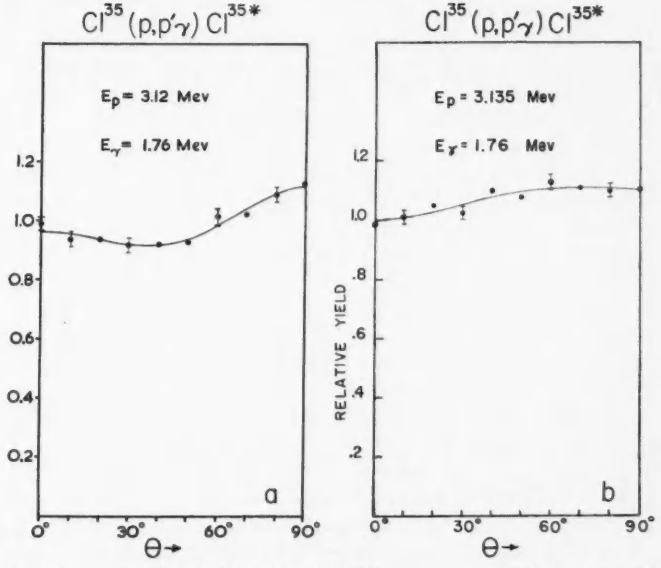

FIG. 4. The angular distribution of the 1.76-Mev gamma ray with respect to the proton beam at resonances $E_p = 3.12$ Mev and $E_p = 3.135$ Mev. Standard deviations are shown by error flags on representative points.

nucleus A^{36}, so that mixed intermediate states will not occur. From the properties of Racah coefficients it is known that an inequality theorem holds for the maximum observable order of Legendre polynomial in a reaction such as this (Racah 1942):

$$0 \leqslant n_{\max} \leqslant \min(2l_1, 2J_1, 2J_2, 2L_2)$$

where l_1 is the orbital angular momentum of the incoming proton measured in units of $\hbar$,

J_1 is the spin of the compound state of A^{36},

J_2 is the spin of the excited state of Cl^{35},

L_2 is the orbital angular momentum carried off by the de-exciting radiation.

The angular distributions for the 1.22-Mev level indicated isotropy in all cases. Because of the short life of the excited levels studied here, isotropy arising from the interaction of extranuclear perturbing fields can be neglected. However, the isotropy at any resonance can arise in several ways:

(*a*) If the ingoing protons are pure *s*-wave protons, then $l_1 = 0$.

(*b*) If the 1.22-Mev excited level has spin 3/2 and de-excites by pure electric quadrupole radiation.

(*c*) By accidental cancellation arising in the population of the magnetic substates, that is, $B_2(J_2) = 0$ (Fagg and Hanna 1959).

(*d*) If the 1.22-Mev level has spin 1/2, independent of the mixing parameter.

Since we have examined the distribution on three well-defined resonances, formation by pure *s*-wave protons in all cases is unlikely. The presence of significant P_4 terms in the distributions of the 1.76-Mev gamma rays shows that *d*-wave protons can form resonances involving this level, and so *d*-wave formation should be expected at resonances of about the same energy involving the 1.22-Mev level. Accidental cancellation causing the magnetic substate population coefficient to be zero in each case seems unlikely. Thus, the remaining information yields 1/2 or 3/2 as likely spin assignments. However, the spin 3/2 is less likely as calculations from the simple Weisskopf independent particle model (Montalbetti 1952) indicate that pure electric quadrupole radiation is decidedly weaker than the magnetic dipole radiation. E_2 enhancement would not be expected for this odd A nucleus since nuclear deformations should be relatively small here (Gove 1960).

Calculations of linear polarization indicates that both (*b*) and (*d*) would yield zero polarization. However, if (*c*) were true, then non-zero linear polarization could only be measured if the spin of the level were greater than 3/2. Thus, polarization measurements would not yield substantiating information on the spin assignment of this level.

The angular distributions for the 1.76-Mev level indicate the existence of a non-zero coefficient for the P_4 term. This shows that J_2 must be at least 5/2. However, beta decay (Kistner, Schwarzschild, Rustad 1956) gives a log *ft* value of 4.5 for beta decay to this level from the 3/2+ ground state of A^{35}. Because this log *ft* value indicates an allowed beta transition the spin value for the 1.76-Mev level must be $\leqslant 5/2$. Thus a definite spin assignment of 5/2 can be made for this level.

The most probable interpretation of the experimental results, then, bearing in mind the beta-ray results of previous workers, is that the spins of the 1.22- and 1.76-Mev levels of Cl^{35} are 1/2 and 5/2, with positive parity in both cases. Such assignments are consistent with shell model predictions in this region.

ACKNOWLEDGMENTS

The authors are greatly indebted to Drs. K. G. McNeill and J. D. Prentice for their interest and advice, and to other members of the Nuclear Physics Group, who assisted in setting up the apparatus. They gratefully acknowledge the provision of facilities by the Ontario Cancer Institute and the helpful co-operation of Drs. H. E. Johns and G. F. Whitmore.

The technical assistance of Mr. G. Woodward of the University of Toronto and of the A.E.R.E. Harwell Isotope Separation Group for preparation of the targets is highly appreciated.

This work was supported by a National Research Council grant BT-84, for which we are grateful.

REFERENCES

ALMQVIST, E., CLARKE, R. L., and PAUL, E. B. 1960. Nuclear Phys. **14**, 472.
BROSTRØM, K. J., MADSEN, B. S., and MADSEN, C. B. 1951. Phys. Rev. **83**, 1265 (L).
ENDT, P. M., PARIS, C. H., SPERDUTO, A., and BUECHNER, W. W. 1956. Phys. Rev. **103**, 961.
FAGG, L. W. and HANNA, S. S. 1959. Revs. Modern Phys. **31**, 711.
GOVE, H. E. 1960. Proceedings of the International Conference on Nuclear Structure, Kingston, p. 438.
HERB, R. G., SNOWDON, S. C., and SALA, O. 1949. Phys. Rev. **75**, 246.
KINSEY, B. B. and BARTHOLOMEW, G. A. 1953. Can. J. Phys. **31**, 537.
KISTNER, O. C., SCHWARZSCHILD, A., and RUSTAD, B. M. 1956. Phys. Rev. **104**, 154.
MONTALBETTI, R. 1952. Can. J. Phys. **30**, 660.
RACAH, G. 1942. Phys. Rev. **62**, 438.
SCHIFFER, J. P., GOSSETT, C. R., PHILLIPS, G. C., and YOUNG, T. E. 1956. Phys. Rev. **103**, 134.

THEORY AND DESIGN OF A COAXIAL SUPPORTING BEAD MADE OF COMPOSITE DIELECTRICS[1]

GILBERT H. OWYANG

ABSTRACT

The effect due to the presence of a single supporting bead made of composite dielectrics in a coaxial line is being studied. A formula correlating the standing wave ratio caused by the bead and the physical parameters of the bead is derived. A bead of this type may be designed to have very low voltage standing wave ratio (VSWR) over a very wide band of frequency. A typical design using quartz and air as dielectrics is given, and the calculated VSWR is below 1.003 over a bandwidth whose maximum to minimum frequency ratio is as high as 13:1.

1. INTRODUCTION

The inner conductor of a coaxial line is generally supported either by a continuous solid dielectric material or by dielectric beads that are spaced along the line. For certain purposes, dielectric beads are preferable. A single simple bead introduced into an air-filled coaxial line will cause a partial reflection of an incident electromagnetic wave. This is due to the change of impedance of the line in the presence of the dielectric material. The magnitude of this reflection depends upon the thickness of the bead and the dielectric material.

The reflection from a dielectric bead may be reduced by adjusting the diametric ratio at the bead so as to hold constant the characteristic impedance. This is accomplished either by undercutting the inner conductor or overcutting the outer conductor or both. By so doing, additional discontinuities are introduced and their effects are great enough to alter the performance of these beads at higher frequencies. A simple and effective way of compensating the shunt-capacity effect caused by the discontinuities (Whinnery and Jamieson 1944) in the case of beads that are thin compared with wavelength is to reduce the characteristic admittance in the beaded section (Ragan 1948, p. 164). However, this requires a larger diametric ratio at the bead and thus introduces more capacitance at the discontinuities. It is obvious that this method is somewhat limited.

The construction of a bead made of composite dielectric material is shown in Fig. 1. This bead may look complicated at the first sight. It is to be noted that either dielectric 1 or 3 may be the same as dielectric 2; the one which is different from dielectric 2 may be air. When the dielectrics are so chosen, such a bead assumes a similar form to the conventional bead except that a portion of it is removed. Such beads require no greater diametric ratio than an equivalent simple bead to hold constant the characteristic impedance. The fringe effect caused by the discontinuity in the conductor can be compensated with a line section of higher characteristic impedance by adjusting the pro-

[1]Manuscript received January 26, 1961.
Contribution from The Radiation Laboratory, Department of Electrical Engineering, University of Michigan, Ann Arbor, Michigan.

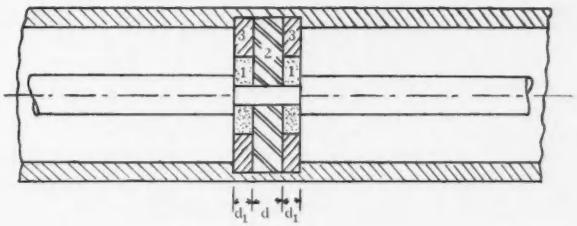

FIG. 1.

portion of composite dielectrics. Since the discontinuities in the conductors are fixed, the problem will automatically be easier to handle. It is found in a typical design (see Section 4) that a bead of this type may have a VSWR less than 1.003 over a ratio of maximum to minimum frequencies of 13:1.

2. TRANSMISSION LINE WITH COMPOSITE DIELECTRICS

Consider an infinitely long transmission line which is concentrically filled with two different dielectrics as shown in Fig. 2. The potential difference

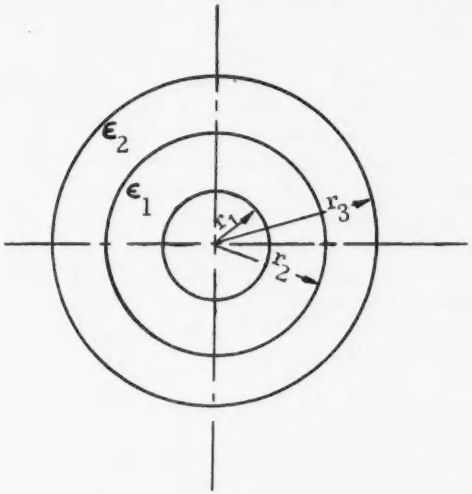

FIG. 2.

between the inner and the outer conductor of the coaxial line is given by

$$V = \int_{r_1}^{r_3} E_r dr = q\left(\frac{1}{C_1}+\frac{1}{C_2}\right), \tag{1}$$

where

$$E_r = \frac{q}{2\pi\epsilon}\frac{1}{r}, \tag{2}$$

$$C_1 = \frac{2\pi\epsilon_1}{\ln r_2/r_1}, \tag{3}$$

$$C_2 = \frac{2\pi\epsilon_2}{\ln r_3/r_2}, \tag{4}$$

where r_1 is the radius of the inner conductor, r_2 is the radius of the interface between the two dielectric materials, and r_3 is the radius of the outer conductor; q is the total charge per unit length on the line. The capacitance per unit length of such a line is given by

$$C = \frac{q}{V} = \left[\frac{1}{C_1}+\frac{1}{C_2}\right]^{-1} \tag{5}$$

$$= \frac{2\pi\epsilon_1\epsilon_2}{\epsilon_1 \ln r_3/r_2+\epsilon_2 \ln r_2/r_1}.$$

From the theory of transmission line, the capacitance per unit length of a coaxial cable filled with a single dielectric is given by

$$C = \frac{2\pi\epsilon}{\ln r_3/r_1}. \tag{6}$$

An equivalent dielectric constant may be defined for the line filled with composite dielectrics by comparing eqs. (5) and (6), thus

$$\epsilon_{12} = \frac{\epsilon_1\epsilon_2 \ln r_3/r_1}{\epsilon_1 \ln r_3/r_2+\epsilon_2 \ln r_2/r_1}. \tag{7}$$

It may thus be concluded that a coaxial line filled with two different dielectric materials behaves in a way similar to an ordinary coaxial line filled with a single dielectric whose equivalent dielectric constant is given approximately by eq. (7). It is not difficult to extend this theory for the case consists of more than two dielectrics. It is to be noted that eq. (7) is a good approximation at lower frequencies (Klopfenstein (1954) should be consulted for more rigorous treatment). For the convenience in design work where ϵ_{12} is usually specified, eq. (7) is rearranged as follows:

$$\frac{r_2}{r_1} = \ln^{-1}\left[\frac{(\epsilon_2/\epsilon_{12})-1}{(\epsilon_2/\epsilon_1)-1}\ln\frac{r_3}{r_1}\right], \tag{8}$$

$$\frac{r_3}{r_2} = \ln^{-1}\left[\frac{(\epsilon_1/\epsilon_{12})-1}{(\epsilon_1/\epsilon_2)-1}\ln\frac{r_3}{r_1}\right]. \tag{9}$$

3. ANALYSIS OF A BEADED LINE SECTION MADE OF COMPOSITE DIELECTRICS

The physical construction of the beaded section to be considered is as shown in Fig. 1 and its equivalent circuit is as shown in Fig. 3. The capacitance C is caused by the discontinuities on the conductor of the line. Y_1 is the characteristic admittance of the line section filled with composite dielectrics, Y_0 is the characteristic admittance of the uniform line, and Y is the characteristic admittance of the line filled with a single dielectric. γ_0, γ_1, and γ are

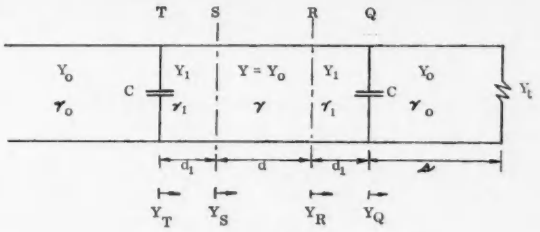

FIG. 3.

the complex propagation constants of the uniform line, the line with composite dielectrics, and the line with single dielectric respectively. The line as a whole is terminated by an admittance Y_t at a distance s from the right surface of the bead; d and d_1 are the corresponding lengths of the portion with single dielectric and that with composite dielectrics.

The input admittance Y_Q, with reference to Y_0, looking to the right at point Q is given by

$$Y_Q = j\omega C + Y_0 \coth(\theta_t' + \gamma s), \tag{1}$$

where $\theta_t' \equiv \coth^{-1}(Y_0/Y_t) = \rho_t + j\phi_t'$ is the complex terminal function, ρ_t is the terminal attenuation function, and ϕ_t' is the terminal phase function. Although the analysis may be carried out with any value of Y_t, the final result is of common interest only when the termination is perfectly matched. Therefore, the case with $Y_t = Y_0$ will be considered. Under such condition, $\phi_t' = \infty$, consequently eq. (1) becomes

$$Y_Q/Y_0 = 1 + jr, \tag{2}$$

where

$$r \equiv \omega C/Y_0. \tag{3}$$

The input admittance Y_Q, with reference to Y_1 is given by

$$Y_Q = Y_1 \coth \theta_{Q1}', \tag{4}$$

where the complex terminal function θ_{Q1}' is defined by eq. (4)

$$\theta_{Q1}' = \coth^{-1}\frac{Y_Q}{Y_1} = \coth^{-1}\left[\frac{1}{r_c}(1+jr)\right], \tag{5}$$

$$r_c \equiv Y_1/Y_0. \tag{6}$$

Equation (2) has been used to obtain eq. (5).

By repeating the above process at points R, S, and T, the input admittance Y_T at point T with reference to Y_1 is given by

$$Y_T = Y_1 \coth(\theta_{S1}' + \gamma_1 d_1) + j\omega C$$

or

$$(7)\quad \frac{Y_T}{Y_0} = jr + \frac{\left\{1-\left(r_c+\frac{1}{r_c}\right)\Omega\Omega_1-\Omega_1^2\right\}+j\left\{(r+\Omega)+\left[2r_c-\left(r_c+\frac{1}{r_c}\right)r\Omega\right]\Omega_1-(r_c^2\Omega+r)\Omega_1^2\right\}}{\left\{(1-r\Omega)-\left[\left(r_c+\frac{1}{r_c}\right)\Omega+\frac{2r}{r_c}\right]\Omega_1-\left(1-\frac{r\Omega}{r_c^2}\right)\Omega_1^2\right\}+j\left\{\Omega+\frac{2}{r_c}\Omega_1-\frac{\Omega}{r_c^2}\Omega_1^2\right\}},$$

where $j\Omega_i \equiv 1/\coth \gamma_i d_i$, and $\gamma_i = j\beta_i$ for lossless dielectric and perfect conductor. The input admittance Y_T can also be expressed in terms of Y_0.

$$Y_T = Y_0 \coth \theta'_T$$

or

$$(8)\quad \theta'_T = \coth^{-1}\frac{Y_T}{Y_0} = \frac{1}{2}\ln\frac{(Y_T/Y_0)+1}{Y_T/Y_0-1} = \frac{1}{2}\ln\frac{M+jN}{jP} \equiv \rho_T + j\phi'_T,$$

$$(9)\quad \rho_T = \frac{1}{2}\ln\frac{(M^2+N^2)^{1/2}}{P},$$

$$(10)\quad \phi'_T = \frac{1}{2}\tan^{-1}\frac{N}{M}-\frac{\pi}{4},$$

$$(11)\quad \frac{M}{2} \equiv (1-r\Omega)-\left[\left(r_c+\frac{1}{r_c}\right)\Omega+\frac{2r}{r_c}\right]\Omega_1+\left(\frac{r\Omega}{r_c^2}-1\right)\Omega_1^2,$$

$$(12)\quad N \equiv [2r+(2-r^2)\Omega]+2\left[\left(r_c+\frac{1}{r_c}\right)(1-r\Omega)-\frac{r^2}{r_c}\right]\Omega_1 + \left\{\left[(r^2-1)\frac{1}{r_c^2}-r_c^2\right]\Omega-2r\right\}\Omega_1^2,$$

$$(13)\quad P \equiv (2-r\Omega)r+2\left[\left(r_c-\frac{1}{r_c}\right)-\left(r_c+\frac{1}{r_c}\right)r\Omega-\frac{r^2}{r_c}\right]\Omega_1 + \left\{\left[\frac{r^2}{r_c^2}+\left(\frac{1}{r_c^2}-r_c^2\right)\right]\Omega-2r\right\}\Omega_1^2.$$

The corresponding formulas for the reflection coefficient

$$(14)\quad \hat{\Gamma}'_T = \Gamma'_T e^{-j\psi'_T} = \frac{Y_T-Y_0}{Y_T+Y_0}$$

are obtained directly from eq. (8). Since

$$(15)\quad \frac{Y_T-Y_0}{Y_T+Y_0} = e^{-2\theta'_T} = e^{-2\rho_T}e^{-j2\phi'_T},$$

therefore

(16) $$\Gamma_T' = e^{-2\rho_T},$$

(17) $$\psi_T' = -2\phi_T'.$$

The voltage or current standing wave ratio is

(18) $$S_T = \coth \rho_T = \coth\left[\frac{1}{2}\ln\frac{(M^2+N^2)^{1/2}}{P}\right].$$

It is to be noticed, from eq. (16) that the reflection coefficient Γ_T' will be small if the attenuation function ρ_T can be made very large, in the limit if $\rho_T = \infty$ then $\Gamma_T' = 0$. This case exists if P in eq. (9) vanishes which requires the following identity to be fulfilled.

(19) $$\Omega_1 = -\frac{A}{2} \pm \left[\left(\frac{A}{2}\right)^2 - B\right]^{1/2},$$

where

(20) $$A \equiv \frac{2}{D}\left[\left(r_c - \frac{1}{r_c}\right) - \left(r_c + \frac{1}{r_c}\right) r\Omega - \frac{r^2}{r_c}\right],$$

(21) $$B \equiv \frac{1}{D}(2 - r\Omega)r,$$

(22) $$D \equiv \left[\frac{r^2}{r_c^2} + \left(\frac{1}{r_c^2} - r_c^2\right)\right]\Omega - 2r.$$

For small values of r, Ω, Ω_1, and $r_c \simeq 1$, the numerator of eq. (8) is of the order of 2. The denominator may be made to vanish at least at one chosen frequency, its value may rise slightly at lower frequencies and approaches the value of $2r$ at zero frequency. By proper choice of the parameters, it is possible to design a bead which is transparent at the chosen upper frequency and whose reflection coefficient remains very small below this frequency.

It is to be noted that the fringing effect due to the discontinuities in the dielectric has been neglected. It has also been assumed that the capacitance due to the discontinuities in the conductors can be accurately determined. These assumptions, especially the latter, may cause substantial difference in the performance of the actual bead from the theoretical prediction.

4. SAMPLE OF DESIGN

It is desired to design a quartz ($\epsilon_2 = 3.8$) bead for a 49.5 ohms air-filled coaxial line. The VSWR caused by such a single bead should be less than 1.003 over a frequency range 100–1000 Mc/s. The I.D. of the outer conductor is .856 in. and the O.D. of the center conductor is .375 in.

The dielectric 1 (Fig. 1) is chosen to be air and dielectrics 2 and 3 are quartz. In order for the line section which is completely filled with quartz to have a characteristic impedance of 49.5 ohms, the ratio of the radii should satisfy the following relation.

$$\frac{r_3}{r_1} = \ln^{-1}\left[\frac{Z_0}{60}\epsilon_2^{1/2}\right] = 4.99 \tag{1}$$

For the present purpose, it is chosen to have $r_3 = .499$ in., therefore $r_1 = .100$ in. The variation of ϵ_{12} as a function of the ratio r_2/r_1 is computed from eq. (2–8) and the result is tabulated in Table I. For the above-chosen dimensions, the composite dielectric constant should not greatly exceed 2.5 for mechanical reason.

TABLE I

r_2/r_1	2.415	1.680	1.350	1.170	1.080
ϵ_{12}	1.5	2.0	2.5	3.0	3.5

In the case when $r_c = 1$ and values of r and Ω are small, eqs. (3.19) to (3.22), which represent the perfectly matched condition, require that Ω_1 be a linear function of frequency in the first-order approximation. In other words, the imposed condition will approximate closely the actuality provided $r_c = 1$. As an example, the following values are chosen.

$$r_c = .85 \quad \text{and} \quad \Omega = .2 \tag{2}$$

The shunt capacitive effect due to discontinuities in the present case is quite complicated since the fringing field caused by the two steps are intimately associated. The following approximate method of treating this problem gives results which agree fairly well with experiment (Ragan 1948, p. 184). An intermediate auxiliary cylindrical sheet of radius $r_{13} = r_{21}$ (properly chosen) could be inserted as indicated in Fig. 4, and the junction capacitance C_{1d} and

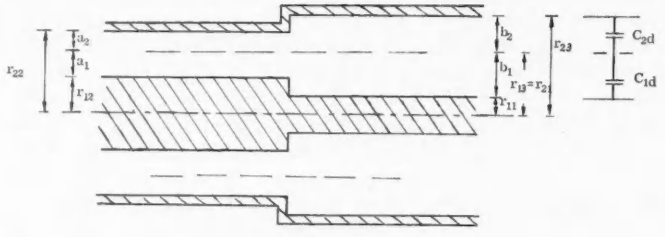

FIG. 4.

C_{2d} of the internal and external lines are formed by the methods for single step discontinuity (Whinnery *et al.* 1944). These junction capacitances are treated first by placing them in series with each other and then by connecting the combination across the line. The value of $r_{13} = r_{21}$ is chosen as that value which makes the total capacitance C_d a maximum. Being at a maximum, the value of C_d is not very sensitive to slight variation of $r_{13} = r_{21}$ from the correct value. For the present case it is found that C_d approaches an almost constant maximum value when $\delta = .8$ to .95, where δ is defined as follows:

$$r_{13} = r_{12} + \delta(r_{22} - r_{12}). \tag{3}$$

The various symbols in the above equation are defined in Fig. 4.

The total capacitance is obtained by computing the series combination of C_{1d} filled with composite dielectrics and C_{2d} filled with a single dielectric. This value does not differ appreciably from that obtained by multiplying the resultant capacitance of the two air-filled capacitors by the resultant composite dielectric constant.

Design data:

$r_1 = .100$ in., $r_2 = .1247$ in., $r_3 = .499$ in.,
$C = .13$ $\mu\mu$f, $\epsilon_{12} = 2.7455$, $r_c = .85$,
$f_M = 1000$ Mc/s (upper limiting frequency),
$\Omega = .20$, $d = .0047159$ m,
$\Omega_1 = .1191$, $d_1 = .0056006$ m.

The theoretical performance is tabulated in Table II and is also plotted in Fig. 5.

TABLE II

f (Mc/s)	S_T
100	1.00039
200	1.00073
300	1.00100
400	1.00119
500	1.00128
600	1.00127
700	1.00115
800	1.00091
900	1.00053
1000	1.00000
1100	1.00068
1200	1.00153
1300	1.00255

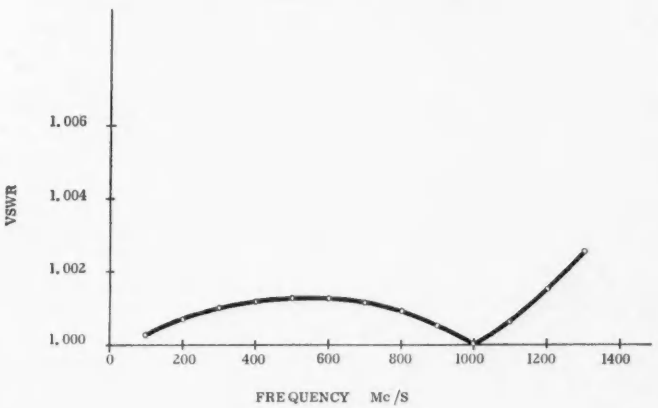

FIG. 5.

ACKNOWLEDGMENT

The author wishes to express his appreciation to Mr. R. E. Hiatt and Dr. D. L. Sengupta for their helpful discussions.

This work was supported by Rome Air Development Center under Contract AF 30(602)-2099.

REFERENCES

KLOPFENSTEIN, R. W. 1954. IRE Trans. **AP-2**, 103.
RAGAN, G. L. 1948. Microwave transmission circuits (McGraw-Hill Book Co.), pp. 164, 184.
WHINNERY, J. R. and JAMIESON, H. W. 1944. Proc. I.R.E. **32**, 98.
WHINNERY, J. R., JAMIESON, H. W., and ROBBINS, T. E. 1944. Proc. I.R.E. **32**, 695.

VARIATIONS IN SOLAR TIME OF EXTENSIVE AIR SHOWERS[1]

B. G. WILSON,[2] J. G. G. DIONNE,[3] AND F. TERENTIUK

ABSTRACT

150,000 extensive air showers of high electron density have been recorded at an altitude of 2283 meters. Analysis of the data in solar time for a wide range of densities shows no evidence for the large semidiurnal variations previously reported by other groups. A possible explanation of this difference may lie in the different methods of selecting the showers.

1. INTRODUCTION

The interaction of an extremely energetic primary cosmic ray with an atmospheric nucleus initiates the development of a complex chain of reactions which continues through several generations, giving rise to a large number of secondary particles. This phenomenon is known as an extensive air shower. Primary energies associated with such showers range from 10^{12} to 10^{18} or 10^{19} electron volts. Studies of their energy spectrum and arrival times may be expected to yield significant information on such cosmological processes as the mechanism for particle acceleration to high energy. They may also throw light on the nature and extension of the galactic magnetic field which retains the particles and randomizes their motions so that their arrival directions appear isotropic.

Even if the retention mechanism is very efficient, leakage of the higher energy particles from the galaxy must be anticipated beyond some finite energy limit. Such a breakdown should be revealed by increasing anisotropy in the arrival directions at the earth of these more energetic particles and perhaps by a discontinuity in the energy spectrum of the particles themselves.

Anisotropy of these incoming particles may be revealed by a study of arrival times of extensive air showers which are the phenomena of consistently highest energy observable on the ground. Such measurements have been performed for many years. Rather unexpectedly, no significant variation in sidereal time has yet been found to be greater than a few per cent and most data do not appear inconsistent with zero variation.

Analysis of the data in solar time has, however, suggested that significant changes in intensity may occur although the mechanism for such variations is not so obvious. Of particular interest are the large semidiurnal variations noted by McCusker and others (McCusker and Wilson 1956; Cranshaw and Galbraith 1957; Wilson 1959; and McCusker, Page, and Reid 1959), which appear to be correlated with the semidiurnal pressure wave. The correlation with this pressure wave has given barometer coefficients of the order of

[1]Manuscript received March 8, 1961.
Contribution from the Division of Pure Physics, National Research Council, Ottawa, Canada, and the Department of Physics, University of Alberta, Calgary, Alberta.
Issued as N.R.C. No. 6311.

[2]National Research Council Sulphur Mountain Laboratory, Banff, Alberta; now at the Department of Physics, University of Alberta, Calgary, Alberta.
[3]Now at Defence Research Board, Valcartier, Que.

$\pm 100\%$ per cm Hg or more. Positive coefficients have been reported for detectors selecting high electron densities, where the detector is necessarily near the shower core, whereas negative coefficients have been reported using extended detectors sensitive to the spread of the showers. Correlations with day-to-day barometric pressure, on the other hand, gave the usual negative coefficients of the order of 10%.

It has been suggested that these large effects may be associated with variations in core size reflecting variations in the height of the primary interaction due to tidal motions in the upper atmosphere. Detectors sensitive to density change at high densities and located within the core region might then show effects in opposite phase to those outside the core. In particular, Pearson and Butler (1960) have investigated the density variations in the core region caused by changes in height of the ozone layer affecting the interaction levels of incoming heavy primaries.

The present experiment was set up to look for time variations in showers with high electron density using an apparatus capable of measuring different particle densities and giving a comparatively high counting rate.

2. EXPERIMENTAL ARRANGEMENT

The apparatus consisted of nine trays each containing two Geiger counters, 4 in. $\times$ 1 in., disposed as in Fig. 1. The trays were arranged in a horizontal plane under the roof of the Sulphur Mountain Laboratory near Banff, Alberta, Canada, at an altitude of 2283 meters (lat. 51.2° N., long. 115.6° W.). The counter array covered an area of 50 square meters.

Events were recorded when any 3 or more of the 18 counters were simultaneously struck. The record of each event was displayed on a 20-pen recorder showing the counters discharged and the arrival time of the shower. The barometric pressure was continuously recorded on two microbarographs. The experiment has been operated since early 1959 and data from July 1, 1959, to August 1, 1960, are included in this analysis.

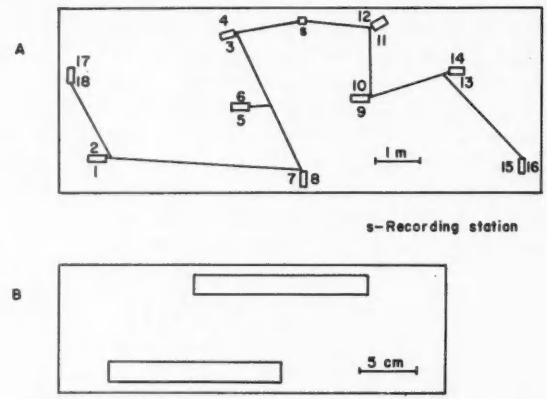

FIG. 1. (*a*) Arrangement of Geiger counter trays in the laboratory. (*b*) Arrangement of Geiger counters in the trays.

3. METHOD OF ANALYSIS

The charts were first analyzed according to the multiplicity of counters struck per event as a function of solar time. The data were then collected on a daily basis giving the total numbers of 3-fold, 4-fold, . . . , 18-fold events. Events involving 3–6, 7–12, and 13–18 discharged counters were also totalled as were the total number of events.

4. SHOWER DENSITIES

Assuming constant density of the showers over the area of the experiment the average particle densities detected vary from 36 to 2800 particles per square meter from 3- to 18-fold. The 3- to 6-, 7- to 12-, and 13- to 18-fold groups have, respectively, average densities of 53, 193, and 881 particles per square meter while the average density for all events is 86 particles per square meter.

5. TIME VARIATIONS

The rates of the three subtotals, 3- to 6-, 7- to 12-, and 13- to 18-fold, and the grand total of all events are plotted as a function of solar time (U.T.) in Figs. 2 and 3. For each case a χ^2 test was applied to the values to determine whether the distribution of the data from the mean rate was normal. P values obtained for these cases are respectively 70, 75, 85, and 60% so that the data are consistent with no variation in solar time. It appears likely, then, that any periodic variation in the data is small for the density ranges selected. The individual multiplicities have also been plotted in solar time. Although in the higher multiplicity events the statistics are less precise, there is no obvious evidence of correlation with the pressure wave.

6. DISCUSSION

A feature of the results is the absence of any variation of the showers in solar time. This appears to be the case for all multiplicities recorded. The total number of events has been analyzed to determine the extent of any correlation with the barometric pressure by comparing the percentage deviations of the mean hourly shower rates and the residual pressure wave over the 24-hour day. The barometric pressure wave for the 13-month period is plotted as a function of solar time in Fig. 4. The calculated correlation coefficient of $r = -0.046$ indicates no apparent correlation.

It is clear that the large percentage changes previously reported are absent from the present data. It has been shown by Antonov *et al.* (1957) that the lateral distribution of showers at mountain altitudes are similar to those at sea level when account is taken of the change in scattering length of the electrons due to change in atmospheric density. The reduction of the data to sea level does not therefore explain the absence of a variation. The selection of high density showers is by itself an insufficient criterion for the establishment of a variation in solar time. From the calculations of Pearson and Butler (1960) it would appear that density changes at the ground due to tidal movements of the interaction layers in the upper atmosphere will be essentially

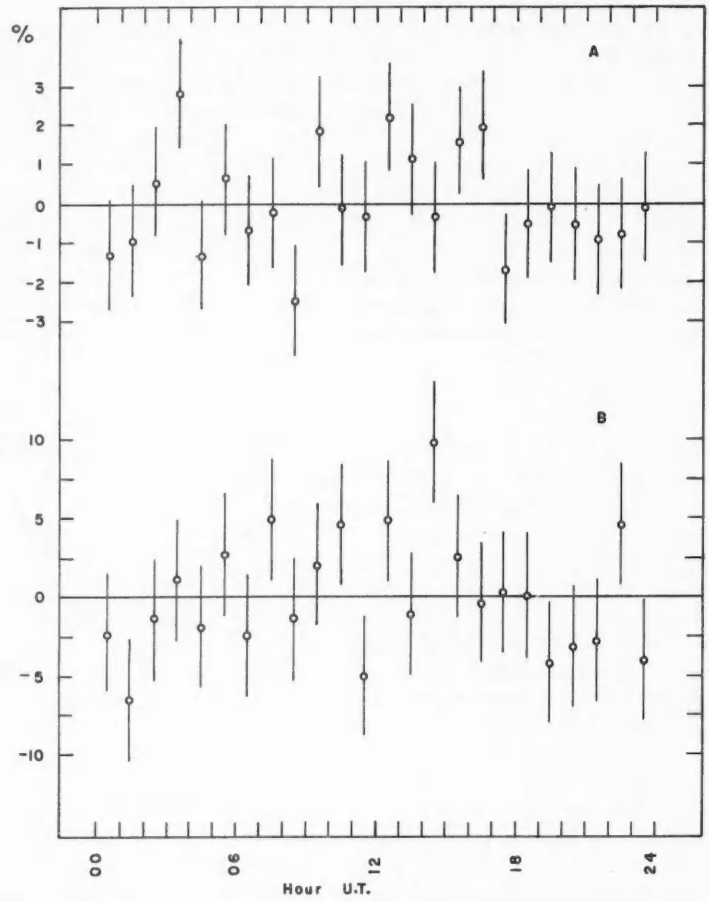

FIG. 2. Percentage deviation from the mean of the hourly extensive air shower rate plotted against universal time for (*a*) 3- to 6-fold events and (*b*) 7- to 12-fold events.

restricted to small areas near the axes of the showers. The present experimental arrangement while sensitive to localized high density showers recorded by adjacent counters in the 3-fold, 4-fold . . . categories will also accept showers from more widely distributed counters in these classes so that a real effect could be masked by these scattered contributions to a particular multiplicity selection. This effect would become smaller as the multiplicity increases until, in a 18-fold event, the selection becomes identical with six 3-counter M-units being set off at the same time in McCusker's experimental arrangement.

The same argument applies to the experimental arrangement used by

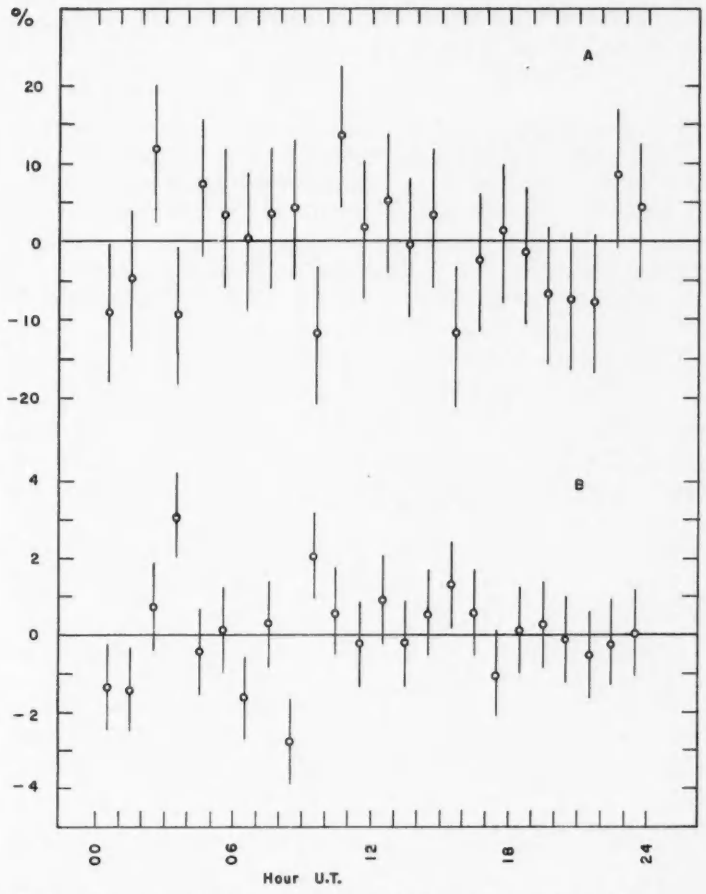

FIG. 3. Percentage deviation from the mean of the hourly extensive air shower rate plotted against universal time for (*a*) 13- to 18-fold events and (*b*) all events.

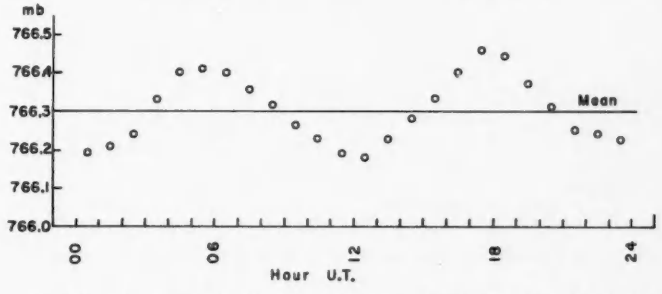

FIG. 4. Average hourly barometric pressure plotted against universal time.

Kellerman and Islam (1960) where the small counters defining a high density shower are separated by 5 meters. The resulting detector is relatively insensitive to small changes in the core structure.

CONCLUSIONS

Variations in solar time of the frequency of extensive air showers of high electron density have been reported by several authors. No such effects have been found at Banff utilizing a detector sensitive to small density changes and with a high counting rate. The conclusion may be drawn that variations in solar time of showers of high electron density are necessarily restricted to measurements close to the axes of the showers. The present negative experimental results are not in disagreement with the theory of Pearson and Butler (1960).

REFERENCES

ANTONOV, I. N., VAVILOV, I. N., ZATSEPIN, V. I., KUTUZOV, A. A., SKVORTSOV, I. V., and KHRISTIANSEN, G. B. 1957. Zhur. Eksptl. i Teoret. Fiz. **32**, 227.
CRANSHAW, T. E. and GALBRAITH, W. 1957. Phil. Mag. **2**, 804.
KELLERMAN, E. W. and ISLAM, M. S. 1960. Nuovo Cimento, **17**, 334.
MCCUSKER, C. B. A., PAGE, D. E., and REID, R. A. 1959. Phys. Rev. **113**, 712.
MCCUSKER, C. B. A. and WILSON, B. G. 1956. Nuovo Cimento, **10**, 188.
PEARSON, C. A. and BUTLER, S. T. 1960. Nuovo Cimento, **18**, 251.
WILSON, B. G. 1959. Can. J. Phys. **37**, 19.

THE CRYSTAL STRUCTURE OF K_2TiCl_6[1]

J. A. BLAND[2] AND S. N. FLENGAS[3]

ABSTRACT

The crystal structure of K_2TiCl_6 was determined from the X-ray diffraction pattern. K_2TiCl_6 is cubic, space group $Fm3m$, and has a cell side of 9.792 $\pm$0.005 Å. The interatomic distances are: Ti–Cl, 2.35$\pm$0.03 Å, and K–Cl, 3.46$\pm$0.03 Å.

During a study of the solubility of titanium tetrachloride vapor in fused alkali chloride mixtures (Flengas 1960) containing potassium chloride, a reaction occurred which produced the compound K_2TiCl_6. This compound was prepared separately in the pure state from KCl and gaseous $TiCl_4$, at a temperature of about 400° C, and its thermal stability was studied by measuring the equilibrium decomposition pressures (Flengas and Ingraham 1960).

Potassium chlorotitanate has a bright yellow color, is stable in dry air, but begins to decompose at about 300° C. At 525° C, the pressure of $TiCl_4$ over the pure compound reaches 1 atmosphere. Upon heating in a vacuum-sealed silica tubing, the color changes to a dull red at about 300° C, and at 695$\pm$5° C, a melt is obtained.

In the present investigation, the density and the crystal structure of K_2TiCl_6 were determined.

X-Ray diffraction patterns were obtained using 11.4 cm and 5.73 cm diameter powder cameras with Cu$K\alpha$ radiation; the positions of the lines were measured using a travelling microscope and the intensities of the strong lines determined with a densitometer, whilst the intensities of the weaker lines were estimated by eye.

Because of the hygroscopic nature of K_2TiCl_6, the specimens for the X-ray work were prepared in a dry box by sealing the powder in glass capillaries.

RESULTS AND DISCUSSION

K_2TiCl_6 is cubic, space group $Fm3m$, with a cell side of 9.792$\pm$0.005 Å; the calculated density is 2.45 g cm^{-3} on the basis of four formula units per cell. The measured density is 2.40$\pm$0.15 g cm^{-3}. It is isomorphous with K_2PtCl_6 and has atoms in the following positions:

(000, 1/2 1/2 0, 1/2 0 1/2, 0 1/2 1/2)+,
K$\pm\frac{111}{444}$,
Ti 000,
Cl$\pm u$,0,0; $\pm$0,u,0; $\pm$0,0,u where $u = 0.240\pm.003$,
Over-all temperature factor, $B = 1.27$.

[1]Manuscript received February 22, 1961.
This work was carried out at the Department of Mines and Technical Surveys, Mines Branch, Ottawa, Canada, and at Imperial Chemical Industries Ltd., Akers Research Laboratories, the Frythe, Welwyn Garden City, Hertfordshire, England.
[2]Imperial Chemical Industries Ltd., Plastics Division, Welwyn Garden City, Hertfordshire, England.
[3]Present address: Department of Metallurgical Engineering, University of Toronto, Toronto 5, Ontario.

A least-squares method was used for scaling the observed and calculated intensities, for obtaining the over-all temperature factor, and for refining the value of the u parameter of the chlorine atom. Corrections for the Lorentz polarization factor and for absorption of X rays in the cylindrical specimen were included in the calculated intensities, and the final values are compared with the film-measured intensities in Table I.

TABLE I

Calculated and observed X-ray data for K_2TiCl_6 (CuKα radiation)

	$a = 9.792 \pm 0.005$ Å			
	d-values		Relative intensities	
hkl	calc.	obs.	calc.	obs.
111	5.652	5.575	90	90
200	4.895	4.840	23	33
220	3.462	3.382	48	30
311	2.951	2.878	39	23
222	2.826	2.809	452	400
400	2.448	2.437	408	398
313	2.246	2.214	6	(8)
420	2.189	2.149	10	(15)
422	1.998	1.985	26	(35)
511, 333	1.884	1.880	45, 3 → 48	65
440	1.725	1.728	312	317
531	1.655	1.653	35	47
442, 600	1.632		4, 2 → 6	(8)
620	1.548	1.569	15	(15)
533			6	—
622	1.476	1.475	200	197
444	1.413	1.412	114	77
551, 711	1.371	1.371	24, 1 → 25	(35)
640	1.358		4	—
642	1.308	1.310	15	(20)
535, 731	1.275	1.283	13, 0 → 13	(23)
800	1.224	1.222	53	(45)
733	1.196		0	—
820, 644	1.187	1.180	2, 3 → 5	(5)
822, 660	1.154	1.150	3, 3 → 6	(8)
751, 555	1.130		5, 7 → 12	(5)
662	1.123	1.124	94	75
840	1.095	1.096	179	200
753, 911	1.075		1, 13 → 14	(8)
842	1.068		17	(8)
664	1.044		5	(4)
931	1.026		16	(22)
844	0.999	0.997	160	136
755, 933, 771	0.984		5, 5, 0 → 10	(8)
10,0,0, 860	0.979		6, 2 → 8	—
10,2,0, 862	0.960		6, 5 → 11	(15)
951, 723	0.947	0.948	36, 1 → 37	(45)

NOTE: Numbers in parentheses are intensities estimated by eye.

The titanium ion is octahedrally co-ordinated by 6 chlorine atoms at 2.35±.03 Å and the potassium ion is co-ordinated by 12 chlorine atoms at 3.46±.03 Å. In Table II, these distances are compared with corresponding

TABLE II

Interatomic distances in M_2TiCl_6 compounds

M	Ti–Cl (6 distances) (Å)	M–Cl (12 distances) (Å)
K	2.35±0.03	3.46±0.03
Rb	2.35±0.05	3.51±0.05
Cs	2.35±0.05	3.62±0.05

distances in Rb_2TiCl_6 and Cs_2TiCl_6 (Engel 1935). The Ti–Cl distances are the same within experimental error, while the alkali metal ion (M) to chlorine distances follow the increasing sizes of the M ions, $r_K < r_{Rb} < r_{Cs}$. This trend is also illustrated in Fig. 1. where the unit cells of M_2PtCl_6, M_2TiCl_6, M_2SnCl_6, and M_2TeCl_6 (Engel 1935) are compared.

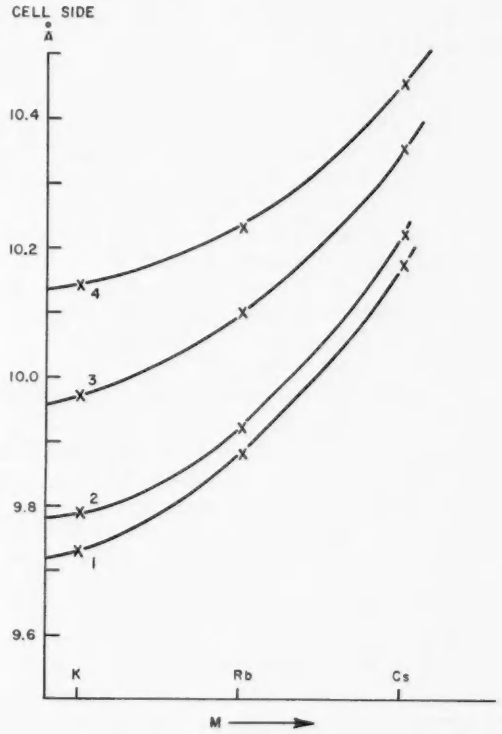

FIG. 1. Comparison of the unit cells of M_2PtCl_6 (curve 1), M_2TiCl_6 (curve 2), M_2SnCl_6 (curve 3), and M_2TeCl_6 (curve 4) where M = K, Rb, and Cs.

ACKNOWLEDGMENTS

We wish to thank Dr. C. M. Mitchell for providing an accurate powder photograph of K_2TiCl_6, and Miss G. G. Reynolds for assistance with the calculations.

REFERENCES

ENGEL, G. 1935. Z. Krist. **90**, 341.
FLENGAS, S. N. 1960. Ann. N.Y. Acad. Sci. **79**, 11, 853.
FLENGAS, S. N. and INGRAHAM, T. R. 1960. Can. J. Chem. **38**, 813.

NOTES

CONCERNING THE DISTRIBUTION COEFFICIENT OF GOLD IN LEAD

J. T. Jubb, E. L. Holmes, and W. C. Winegard

It has been suggested by Holmes *et al.* (1957) that the onset of dendritic freezing in binary alloys under given growth conditions depends upon the average solute concentration at the solid–liquid interface independent of the particular solute present. This suggestion was based upon a comparison between the results of Tiller and Rutter (1956) and those of Holmes *et al.* (1957) concerning the growth conditions for the stability of a cellular solid–liquid interface in lead–tin and lead–silver alloys respectively. It was shown that the two systems could be related by expressing the concentration as C_0/k_0, i.e., transition from cellular to dendritic growth occurred at the same $G/R^{1/2}$ ratio for the same C_0/k_0 concentration, where C_0 is the concentration of solute in atomic per cent, k_0 is the distribution coefficient, taken as 0.57 for tin in lead and 0.04 for silver in lead, G is the temperature gradient in the liquid, ahead of the solid–liquid interface, and R is the rate of growth.

This original suggestion has received support from the work of Plaskett and Winegard (1960) on tin-base binary alloys.

In view of these results, it was felt that an investigation of the conditions for the transition from cellular to dendritic growth in the lead–gold system and a comparison with the other systems investigated would yield a value for the distribution coefficient of gold in lead, a value which is not readily available from other experimental results.

The experimental results for the lead–gold system, obtained by using similar techniques to those of the previous investigators, are plotted in Fig. 1 in the form of C_0 vs. $G/R^{1/2}$.

For these results to be consistent with the results obtained on the lead–tin and lead–silver systems, a value of the distribution coefficient k_0, equal to 0.015 for gold in lead would be required. The results of the three systems investigated to date, using a k_0 of 0.015 for gold in lead, are shown in Fig. 2.

It is interesting to compare this value with values of the distribution coefficient from other sources. The value obtained from the published phase diagram, assuming straight solidus and liquidus lines from the melting point to the eutectic composition and the limit of solubility respectively, is 0.007. Aust and Rutter (1960) from observations made on the critical conditions for the formation of the hexagonal cell structure on the solid–liquid interface of lead specimens containing known amounts of gold, concluded that the distribution coefficient was approximately 0.04. The derivation of this value, however, depended upon the use of a relationship developed by Tiller *et al.* 1953), which requires a knowledge of both the slope of the liquidus line and the diffusion coefficient of gold in liquid lead.

The advantage of the method outlined in the present paper is that a

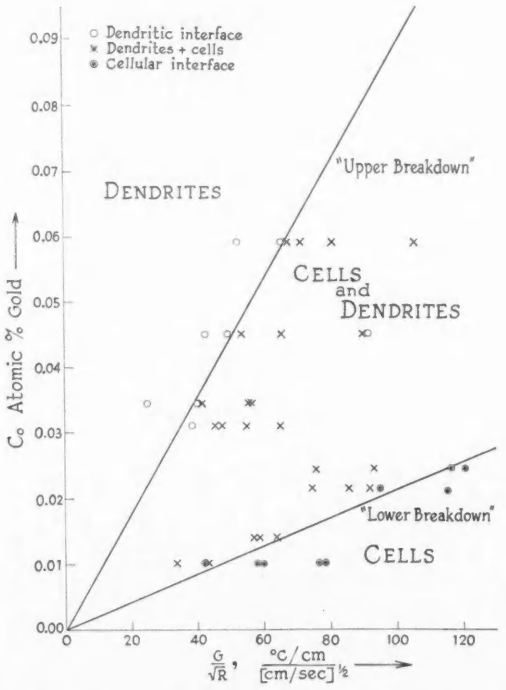

FIG. 1. The conditions for the onset of dendritic growth in the lead–gold system.

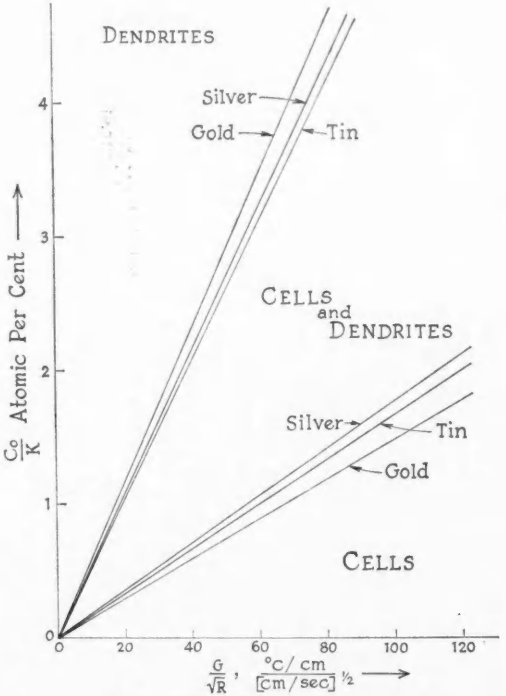

FIG. 2. The conditions for the onset of dendritic growth in the lead–tin, lead–silver, and lead–gold systems.

knowledge of the value of the distribution coefficient of tin in lead, which can be obtained with reasonable accuracy from published phase diagrams, is the only prerequisite. Using the value 0.57 as the distribution coefficient for tin in lead, the value 0.015 is obtained for the distribution coefficient for gold in lead.

AUST, K. T. and RUTTER, J. W. 1960. Trans. Am. Inst. Mining Met. Engrs. **218**, 682.
HOLMES, E. L., RUTTER, J. W., and WINEGARD, W. C. 1957. Can. J. Phys. **35**, 1223.
PLASKETT, T. S. and WINEGARD, W. C. 1960. Can. J. Phys. **38**, 1077.
TILLER, W. A., JACKSON, K. A., RUTTER, J. W., and CHALMERS, B. 1953. Acta Met. **1**, 428.
TILLER, W. A. and RUTTER, J. W. 1956. Can. J. Phys. **34**, 96.

RECEIVED FEBRUARY 22, 1961.
DEPARTMENT OF METALLURGICAL ENGINEERING,
UNIVERSITY OF TORONTO,
TORONTO, ONTARIO.

VACANCIES AND THE KIRKENDALL EFFECT

H. H. BLEAKNEY

The subject of this discussion is the revolutionary implications contained in the greatly changed concept of the volume of a vacancy, reported by Seitz in his 1959 Institute of Metals lecture.

The nucleus of the congeries of ideas comprising contemporary theories of lattice vacancies is, of course, the vacancy itself. The accepted picture of a vacancy was established in 1942 by Huntington and Seitz, and Lomer (1957) described it as follows: "The vacancy in copper is believed to be very nearly described by stating that one of the copper atoms has been removed and that the rest have remained very near their original lattice positions. This was deduced by Huntington and Seitz in their classic papers on diffusion in noble metals; and the conclusion rests on the assumption that the closed shell interaction between atoms is a strong rapidly increasing repulsion, so that to a reasonable approximation the atoms behave like hard balls. So far as the author is aware there has been no serious objection to this conclusion." This picture of the volume of a lattice vacancy is closely related to its physical influence in the lattice. Specifically it placed limitations on the possible explanations for the role of vacancies in the Kirkendall effect. Obviously if the loss of zinc atoms from the brass lattice, for example, did not, per se, bring about a contraction of the lattice, then from this point of view the vacancies so created did not influence the shift of the interface. Nevertheless, the interface movement is clearly a result of the net loss of atoms from the brass and therefore required that the part played by the vacancies be explained. An explanation was found and accepted by the great majority of physical metallurgists interested in the problem. It postulates that the vacancies must

migrate in a direction away from the interface to dislocations in the brass side of the couple, and by changing places with atoms on the dislocation lines permit shrinkage of the lattice to occur at those points. The observed shift in the interface is attributed to the sum of the resulting strains. Grain boundaries are also said to be sinks where vacancies can disappear (Seitz 1953), but dislocations are believed to be more important, in the Kirkendall effect, probably because of their greater availability.

The radically different picture of a vacancy, mentioned at the beginning of this discussion, affords a much more direct and much simpler explanation for the Kirkendall effect. This picture may best be described in the words of its author: "Tewordt has also estimated the change in volume of the lattice anticipated when an atom is withdrawn to form a vacancy and when one is added from the outside and placed in an interstitial position. As might be expected the lattice contracts when a vacancy is formed by the removal of an atom, and expands when one is placed in an interstitial position. The estimated value of the contraction associated with the first process lies between 0.45 and 0.53 Va, in which Va is the atomic volume." It is at once apparent that contraction of the lattice as a direct result of vacancy formation should be quite sufficient to account for the interface movements observed in experiments of the Kirkendall type. The stresses generated in a brass–copper diffusion couple by the unequal diffusion rates of copper and zinc are indeterminate because the elastic modulus for copper at the temperature of diffusion is not known. Nevertheless some useful purpose may be served by calculating the triaxial stresses necessary to expand the copper lattice, at room temperature, to an extent equivalent to the contraction in the Kirkendall experiment, and thus obtain a rough qualitative estimate of the forces available to bring about the lattice contraction which constitutes the Kirkendall effect.

An element of volume beside the interface on the brass side, shortly after the beginning of diffusion, will contain about 22.5% of zinc (Smigelskas and Kirkendall 1947). The original zinc content of the brass was 30.5%, hence eight vacancies have been created for every 100 atoms of alloy. However, taking the diffusion rate of copper as 1/5 that of zinc, it may be assumed that 1.6 of these vacancies will be eliminated by copper atoms. The remaining 6.4 vacancies, therefore, represent a loss of volume of approximately 6.4/2%. Taking $e = 3(1-2\nu)p/E$ (Timoshenko and Goodier 1951) where e is the volume strain $\approx .064/2$, ν is Poisson's ratio $= 0.33$ for copper, E, Young's modulus, $= 17.5\times10^6$ p.s.i. for copper, and p is the triaxial stress, then

$$p = \frac{.032\times17{,}500{,}000}{3\times.34} = 550{,}000 \text{ p.s.i.}$$

This figure is only distantly related to the stresses which cause the bulk movements responsible for the Kirkendall effect; but it is not unreasonable to assume that the diminution of the elastic modulus with rising temperature is comparable to the diminution of flow stress within an order of magnitude. Granted the validity of this assumption, it is evident that ample stress is created to cause not only the interface movements, but also the occurrence

of porosity observed in those couples where the cohesive strength of the metal has been impaired by impurities.

Some other evidence also suggests that the Kirkendall effect and the porosity which sometimes accompanies it may not be products of vacancy migration. This evidence indicates the improbability of vacancy migration toward the brass side of a brass–copper diffusion couple. In the discussion which follows, for simplicity's sake, only net movement of atoms across the interface will be considered.

In order that vacancies might migrate toward the brass side of the couple they must exchange places with atoms moving in the opposite direction. Considering again the element of volume beside the interface, the constancy of zinc concentration makes it clear that no net movement of vacancies can occur as a result of the diffusion of zinc atoms, since for every vacancy destroyed by a zinc atom arriving from the brass, another vacancy is created by a zinc atom departing toward the copper. Only copper atoms, therefore, could produce the required migration of vacancies in the required direction. But the existence of the Kirkendall effect is a result of the failure of copper atoms to diffuse as rapidly as zinc atoms. If copper atoms cannot move fast enough to fill the vacancies formed in the element of volume under consideration by moving in the direction which a relatively enormous concentration of vacancies would invite, and which their own concentration gradient would promote, surely they cannot move fast enough in the opposite direction to satisfy the accepted explanation for the Kirkendall effect.

If one adopts the more convenient and popular procedure of considering vacancy movements, rather than atom movements, the question of the direction of movement remains, if anything, in more insistent form. The explanation offered for the Kirkendall effect is that migration of zinc atoms across the interface from the brass to the copper creates excess vacancies which immediately migrate to dislocations on the brass side of the interface. Balluffi (1954) describes the kinetics as follows: "If only one site in every thousand along the dislocation line is capable of acting as an effective sink the vacancy must make about 10^{10} jumps before capture since about one site in 10^{7} lies on a dislocation line according to current estimates. The lifetime (of the vacancy) under these conditions is about 10 seconds." The above-mentioned question then is, Why is all this feverish activity necessary when the vacancy need only jump across the interface to the copper side? There it would be immediately welcomed as compensation for a vacancy, previously in equilibrium with its surroundings, which was destroyed by the intrusion of one of the immigrant zinc atoms. It should be remembered that this discussion envisages an element of volume very close to the interface on the brass side of the couple in the earliest stages of diffusion. The justification for this simplification of the problem is the assumption that whatever movements take place in the early stages of diffusion will characterize subsequent behavior.

A second related question also arises in connection with the movement of vacancies postulated by current theory. This theory requires that the

concentration of vacancies be maintained very close to the equilibrium value during diffusion; and that maintenance of this equilibrium requires a net flow of vacancies, continuously contributed by dislocations on the copper side, across the interface and on into the brass until absorbed there by dislocations in the brass. Hence, as soon as a zinc atom crosses the interface by jumping into a vacancy on the copper side of the couple, equilibrium is upset and must be restored by the contribution of a vacancy from the nearest dislocation. But the nearest dislocation, on the average, will be several thousand lattice spacings away, and the question then presents itself, How does the dislocation know that it must contribute a vacancy to the lattice?

The "condensation" of excess vacancies, to form the porosity sometimes seen in the Kirkendall type of experiment, appears to be equally improbable. The evidence indicates that such porosity results from the presence of impurities which destroy the cohesive strength of the metal. The results reported by Resnick and Seigle (1957) are an impressive contribution to this evidence, and especially so when related to the remarkable difference in ductility between tough pitch and O.F.H.C. copper at elevated temperatures (Bleakney 1954). The results reported by da Silva and Mehl (1951) should also be given serious consideration. They reported that "Cu/Zn couples exhibit apparent traces of porosity in the diffusion zone while no such porosity could be found in other systems". The most impressive evidence, however, is found in a recent paper by Puttick (1959). One of his illustrations shows a longitudinal section through the neck of a copper tension test piece which displays porosity remarkably similar to that revealed in Fig. 4 of the Smigelskas and Kirkendall (1947) paper. The evidence constitutes a prima facie case that both occurrences have their origins in the same cause: the action of multiaxial stresses on centers of impaired cohesive strength.

To the author the questions raised in this discussion appear to demand answers if the vacancy mechanism of diffusion is to maintain its present pre-eminent position. The favored position of vacancies over interstitials in diffusion is based entirely on energy considerations; but in Seitz's Institute of Metals lecture (1959) a very changed picture of the vacancy and a modified estimate of its energy relationships would seem to make the interstitial mechanism much more respectable than previous concepts would allow. Specifically Seitz quotes 1.5 ev as the required energy of vacancy formation, but he has reduced the estimate of energy for interstitial formation from 5 ev to 2.6 ev. At the same time he suggests 1.0 ev as the activation energy for the motion of a vacancy, but only 0.1 for the motion of an interstitial. He warns that these figures are approximate and must be interpreted discreetly; but the evidence as shown indicates the greatly improved energy position of interstitials as compared with previous figures.

Whether the motive force for the contraction that constitutes the Kirkendall effect is a result of vacancy migration, or alternatively, a direct result of the formation of vacancies, the mechanism is probably one of slip involving movement of dislocations. Obviously a concentration of vacancies of the magnitude indicated earlier cannot exist indefinitely in the metal. On the other hand it has been shown that there are serious objections to the vacancy

migration hypothesis. However, an explanation involving absorption of the excess vacancies by moving dislocations would meet both objections. It has been shown that the formation of excess vacancies on the brass side of the couple used in the Kirkendall experiment should, itself, provide more than sufficient energy to induce slip. Dislocations so activated, moving through the brass, would inevitably pick up and thus eliminate the excess vacancies. This explanation is very much oversimplified, but it provides a basis for an explanation involving some sort of recrystallization process needed to restore the normal lattice.

As a result of the studies described in this discussion, the author has come to believe that the Kirkendall effect, heretofore regarded as a buttress of the vacancy diffusion hypothesis, actually indicates the probability that diffusion occurs by an interstitial mechanism.

BALLUFFI, R. W. 1954. Acta Met. **2**, 201.
BLEAKNEY, H. H. 1952. Can. J. Technol. **30**, 345.
DA SILVA, L. C. C. and MEHL, R. F. 1951. Trans. A.I.M.E. **191**, 173.
HUNTINGTON, H. B. and SEITZ, FREDERICK. 1942. Phys. Rev. **61**, 315, 325.
LOMER, W. M. 1957. Institute of Metals Symposium, Monograph and Report Series 23, 81.
PUTTICK, K. E. 1959. Phil. Mag. Ser. 8, **4**, Plate 111.
RESNICK, R. and SEIGLE, L. L. 1957. J. Metals, **9**, 87.
SEITZ, FREDERICK. 1953. Acta Met. **1**, 359.
——— 1959. Trans. A.I.M.E. **215**, 359.
SMIGELSKAS, A. D. and KIRKENDALL, E. O. 1947. Trans. A.I.M.E. **171**, 132.
TIMOSHENKO, S. and GOODIER, J. N. 1951. Theory of elasticity (McGraw-Hill Book Company Inc., New York), p. 10.

RECEIVED OCTOBER 31, 1960.
KIRK'S FERRY, QUE.

MATHEMATICAL TREATMENT OF A FOUR-COMPONENT FURNACE*

M. J. LAUBITZ

INTRODUCTION

The past few years have witnessed an ever-increasing interest in the field of high temperature research. The generation of high temperatures in the laboratory requires almost invariably the construction of a furnace, and in many applications it is necessary to know precisely the temperature distributions in the furnace, and the way in which these distributions are affected by changing furnace parameters or conditions of operation. The performance of a furnace can be determined either experimentally or by calculation, the latter approach being far more illuminating as regards relationship among factors affecting the performance. Remarkably complex furnaces can be analyzed theoretically under some very general conditions with only a modicum of mathematical knowledge, the derivation of formulae for temperature distribution being more a matter of perseverance than mathematical ingenuity.

*Issued as N.R.C. No. 6317.

Having been once through that tedious labor of deriving temperature distribution formulae for quite a general cylindrical furnace, the author has decided to facilitate the work of others by making these results generally available, together with a few useful comments. The formulae given herein are in a form particularly useful for analysis of equipment used for measuring thermal conductivity, but can easily be rearranged to suit other purposes.

DESCRIPTION OF THE FURNACE AND TEMPERATURE DISTRIBUTION FORMULAE

The furnace analyzed is shown in Fig. 1. It has cylindrical symmetry, with four components, A, B, C, and D with conductivities k_1, k_2, k_3, and k_4 re-

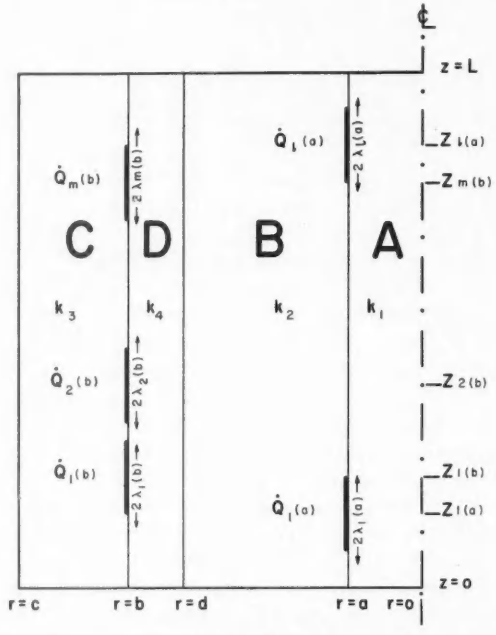

FIG. 1. General arrangement of a four-component furnace.

spectively. Component A, of radius a, has l heaters wound on it, the lth heater, located at $z_l(a)$ and of length $2\lambda_l(a)$, dissipating power $\dot{Q}_l(a)$ *per unit length*. Component D, of thickness $(b-d)$, has m heaters wound on it; the mth heater located at $z_m(b)$ has a length $2\lambda_m(b)$, and dissipates power $\dot{Q}_m(b)$ per unit length. The outside radius of the furnace is c, and its length L. The conditions assumed are as follows:

1. Radial symmetry.
2. $T(c,z) = 0$.
3. $T(r,L) = T(r,0) = 0$.

4. All conductivities, k, independent of temperature. $T(r,z)$ stands for the temperature at point (r,z). Under these conditions, the temperature in region X, where X stands for A, B, C, or D, is given by

$$T(r,z) = \sum_n [F_n(X) I_0(\alpha_n r) + G_n(X) K_0(\alpha_n r)] \sin \alpha_n z$$

where

$$\alpha_n = \frac{n\pi}{L}.$$

I_i and K_i are associated Bessel functions, and F and G are arbitrary constants for each region X. $G(A)$ is, of course, zero. The constants $F_n(X)$ and $G_n(X)$ are so selected as to satisfy the continuity conditions at the boundaries a, b, and d, and the boundary condition of c.

The formulae for $F_n(X)$ and $G_n(X)$ are given below. To facilitate their presentation a number of functions are first defined. These functions have no physical meaning whatsoever. Their only purpose is to keep the formulae to manageable lengths.

We therefore define

$$R_i(y) = \frac{I_i(y)}{K_i(y)},$$

$$S(y) = R_0(y) + R_1(y),$$

$$q_i(a) = \frac{\dot{Q}_i(a)}{2\pi k_2 a},$$

$$q_m(b) = \frac{\dot{Q}_m(b)}{2\pi k_3 b},$$

$$\rho_{i,j} = \frac{k_i}{k_j},$$

$$\alpha_n = \frac{n\pi}{L},$$

$$\beta_n = \frac{S(\alpha_n a)}{(\rho_{1,2}-1)\cdot R_1(\alpha_n a) + S(\alpha_n a)},$$

$$\gamma_n = \frac{(\rho_{1,2}-1) R_1(\alpha_n a) R_0(\alpha_n a)}{(\rho_{1,2}-1)\cdot R_1(\alpha_n a) + S(\alpha_n a)},$$

$$\theta_n = \frac{1}{\rho_{4,2}}\left\{1 + \frac{(\rho_{4,2}-1)[R_0(\alpha_n d) - \gamma_n]}{S(\alpha_n d)}\right\},$$

$$\phi_n = \frac{(\rho_{4,2}-1)}{\rho_{4,2}\cdot S(\alpha_n d)},$$

$$\chi_n = \frac{1}{\rho_{4,2}}\left\{\gamma_n - \frac{(\rho_{4,2}-1) R_1(\alpha_n d)[R_0(\alpha_n d) - \gamma_n]}{S(\alpha_n d)}\right\},$$

$$\xi_n = \frac{1}{\rho_{4,2}}\left[1+\frac{(\rho_{4,2}-1)R_1(\alpha_n d)}{S(\alpha_n d)}\right],$$

$$\mu_n = \left[\frac{R_0(\alpha_n c)S(\alpha_n b)}{R_0(\alpha_n c)-R_0(\alpha_n b)}+(\rho_{4,3}-1)R_1(\alpha_n b)\right]\cdot\theta_n-\left[\frac{S(\alpha_n b)}{R_0(\alpha_n c)-R_0(\alpha_n b)}-(\rho_{4,3}-1)\right]\cdot\chi_n,$$

$$\nu_n = \left[\frac{R_0(\alpha_n c)S(\alpha_n b)}{R_0(\alpha_n c)-R_0(\alpha_n b)}+(\rho_{4,3}-1)R_1(\alpha_n b)\right]\cdot\phi_n+\left[\frac{S(\alpha_n b)}{R_0(\alpha_n c)-R_0(\alpha_n b)}-(\rho_{4,3}-1)\right]\cdot\xi_n,$$

$$\eta_n = \frac{4}{L\alpha_n^2}\cdot\frac{\gamma_n}{(\rho_{1,2}-1)I_1(\alpha_n a)}\cdot\sum_l q_l(a)\cdot\sin\alpha_n\lambda_l(a)\cdot\sin\alpha_n z_l(a),$$

$$\sigma_n = \frac{4}{L\alpha_n^2}\cdot\frac{R_1(\alpha_n b)}{I_1(\alpha_n b)}\cdot\sum_m q_m(b)\cdot\sin\alpha_n\lambda_m(b)\cdot\sin\alpha_n z_m(b).$$

Using these definitions the constants $F_n(X)$ and $G_n(X)$ are given by

$$F_n(A) = \frac{\beta_n}{\mu_n}\cdot\sigma_n+\left[\frac{1}{R_0(\alpha_n a)}-\frac{\beta_n\cdot\nu_n}{\mu_n}\right]\cdot\eta_n,$$

$$G_n(A) = 0,$$

$$F_n(B) = \frac{\sigma_n}{\mu_n}-\frac{\nu_n}{\mu_n}\cdot\eta_n,$$

$$G_n(B) = -\frac{\gamma_n}{\mu_n}\cdot\sigma_n+\left(\frac{\gamma_n\cdot\nu_n}{\mu_n}+1\right)\cdot\eta_n,$$

$$F_n(D) = \frac{\theta_n}{\mu_n}\cdot\sigma_n+\left(\phi_n-\frac{\theta_n\cdot\nu_n}{\mu_n}\right)\cdot\eta_n,$$

$$G_n(D) = -\frac{\chi_n}{\mu_n}\cdot\sigma_n+\left(\xi_n+\frac{\chi_n\cdot\nu_n}{\mu_n}\right)\cdot\eta_n,$$

$$F_n(C) = \left\{\frac{1}{S(\alpha_n b)}+\frac{\theta_n}{\mu_n}+\frac{(\rho_{4,3}-1)[R_1(\alpha_n b)\cdot\theta_n+\chi_n]}{\mu_n S(\alpha_n b)}\right\}\cdot\sigma_n+\left\{\left(\phi_n-\frac{\theta_n\cdot\nu_n}{\mu_n}\right)+\frac{(\rho_{4,3}-1)[(\mu_n\cdot\phi_n-\theta_n\cdot\nu_n)R_1(\alpha_n b)-(\mu_n\cdot\xi_n+\nu_n\cdot\chi_n)]}{\mu_n S(\alpha_n b)}\right\}\cdot\eta_n,$$

$$G_n(C) = -R_0(\alpha_n c)\cdot F(c).$$

Thus, the temperature distributions are described throughout the furnace. The temperatures along two surfaces, $r = a$ and $r = b$, are of particular interest in systems used for measuring thermal conductivity. These two temperature distributions are given more explicitly by the following equations, where x stands for a or b.

$$T(x,z) = \sum_{l}\sum_{n} q_l(a)\cdot f_n(x)\cdot \sin\alpha_n\lambda_l(a)\cdot \sin\alpha_n z_l(a)\cdot \sin\alpha_n z$$

$$+\sum_{m}\sum_{n} q_m(b)\cdot g_n(x)\cdot \sin\alpha_n\lambda_m(b)\cdot \sin\alpha_n z_m(b)\cdot \sin\alpha_n z$$

where

$$f_n(a) = \frac{4}{L\alpha_n^2}\cdot\frac{\gamma_n}{(\rho_{1,2}-1)}\cdot\frac{K_0(\alpha_n a)}{I_1(\alpha_n a)}\cdot\left[1-\frac{\beta_n\cdot\nu_n\cdot R_0(\alpha_n a)}{\mu_n}\right],$$

$$f_n(b) = \frac{4}{L\alpha_n^2}\cdot\frac{\gamma_n}{(\rho_{1,2}-1)}\cdot\frac{K_0(\alpha_n b)}{I_1(\alpha_n a)}\cdot\left\{\left[\phi_n\cdot R_0(\alpha_n b)+\xi_n\right]-\left[\theta_n\cdot R_0(\alpha_n b)-\chi_n\right]\cdot\frac{\nu_n}{\mu_n}\right\},$$

$$g_n(a) = \frac{4}{L\alpha_n^2}\cdot\frac{I_0(\alpha_n a)}{K_1(\alpha_n b)}\cdot\frac{\beta_n}{\mu_n},$$

$$g_n(b) = \frac{4}{L\alpha_n^2}\cdot\frac{K_0(\alpha_n b)}{K_1(\alpha_n b)}\cdot\frac{\theta_n\cdot R_0(\alpha_n b)-\chi_n}{\mu_n}.$$

The number of terms that has to be taken in the summation obviously depends on the accuracy required. In a system analyzed by the author it was found that 12 terms gave a distribution differing by less than 0.5% from that given by 24 terms, while 6 terms gave one which differed by up to 5% from the 24-term distribution.

The only limitation of the theory is the assumption of temperature independence of the conductivities. By comparing calculated with experimental distributions, it was found, however, that this limitation is not serious, particularly in the central region of the furnace.

RECEIVED MARCH 3, 1961.
DIVISION OF APPLIED PHYSICS,
NATIONAL RESEARCH COUNCIL,
OTTAWA, CANADA.

Frequency Measurement of Standard Frequency Transmissions[1,2]

Measurements are made at Ottawa, Canada, using N.R.C. caesium-beam frequency resonator as reference standard (with an assumed frequency of 9 192 631 770 c.p.s.). Frequency deviations from nominal are quoted in parts per 10^{10}. A negative sign indicates that the frequency is below nominal.

Date, March 1961	MSF, 60 kc/s	GBR, 16 kc/s		WWVB, 60 kc/s
		5-hour average*	24-hour average†	
1	−158	−140	−143	N.M.
2	−157	−148	−150	N.M.
3	N.M.	−145	−147	N.M.
4	−146	−146	−146	N.M.
5	−150	−140	−143	N.M.
6	−167	−142	−145	N.M.
7	N.M.	−150	−151	−154
8	−159	−148	−149	−148
9	N.M.	−146	−145	−145
10	N.M.	−155	−153	N.M.
11	N.M.	−151	−154	N.M.
12	N.M.	−152	−151	N.M.
13	−174	−150	−152	−154
14	−162	−147	−150	−154
15	−164	−141	−148	−150
16	−160	−146	−151	−152
17	−158	−150	−149	−146
18	−145	−147	−146	−149
19	N.M.	−145	−144	N.M.
20	−151	−142	−142	−154
21	−140	−144	−145	−157
22	−143	−136	−139	−149
23	−153	−142	−144	−152
24	−146	−142	−141	−147
25	−140	−139	−139	−144
26	−144	−139	−141	−147
27	−147	−141	−141	−151
28	N.M.	−132	−137	−149
29	−161	−139	−141	−154
30	−155	−146	−150	−152
31	−141	−144	−148	−142
Average	−153	−144	−146	−150
Midmonthly mean of WWV	−148			

NOTE: N.M. no measurement.
*Time of observations: 00.00 to 05.00 hours U.T.
†Time of observations: 15.00 to 15.00 hours U.T.

RECEIVED APRIL 14, 1961.
S. N. KALRA
DIVISION OF APPLIED PHYSICS,
NATIONAL RESEARCH COUNCIL,
OTTAWA, CANADA.

[1]Issued as N.R.C. No. 6296.
[2]Cf. Kalra, S. N. 1959. Can. J. Phys. **37**, 1328.

NOTES TO CONTRIBUTORS

Canadian Journal of Physics

MANUSCRIPTS

General.—Manuscripts, in English or French, should be typewritten, double spaced, on paper 8½×11 in. **The original and one copy are to be submitted.** Tables and captions for the figures should be placed at the end of the manuscript. Every sheet of the manuscript should be numbered. Style, arrangement, spelling, and abbreviations should conform to the usage of recent numbers of this journal. Greek letters or unusual signs should be written plainly or explained by marginal notes. Characters to be set in boldface type should be indicated by a wavy line below each character. Superscripts and subscripts must be legible and carefully placed. Manuscripts and illustrations should be carefully checked before they are submitted. Authors will be charged for unnecessary deviations from the usual format and for changes made in the proof that are considered excessive or unnecessary.

Abstract.—An abstract of not more than about 200 words, indicating the scope of the work and the principal findings, is required, except in Notes.

References.—References should be listed **alphabetically by authors' names,** unnumbered, and typed after the text. The form of the citations should be that used in current issues of this journal; in references to papers in periodicals, titles should not be given and only initial page numbers are required. The names of periodicals should be abbreviated in the form given in the most recent *List of Periodicals Abstracted by Chemical Abstracts.* All citations should be checked with the original articles and each one referred to in the text by the authors' names and the year.

Tables.—Tables should be numbered in roman numerals and each table referred to in the text. Titles should always be given but should be brief; column headings should be brief and descriptive matter in the tables confined to a minimum. Vertical rules should not be used. Numerous small tables should be avoided.

ILLUSTRATIONS

General.—All figures (including each figure of the plates) should be numbered consecutively from 1 up, in arabic numerals, and each figure referred to in the text. The author's name, title of the paper, and figure number should be written in the lower left corner of the sheets on which the illustrations appear. Captions should not be written on the illustrations.

Line drawings.—Drawings should be carefully made with India ink on white drawing paper, blue tracing linen, or co-ordinate paper ruled in blue only; any co-ordinate lines that are to appear in the reproduction should be ruled in black ink. Paper ruled in green, yellow, or red should not be used. All lines must be of sufficient thickness to reproduce well. Decimal points, periods, and stippled dots must be solid black circles large enough to be reduced if necessary. Letters and numerals should be neatly made, preferably with a stencil (**do NOT use typewriting**) and be of such size that the smallest lettering will be not less than 1 mm high when the figure is reduced to a suitable size. Many drawings are made too large; originals should not be more than 2 or 3 times the size of the desired reproduction. Whenever possible two or more drawings should be grouped to reduce the number of cuts required. In such groups of drawings, or in large drawings, full use of the space available should be made; the ratio of height to width should conform to that of a journal page (4¼×7⅛ in.), but allowance must be made for the captions. **The original drawings and one set of clear copies (e.g. small photographs) are to be submitted.**

Photographs.—Prints should be made on glossy paper, with strong contrasts. They should be trimmed so that essential features only are shown and mounted carefully, with rubber cement, on white cardboard, with no space between those arranged in groups. In mounting, full use of the space available should be made. **Photographs are to be submitted in duplicate;** if they are to be reproduced in groups one set should be mounted, the duplicate set unmounted.

REPRINTS

A total of 100 reprints of each paper, without covers, are supplied free. Additional reprints, with or without covers, may be purchased at the time of publication.

Charges for reprints are based on the number of printed pages, which may be calculated approximately by multiplying by 0.6 the number of manuscript pages (double-spaced typewritten sheets, 8½×11 in.) and including the space occupied by illustrations. Prices and instructions for ordering reprints are sent out with the galley proof.

Contents

Printed in Canada *by* University of Toronto Press